BRNO UNIVERSITY OF TECHNOLOGY

VYSOKÉ UČENÍ TECHNICKÉ V BRNĚ

FACULTY OF MECHANICAL ENGINEERING

FAKULTA STROJNÍHO INŽENÝRSTVÍ

INSTITUTE OF AEROSPACE ENGINEERING

LETECKÝ ÚSTAV

EFFECT OF VIBRATIONS ON FATIGUE LIFE OF L 410 NG AIRPLANE FLAPS

VLIV VIBRACÍ NA ŽIVOTNOST VZTLAKOVÝCH KLAPEK LETOUNU L 410 NG

MASTER'S THESIS

DIPLOMOVÁ PRÁCE

AUTHOR — Bc. Lubomír Častulík

AUTOR PRÁCE

SUPERVISOR — Ing. Dalibor Vlček

VEDOUCÍ PRÁCE

BRNO 2017

BRNO UNIVERSITY OF TECHNOLOGY
FACULTY OF MECHANICAL ENGINEERING

Master's Thesis Assignment

Institut:	Institute of Aerospace Engineering
Student:	**Bc. Lubomír Častulík**
Degree programm:	Mechanical Engineering
Branch:	Aircraft Design
Supervisor:	**Ing. Dalibor Vlček**
Academic year:	2016/17

As provided for by the Act No. 111/98 Coll. on higher education institutions and the BUT Study and Examination Regulations, the director of the Institute hereby assigns the following topic of Master's Thesis:

Effect of vibrations on fatigue life of L 410 NG airplane flaps

Brief description:

The goal of master's thesis is to determine the effect of vibrations on fatigue life of L 410 NG airplane flaps. In the first part of the thesis overview of different methods for evaluation of effect of vibrations on fatigue life of aircraft structures will be made. In the second one results of in-flight strain gauge measurements will be analyzed. The crucial task will be focused on the development of methodology for prediction of fatigue life of flap structure under the vibration loads. Proposed method will include both the initiation and propagation of fatigue cracks in analyzed structure.

Master's Thesis goals:

Master's thesis will be directly applicable by Aircraft Industries in the frame of development and certification of L 410 NG airplane.

Bibliography:

SCHIJVE, J.: Fatigue of Structures and Materials. Springer, Dordrecht, The Netherlands, 2009.

KAHÁNEK, V.: Únavová životnost letadlových konstrukcí, VŠD v Žiline, 1977.

BURIAN, P.: Vliv vibrací na únavovou pevnost a rychlost šíření únavové trhliny v Al-slitinách, zpráva R-2695/1992, VZLÚ, 1992.

Students are required to submit the thesis within the deadlines stated in the schedule of the academic year 2016/17.

In Brno, 10. 11. 2016

L. S.

doc. Ing. Jaroslav Juračka, Ph.D.
Director of the Institute

doc. Ing. Jaroslav Katolický, Ph.D.
FME dean

ABSTRACT

The thesis deals with the design of methodology for determination of vibrations effect on fatigue durability and crack growth rate of L 410 NG airplane flaps. The introductory part contains necessary information about the airplane and loading of flaps. Means for quantitative description of fatigue process by the stress-life approach are described afterwards. Definition of general random process and description of techniques applied to data, which were obtained by a strain gauge survey, are presented to clarify the proposed methodology. The main part of the thesis contains a detailed description of the proposed methodology. At the same time, the methodology is applied to data obtained from the strain gauge survey on L 410 UVP-E20.

KEYWORDS

Fatigue, random cyclic loading, vibration

ABSTRAKT

Diplomová práce se zabývá návrhem metodiky pro stanovení vlivu vibrací na únavovou životnost a rychlost šíření trhlin u vztlakových klapek letounu L 410 NG. Úvodní část práce obsahuje potřebné informace o letounu a zatížení vztlakových klapek. Poté jsou popsány prostředky pro kvantitativní popis únavového procesu s využitím napěťového přístupu. Pro objasnění navrhované metodiky je uvedena definice obecného náhodného procesu a popis postupů aplikovaných na data získaná z letového měření. Hlavní část práce obsahuje podrobný popis navržené metodiky. Ta je zároveň aplikována na data získaná z měření na letounu L 410 UVP-E20.

KLÍČOVÁ SLOVA

Únava, náhodné cyklické zatěžování, vibrace

BIBLIOGRAPHIC CITATION

BIBLIOGRAFICKÁ CITACE

ČASTULÍK, L. *Effect of vibrations on fatigue life of L 410 NG airplane flaps.* Brno: Vysoké učení technické v Brně, Fakulta strojního inženýrství, 2017. 137 p. Master's thesis supervisor Ing. Dalibor Vlček.

AFFIDAVIT

I declare that I developed my master's thesis „Effect of vibrations on fatigue life of L 410 NG airplane flaps" on my own under the supervision of the master's thesis supervisor and with usage of the literature and additional information sources that are all cited in the thesis and stated in a list at the end of the thesis.

ČESTNÉ PROHLÁŠENÍ

Prohlašuji, že svou diplomovou práci na téma „Vliv vibrací na životnost vztlakových klapek letounu L 410 NG" jsem vypracoval samostatně pod vedením vedoucího diplomové práce a s použitím odborné literatury a dalších informačních zdrojů, které jsou všechny citovány v práci a uvedeny v seznamu literatury na konci práce.

In Brno on May 20, 2017

……

Lubomír Častulík

ACKNOWLEDGEMENT

I am very grateful that *Aircraft Industries, a.s.* offered me to work on the topic "Effect of vibrations on fatigue life of L 410 NG airplane flaps." My thanks belong to the staff of *Stress and F&DT department* and to Ing. Dalibor Vlček personally. It was an honour to work on a master's thesis under his supervision.

At the same time, I would like to express my thanks to my parents and all my relatives for their support during my university studies.

PODĚKOVÁNÍ

Jsem velmi vděčný, že mi v *Aircraft Industries, a.s.* nabídli možnost pracovat na tématu "Vliv vibrací na životnost vztlakových klapek letounu L 410 NG." Mé poděkování patří zaměstnancům *Oddělení Statických a F&DT* analýz a osobně pak Ing. Daliboru Vlčkovi. Byla čest pracovat na diplomové práci pod jeho vedením.

Současně bych rád poděkoval svým rodičům a všem příbuzným za jejich podporu během mých studií na vysoké škole.

CONTENTS

1 INTRODUCTION

Fatigue due to vibrations is an important issue throughout the industry, not only in the aerospace engineering. The significance of the term corresponds to the fact, that vibration of the structure may cause a fatigue failure earlier than expected by the analysis, if the analysis does not cover vibration effects. As can be expected, vibration will be much more severe, when the sources of vibration correspond to the natural frequency of the structure.

The airplane is loaded by various loads during each flight. Some of them are deterministic, some of them purely stochastic. The thesis analyses vibrations, which occur on the flaps. It is presumed that the main source of vibration is the propeller slipstream. Vibration is dealt as a stochastic event, which might be described by means of statistics. The stress/strain response of the structure might be directly measured via strain gauges fixed in the analysed locations. The stress/strain time history is then processed using the time-domain approach.

The introductory chapter contains basic information about analysed aircraft and the detailed description of flap's design. Additional information about aircraft's power-plant and typical operational conditions in the form of a typical flight profile are also mentioned.

1.1 Description of L-410 NG

L-410 NG is a twin-engine turboprop commuter category airplane designed in line with FAR-23 regulation. The airplane is capable to seat up to 19 passengers. Thanks to a brand-new wing structure carrying an integral fuel tank with higher volume capacity, the airplane is meant to be the successor of the L 410 UVP-E20. Comparing to L 410 UVP-E20, L410 NG aircraft has significantly higher range and flight endurance. At the same time, the MTOW and payload increased. The baggage compartment was enlarged and the aircraft is able to carry 400kg of load more than UVP-E20 version. L-410 NG is equipped with more efficient turboprop engine GE H85-200 and a five-blade propeller AV 725.

Another benefit of the aircraft is connected with the improved utility characteristics. The aircraft is designed to be easily accessible during maintenance procedures. At the same time, the operational life significantly increased by implementing the "Damage tolerance" design philosophy.

A brief comparison between L410 UVP-E20 and L410 NG is summarized in Table 1.1.

Airplane	L 410 NG	L 410 UVP-E20
Maximum take-off weight	7000 kg	6600 kg
Empty weight	4200 kg	4200 kg
Wingspan	19.48 m	19.98 m
Payload	2200 kg	1800 kg
Passengers	19	19
Engines	GE H85-200	GE H80-200
Propellers	Avia 725 (5-blade)	Avia 725 (5-blade)
Maximum speed (TAS)	412 km/h	398 km/h
Maximum range (ISA, 45min. res.)	2840 km	1520 km
Service life	30 000 FH/FC	20 000 FH/FC

Table 1.1 – Comparison between L410 UVP-E20 and L410 NG aircraft

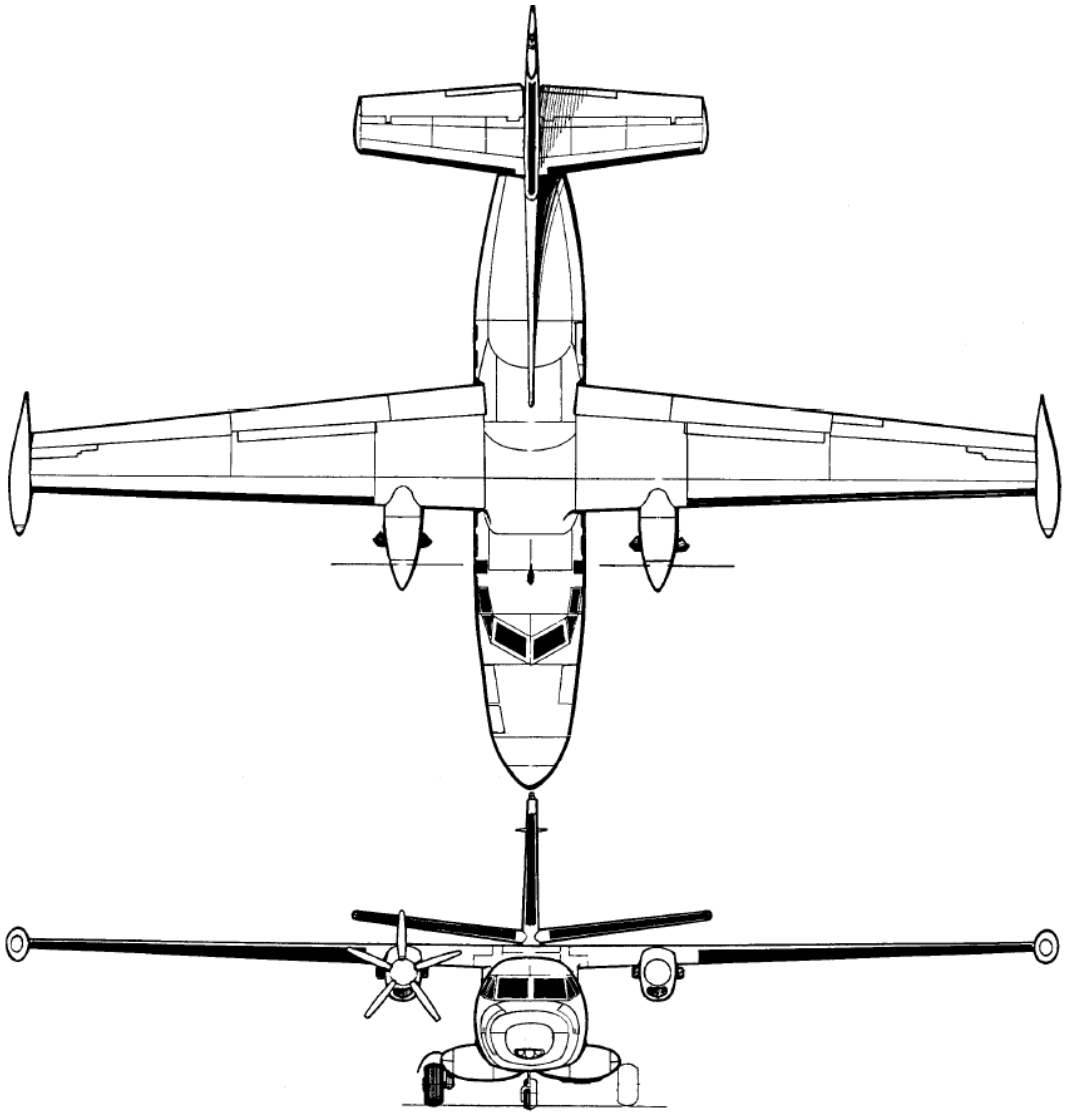

Figure 1.1 – L 410 NG airplane [1]

1.2 Regulatory background

FAR 23.572 Metallic wing, empennage and associated structures [9]

FAR 23.572(b)(3) is directive to normal, utility and aerobatic category only, but it is mentioned here to point out, that propeller slipstream might have a significant effect on aircraft fatigue durability. It prescribes to investigate any significant effect of propeller slipstream on fatigue behaviour of the metallic wing or fuselage, including any associated structure:

"FAR 23.572(b)(3) *Metallic wing, empennage and associated structures:*

a) For normal, utility, and *aerobatic category airplanes, the strength, detail design, and fabrication of those parts of the airframe structure whose failure would be catastrophic must be evaluated under one of the following unless it is shown that the structure, operating stress level, materials and expected uses are comparable, from a fatigue standpoint, to a similar design that has had extensive satisfactory service experience:*

(1) A fatigue strength investigation in which the structure is shown by tests, or by analysis supported by test evidence, to be able to withstand the repeated loads of variable magnitude expected in service;

(2) A fail-safe strength investigation in which it is shown by analysis, tests, or both, that catastrophic failure of the structure is not probable after fatigue failure, or obvious partial failure, of a principal structural element, and that the remaining structure is able to withstand a static ultimate load factor of 75 percent of the critical limit load factor at Vc. These loads must be multiplied by a factor of 1.15 unless the dynamic effects of failure under static load are otherwise considered.

(3) The damage tolerance evaluation of CS 23.573(b).

b) Each evaluation required by this paragraph must:

(1) Include typical loading spectra (e.g. taxi, ground-air-ground cycles, manoeuvre, gust)

(2) Account for any significant effects due to the mutual influence of aerodynamic surfaces

(3) ***Consider any significant effects from propeller slipstream loading****, and buffet from vortex impingements"*

AC 25.571-1D [10]

This advisory circular provides guidelines to comply with FAR 25 and also FAR 23 airworthiness standards, if the damage tolerance approach is opted for. **Section 5.b.** deals with the typical loading spectrum expected in service:

"Loading spectrum used for crack-growth and fatigue crack initiation assessments (tests or analyses) should be based on measured statistical data of the type derived from government and industry load-history studies and, where data is insufficient or unavailable, on a conservative estimate of the anticipated use of the airplane. The principal loads that should be considered in establishing a loading spectrum are flight loads (gust and manoeuver), ground loads (taxiing,

landing impact, turning, engine run-up, braking, thrust reversing, and towing), and pressurization loads. The development of the loading spectrum includes the definition of the expected flight plan, which involves climb, cruise, descent, flight times, operational speeds and altitudes, and the approximate time to be spent in each of the operating regimes. Operations for crew training and ***other pertinent factors, such as the dynamic stress characteristics of any flexible structure excited by turbulence or buffeting, should also be considered****. For pressurized cabins, the loading spectrum should include the repeated application of the normal operating differential pressure, and the superimposed effects of flight loads and external aerodynamic pressures."*

1.3 F&DT Approaches valid for L 410 NG

Because L 410-NG aircraft consists of newly designed structure as well as structure inherited from L 410 UVP-E20, altogether three possible F&DT approaches are proposed over the F&DT evaluation of the structure [18]:

- **DTA** – Damage tolerance approach for newly designed structure and structure inherited from L 410 UVP-E20
- **SLA-1** – Safe life approach for traditional safe life structure (landing gear, landing gear beam, engine mounts)
- **SLA-2** – Safe life approach for structure inherited from L 410 UVP-E20 which is not included within SLA-1 category and where damage tolerance approach (DTA) is not practical

Report [18] describes relevant usage of the approaches in more detail. There are also stated inspection aims, together with the design service goal of the structure. The airframe shall be designed to withstand 30 000 flight hours or 30 000 landings (flight cycles), whichever comes first.

1.4 Flaps structure

The wing of L410 NG airplane is equipped with all-metal flaps to increase lift of the aircraft, mainly during take-off and landing flight phase.

Flaps are divided into two sectors along the wingspan – inner flap and outer flap (see Figure 1.2). Each of them consists of two segments. These two segments are tied together by a unique kinematic coupling, which enables them to deflect differently. The slot (first segment) improves flap's efficiency when deflected to the landing configuration. The kinematic coupling is displayed in Figure 1.3.

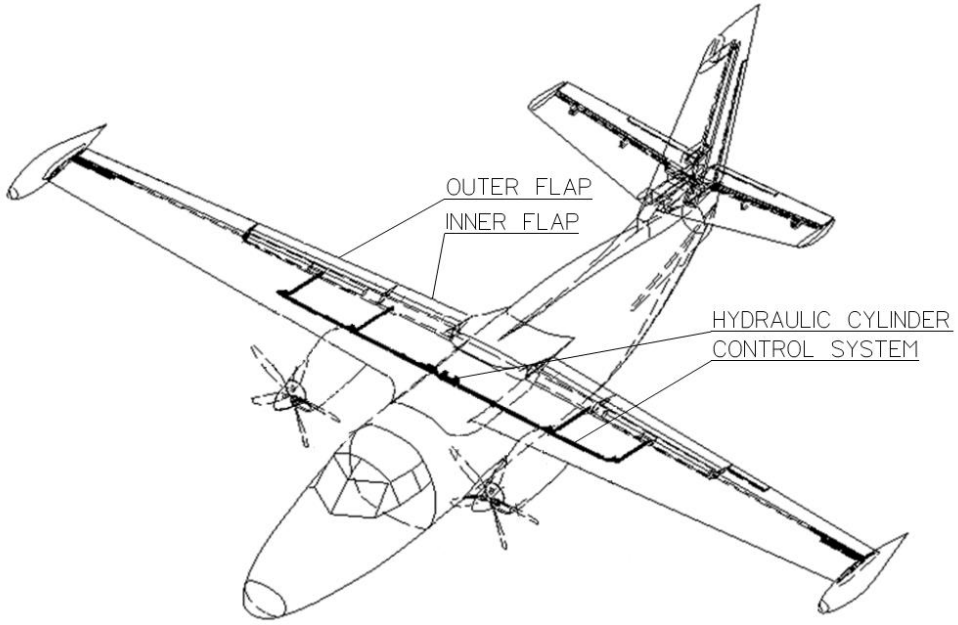

Figure 1.2 – Flaps scheme [3]

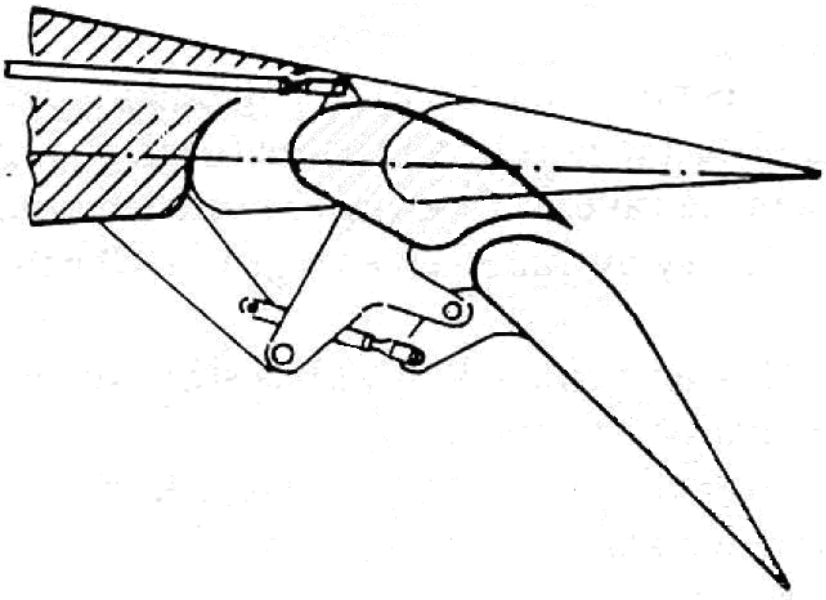

Figure 1.3 – Kinematic coupling of flaps [3]

Flaps are controlled by the control system, which scheme can be seen in Figure 1.4. Executive member of the system is the hydraulic cylinder located in the symmetry plane of the aircraft. The hydraulic cylinder drives the system of rods, which transmits the motion onto the inner and outer flap at different rates. The outer sector is deflected less than the inner sector, which provide the aircraft with convenient stalling characteristics.

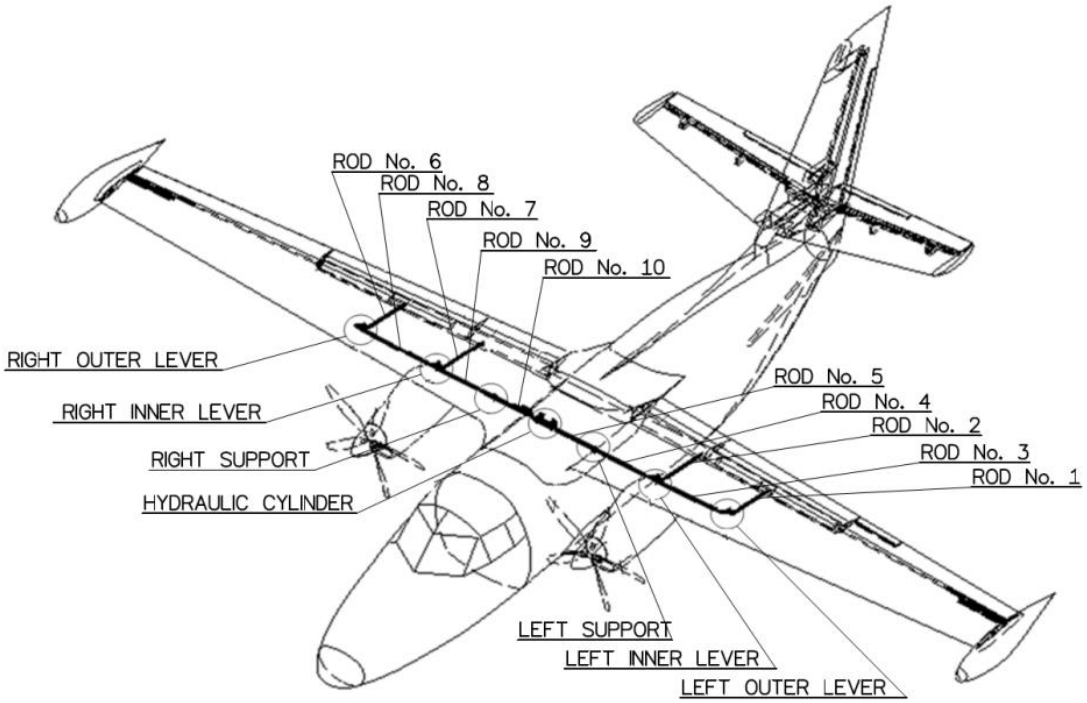

Figure 1.4 – Flaps control system [3]

1.5 Power-plant

It has been already mentioned in Table 1.1 that L410 NG is powered by two turboprop engines GE-H85-200 and a five-blade AV-725 propeller. The output shaft revolutions of the engine are 2080 RPM according to the engine manufacturer. Maximal output power is equal to 850 SHP. Comparing to that, L 410 UVP-E20 is powered by GE-H80-200. The main difference between these engines are the performance characteristics.

Sea level – standard day	
Power Output	shp 850 eshp 898
RPM	gas gen (98.7%) – 36,183 shaft output – 2,080
Propeller Rotation	cw from rear
Weight (basic dry mass)	390 lbs
Airflow	8.4 lb/s
Fuel	Jet A, Jet A-1
Oil	Mil-L 23699C
Electrical	28 VDC
Bleed Air	4% (max continuous)
TBO	Hours – 3,600
	Cycles – 6,600
Basic Warranty (whichever occurs first)	Hours – 1,000
	Cycles – 1,100
	Months – 24

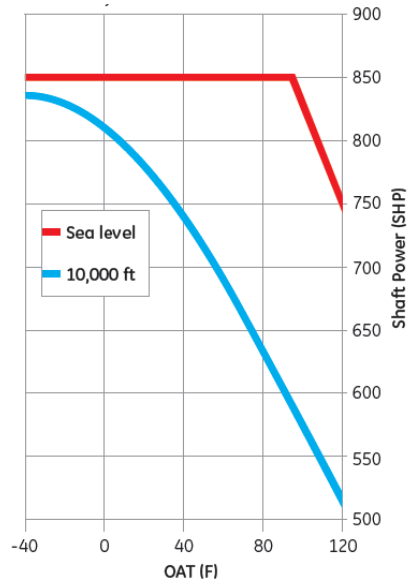

Figure 1.5 – Specifications and maximum take-off power of GE-H85 [7]

Sea level – standard day	
Power Output	shp 800 eshp 845
RPM	gas gen (97.8%) – 35,854 shaft output – 2,080
Propeller Rotation	cw from rear
Weight (basic dry mass)	390 lbs
Airflow	8.2 lb/s
Fuel	Jet A, Jet A-1
Oil	Mil-L 23699C
Electrical	28 VDC
Bleed Air	4% (max continuous)
TBO	Hours – 3,600
	Cycles – 6,600
Basic Warranty (whichever occurs first)	Hours – 1,000
	Cycles – 1,100
	Months – 24

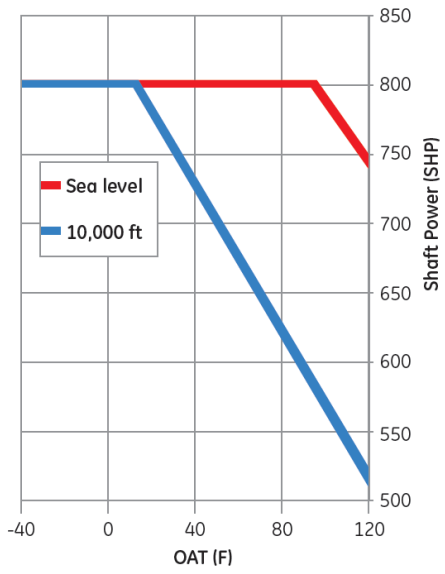

Figure 1.6 – Specifications and maximum take-off power of GE-H80 [8]

1.6 Effect of propeller slipstream

Thrust produced by the propeller affect a part of flaps, which is located directly in the propeller slipstream. The area affected by the propeller slipstream was adopted from [4] and can be seen below.

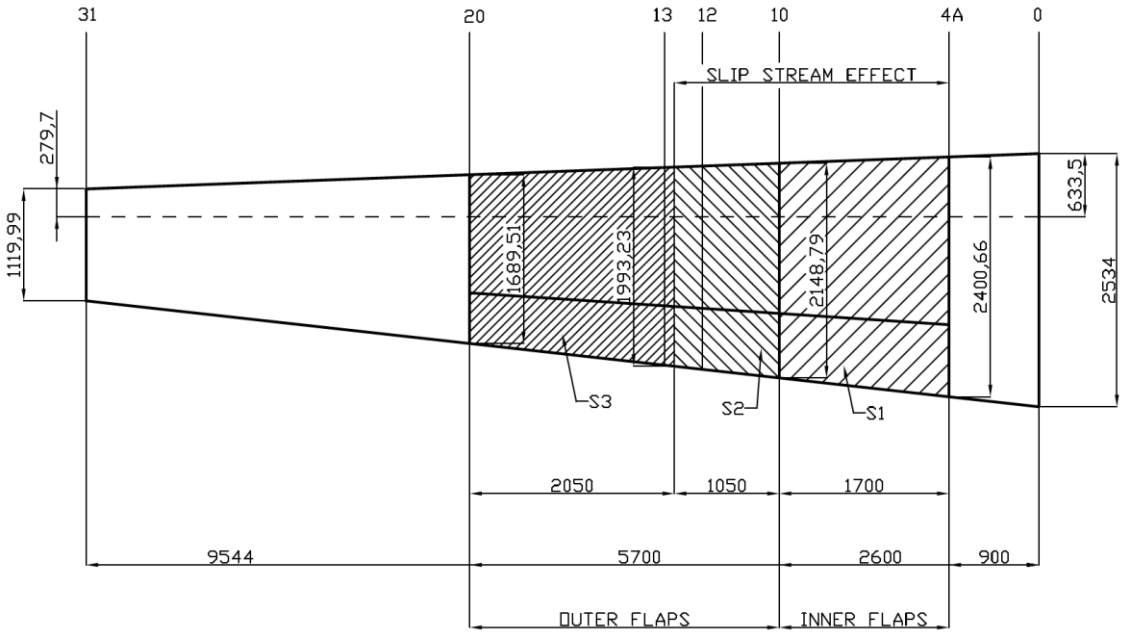

Figure 1.7 – Area of flaps affected by the propeller slipstream [4]

According to [5], the effect of propeller slipstream on the flap's loading can be described by an increase of the dynamic pressure on the affected flaps area. The dynamic pressure increase corresponds to the air acceleration caused by the propeller. Assuming linear propulsion theory, the airspeed beyond the propeller can be calculated as a sum of the airspeed V_∞ and the induced airspeed w_0:

$$V_0 = V_\infty + w_0$$

Where:

$$w_0 = V_\infty \cdot \left(-1 + \sqrt{1 + k_q}\right)$$

$$k_q = \frac{F}{q \cdot S_{VD}}$$

k_q	Dynamic pressure increase coefficient
F	Thrust produced by the propeller
q	Dynamic pressure of the undisturbed air
S_{VD}	Propeller disc area

Detailed description of the effect of propeller slipstream on loading of wing's structure and high-lift devices might be found in [2] and [5].

The assumption described above gives us an information about an average loading of the structure due to the propeller slipstream. However, it shall be pointed out, that the increase of the dynamic pressure is not uniform. The dynamic pressure increases each time, when the propeller blade passes through particular point and then decreases again. Such passes produce impulses with frequency proportional to the propeller revolutions.

These pressure pulses act upon the structure and depending on the natural frequency of the structure and other impacts, they contribute to the dynamic loading of the structure.

The frequency of pressure pulses can be estimated by the following equation:

$$\omega\ [Hz] = \frac{n \cdot z}{60}$$

Where:

$n\ [min^{-1}]$	propeller revolutions per minute
$z\ [-]$	number of propeller blades

As a conclusion, it can be expected, that pressure pulses generated by the propeller will vary with flight mode, especially with revolutions of the propeller and thrust delivery.

1.7 Operational conditions

Operational conditions of an airplane might alternate from one operator to another. It is vitally important to determine representative conditions in a form of a flight profile which will be used during the fatigue analysis and which will cover operational conditions of most of the aircraft in service. Therefore, it is recommended to gather flight data from the operated aircraft and to update flight profile accordingly.

1.7.1 Typical flight profile

There is a long-time experience with L410 aircraft family and its operational conditions. Several flight profiles have been derived from the obtained data and the typical flight profile was established.

Flight is separated into altogether seven phases, described in more detail in Table 1.2.

Section mark	Flight regime	Description of the section
A	Take-off	Airplane stay on line-up at take-off configuration (flaps 18 deg.) -> take-off rating setting -> brakes release -> ground run -> lift-off -> achieving of height 35 ft (10.7 m) above runway surface
	Initial climb	1st segment of climb: landing gear retracting 2nd segment of climb: climbing to altitude 400 ft (122 m) above runway surface Accelerate segment: airplane acceleration and flaps retracting Final take-off segment: climbing to 1500 ft (457 m) above runway surface
B	En-route climb	Climbing from 1500 ft (457 m) above runway surface to cruise level
C	Cruise flight	Setting of the selected rating in cruise altitude -> steady horizontal flight
D	Descent	Setting required rating for descent -> descent with comfortable rate of descent -> continue in descent to altitude 1500 ft (457 m) above runway surface
E	Approach	Initiation of the approach at altitude 1500 ft (457 m) above runway surface -> extension of the landing gear -> setting flaps to 18 deg. -> propellers fine pitch angle -> achieving of the decision altitude 200 ft (61 m) above runway surface -> setting flaps to 42 deg. -> Idle at both engines -> achieving of threshold altitude 50 ft (15 m) above runway surface
F	Landing	Altitude 50 ft (15 m) above runway surface, VREF speed-> touch down -> (reverse thrust setting) -> spoilers deflection -> wheels braking -> ground run

Table 1.2 – Flight phases [6]

Besides the profile presented above, other ground phases such as straight taxi or turns during taxi are also determined, but won't be studied in detail. It is assumed, that loading of flaps during straight taxiing, or turns etc. is quite small in comparison to loading during take-off and landing. Therefore, such ground phases are neglected. The reverse thrust is used within 50% of landings according to [6]. The average duration of thrust reversals is 8 seconds.

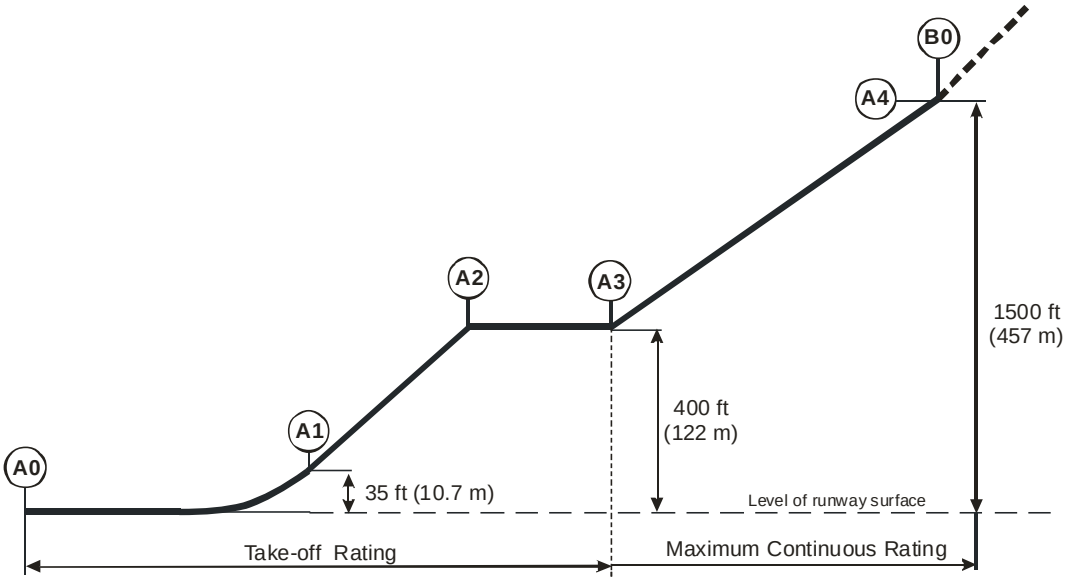

Figure 1.8 Take-off flight phase[6]

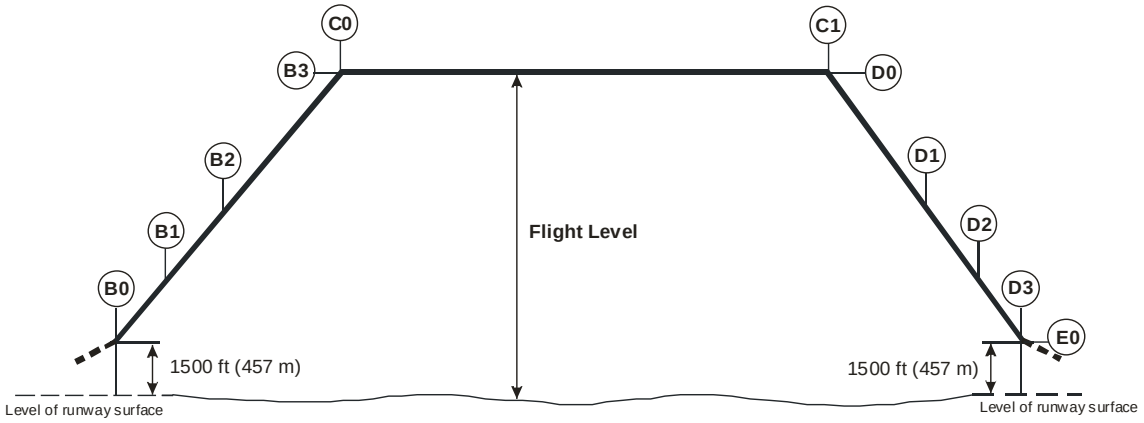

Figure 1.9 En-route flight phase[6]

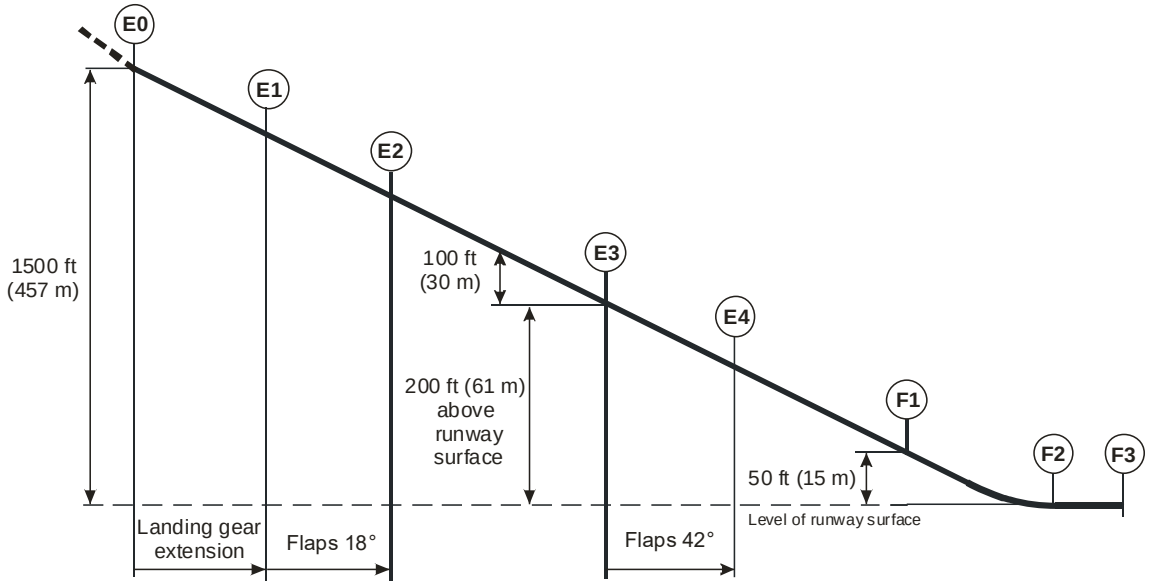

Figure 1.10 Approach and landing flight phases[6]

Block time	Block fuel	Block distance
min.	kg	km
60	382	377

Take-off weight	Landing weight	Total fuel	Payload
kg	kg	kg	kg
6835	6453	689	1700

Wing tip tanks	
Fuel	NO
Installed	NO

Flight phase	Segment	Segment point	Flight time	Distance	Pressure altitude	Airplane weight	Airspeed			Rate of climb	Fuel consumption	Engines Rating	One engine Power	One engine Thrust	Propeller speed	Flaps	Landing gear
							IAS	EAS	TAS			TRQ					
			min	km	ft	kg	km/h	km/h	km/h	m/s	kg	%	kW	N	RPM	deg.	-
Brakes release	A	0	0	0.0	1000	6835		0	0	0.0	0	100	634	12 873	1950	18	DOWN
Take-off to 35 ft AGL		1	0.4	0.6	1035	6832		173	178	7.9	2.9	100	634	8 681	1950	18	DOWN
Take-off climb to 400 ft AGL (2nd segment)		2	0.6	1.3	1400	6831		173	179	8.5	4.6	100	634	8 660	1950	18	UP
Flaps retracting 400 ft AGL		3	0.7	1.7	1400	6829		192	199	0.0	5.6	100	634	8 174	1950	0	UP
Climb to 1.500 ft AGL (Final take-off segment)		4	1.3	3.7	2500	6825		192	202	9.5	10.3	100	634	8 051	1950	0	UP
Start En-route climb	B	0	1.3	3.7	2500	6825		300	317	5.0	10.3	100	553	5 251	1700	0	UP
Climb		1	2.1	8.0	3315	6819		297	317	5.0	16.2	100	553	5 193	1700	0	UP
Enroute climb 1/2 Pressure Altitude		2	3.8	17.2	5000	6807		295	323	5.0	28.4	100	553	5 133	1700	0	UP
End of climb (cruise altitude)		3	10.6	56.1	10000	6761		310	367	2.5	74.3	95	525	4 320	1700	0	UP
Start: Cruise flight in given FL	C	0	10.6	56.1	10000	6761		337	400	0.0	74.3	95	525	4 029	1700	0	UP
Cruise flight in given FL		1	27.5	168.4	10000	6651		337	400	0.0	184.0	95	525	4 029	1700	0	UP
End of cruise flight		2	44.3	280.8	10000	6541		337	400	0.0	293.6	95	525	4 029	1700	0	UP
Start Descent	D	0	44.3	280.8	10000	6541		362	429	-3.0	293.6	95	525	3 729	1700	0	UP
Descent (1/2 Pressure Altitude)		1	52.8	339.7	5000	6486		373	409	-3.0	349.0	95	525	3 911	1700	0	UP
Descent		2	55.6	358.8	3315	6467		376	402	-3.0	368.1	95	525	3 978	1700	0	UP
		3	55.8	360.1	3200	6466		376	401	-3.0	369.5	95	525	3 977	1700	0	UP
Transition from descent to approach		4	56.0	361.2	3100	6465		358	382	-3.0	370.3	20	111	667	1700	0	UP
		5	56.1	362.3	3000	6464		331	352	-3.0	370.8	20	111	768	1700	0	UP
		6	56.3	363.2	2900	6464		311	331	-3.0	371.3	15	83	549	1700	0	UP
		7	56.5	364.1	2800	6463		293	311	-3.0	371.8	10	55	288	1700	0	UP
		8	56.6	365.0	2700	6463		275	292	-3.0	372.3	10	55	335	1700	0	UP
		9	56.8	365.9	2600	6462		261	276	-2.5	372.8	10	55	374	1700	0	UP
Approach FL0 (1.500 ft AGL)	E	0	57.1	366.9	2500	6462		241	254	-2.0	373.4	10	55	392	1700	0	UP
Landing gear extended		1	57.2	367.4	2450	6461		229	242	-2.4	373.7	10	63	447	1950	0	DOWN
Flaps extended - FL18		2	57.3	367.7	2410	6461		223	235	-2.6	373.9	10	63	477	1950	18	DOWN
Approach to Decision Height: 200 ft AGL		3	58.0	370.5	2000	6459		193	202	-2.9	376.4	20	127	1 638	1950	18	DOWN
		4	59.4	375.2	1200	6454		187	194	-2.8	380.9	10	61	627	1870	18	DOWN
Landing flaps extension		5	59.5	375.4	1154	6454		182	188	-2.8	381.1	10	61	644	1870	42	DOWN
Landing from 50 ft AGL	F	1	59.7	376.0	1050	6453		157	162	-2.4	381.7	10	61	682	1870	42	DOWN
Touch-down		2	59.8	376.3	1000	6453		154	159	-0.5	381.8	Idle	-	-	1870	42	DOWN
Ground run (reverse- if it use)		3	60.0	376.5	1000	6453		0	0	0	382.1	Idle	-	-	1870	42	DOWN

Table 1.3 Typical flight profile[6]

1.7.2 Flap – duty cycles

Flaps are loaded predominantly during take-off and landing flight phase, when they are in an extended position. Together with other significant loading conditions, which are repeated flight by flight, so-called flap duty cycles might be determined. The flap duty cycles can be derived from the typical flight profile. Altogether 5 significant states can be determined:

1.	Taxiing	Flaps retracted	$\delta_{FL} = 0°$
2.	Take-off	Flaps deflected	$\delta_{FL} = 18°$
3.	En-route flight	Flaps retracted	$\delta_{FL} = 0°$
4.	Approach	Flaps deflected	$\delta_{FL} = 18°$
5.	Landing	Flaps deflected	$\delta_{FL} = 42°$

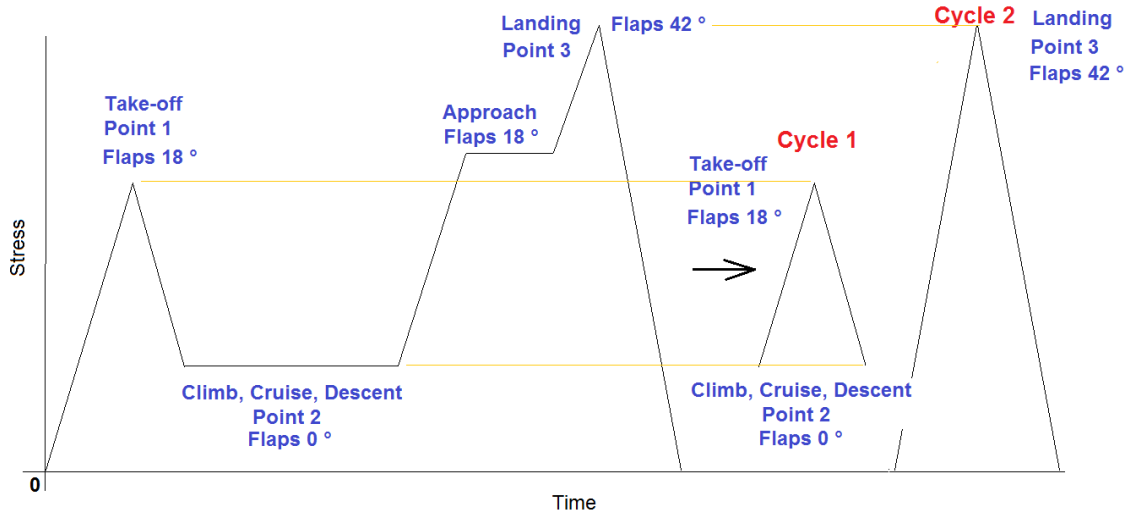

Figure 1.11 Flap-duty cycles [3]

Maximum loading during take-off and minimum loading during cruise flight form the flap-duty cycle n°1. Flap-duty cycle n° 2, which consists of load during landing and ground loading condition, is the main flap-duty cycle.

There can be seen, that the assumption of unloaded flaps on the ground and in cruising configuration will give conservative results, because the loading range of both cycles will be higher than expected in service.

1.7.3 Strain gauge survey

The in-flight strain gauge survey (further in-flight measurement) was performed on L 410 UVP-E20, primarily to gain information about maximal forces acting upon flap's control system. Report [11] contains detailed description of the survey and results summary.

The loading of control rods at the end of the control system was measured. Measured areas correspond to rods n° 1, 2, 6 and 7 in Figure 1.4. These rods were equipped with strain gauges, plugged in a full bridge. The notation of the strain gauges among all other sensors is introduced in Table 1.4.

Terminal rod (SG notation)	Left side	Right side
Inner flap	B53400N (334)	B536401N (356)
Outer flap	B5450062N (338)	B450063N (357)

Table 1.4 – Denotation of strain gauges

Altogether two flights have been carried out to obtain desired data. The entire records, designated as F2202_01 and F2202_02 are displayed in Figure 1.12 and Figure 1.13. Except the flap's control forces, the additional data are provided, including angle of flaps extension, propeller revolutions, IAS, OAT and ALT.

The maximum forces in the flap's control system were obtained during each flight with flaps extended and IAS near its maximum permissible value. Such loading is not important from the fatigue point of view, because it is rarely reached during an ordinary operation. However, apart from these extreme cases, the flight record contains flight phases repeated during any flight. Because the flaps control rods are evidently loaded predominantly when flaps are extended, the following flight phases were extracted (see chapter 1.7.2):

- Take-off
- Approach
- Landing

The take-off flight phase comprises flight segments between points A0 to A2 according to the typical flight profile (Table 1.3) and Figure 1.8.

The approach corresponds to a flight segment, bounded by points E1 and E5. The landing flight phase is assumed as a flight segment lasting from point E5 to F2. It means, that the extracted segment for landing does not cover the loading after touch down.

The detailed description and graphical interpretation of all flight phases extracted from the flight record are attached in the Appendix A.

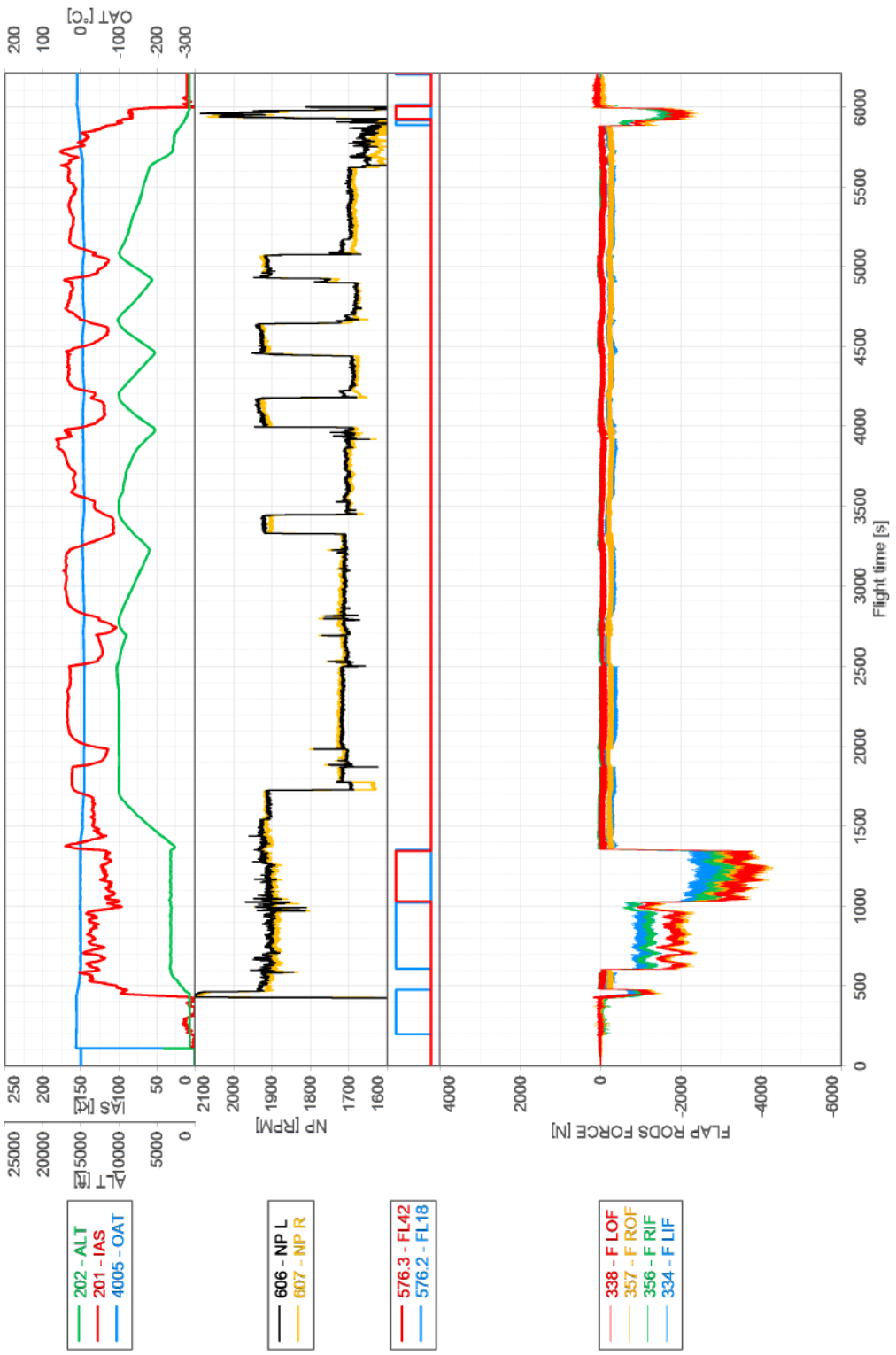

Figure 1.12 – Flight record F2202_01

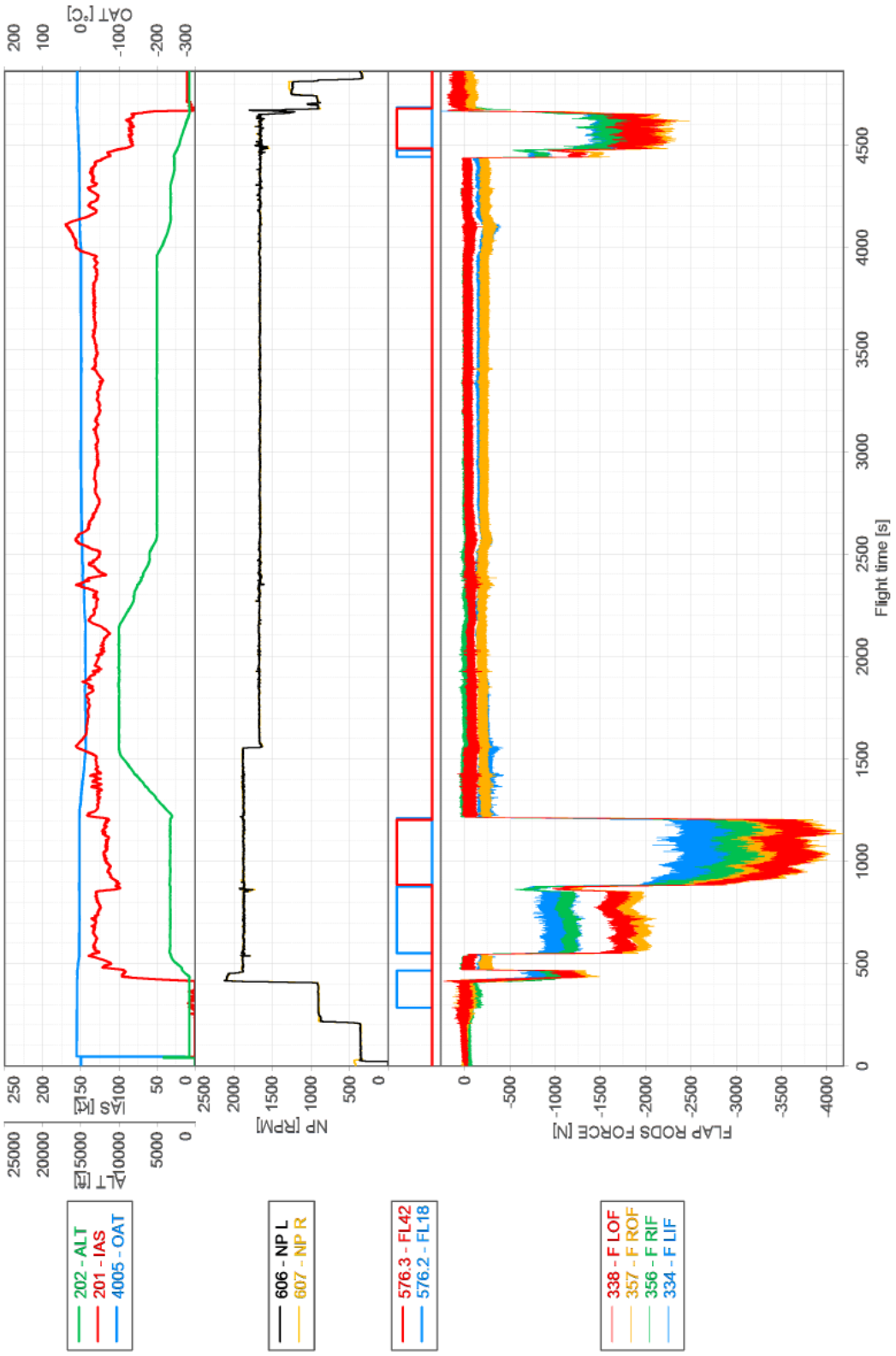

Figure 1.13 – Flight record F2202_02

2 F&DT analysis

To perform F&DT evaluation of any structure, it is necessary to gain appropriate information about loading of the structure, material properties and some presumptions about the state of the structure first time it reaches its operational engagement.

The following chapter defines basic terms related to F&DT analysis. The F&DT approaches corresponding to F&DT evaluation of L 410 NG have been already mentioned in chapter 1.3.

2.1 Basic terms

2.1.1 Stages of fatigue life

Fatigue life until failure of the structure might be divided in line with [20] into altogether two periods, as shown in Figure 2.1.

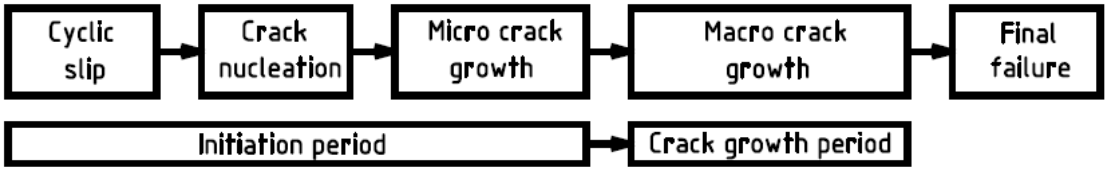

Figure 2.1 – Periods of fatigue life

Fatigue cracks are initiated on a microscopic scale in slip bands, usually very early in the fatigue life. Fatigue is a material surface phenomenon in the crack initiation period. The initiation of the microcrack is affected by surface conditions, as for example roughness or surface corrosion. After some microcrack propagation, more regular crack growth is observed. However, microcrack growth is usually still very slow process due to micro structure effects, as grain boundaries, etc.

In the case of a laboratory specimen, the remaining fatigue life after cracks become visible represents usually only a small percentage of the total life. For real structures however, the latter percentage may be significantly larger. The direction of macrocracks propagation is usually dependent mostly on loading conditions of the structure. Surface conditions have just a negligible effect on macrocrack growth.

As a consequence, the fatigue prediction methods are different for the two periods mentioned in Figure 2.1. The stress concentration factor is an important parameter from the crack initiation point of view. For the crack growth description, concept of stress intensity factor has been established.

Further information about particular stages of fatigue life might be found in [20].

2.1.2 Description of cyclic loading

Cyclic loading is described by a sequence of load/stress cycles. Each load cycle is represented by a change of load between points A and B, as shown on harmonic loading in Figure 2.2. Points A and B are stress levels at which the loading direction is reversed. They are so-called reversal points. Apart from reversals, standard [14] further distinguishes between peaks and valleys.

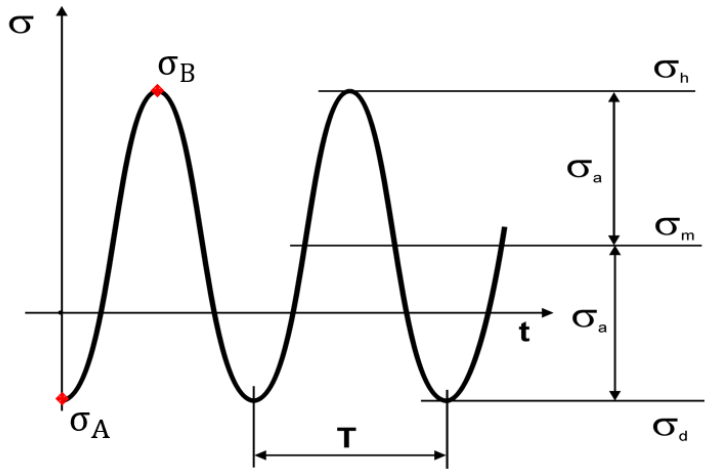

Figure 2.2 Harmonic loading – Description of load cycle

Each stress cycle can be described by the following parameters:

σ_A	Starting stress level
σ_B	Target stress level
$\sigma_h = max\{\sigma_A; \sigma_B\}$	Maximum stress (Upper stress level)
$\sigma_d = min\{\sigma_A; \sigma_B\}$	Minimum stress (Lower stress level)
$\sigma_m = \frac{\sigma_B + \sigma_A}{2} = \frac{\sigma_h + \sigma_d}{2}$	Mean stress
$\sigma_a = \frac{\lvert\sigma_B - \sigma_A\rvert}{2} = \frac{\sigma_h - \sigma_d}{2}$	Stress amplitude
$R = \frac{\sigma_d}{\sigma_h}$	Stress ratio
$\Delta\sigma = \sigma_h - \sigma_d$	Stress range
T	Cycle period
$\omega = \frac{1}{T}$	Cycle frequency

The information about loading of the structure might have a form of load spectra for fatigue analysis or a form of a loading sequence for DT analysis. Contrary to load spectra, loading sequence does not contain only the information about quantity and type of loading acting upon structure, but contains also an information about time sequence of loads.

2.1.3 Fatigue properties of material

The thesis is focused on fatigue analysis using stress-life approach only. Determination of fatigue life using strain-life approach is usually recommended for low-cycle fatigue. This approach is not applied in the thesis.

According to [20], fatigue properties of any material might be described by one of the following methods:

- S-N curve
- Fatigue limit
- Fatigue diagrams

S-N curve

S-N curve is a graphical interpretation of the fatigue durability of specimens, loaded at different stress levels. To obtain the S-N curve, the test specimens are usually loaded by a loading with a constant mean stress or by a loading with a constant stress ratio.

In the case of the constant mean stress loading, the S-N curve represents a relationship between stress amplitude and fatigue durability (number of cycles to failure), as shown below.

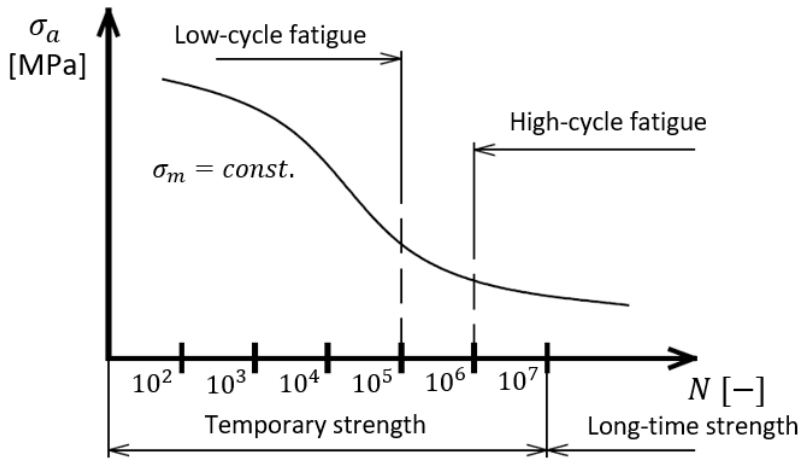

Figure 2.3 S-N curve for a constant mean stress loading [19]

In log-log coordinates, the relationship can be mathematically described by a linear relation, which is known as a Basquin equation [20]:

$$\sigma_a{}^m \cdot N = A$$

Where:

m Slope of an S-N curve

N Number of cycles to failure

A Constant of the S-N curve

Fatigue limit

There has been observed a certain threshold of stress amplitude for which the fatigue durability rapidly increases much above the order of 10^6 cycles, if the specimen is loaded by a constant amplitude loading. When the stress amplitude goes down below this level, it becomes very difficult for microcracks to grow until failure. Such threshold is called a fatigue limit.

However, it can be defined for some materials only, typically for steel. For other materials, as aluminium alloys, it is impractical to establish the concept of fatigue limit. There has not been observed any stress limit below which the fatigue durability would increase such rapidly.

It is necessary to note, that the fatigue limit is a term related to loading by a constant amplitude only. In the case of variable amplitude loading, cycles with amplitudes below the fatigue limit participate on fatigue process leading to failure. To account for the damaging effect of cycles below the fatigue limit, various methods of SN-curve extrapolation are suggested in [20].

One of the methods presumes, that the Basquin equation is valid for the stress amplitudes below the fatigue limit in the same form as for the stress amplitudes above the fatigue limit.

Method suggested by Haibach extrapolates the SN-curve below the fatigue limit by modifying the SN-curve slope from original value m_1 to value m_2, which is applied to amplitudes lying below the fatigue limit:

$$m_2 = 2 \cdot m_1 - 1$$

Fatigue diagrams

S-N curve describes fatigue durability of the specimen loaded by a variable amplitude and a constant mean stress. A higher mean stress will give a lower S-N curve. Principle of fatigue diagram derivation from a series of S-N curves is apparent from Figure 2.4. The lines in a fatigue diagram (also called Goodman or Haigh diagram) represent possible combination of mean stress and its amplitude, which will lead to a given fatigue life. Where possible, the line corresponding to fatigue limit can also be determined.

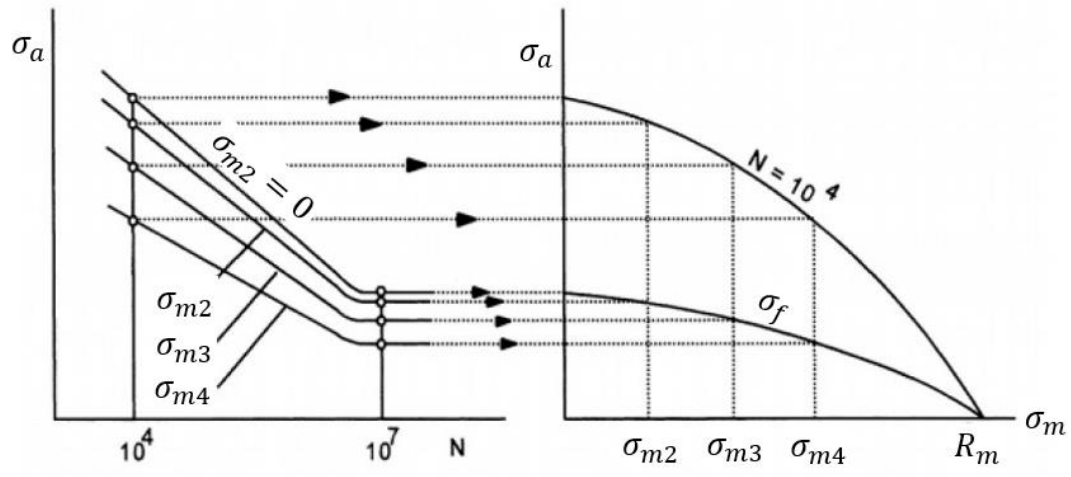

Figure 2.4 – Fatigue diagram [20]

Based on experience, Schijve [20] declares, that the effect of stress amplitude on fatigue is higher than the effect of mean stress. It is in line with a fact, that fatigue failure is primarily a consequence of cyclic loading.

Another way, how to represent the effect of mean stress on fatigue life is offered by a so-called Smith diagram. It is derived for one specific fatigue life, very often for a fatigue limit, or for a fatigue life above 10^6 cycles. It consists of two lines corresponding to minimal and maximal stress in a cycle σ_{min} and σ_{max}. We get the exact combination of σ_{min} and σ_{max} by connecting these two lines vertically, as shows Figure 2.5.

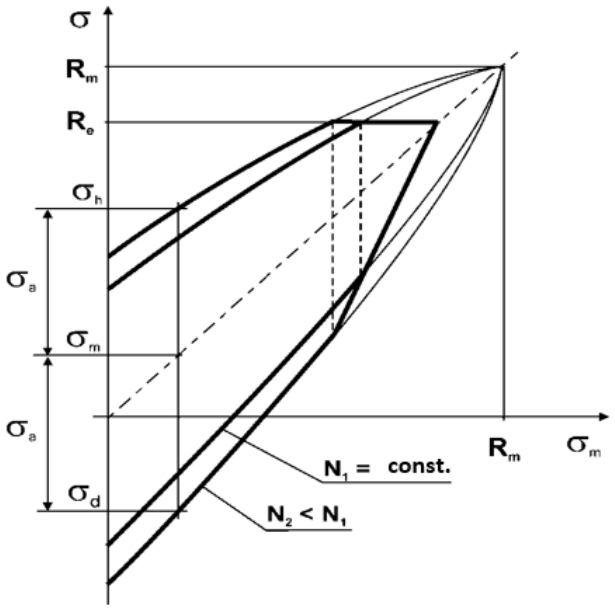

Figure 2.5 – Smith diagram [20]

2.1.4 Mean stress effects

By comparing two variable loadings with the same amplitude and different mean stresses, higher maximum stress in a cycle is present for a higher mean stress. As a result, opening of microcracks is more severe for higher maximum stresses, which will cause shorter fatigue life. The mean stress correction of an S-N curve might be performed by its vertical transformation using one of the following equations:

- Goodman:

$$\sigma_a = \left(1 - \frac{\sigma_m}{R_m}\right) \cdot (\sigma_a)_{\sigma_m=0}$$

- Gerber:

$$\sigma_a = \left[1 - \left(\frac{\sigma_m}{R_m}\right)^2\right] \cdot (\sigma_a)_{\sigma_m=0}$$

- Soderberg:

$$\sigma_a = \left(1 - \frac{\sigma_m}{R_e}\right) \cdot (\sigma_a)_{\sigma_m=0}$$

- Oding:

  a) $\sigma_m \geq 0$

$$\sigma_{h,ekv} = \sqrt{2 \cdot \sigma_a \cdot (\sigma_a + \sigma_m)}$$

  b) $\sigma_m \in \langle 0, -2.857 \cdot \sigma_a \rangle$

$$\sigma_{h,ekv} = \sqrt{2 \cdot \sigma_a{}' \cdot (\sigma_a{}' + |\sigma_m|)}$$

$$\sigma_a{}' = \sigma_a - |0{,}35 \cdot \sigma_m|$$

  c) $\sigma_m < -2.857 \cdot \sigma_a$

$$\sigma_{h,ekv} = 0$$

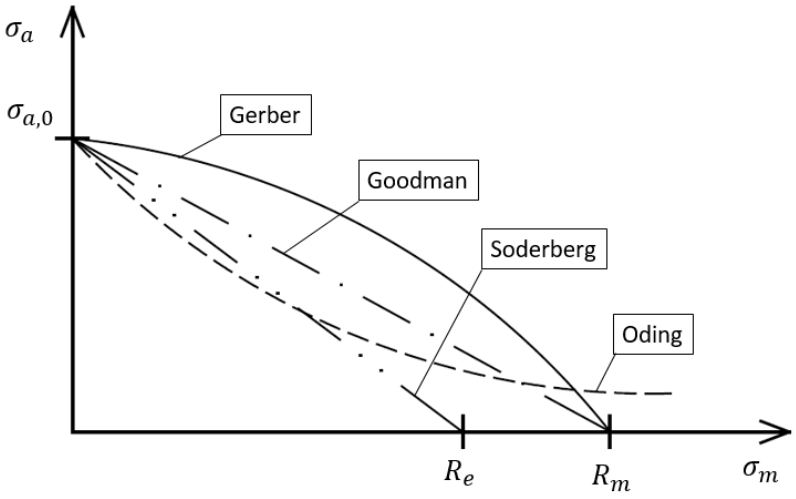

Figure 2.6 – Mean stress correction

Figure 2.6 shows graphical comparison between equations mentioned above for $\sigma_m \geq 0$. All of the relations are often cut above the line $\sigma_{max} > R_e$, which is an area, where macroscopic plastic deformation occurs. Such treatment of a fatigue diagram is shown in Figure 2.7.

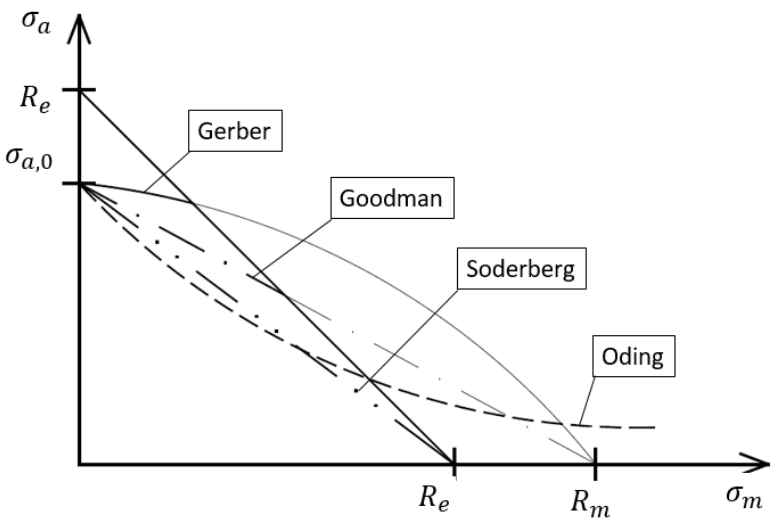

Figure 2.7 – Additional treatment of the mean stress correction

However, as stated in [20], fatigue is rarely a practical problem for a negative mean stress, due to crack closing under compression. The negative part of the cycle may be expected as non-damaging. Reversed loading is significant in view of reversed plasticity in the area of a crack tip, but crack opening is still necessary for crack extension and also for reversed plasticity in the crack tip plastic zone. Amplitude required for a crack opening is much larger for negative mean stress.

Therefore, the Oding's mean stress correction might be modified into the following form, which does not count cycles with $\sigma_{max} < 0$ as damaging:

a) $\sigma_m \geq 0$

$$\sigma_{h,ekv} = \sqrt{2 \cdot \sigma_a \cdot (\sigma_a + \sigma_m)}$$

b) $(\sigma_m < 0) \cap (\sigma_m + \sigma_a \geq 0)$

$$\sigma_{h,ekv} = (\sigma_a + 0.2 \cdot \sigma_m) \cdot \sqrt{2}$$

c) $\sigma_m + \sigma_a < 0$

$$\sigma_{h,ekv} = 0$$

2.2 Cumulative damage hypothesis

To obtain an S-N curve, fatigue test specimen is loaded by a constant amplitude loading, as was already described earlier. Contrary to that, the service operation of real structural parts covers variable loading conditions. The cumulative damage hypothesis was therefore introduced to account for the effects of loading variability. During variable loading of the test specimen, each load cycle reduces the fatigue resistance of the specimen accordingly its amplitude and mean stress.

The fatigue damage D caused by n cycles of a particular stress level with constant σ_m, σ_a is defined in [20] as follows:

$$D = \left(\frac{n}{N}\right)^m$$

Where:

$m = 1$	Linear damage accumulation (Palmgren-Miner Rule)
$m \neq 1$	Non-linear damage accumulation
$D = 0$	Initial stage of specimen loading
$D = 1$	Failure of the specimen
N	Number of cycles to failure (Fatigue life endurance)

The failure caused by a variable loading consisting of p different load levels occurs, when the accumulated fatigue damage reaches its limit value:

$$D = \sum_{i=1}^{p} D_i = 1$$

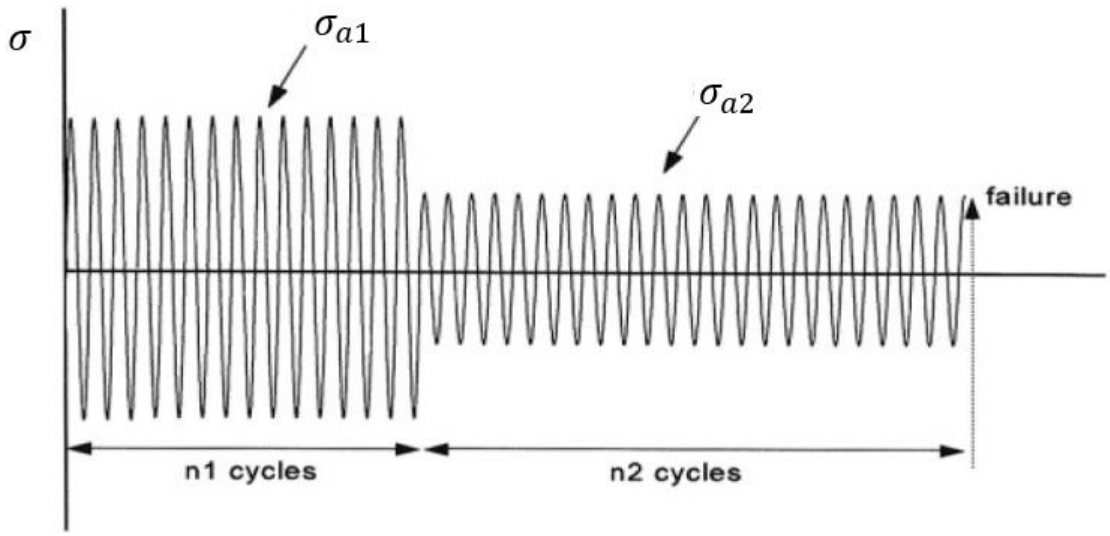

Figure 2.8 – Two blocks of constant amplitude loading [20]

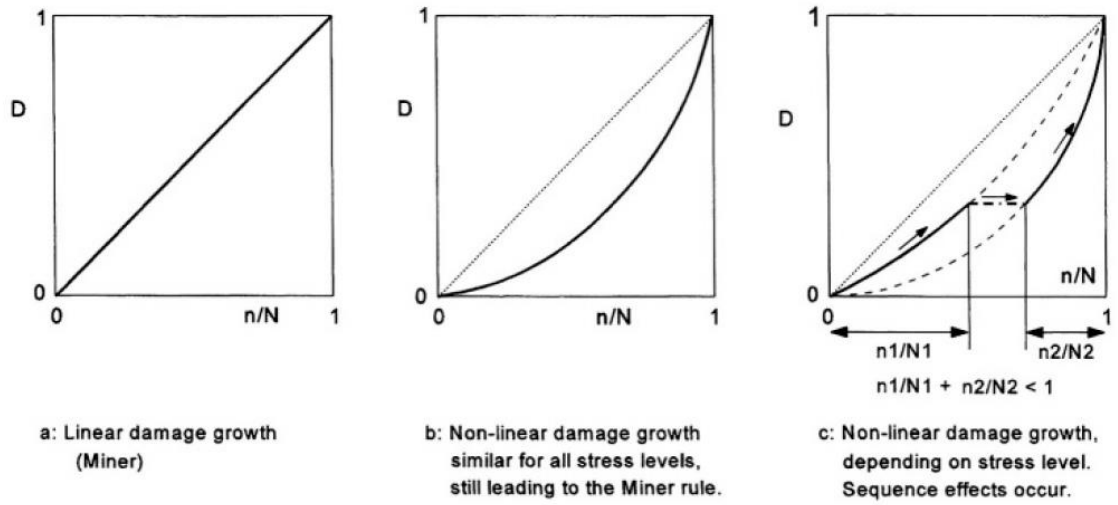

Figure 2.9 – Comparison between damage accumulation theories [20]

According to [20], the basic shortcoming of the Miner-rule is the fact, that cumulative fatigue damage is a function of one parameter only, which integrates from zero to unity.

The process of the crack growth (fatigue damage accumulation) is much more complicated, than predicted by the Miner-rule and many other methods. It includes repeated crack tip plasticity, local strain hardening in the crack tip zone, residual stresses around the crack tip, and for notched elements also macro plasticity in the root of the notch. It implies, that the fatigue damage increment depends on the material fatigue condition, caused by the previous cycles. These effects are called interaction effects.

Another problem related to the use of Miner-rule is the assumption, that S-N curve is a curve of a constant fatigue damage. This isn't unfortunately a real assumption, because the crack length at failure depends on the maximal stress σ_h of the last cycle. This shortcoming of the Miner-rule may not be so serious, if the fatigue life spent in the macro-crack growth period was relatively short.

One of the ways, that was suggested to deal with the sequence effects within fatigue life prediction models, was to define an exponent m in the definition of fatigue damage as a function of the load level. It was believed, that such description might cover the sequence effects correctly.

The idea is presented in the Figure 2.9. There is displayed, how different damage accumulation methods deals with a simple VA loading consisting of two blocks of CA cycles from Figure 2.8. Using non-linear damage accumulation method with variable exponent m, the damage parameter increases along the upper curve during the first block and along the lower curve during the second block of CA cycles. Transition to another damage curve causes, that the sum of the two contributions $\left(\frac{n_i}{N_i}\right)^{m_i}$ is smaller than 1. At the same time, the reversed order of the two blocks would lead to the sum greater than 1.

However, according to [20], models with such a non-linearly increasing single damage parameter have not led to an improved Miner-rule giving reliable predictions with a general validity. The problem is still the use of a single damage parameter, which is in conflict with the up to date understanding of fatigue damage. Therefore, the shortcomings of the Miner-rule are not removed by assuming a non-linear damage function.

Although it is not possible to describe the fatigue process by a single damage parameter correctly, due to its simplicity, the Miner-Rule is still the most common way, how to deal with fatigue analysis of the structural element subjected to a variable loading in the sense of determination of its fatigue life.

2.3 Crack growth prediction

Fatigue life prediction might be replaced by a crack growth prediction, if we assume, that the initial stages of the fatigue life corresponding to initiation of macrocracks, as defined in chapter 2.1.1, are negligible. As an initial flaw is supposed to be a small defect, typically a surface damage created during a manufacturing process. Crack growth is then predicted using methods of linear fracture mechanics. Methods of linear fracture mechnics are already applicable for rather small cracks.

Crack growth predictions form an essential part of the damage tolerance analysis of the L410 NG structure. Crack propagation curves, validated by the test evidence are used for planning the maintenance procedures, especially for determination of the inspection threshold and the interval between two adjacent inspections.

A flaw of any length is a source of a stress concentration at the crack tip within the structural element of any geometry. Each crack might be loaded in the so-called **opening modes**, as shown in Figure 2.10. The most important way of loading from the practical point of view is represented by the tensile opening (Mode I).

Mode I - Tensile opening

Mode II - In-plane shear

Mode III - Anti-plane shear

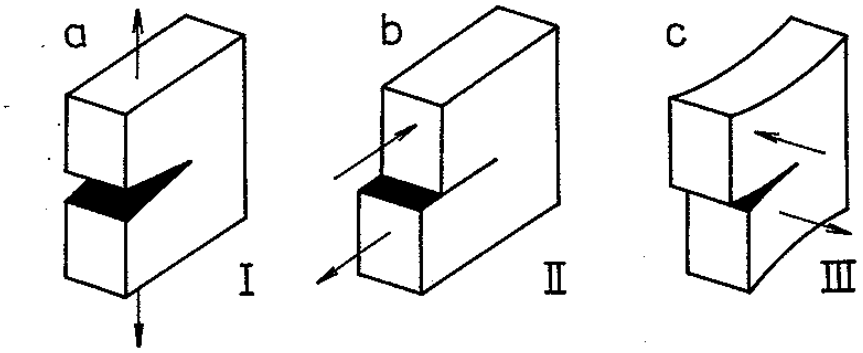

Figure 2.10 – Crack opening modes [25]

According to theoretical predictions, the stress reaches an infinite value in the vicinity of the crack tip. Therefore, it is impossible to describe the vicinity of the crack tip by the use of a stress concentration factor, which is usually defined for a notch of a particular shape, loaded by specific conditions. The most widely used instrument for a description of the stress field at the crack tip area is the stress intensity factor K, which accounts for type and magnitude of applied load as well as geometric arrangement.

The stress intensity factor is usually presented in the following form for Mode I:

$$K_I = \beta \cdot \sigma \cdot \sqrt{\pi \cdot a}$$

where:

σ nominal stress in the area unaffected by the crack occurrence

a crack length

β shape function

The shape function β (also called correction factor or simply β-function) accounts for the geometric arrangement, type of loading etc.

Theoretical approach assuming an infinitely high stress magnitude at the crack tip is not acceptable for a real material. For a real material, the yield strength is exceeded and a plastic zone of a particular size is created at the crack tip area. The primary plastic zone is followed by a reverse (secondary) plastic zone, which occurs as soon as the object is unloaded again. The reverse plastic zone is represented by residual compression stress field at the crack tip, which causes closing of the crack.

The crack propagation under CA loading might be characterized by $\frac{da}{dN} = f(\Delta K)$ relation, depicted in the Figure 2.11. The curve represents crack length increment per cycle as a function of the stress intensity factor range ΔK, defined by:

$$\Delta K = K_{max} - K_{min}$$

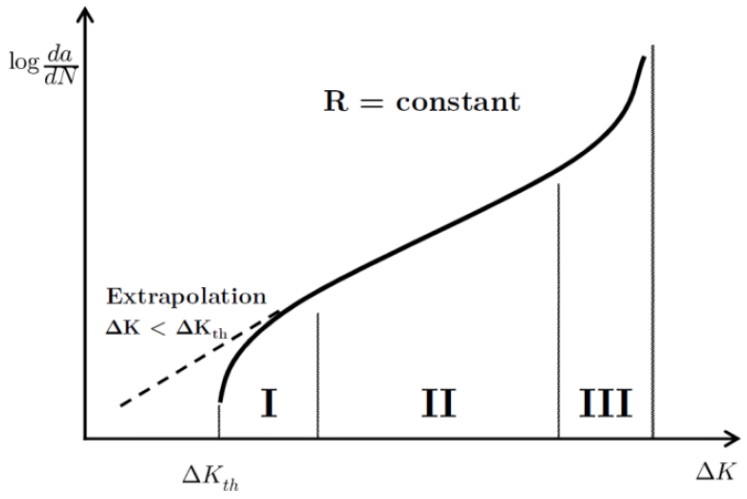

Figure 2.11 – Typical shape of $\frac{da}{dN} = f(\Delta K)$ curve [25]

The typical curve can be divided into three regions:

I) **The Threshold region** – might be represented by the threshold value ΔK_{th} valid for a macro-crack only, which implies, that macro-crack won't grow due to stress intensity factor lower than the threshold value. However, such assumption is valid for a constant amplitude loading only. In the case of variable amplitude loading, even cycles providing ranges of stress intensity factor below the threshold value participate on a crack propagation. Therefore, an extrapolation of the Paris region below the threshold value is made to account for the damaging effect of cycles with relatively low amplitudes.

II) **The Paris region** – corresponds to the stable growth of a macro-crack

III) **The stable tearing crack growth** – the crack growth rate in this region is high, its magnitude is approximately of order $10^{-5}\ m/cycle$ according to [25]

Various equations describing crack growth in regions discussed above were developed. They might be found for example in [20] or [25].

As stated in [25], due to a reverse plastic zone and the corresponding compressive stress field at the crack tip, the crack closure is induced in the lower part of the load cycle. As a result, the crack tip is being opened only during a part of the load cycle. Based on this fact, the effective stress range $\Delta\sigma_{eff}$ and corresponding effective stress intensity factor range ΔK_{eff} were defined:

$$\Delta K_{eff} = K_{max} - K_{op}$$

The value of ΔK_{eff} is usually defined by a semi-empirical approach with the use of the function $U = f(R)$:

$$\Delta K_{\mathrm{eff}} = U \cdot \Delta K$$

With the knowledge of the closure effect, the description of the crack propagation under CA loading becomes a little bit complicated, as described above.

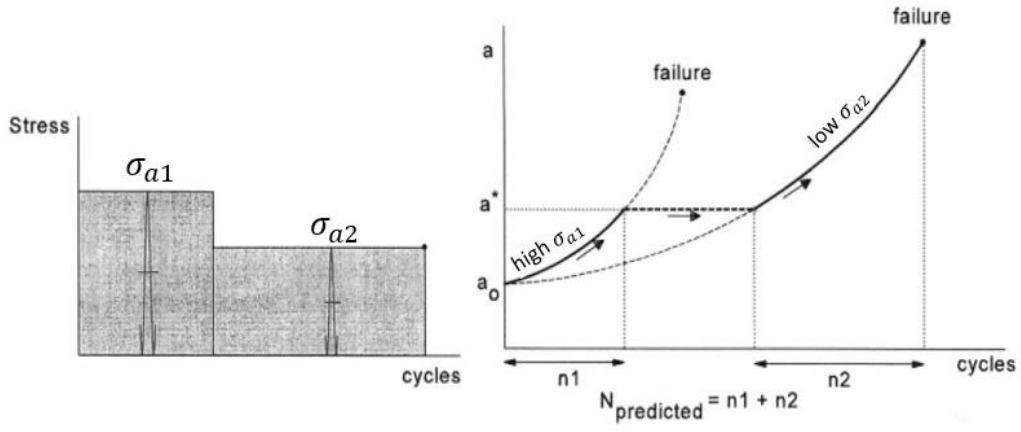

Figure 2.12 – Non-interaction fatigue crack growth in a 2-block VA test [20]

The situation is then even magnified for VA loading. Schijve compares in [20] the crack propagation without assuming the interaction effects with the test results obtained on 2024-T3 Al-alloy specimens under a 2-block VA loading.

The crack growth prediction based on the presumption, that previous loads do not affect the crack growth caused by the current cycle, is shown in Figure 2.12.

However, the test evidence has shown that the crack growth in the second block is affected by the crack growth in the first block. After the reduction of stress amplitude from 54 MPa to 24 MPa, a crack growth retardation during a crack length increment of 1 to 3 mm occurred. After a retardation period, the crack growth curves became parallel to the original crack growth curves again, obtained without assuming the interaction effects. The situation is displayed in Figure 2.13.

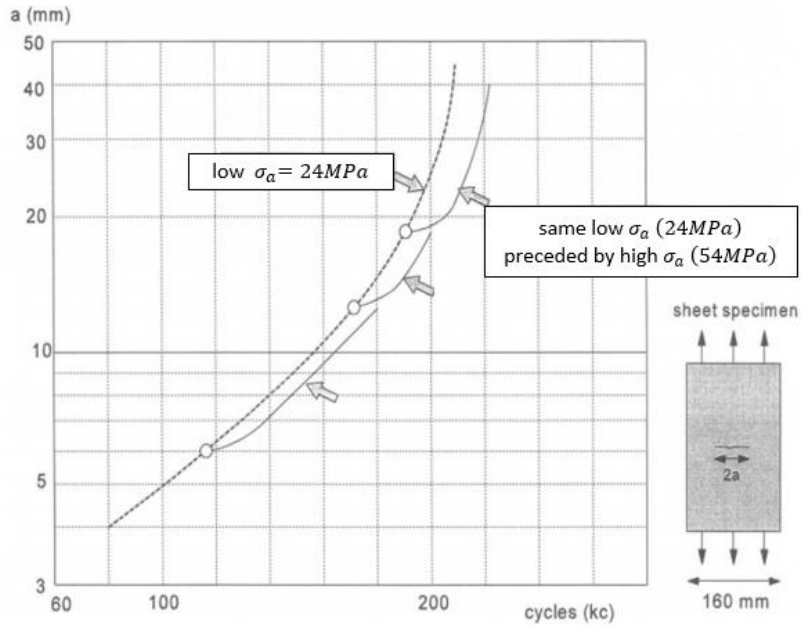

Figure 2.13 – Results of the crack growth tests on specimens made of 2024-T3 Al-alloy [20]

As a result, it might be noted, that the load interaction is an important issue affecting the crack propagation. In the case of structural elements subjected to variable loading with peaks separated by a relatively moderate loading, it is sufficient to include the interaction effects to the crack growth predictions without any doubts. On the other hand, such structural element, as for example pressurized cabin, which is loaded predominantly by pressurization, will not be strongly affected by the interaction effects.

The crack growth prediction under VA loading comprises several steps, which are schematically ordered in the Figure 2.14:

- Stress analysis in order to obtain shape function β
- Calculation of the stress range $\Delta\sigma$
- Computation of the stress intensity factor range (or its effective value) ΔK (ΔK_{eff})
- Determination of the crack growth increment per applied cycle $\frac{da}{dN}$
- Adding the increment to the crack growth curve $a = f(N)$

The paradox of this approach is the use of material data obtained under CA tests for prediction of the crack growth propagation under VA loading. However, this procedure is widely accepted in practice.

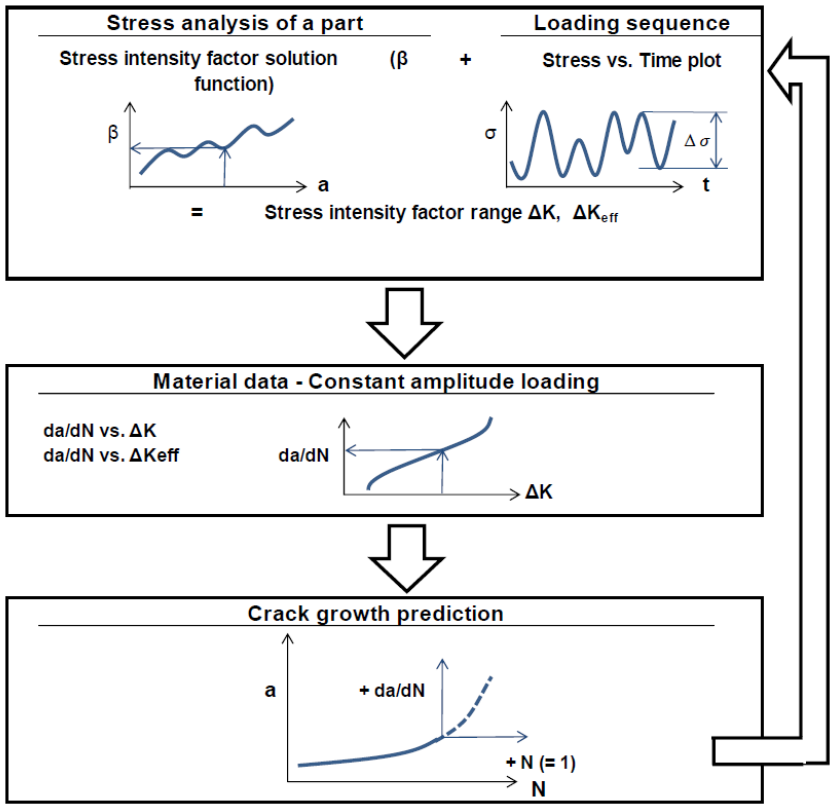

Figure 2.14 – Solution of the crack growth under VA loading [25]

2.4 AFGROW loading sequence

AFGROW software is used by AI to analyse fatigue crack growth and fracture of metallic structures. AFGROW is a Damage Tolerance Analysis framework, which was originally developed by The Air Force Research Laboratory and now it is developed and maintained by LexTech, Inc.

The software contains classic stress intensity factor library providing solutions for over 30 different crack geometries/loading conditions. It also implements five different crack growth rate models to determine crack growth per applied load cycle.

The spectrum of loads is loaded into an AFGROW via the spectrum dialog. The user is supposed to specify the Stress Multiplication Factor of the loaded spectrum and limit stress for Residual Strength calculation, denoted as Residual Stress Strength Requirement.

Stress multiplication factor (SMF) [27]

"Each maximum and minimum value in the user input stress spectrum is multiplied by SMF. This allows the user to input spectra, which are normalized and simply use one factor to predict the life for different stress levels."

Residual Stress Strength Requirement (Pxx) [27]

"Pxx is simply the value of stress (or load for models using load instead of stress input), which the structure must be able to carry at all crack sizes. This value is not multiplied by SMF. It is very useful for cases in which the user does not know when the maximum stress (or load) will occur and wishes to check for failure at all times for this condition. If the user set this value to zero (default), failure will occur based on the current applied stress (or load)."

AFGROW offers an opportunity of defining constant amplitude loading, or creating a new spectrum file using the Spectrum wizard, that guides the user throughout the process of spectrum generation.

To specify any spectrum for AFGROW, at least two files are required. The first file is called a Spectrum Information File. Its name is in a form of [filename].sp3. The subsequent file(s) contain the actual spectrum data. In line with [27], when generating spectrum via Spectrum wizard, the filename convention is [filenameXX].sub, where XX is a two digit file number (from 01 to 99). When importing an already complete spectrum file, it is possible to load an unlimited number of sub-spectra.

The Spectrum Information File (ASCII text file) of the form [filename].sp3 is constructed as follows:

[title]

[sub-spectrum label] (i.e. Flight, Block, Hour, etc.)

[type of spectrum] (Either BLOCKED or CYCLExCYCLE)

[number of files to follow]

The subsequent files associated with the spectrum contain information about the actual stress (or load). If the spectrum is specified as CYCLExCYCLE, then there might not be specified more than one cycle for any stress (or load) level. The spectrum is supposed to be cycle-counted.

The spectrum data files (ASCII text files) are named [filename01].sub, [filename02].sub, …, etc. Each of these files is constructed as follows:

[Sub-spectrum number] [number of levels]

[max] [min] [cycle]

… … …

… … …

Note that if two files are specified in the [filename].sp3 file, there must be a [filename02].sub file. The maximum and minimum values are floating point values and the cycles are expressed as integer values only.

3 DATA PROCESSING

The following chapter describes techniques which will be used for determination of vibration effects on the fatigue damage of flaps and flaps control system, caused by an aircraft operation.

First of all, various types of processes and sampling frequency suitable for their measurement are defined. Main part of the chapter describes specific techniques of data processing in detail:

- The purpose of **data filtration** is to get rid of the noise induced by a sensor and to reduce the volume of data. Chapter 3.4 describes the basic principles of an amplitude filtration based on a 4-point algorithm.
- Loading cycles might be detected and counted by various **cycle counting** methods. The method used for determination of vibrations effect on fatigue life of flaps is mentioned in chapter 3.5.
- **Loading history** of user-defined length is reconstructed, enabling a normalization of the flight duration. Chapter 3.6 provides detailed description of the load reconstruction method applied in the proposed methodology.
- Random processes might be characterized by a PDF. The PDF of detected cycles is estimated using one of **non-parametric estimation methods**. This method is described in the chapter 3.7.

3.1 Classification of variable loading

Variable loading as a general process might be divided into classes according to [13] as shown in Figure 3.1.

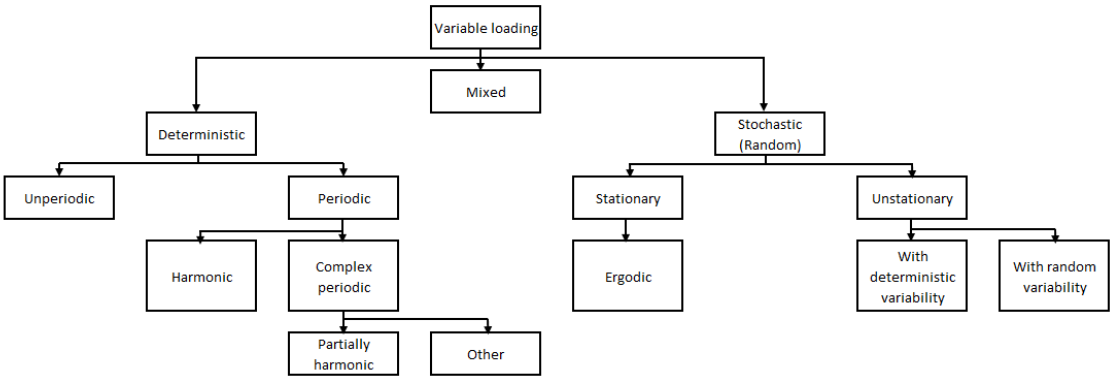

Figure 3.1 – Classification of variable loading

3.2 Sampling frequency

It is convenient not to record data continuously in time, but to sample any measurement of load-time history with proper sampling frequency. It means, that only values in specific moments, separated by a gap with constant width (sampling period), will be recorded, as shown in Figure 3.2.

T_v Sampling period

$\omega_v = \frac{1}{T_v}$ Sampling frequency

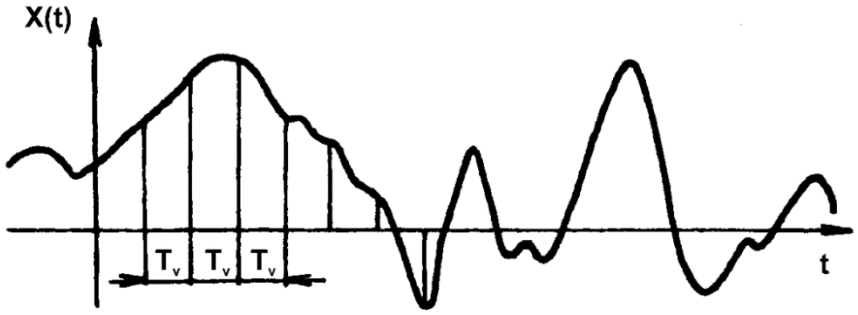

Figure 3.2 – Data sampling

It is necessary to choose sampling frequency to be greater than a maximum frequency of any process ω_{max}, which is desired to be measured. Minimum permissible Nyquist sampling frequency is equal to $\omega_{NGT} = 2 \cdot \omega_{max}$. When the characteristics of local extremes are desired, it is recommended to choose frequency as follows, according to [13]:

$$\omega_v \geq 10 \cdot \omega_{max}$$

It is presumed, that vibrations on flaps and flaps control system are caused by propeller slipstream. As stated in chapter 1.6, each pass of one of the propeller blades causes an increase of dynamic pressure. Such increase might be presumed as a source of flap's buffeting. Therefore, the minimal and recommended sampling frequencies might be derived from maximum propeller revolutions per minute n_{max} and number of blades z:

$$\omega_{max} = \frac{n_{max} \cdot z}{60} = \frac{2080 \cdot 5}{60} = 173\ Hz$$

$$\omega_{NGT} = 2 \cdot \omega_{max} = 346\ Hz$$

$$\omega_{vmin} = 10 \cdot \omega_{max} = 1730\ Hz$$

3.3 Random process

It has been already mentioned without further justification, that vibration loading might be assumed as a random process. The state of such process can't be determined in any time. However, its behaviour can be described statistically, as for example by the probability density function.

3.3.1 Definition of a random process

- Random sample time history [12]:

"A system produces a certain response under excitation. If the excitation or the response motion $X(t)$ is unpredictable, the system is in random vibration, because the exact value of $X(t)$ cannot be precisely predicted in advance. It can only be described probabilistically."

- Random process [12]:

Random process is any process comprised of an infinite number of sample time histories $X_1(t)$, $X_2(t)$, $X_3(t)$, … Each time history is represented by a separate experiment.

Figure 3.3 shows random process defined by an ensemble of load-time histories.

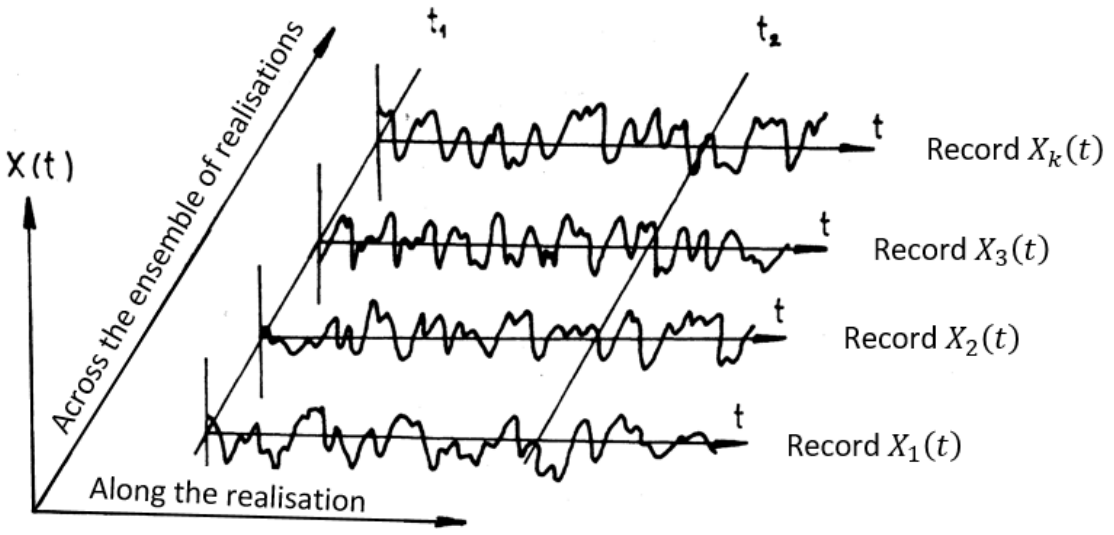

Figure 3.3 – Ensemble of time histories creating a random process [13]

3.3.2 Statistical characteristics of a random process

It is distinguished between characteristics of the first and the second order according to [13]. When only one section of a process $X(t)$ in a random time t is assumed, the following characteristics can be defined:

- Distribution function :

$$F(x,t) = P[X(t) \leq x]$$

- Probability density function :

$$f(x,t) = \frac{dF(x,t)}{dx} = P[x < X(t) \leq x + dx]$$

- Mean value:

$$\mu(t) = \int_{-\infty}^{\infty} f(x,t) \cdot dx$$

- Variance:

$$\sigma^2(t) = \int_{-\infty}^{\infty} [x - \mu(t)]^2 \cdot f(x,t) \cdot dx$$

Characteristics of the second order correspond to two different sections of a process in random times t_1 and t_2:

- Two-dimensional distribution function:

$$F(x_1, x_2, t_1, t_2) = P[\mathrm{X}(t_1) \leq x_1, X(t_2) \leq x_2]$$

- Two-dimensional probability density function:

$$f(x_1, x_2, t_1, t_2) = \frac{\partial^2 F(x_1, x_2, t_1, t_2)}{\partial x_1 \cdot \partial x_2}$$

- Auto-correlation function:

It describes a correlation between two values of a random process in two different times, which indicates a speed of change of the process.

$$R(t_1, t_2) = \int_{-\infty}^{\infty} \int_{-\infty}^{\infty} x_1 \cdot x_2 \cdot f(x_1, x_2, t_1, t_2) \cdot dx_1 \cdot dx_2$$

Characteristics of the first and second order will be used for proper definition of the basic types of random processes discussed in the following chapter.

3.3.3 Basic types of random processes

- Gaussian process [12]:

The process $X(t)$ is called Gaussian if its PDF $f(x)$ follows a bell-shape distribution (also called normal distribution), given by the following equation:

$$f(x) = \frac{1}{\sigma_X \cdot \sqrt{2\pi}} \cdot exp\left[-\frac{1}{2} \cdot \left(\frac{x - \mu_X}{\sigma_X}\right)^2\right] \; for \; x \in (-\infty; \infty)$$

Where:

μ_X mean value of the process $X(t)$

σ_X standard deviation of the process $X(t)$

- Gaussian random process [12]:

The ensemble of probability densities at each time instant and at any two time units must be gaussian for a gaussian random process.

- Stationary random process [13]:

Characteristics of the first order are time invariant for a stationary random process. It means that the probability distribution for the ensemble remain the same (stationary) for each time instant.

The difference between stationary and non-stationary random process can be seen by comparing Figure 3.4 and Figure 3.5.

.

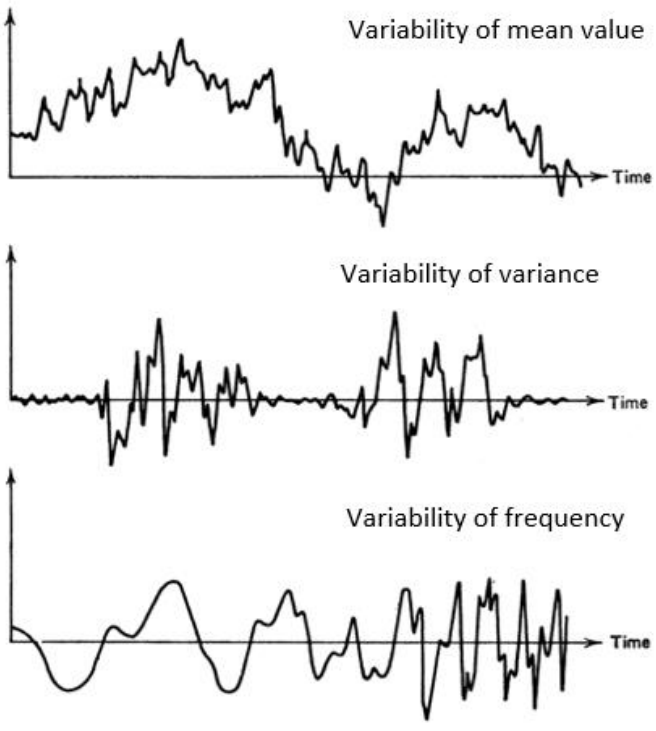

Figure 3.4 – Non-stationary random processes [13]

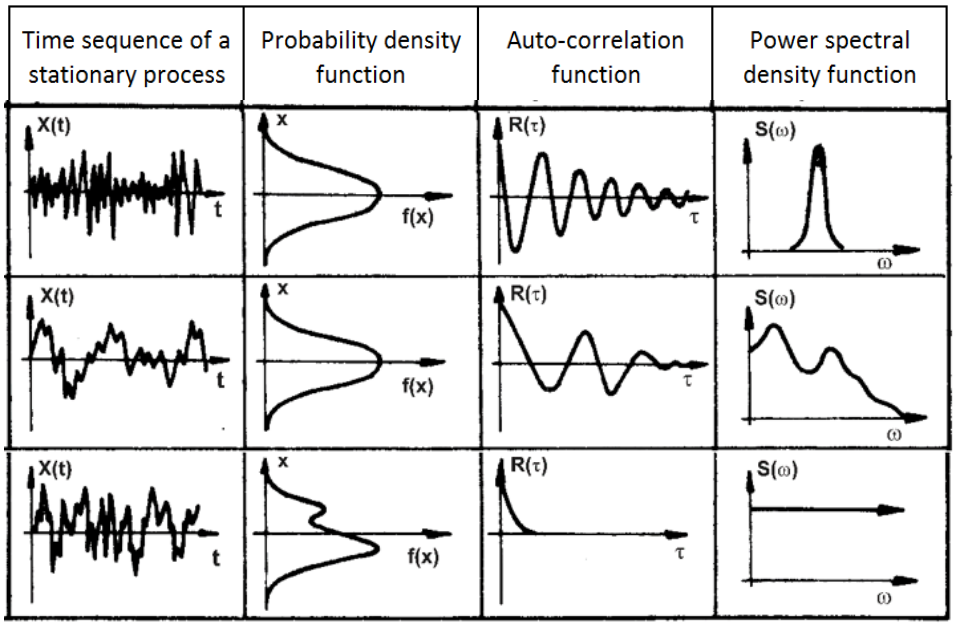

Figure 3.5 – Stationary random processes [13]

- Ergodic process [12]:

„A stationary process is called ergodic if the statistical properties along any single sample are the same as properties taken across the ensemble.“

Therefore, characteristics of an ergodic process might be replaced by the characteristics calculated along any of its samples.

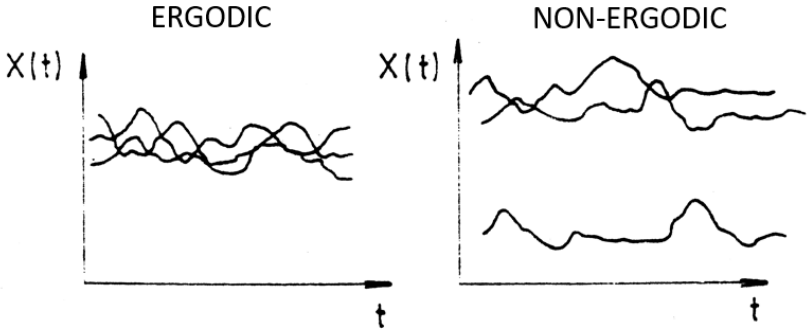

Figure 3.6 – Difference between an ergodic and a non-ergodic process [13]

3.4Data filtration

Raw data might contain a noise produced by the sensor which was used for the measurement. Sometimes, it might be also beneficial to eliminate cycles with stress ranges which are too small to produce fatigue damage of similar severity to fatigue damage produced by other loading cycles in the sequence.

Therefore, the purpose of the filter is to remove cycles with load range R less than significant value for fatigue R_{min}. Appropriate value of R_{min} must be established prior to data filtering.

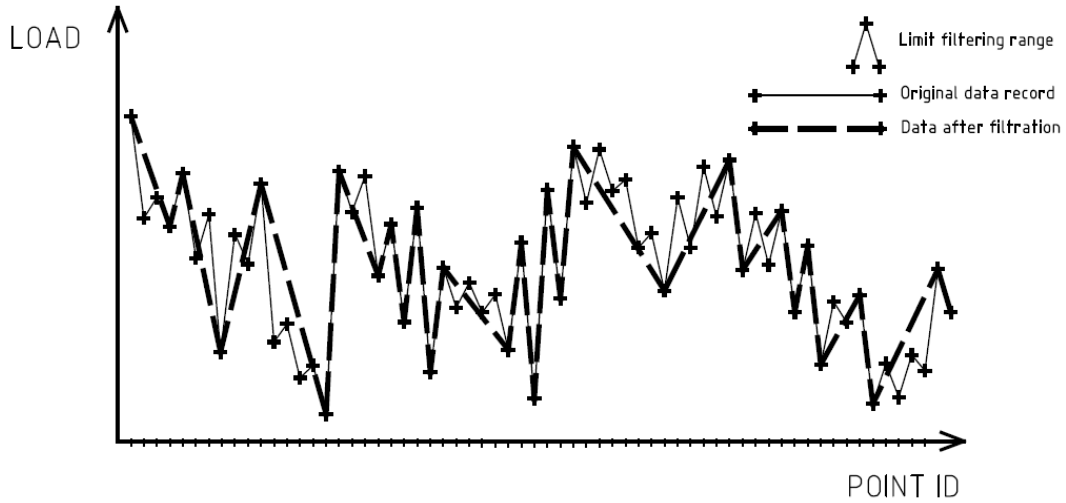

Figure 3.7 Rain-flow filtering

Figure 3.7 displays the rain-flow filtering of a sequence of peaks detected in a time record of load.

Procedure consists of two steps. Peaks are found and data between peaks are extracted from the signal in the first step. Second step is based on ASTM 4-point algorithm, mentioned also in [21]:

1. For any set of 4 consecutive turning (reversal) points compute the three corresponding ranges (absolute values)
2. If the middle range is smaller than the checked minimum value R_{min} and both outer ranges, extract a cycle of that range from the signal.
3. Repeat step 1-3 until no cycle can be removed from the signal.

3.5Cycle counting methods

Standard [14] defines acceptable procedures for cycle-counting methods employed in fatigue analysis. Basic parameters of cyclic loading are displayed in Figure 2.2 and Figure 3.8. Detailed description of any term might be found in [14].

Cycle counting methods are used to summarize irregular load-time histories by counting quantity of particular cycle's occurrence in the history. Although the definition of cycle might vary with the cycle counting method, the definition of cycle parameters defined in the previous chapters is of general applicability.

Procedures of cycle counting might be divided into one-parameter and two-parameter procedures. One-parameter methods provide the analyst with one-parametric information about the cycle, for example number of cycles with its peak in selected interval or number of cycles with its range of selected magnitude.

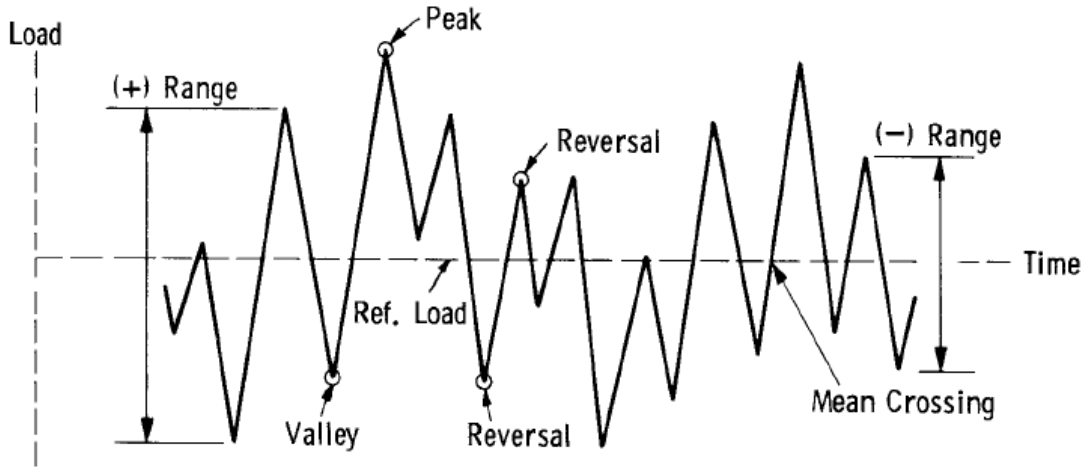

Figure 3.8 – Basic parameters of cyclic loading [14]

Two-parameter methods register not only range of a cycle, but also its mean value. The results of such procedures might be presented in a form of range-mean matrix, from-to matrix or other relevant forms.

- One-parameter procedures:
  - Level-crossing counting
  - Peak counting
  - Simple-range counting
- Two-parameter procedures:
  - Range-pair counting
  - Rain-flow counting
  - Simplified rain-flow counting for repeating histories

Further in the text only two-parameter procedures will be described with a scope on the rain-flow counting and the simplified rain-flow counting and the difference between them.

Rain-flow counting method [14]:

Rules for this method are as follows:

"Let X denote range under consideration; Y previous range adjacent to X; and S starting point in the history.

(1) Read next peak or valley. If out of data, go to Step 6.

(2) If there are less than three points, go to Step 1. Form ranges X and Y using the three most recent peaks and valleys, that have not been discarded.

(3) Compare the absolute values of ranges X and Y.

(a) If X < Y, go to Step 1.

(b) If X ≥ Y, go to Step 4.

(4) If range Y contains the starting point S, go to Step 5; otherwise, count range Y as one cycle; discard the peak and valley of Y; and go to Step 2.

(5) Count range Y as one-half cycle; discard the first point (peak or valley) in range Y; move the starting point to the second point in range Y; and go to Step 2.

(6) Count each range that has not been previously counted as one-half cycle."

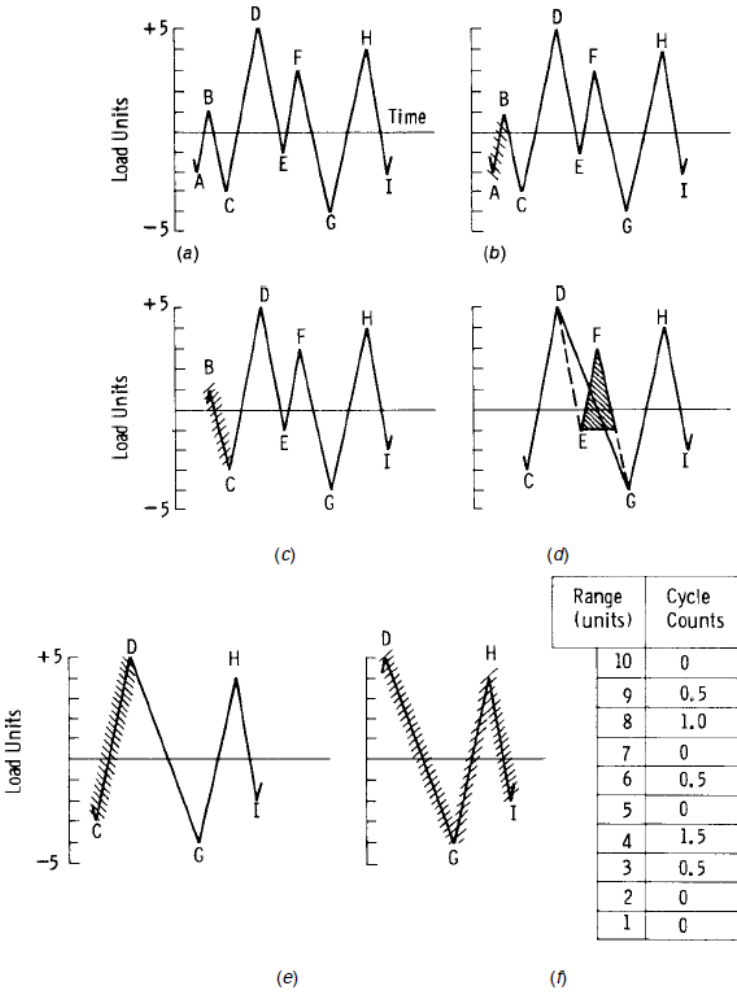

Range (units)	Cycle Counts	Events
10	0	
9	0.5	D-G
8	1.0	C-D, G-H
7	0	
6	0.5	H-I
5	0	
4	1.5	B-C, E-F
3	0.5	A-B
2	0	
1	0	

Figure 3.9 – Rainflow counting example [14]

Simplified rainflow counting method [14]:

Rules for obtaining cycle count, called “simplified rainflow counting for repeating histories” are the following:

„Let X denote range under consideration; and Y previous range adjacent to X.

(1) Arrange the history to start with either the maximum peak or the minimum valley.

(2) Read the next peak or valley. If out of data, STOP.

(3) If there are less than three points, go to Step 2. Form ranges X and Y using the three most recent peaks and valleys that have not been discarded.

(4) Compare the absolute values of ranges X and Y.

(a) If X < Y, go to Step 2.

(b) If X ≥ Y, go to Step 5.

(5) Count range Y as one cycle; discard the peak and valley of Y; and go to Step 3.“

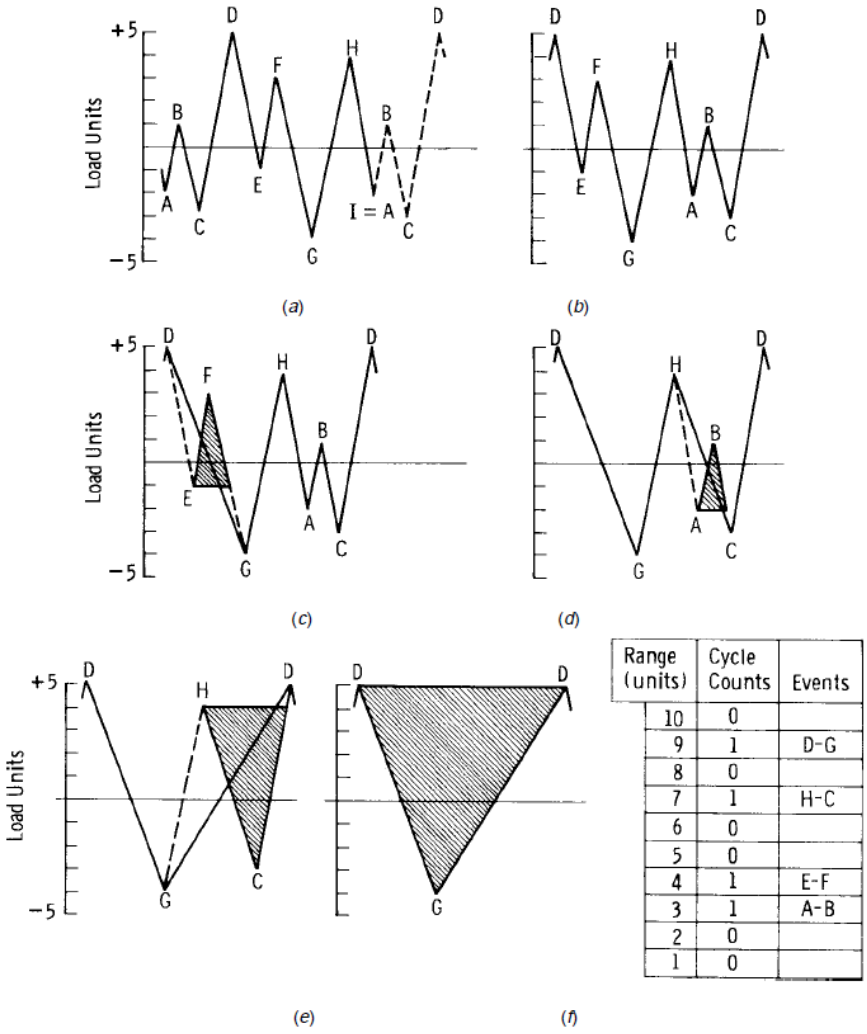

Range (units)	Cycle Counts	Events
10	0	
9	1	D-G
8	0	
7	1	H-C
6	0	
5	0	
4	1	E-F
3	1	A-B
2	0	
1	0	

Figure 3.10 – Simplified rain-flow counting example [14]

The simplified rain-flow counting method was developed specifically for repeating load histories. By the time when the maximum peak or valley is reached for the first time, the resulting loading sequence produced by this method is the same as loading sequence produced by the rain-flow counting procedure. Sequence of such a repeating history does not contain any half cycles, only full cycles.

In the case, that the analysed load-history isn't repeated "all round", the sequences produced by the methods mentioned above might differ. The significance of the difference depends on the history length, which is analysed.

3.6 Fatigue loading history reconstruction

Sometimes, it might be beneficial to reconstruct a loading history after data processing using one of the cycle counting procedures mentioned above. Such reconstruction methods can be found in [15]. Altogether three methods based on rain-flow cycle counting matrix are presented in detail. Histories reconstructed by any of this method produce a rain-flow matrix identical to rain-flow matrix of the original history. Therefore, it is expected that a fatigue life similar to the original history will be produced, when using any of the reconstruction methods. This expectation was verified by a limited number of cases, as stated in [16] or [17].

All methods which are described in [15] can be used conveniently for reconstruction of irregular loading histories in a form of a time sequence.

Rain-flow reconstruction method based on a 2-D matrix will be described in detail. The use of 3-D matrix is not considered due to greater demands on computational time.

The reconstruction method based on a 2-D matrix requires a rain-flow matrix as an input. The rain-flow matrix can be defined in two forms. In the first form (range-mean matrix), all values above the matrix diagonal are zero. Such matrix does not account the direction of detected cycles. When indication of cycle's direction is of interest, it is necessary to use a rainflow matrix in a form of from-to matrix. Such matrix distinguishes between ascending and descending cycles, as can be seen in Figure 3.11.

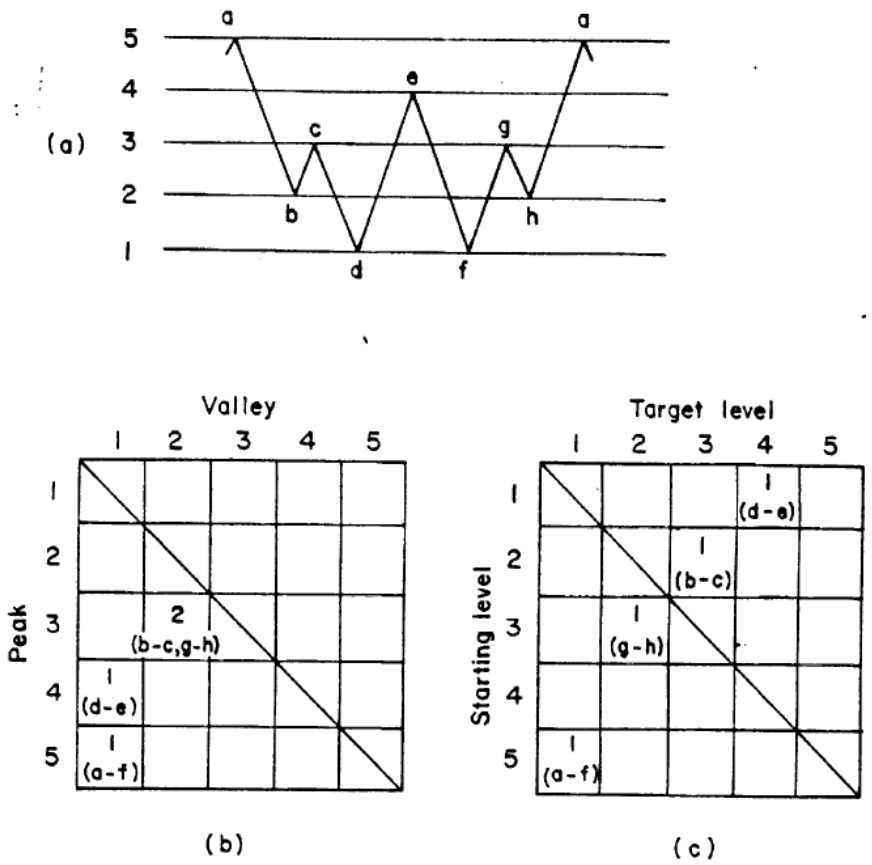

Figure 3.11 – Types of rain-flow matrices [15]

When working with range-mean matrix, the loading history reconstruction procedure is as follows according to [15]:

1. The bottom-most row of a matrix is considered first.
2. The largest cycle in a row, corresponding to the left-most column is considered and reconstructed first. Then all of the columns corresponding to the same row are considered in increasing order.
3. The procedure continues, until all elements of the matrix are covered.
4. A cycle can be placed within any cycle in the matrix with equal or more extreme peak and valley, that is, greater or equal row number and less or equal column number.
5. A random location is chosen among all the possibilities, and then the partially reconstructed sequence is rearranged accordingly.

It is possible to place cycles with the same peak and valley into a sequence in various ways. They all might be placed in the same location which gives the simplest reconstructed history. However, if more diverse loading history is desired, it is necessary to place the cycles with the same peak and valley to different locations. They might be placed one-by-one, or by groups created by n cycles. Diversity of the reconstructed history increases with decreasing number n of cycles in each group.

Unfortunately, this claim isn't sufficiently accurate. It is meaningful to decrease number n of cycles in each group to a specific point. Before beginning to place cycles with particular peak and valley, the number of groups shouldn't become higher than the number of possible locations for placing these cycles. Otherwise, the diversity of the reconstructed sequence stays the same and the computational time increases redundantly. In addition, when assuming the direction of cycles, it might happen that the direction of particular group will be changed unwillingly.

The procedure for loading history reconstruction from a 2-D matrix with values on both sides of the diagonal is as follows:

The elements within the matrix are chosen according to cycle's range in descending order. The typical order of cycle's consideration for 32 by 32 matrix is displayed in Figure 3.12.

There are altogether four rules for inserting a cycle into a partially reconstructed history according to [15]:

"If the cycle that is being inserted (inserting cycle) has a greater row than column, that is, if it is ordered peak-valley, then it can be placed within any cycle (receiving cycle), provided:

1. If the receiving cycle is ordered valley-peak, that is, if it has a row less than the column, then the receiving row must be less than or equal to the inserting column, and the receiving column must be greater than or equal to the inserting row. Figure 3.13 illustrates this case.
2. If the receiving cycle is ordered peak-valley, that is, if it has a row greater than column, then the receiving row must be greater than or equal to the inserting row, and the reiving column must be less than or equal to the inserting column. Figure 3.14 illustrates this case.

On the other hand, if' the inserting cycle has a column greater than a row, that is, if it is ordered valley-peak, then it can be placed within any cycle, provided:

1. If the receiving cycle is ordered peak-valley, that is, if it has a row greater than the column, then the receiving row must be greater than or equal to the inserting column, and the receiving column must be less than or equal to the inserting row. Figure 3.15 illustrates this case.
2. If the receiving cycle is ordered valley-peak, that is, if it has a row less than column, then the receiving row must be less than or equal to the inserting row, and the receiving column must be greater than or equal to the inserting column. Figure 3.16 illustrates this case.

In addition, the reconstruction must alternate between peaks and valleys. This results in the insertion being made in the rising branch of the receiving cycle for cases 1. and 2., and in the falling branch for 3. and 4. Also, the envelope cycle could be considered to be either a peak-valley or a valley-peak cycle."

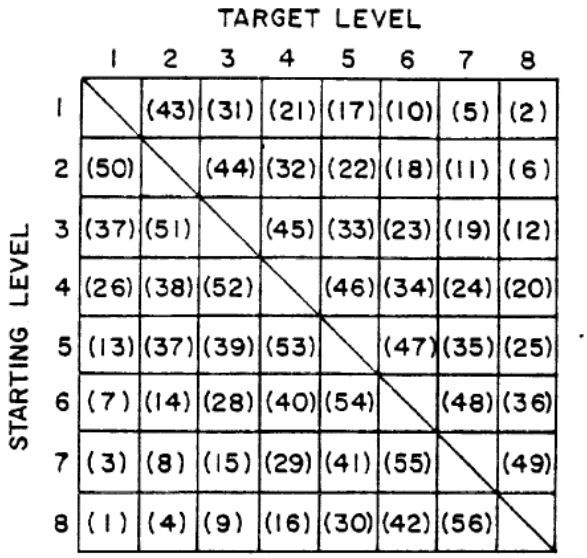

Figure 3.12 – Order of cycle's insertion [15]

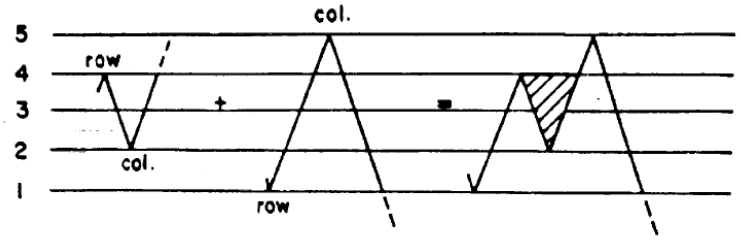

Figure 3.13 – Insertion of cycle into a loading history - case 1 [15]

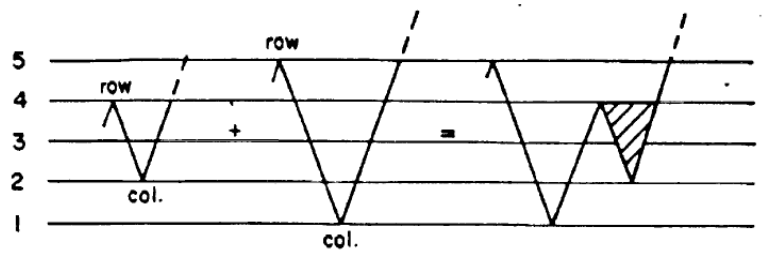

Figure 3.14 – Insertion of cycle into a loading history - case 2 [15]

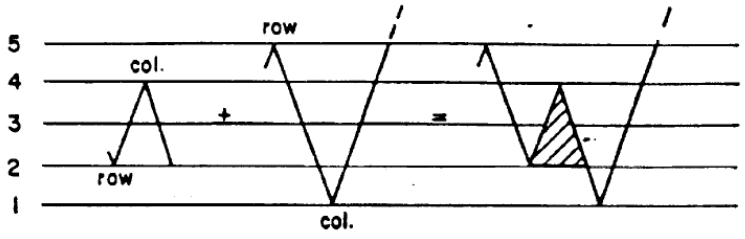

Figure 3.15 – Insertion of cycle into a loading history - case 3 [15]

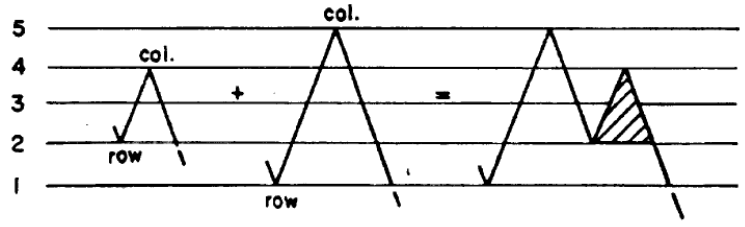

Figure 3.16 – Insertion of cycle into a loading history - case 4 [15]

The reconstructed loading history is never the same as the original loading history, as might be expected. The reason is very simple. There is usually more than one possibility of placing an inserting cycle. However, the fatigue damage of the reconstructed history will be the same as the fatigue damage calculated from the original history, because the rain-flow matrices of the original history and the reconstructed history are identical.

When defining the rain-flow matrix in a different way (not directly by rain-flow cycle counting of the original history), as will be described further in the text, it is vitally important to remember, that the envelope cycle must be included in the rain-flow matrix which sequence is desired to be reconstructed.

The envelope cycle is any cycle which has more extreme or equal peak and valley as the rest of the cycles in the matrix. If such cycle does not exist, it is impossible to reconstruct the loading history by the procedure described above.

3.7 PDF estimation using kernel density estimator

An output from any of the cycle counting methods mentioned in chapter 3.5 would be a sufficient input for further fatigue and DT analysis only if the analysed structure was not loaded by any cycles other than those detected by a measurement.

It is hard to meet such a strict requirement on real measurement results. The typical process meeting this requirement is an ergodic process for which the characteristics of the whole process might be replaced by the characteristics calculated along any of its sample, as stated before. To work with ergodic processes only, it would be necessary to divide the whole measurement record into sections, where each of them might be assumed as representatives of an ergodic process. Such sections could be analysed separately and compiled together after the analysis to follow the same order as observed during measurements.

In general, the loading of any aircraft's structure is generated by various sources. In our case, it can be distinguished between three basic sources of loading:

- Manoeuvers (Take off, Approach, Landing, Cruise flight)
- Gusts
- Vibrations

Although a certain simplification is often made by considering manoeuvers as deterministic processes, the fact is, that it is not possible to perform specific manoeuver exactly in the same way two times in a row. Therefore, all of the three loading types mentioned above might be considered as more or less stochastic events. As a result, the recorded data obtained by an in-flight measurement vary from one to each other. Due to stochastic nature of manoeuvres and gust loads, it is impossible to separate a single section following conditions of an ergodic process.

Therefore, data extrapolation is an essential procedure for determination of long-term load spectrum from a short-term one.

One possible way, how to extrapolate detected loading cycles, is to describe the process by its probability density function (PDF). PDF can then be used for predicting a cycle occurrence in any time interval. An extrapolation of measured data is practically made by generating random events in a form of loading cycles of desired quantity in line with the PDF of the process.

Kernel density estimator is one of the non-parametric methods used for PDF estimation. Contrary to parametric methods of PDF estimation, non-parametric methods are able to predict PDF of a general shape.

3.7.1 Kernel method for univariate data

In this chapter, a PDF estimation $\hat{f}$ of a sample $X_1, \dots X_n$ of n independent, identically distributed observations from a continuous univariate distribution with probability density function f using a kernel method according to [22] will be described.

The probability density function can be defined according to [22] as a probability of observation's occurrence in an incremental interval $(x-h, x+h)$:

$$f(x) = lim_{h\to 0} \frac{1}{2h} P(x-h < X > x+h)$$

For any given h, $P(x-h < X > x+h)$ can be estimated by the proportion of the sample falling in the interval $(x-h, x+h)$. Therefore, the natural estimator $\hat{f}$ is given by choosing a relatively small bandwidth h and setting:

$$\hat{f}(x) = \frac{1}{2 \cdot h \cdot n} [no. of\ X_1, \dots X_n\ falling\ \text{in}\ (x-h, x+h)]$$

The naive estimator might be also expressed as follows:

$$\hat{f}(x) = \frac{1}{n} \cdot \sum_{i=1}^{n} \frac{1}{h} \cdot w\left(\frac{x - X_i}{h}\right)$$

Where $w(u)$ is a weight function, defined by:

$w(u) = \frac{1}{2}$ if $|u| < 1$

$w(u) = 0$ otherwise

The kernel estimator is made by replacing the weight function $w(u)$ by a kernel function $K(x)$. Kernel function $K(x)$, used for PDF estimation, is usually any symmetric function, satisfying the following conditions:

$$\int_{-\infty}^{\infty} K(x) \cdot dx = 1$$

$$\int_{-\infty}^{\infty} x \cdot K(x) \cdot dx = 0$$

$$\int_{-\infty}^{\infty} x^2 \cdot K(x) \cdot dx \neq 0$$

The kernel estimator with constant bandwidth (also called smoothing parameter) can be then defined:

$$\hat{f}(x) = \frac{1}{nh} \cdot \sum_{i=1}^{n} K\left(\frac{x - X_i}{h}\right)$$

The kernel estimator is nothing more than a sum of 'bumps', which are placed above each observation. Kernel function $K(x)$ determines a shape of the bump, while the bandwidth h affects its width. Some kernel functions for univariate data can be found in [23]:

- Gaussian kernel:

$$K(u) = \frac{1}{\sqrt{2\pi}} \cdot \exp\left(-\frac{u^2}{2}\right)$$

- Epanechnikov (Parabolic) kernel:

$\mathrm{K}(u) = \frac{3}{4} \cdot (1 - u^2)$ if $u \leq 1$

$K(u) = 0$ otherwise

- Biweight kernel:

$K(u) = \frac{15}{16} \cdot (1 - u^2)^2$ if $u \leq 1$

$K(u) = 0$ otherwise

- Triangular kernel

$\mathrm{K}(u) = 1 - |u|$ if $u \leq 1$

$K(u) = 0$ otherwise

The influence of bandwidth selection and kernel function on the PDF estimation might be found in [22]. Because it turned out to be inconvenient to use constant bandwidth for the PDF estimation in some specific situations, especially for a long-tail probability distribution, various methods enabling to use alternating bandwidth were developed.

Nearest neighbour method

The amount of smoothing is controlled by an integer k, which enables to adapt the degree of smoothing to the local density of data.

Distance between two points on a line $d(x)$ can be defined as $|x - X|$. The distances between particular point x and the points of the sample, are arranged in the ascending order:

$$d_1(x) \leq d_1(x) \leq \cdots \leq d_n(x)$$

The k-th nearest neighbour density estimate is then defined by:

$$\hat{f}(x) = \frac{1}{n \cdot d_k(x)} \cdot \sum_{i=1}^{n} K\left(\frac{x - X_i}{d_k(x)}\right)$$

Contrary to the kernel estimator with constant bandwidth, which is based on the number of observations falling in a box of fixed width centered at the point of interest, the bandwidth of the nearest neighbour estimate is proportional to the size of the box needed to contain a given number of observations. As a consequence, the nearest neighbour estimate is not itself a probability density, since it does not integrate to unity. Another drawback of this method are heavy tails at both ends of the estimate.

Variable kernel method

As well as the Nearest neighbour method, variable kernel method adapts the amount of smoothing to the local density of data. The estimate is constructed similarly to the kernel estimate, but the scale parameter of the bandwidth is allowed to vary from one data point to another.

The distance $d_{i,k}(x)$ is defined as a distance between i-th observation X_i to the k-th nearest point in the set consisting of $n - 1$ data points. Then the variable kernel estimate with bandwidth h is defined by:

$$\hat{f}(x) = \frac{1}{n} \cdot \sum_{i=1}^{n} \frac{1}{h \cdot d_{i,k}(x)} K\left(\frac{x - X_i}{h \cdot d_{i,k}(x)}\right)$$

It is apparent from the definition above, that the window width of the kernel placed above the observation X_i is proportional to the distance $d_{i,k}(x)$. It is ensured, that in regions with data points close to each other is used proportionally narrow window width and vice-versa.

For any fixed k, the overall degree of smoothing depends on the bandwidth h. The choice of k influences the sensitivity of the variable kernel estimator to the local details.

Contrary to the nearest neighbour method, the variable kernel method produces a PDF itself. At the same time, the method does not suffer from heavy tails. Comparing to kernel method with constant bandwidth, it might be used to eliminate the noise in the tails for a long-tailed distributions, when using appropriate parameters.

Adaptive kernel estimator

The natural way, how to deal with long-tailed densities is to use a broader kernel in regions of low density. The basic idea of an adaptive kernel estimator is to construct an estimator consisting of kernels placed above the observations and to allow the window width to vary from one point to another. One of the practical problems related to the method is deciding whether or not an observation lies in a region of low density. The adaptive kernel approach according to [22] copes with this problem by the use of a two-stage procedure:

1) Find a pilot estimate $\tilde{f}(x)$, that satisfies $\tilde{f}(x) \geq 0$ for all observations X_i

2) Define local bandwidth factors λ_i by:

$$\lambda_i = \left\{\frac{\tilde{f}(X_i)}{g}\right\}^{\alpha}$$

where g is the geometric mean of the pilot estimate $\tilde{f}(X_i)$:

$$\log g = \frac{\sum_{i=1}^{n} log\ \tilde{f}(X_i)}{n}$$

and α is the sensitivity parameter, a number satisfying $\alpha\epsilon\langle 0; 1\rangle$

3) Define the adaptive kernel estimate $\hat{f}(x)$ by:

$$\hat{f}(x) = \frac{1}{n} \cdot \sum_{i=1}^{n} \frac{1}{h \cdot \lambda_i} K\left(\frac{x - X_i}{h \cdot \lambda_i}\right)$$

The sensitivity of the method to variations in the pilot density increases with higher values of sensitivity parameter α. The value $\alpha = 0$ transforms the method into the kernel method with constant bandwidth independent from the pilot estimate. According to [22], there are good reasons for setting $\alpha = 0{,}5$. Literature [22] also suggests to construct the pilot estimate to be sensitive to local variability of the density on the same sort of scale as the final estimate. It implies to generate the pilot estimate by means of a fixed kernel estimator of bandwidth h, the same as for the final estimate.

3.7.2 Measures of discrepancy

To evaluate the discrepancy between an estimator $\hat{f}$ and the original unknown function f in single points, the mean square error (MSE) might be used. MSE is defined by:

$$MSE_x(\hat{f}) = E\left[\hat{f}(x) - f(x)\right]^2$$

Using standard elementary properties of mean and variance, the MSE might be expressed as a sum of the squared bias and the variance at x:

$$MSE_x(\hat{f}) = \left[E\hat{f}(x) - f(x)\right]^2 + \mathrm{E}\left[\left(\hat{f}(x) - E\left[\hat{f}(x)\right]\right)^2\right]$$

$$MSE_x(\hat{f}) = Bias\left(\hat{f}(x), f(x)\right)^2 + var\left(\hat{f}(x)\right)$$

As mentioned in [22], there is a trade-off between the bias and the variance terms, which means that the bias can be reduced at the expense of increasing the variance and vice versa by adjusting the amount of smoothing.

The most widely used way, how to measure global accuracy of the density estimate $\hat{f}$ is the mean integrated square error (MISE):

$$MISE_x(\hat{f}) = E\int_{-\infty}^{\infty}\left[\hat{f}(x) - f(x)\right]^2 dx$$

In the case of non-negative integrand, the order of integration and expectation might be reversed to give a different form of MISE:

$$MISE_x(\hat{f}) = \int_{-\infty}^{\infty} E\left[\hat{f}(x) - f(x)\right]^2 dx$$

$$MISE_x(\hat{f}) = \int_{-\infty}^{\infty} MSE_x(\hat{f})\, dx$$

$$MISE_x(\hat{f}) = \int_{-\infty}^{\infty} Bias\left(\hat{f}(x), f(x)\right)^2 dx + \int_{-\infty}^{\infty} var\hat{f}(x)\, dx$$

3.7.3 Choice of the smoothing parameter

Choice of the smoothing parameter strongly affect the result obtained by the PDF estimator. Its choice is therefore crucially important.

As stated in [22]: "The appropriate choice of smoothing parameter is always influenced by the purpose for which the density estimate is to be used." In the case of detected load cycles extrapolation, it would be definitely appropriate to choose such a value of the smoothing parameter which will give conservative results in a form of fatigue damage, or a crack growth rate. Too low bandwidth causes under-smoothing of data and therefore does not enable their extrapolation at all. On the other hand, too high value of bandwidth might over-smooth the measured data and cause a loss of basic patterns detected by the measurement.

Various methods for choosing optimal bandwidth for PDF estimation are suggested in [22]:

a) Subjective choice
b) Reference to a standard distribution
c) Least-square cross validation
d) Likelihood cross validation

Subjective choice is made by comparing several curves produced by the estimator using various smoothing parameters. However, the choice is fully subjective, because it reflects one's prior ideas about the density.

The use of a standard distribution requires to predict a shape of the distribution in advance, which might be inconvenient when predicting for example a PDF of a complex process comprising several sub-processes, although each of them might follow a normal distribution. It would be necessary to extract sub-processes from the record before estimating their PDF.

Methods providing fully automatic choice independent from any standard distribution or a subjective idea about the density being estimated are the cross validation methods mentioned above. These methods will be described in more detail.

Least square cross validation

The method was suggested by [24] and is based on a simple idea. For a given estimation $\hat{f}(x)$ of the PDF $f(x)$, the integrated square error can be written as:

$$\int_{-\infty}^{\infty}\left(\hat{f}(x)-f(x)\right)^2 dx = \int_{-\infty}^{\infty}\hat{f}(x)^2 dx - 2\cdot\int_{-\infty}^{\infty}\hat{f}(x)\cdot f(x)dx + \int_{-\infty}^{\infty}f(x)^2 dx$$

The last term in the equation does not depend on the estimation $\hat{f}(x)$. Therefore, the ideal choice of a window width in the sense of minimizing integrated square error corresponds to minimizing the quantity $R(\hat{f})$, defined by:

$$R(\hat{f}) = \int_{-\infty}^{\infty} \hat{f}(x)^2 dx - 2 \cdot \int_{-\infty}^{\infty} \hat{f}(x) \cdot f(x) dx$$

An estimate of the quantity $R(\hat{f})$ is computed directly from the data themselves within least square cross validation method. $R(\hat{f})$ is then minimized over h to obtain an optimal value of bandwidth. The whole process step by step is as follows:

a) Term $\int_{-\infty}^{\infty} \hat{f}(x)^2 dx$ is calculated directly from the estimate $\hat{f}(x)$ for a given h

b) Density estimate constructed from all the data points except the i-th observation X_i is computed for $i = 1,2, \dots, n$. For a kernel estimator with constant bandwidth:

$$\hat{f}_{-i}(x) = \frac{1}{(n-1) \cdot h} \cdot \sum_{j \neq i} \mathrm{K}\left(\frac{x - X_j}{h}\right)$$

c) Score function $M_0(h)$ is defined by:

$$M_0(h) = \int_{-\infty}^{\infty} \hat{f}(x)^2 dx - \frac{2}{n} \cdot \sum_{i=1}^{n} \hat{f}_{-i}(X_i)$$

The idea of the least square cross validation is to minimize the score function over h. Literature [22] provides a derivation of equality between minimizing the $EM_0(h)$ and minimizing $ER(\hat{f})$.

Likelihood cross validation

The method is based on an idea to use likelihood to judge, how the statistical model matches measured data. It is of general applicability, not just in the estimation of a PDF.

It is supposed, that there is an additional independent observation Y to the original data set $X_1, X_2, \dots, X_n$ from the same PDF $f(x)$ available. Then the likelihood of $\hat{f}(x)$ as a density underlying the observation Y would be $\log \hat{f}(Y)$. Assuming, that $\hat{f}(x)$ is actually a parametric family of densities depending on the bandwidth h, the log likelihood $\log \hat{f}(Y)$ is also a function of h.

Since an independent observation Y is not available, one of the original observations X_i from the sample might be omitted. This would give log likelihood $\log \hat{f}_{-i}(X_i)$, where $\hat{f}_{-i}(x)$ is the same as defined above. To discharge a necessity to choose which observation from the original data set to leave, the log likelihood is averaged over each possible choice of X_i omitted, to give the score function defined by:

$$CV(h) = \frac{1}{n} \cdot \sum_{i=1}^{n} \log \hat{f}_{-i}(X_i)$$

The optimal bandwidth in the sense of likelihood cross validation is such a value of bandwidth which maximizes the score function $CV(h)$ for the given data set.

3.7.4 Kernel method for multivariate data

The definition of the kernel estimator with constant bandwidth mentioned earlier might be easily generalized to the multivariate data set $\boldsymbol{X_1}, \boldsymbol{X_2}, \ldots, \boldsymbol{X_n}$:

$$\hat{f}(\boldsymbol{x}) = \frac{1}{nh^d} \cdot \sum_{i=1}^{n} K\left\{\frac{\boldsymbol{x} - \boldsymbol{X_i}}{h}\right\}$$

where bold face is used for definition of points in d-dimensional space. The same generalization can be made for other methods, which have been already defined for univariate data.

The kernel function in the case of d-dimensional variable $\boldsymbol{x}$ satisfies the following conditions:

$$\int K(\boldsymbol{x}) \cdot d\boldsymbol{x} = 1$$

$$\int \boldsymbol{x} \cdot K(\boldsymbol{x}) \cdot d\boldsymbol{x} = 0$$

$$\int \boldsymbol{x}^2 \cdot K(\boldsymbol{x}) \cdot d\boldsymbol{x} \neq 0$$

The kernel function is usually a radially symmetric unimodal probability density function. Two different kernel functions used for multivariate data according to [22], which are frequently used, are:

- Standard multivariate normal density function:

$$K(u) = \left(\frac{1}{2\pi}\right)^{\frac{d}{2}} \cdot \exp\left(-\frac{\boldsymbol{u^T} \cdot \boldsymbol{u}}{2}\right)$$

- Multivariate Epanechnikov kernel function:

$$\mathrm{K}(u) = \frac{1}{2 \cdot c_d} \cdot (d+2) \cdot (1 - \boldsymbol{u}^{\boldsymbol{T}} \cdot \boldsymbol{u}) \qquad \text{if } \boldsymbol{u}^{\boldsymbol{T}} \cdot \boldsymbol{u} \leq 1$$

$$K(u) = 0 \qquad \text{otherwise}$$

where c_d is the volume of the unit d-dimensional sphere, which gives:

$c_1 = 2$, $c_2 = \pi$, $c_3 = \frac{4\pi}{3}$, etc.

When using just a single smoothing parameter h according to equation above, the kernel function is scaled equally in all directions. In certain circumstances, typically in the case where the data are spread greater in one direction than the others, it may be beneficial to use a vector of smoothing parameters or even a matrix of scaling coefficients.

According to [22], it is possible to pre-scale the data to avoid extreme differences of spread in the various coordinate directions. If this is done, then there is no need to consider more complicated forms of the kernel density estimate than the form involving a single smoothing parameter.

4 PROPOSED METHODOLOGY

As might be derived from the strain-gauge survey (see chapter 1.7.3), flaps are loaded predominantly by the flap-duty cycles. Apart from the flap-duty cycles, variable loading of low-frequency might occur due to variability of aircraft's airspeed, head-on gusts etc. High-frequency loading is supposed to be caused by the effects of propeller slipstream described in chapter 1.6.

As already mentioned, it is not possible to perform take-off or landing in the same way two times in a row. Apart from that, loading by gusts, as well as loading by vibrations, are stochastic processes from nature. Therefore, it is reasonable to presume, that any two data records from a long row of in-flight measurements would not be the same. They might vary from the load levels as well as from the time duration point of view.

These facts make the determination of vibrations effect on fatigue life of flaps and flap's control system a complex problem.

An alternative approach, especially suitable for a quick and easy estimation of vibrations effect, might be inspired by [26]. The report contains a summary of methods describing the effect of vibrations on fatigue life and crack propagation in aluminium alloys and partially in steel.

The vibration cycles might be supposed to be cycles with high frequency. The vibration cycles are superposed onto basic cycles of low frequency. The vibration cycles, as well as basic cycles are presumed to be harmonic loadings. Therefore, the resulting loading has a biharmonic character with the following parameters:

σ_{aH}	Amplitude of vibration cycles
σ_{aL}	Amplitude of basic cycles
σ_{mL}	Mean value of basic cycles
$\sigma_c = \sigma_{aL} + \sigma_{aH}$	Amplitude of the biharmonic loading

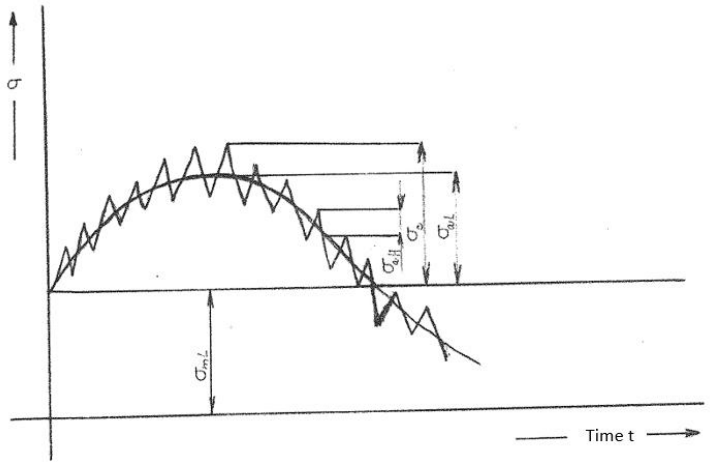

Figure 4.1 – Superposition of basic and vibration cycles [26]

The effect of biharmonic loading on the reduction of fatigue life can be expressed by a ratio between fatigue durability under biharmonic loading and fatigue durability under monoharmonic loading in a form of a basic cycle.

The validity of the following equation suggested in [26] was demonstrated on specimens made of aluminium alloy D16T. The equation describes the effect of biharmonic loading as a relative reduction of fatigue durability under monoharmonic loading with frequency ω_L and loading amplitude σ_c:

$$\frac{N_c - N_{LF}}{N_c} = 1 - \frac{1}{\left[1 + \left(\frac{\omega_H}{\omega_L}\right)^{\frac{2}{m}} \cdot \left(\frac{\sigma_{aH}}{\sigma_{aL}}\right)^2\right]^{\frac{m}{2}}}$$

The equation works with parameters of the basic cycle, vibration cycle and corresponding fatigue durability:

N_c	Fatigue life due to monoharmonic loading with frequency ω_L and loading amplitude σ_c
N_{LF}	Fatigue life due to biharmonic loading
ω_H	Frequency of vibration cycles
ω_L	Frequency of basic cycles
m	SN-curve exponent

Analysis of fatigue durability of specimens made of aluminium alloys might be carried out using this equation, if the parameters of basic cycle as well as parameters of vibration loading are determined.

In practical applications, necessity to choose representative parameters of vibration cycles and parameters of basic cycles arises. In the case of an inappropriate choice, such approaches might become unconservative, or far conservative, leading to under or overestimating the effect of vibrations in a form of a ratio between fatigue damage caused by the biharmonic loading and fatigue damage due to basic cycle.

Therefore, the aim of the proposed methodology is to perform complex analysis of the in-flight measurement to reach as much information about the loading as possible. To accomplish this task, an algorithm consisting of several scripts was developed.

To determine the effect of vibrations, each flight is divided into three flight phases, which are analysed separately. For further details about separated flight phases, see chapter 1.7.3 and Appendix A.

PDF of loading cycles is determined for each flight phase. The sequence of length corresponding to time duration of the typical flight profile is reconstructed and the entire flight is formed. The methodology provides a loading sequence for crack growth calculations using AFGROW and ratio between fatigue damage due to vibrations and fatigue damage due to flap duty cycles.

4.1 Description of the algorithm

The algorithm leading to determination of vibration effects comprises altogether six steps, that are displayed in a form of a flowchart on the figure below.

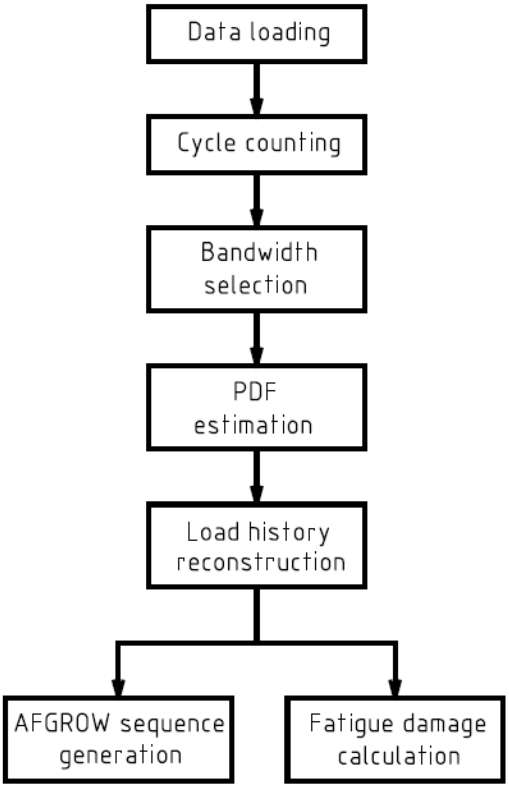

Figure 4.2 – Basic flowchart

The data processing is made with the use of Matlab or Octave depending on the choice of the user. An excel file AIVIB.xlsx contains all important parameters which have an influence on the final result. The excel file acts also as an interface providing all major sub-results and links on files created during data processing to the user.

The AIVIB.xlsx file is composed of the following sheets:

- INPUT_DATA
- PARAM
- TAKO
- APP
- LNG
- OUTPUT

INPUT_DATA

It is a spreadsheet containing all necessary information for data loading. The user is requested to input directory of input files as well as an output directory.

PARAM

It is an excel sheet containing all parameters which are requested during the data processing.

TAKO – APP – LNG

These sheets contain sub-results obtained by the algorithm, links on the output files in the output directory, as well as some additional parameters related to the corresponding flight phase only. The user has to define especially the bandwidth for the final PDF estimation and boundaries of the area, where the PDF will be established.

OUTPUT

The final results of the algorithm are stated in this spreadsheet. The results have two forms. First of them is represented by a vibration factor describing the effect of vibrations on the fatigue durability. The second one is a loading sequence for further crack growth analysis using AFGROW. The sheet contains a link on the loading sequence files .sp3 and .sub (see chapter 2.4 for more detail).

4.2 Data loading

To load desired data, it is necessary to fill the following entries into the spreadsheet INPUT_DATA of AIVIB.xlsx file and call the script DLOAD.m:

- **Output files notation (OFN)** – Forms a core of the output filename. The output filename is formed from the input OFN at the first place, followed by other relevant chars.

  Output directory – Name of a directory containing all output files.

- **Number of input files** – Number of files which are desired to be loaded. If the entered value is lower than number of entered filenames, the filenames with IDs higher than desired number of input files won't be loaded. If the entered value is higher than number of entered filenames, an error message will occur.

- **Slot no.** – Measurement unit usually receives signals from several sensors. The slot n° indicates the sensor which signal will be analysed.

- **Directory of measured data** – Directory containing all input files.

- **Flight phase** – Indicates which flight phase is represented by the corresponding input file. Altogether three possibilities are accepted:
  - TAKO – Take-off (Flaps deflected $\delta_{FL} = 18°$)
  - APP – Approach (Flaps deflected $\delta_{FL} = 18°$)
  - LNG – Landing (Flaps deflected $\delta_{FL} = 42°$)

- **Input filename** – Name of file containing the data of the in-flight measurement, including suffix. Be aware, that only input files of the same format as specified in Appendix B might be loaded.

Apart from the INPUT_DATA sheet, the user is requested to specify the stress multiplication factor (SMF) and desired data unit in the sheet called PARAM, prior to data loading:

- **SMF** – Stress multiplication factor has the same meaning as defined in the case of AFGROW sequence (see chapter 2.4). Each value obtained by the measurement is multiplied by the user-defined SMF. SMF enables to convert the data from original units to user-defined units.

The functionality of the algorithm will be demonstrated using the results of the in-flight measurement on L410 UVP – E20 aircraft (see chapter 1.7.3). Data from slot n°334 (see Table 1.4) will be used for the analysis. It will be assumed, that it is necessary to analyse a structural detail loaded in tension for which the relationship between measured loading $F\ [N]$ and the normal stress $\sigma_N\ [MPa]$ might be described by the following value of SMF:

$$SMF = \frac{\sigma_N}{F} = -0.05$$

Table 4.1 and Table 4.2 summarize all necessary parameters to be filled in the INPUT_DATA and PARAM spreadsheets prior to calling the script DLOAD.m.

Stress multiplication factor	SMF	[-]	-0.05
Data unit after multiplying by SMF	unit	[MPa]	

Table 4.1– Necessary parameters for the initial loading of data – PARAM spreadsheet

INPUT/OUTPUT FILES		
Output files notation	[-]	SLOT_NO_334
Output directory	[-]	C:\VIBRATION_ANALYSIS\OUTPUT
MEASURED DATA		
Number of input files	[-]	6
Slot no.	[-]	334
Directory of measured data	[-]	C:\VIBRATION_ANALYSIS\AIVIB\DATA
ID	FLIGHT PHASE	INPUT FILENAME
1	TAKO	F220201 TAKO.xlsx
2	APP	F220201 APP.xlsx
3	LNG	F220201 LNG.xlsx
4	TAKO	F220202 TAKO.xlsx
5	APP	F220202 APP.xlsx
6	LNG	F220202 LNG.xlsx

Table 4.2 – Necessary parameters for the initial loading of data – INPUT_DATA spreadsheet

After filling all entries mentioned above, the script DLOAD.m shall be called. The script opens all input files and finds the data corresponding to desired slot number.

Raw data are sorted out based on the flight phase which they refer to. All data referring to the same flight phase are merged together and multiplied by SMF. During their merging, the last point of one record is replaced by the first point of the following record. The resulting record has therefore n_{org} number of data points. Such merging guarantees, that there won't be any time extension of measured data:

$$n_{org} = \sum_{i=1}^{n_{RD}} n_{Fi} - (n_{RD} - 1)$$

where:

n_{RD} number of data files corresponding to the same flight phase

n_{Fi} number of data points in particular file of index i

The time duration of merged data t_{org} is therefore equal to a sum of time durations of the data before merging t_{Fi}:

$$t_{org} = \sum_{i=1}^{n_{RD}} t_{Fi}$$

Excel spreadsheet (TAKO, APP, LNG) contains the summary of data loading, as shown in Table 4.4 to Table 4.6. The resultant records are shown in Figure 4.3 to Figure 4.5 for each flight phase.

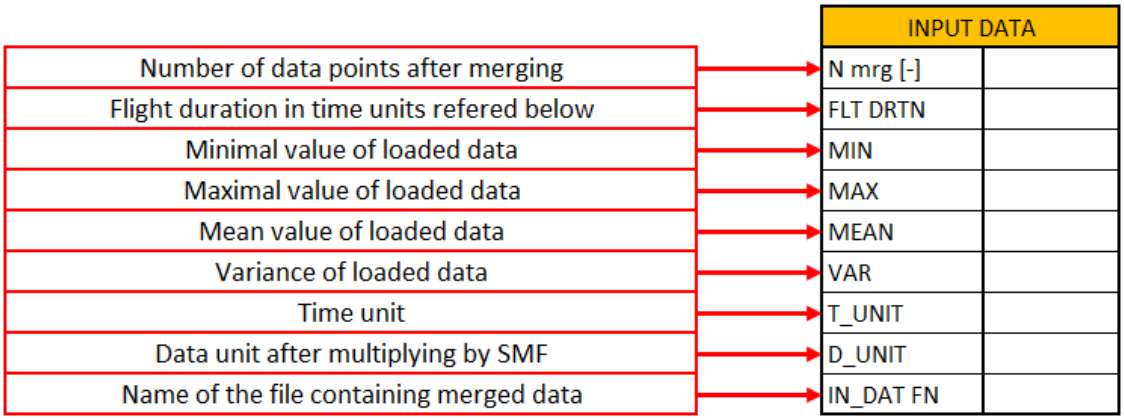

Table 4.3 – Data loading output summary – description

INPUT DATA	
N mrgD[-]	140002
FLT DRTN	140
MIN	-2.98
MAX	55.12
MEAN	27.03
VAR	320.85
T_UNIT	[s]
D_UNIT	[MPa]
IN_DAT FN	INPUT_DATA\SLOT_NO_334_INPUT_DATA_TAKO.txt

Table 4.4 – Data loading output summary – TAKO

INPUT DATA	
N mrgD[-]	64002
FLT DRTN	64
MIN	25.17
MAX	47.92
MEAN	35.71
VAR	22.98
T_UNIT	[s]
D_UNIT	[MPa]
IN_DAT FN	INPUT_DATA\SLOT_NO_334_INPUT_DATA_APP.txt

Table 4.5– Data loading output summary – APP

INPUT DATA	
N mrgD[-]	220002
FLT DRTN	220
MIN	59.11
MAX	109.24
MEAN	82.80
VAR	47.35
T_UNIT	[s]
D_UNIT	[MPa]
IN_DAT FN	INPUT_DATA\SLOT_NO_334_INPUT_DATA_LNG.txt

Table 4.6 – Data loading output summary – LNG

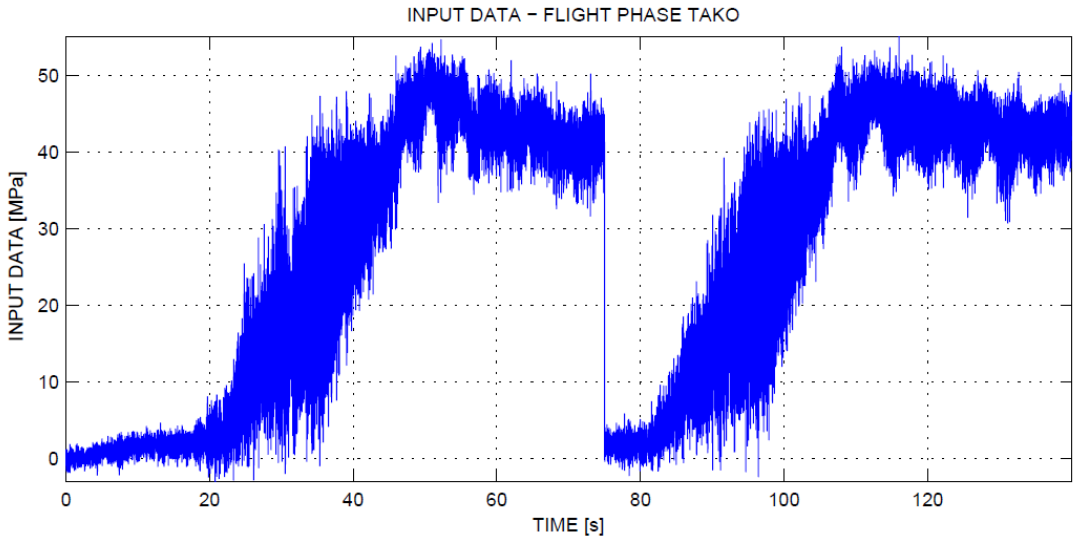

Figure 4.3 – Merged data – TAKO

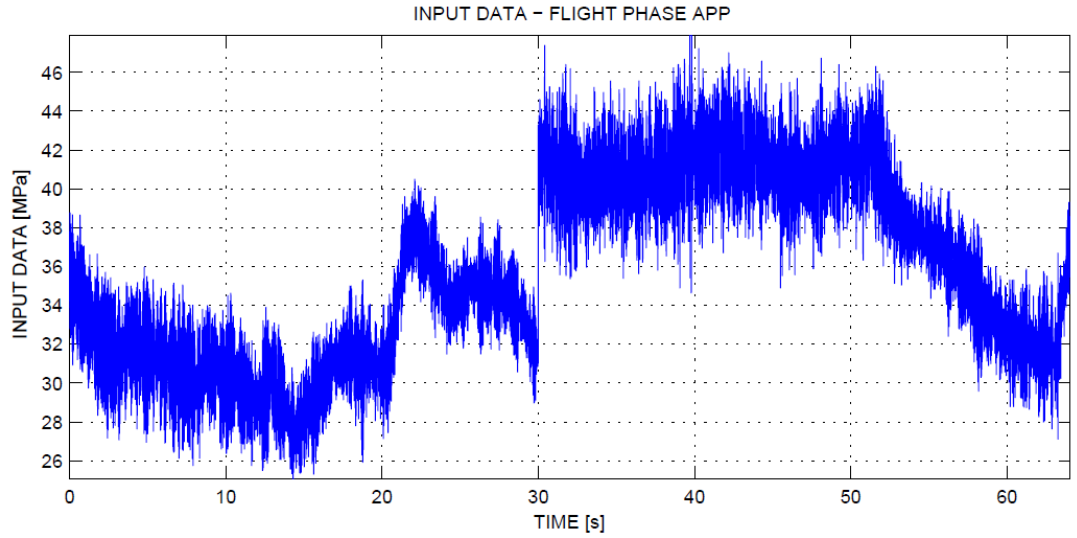

Figure 4.4 – Merged data – APP

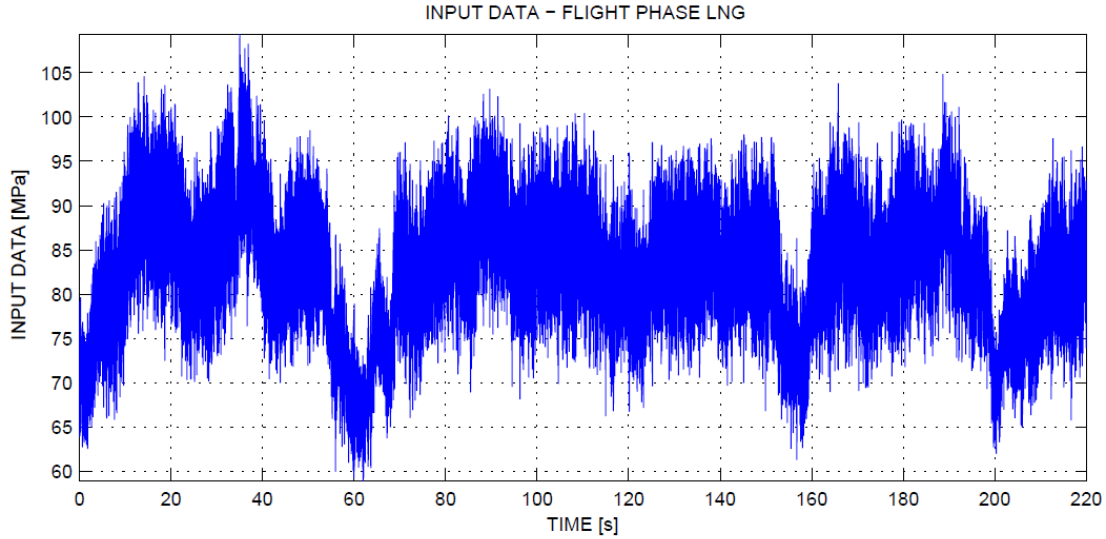

Figure 4.5 – Merged data – LNG

4.3 Cycle counting

The proposed methodology continues with separating peaks in the merged loading history of particular flight phase by calling the script CC.m. After the peaks are separated, the simplified rainflow counting method for repeating histories is applied as described in chapter 3.5. Detected cycles are registered in two vectors, representing the starting and target level of each cycle.

To provide an instrument for a quick and easy check of the performed cycle count by the user, the scatter plot of detected cycles is created. The scatter plots of cycles derived from the in-flight measurement can be seen in Figure 4.6 to Figure 4.8.

It is evident, that most cycles lie nearby the diagonal. Such cycles are characterized by a low amplitude, which is defined as an absolute value of the difference between target and starting load level.

After the cycles are counted, corresponding fatigue damage is calculated by the linear damage accumulation hypothesis (see chapter 2.2) and the user-specified mean stress correction method (in line with chapter 2.1.4). The fatigue damage is related to the user-defined duration of flight phase in PARAM spreadsheet. It is recommended to specify the flight duration in line with the typical flight profile and definition of the analysed flight phases, as defined in chapters 1.7.1 and 1.7.3.

All necessary parameters to be specified in the PARAM spreadsheet prior to calling the script CC.m are summarized in the Table 4.7.

	FLIGHT PROFILE		
Time duration of take-off	T_TAKO	[min]	0.7
Time duration of approach	T_APP	[min]	2.3
Time duration of landing	T_LNG	[min]	0.3
	MEAN STRESS CORRECTION		
Mean stress correction method	Method	[-]	ODING
	SN CURVE		
Rerefence number of cycles	N_ref	[-]	1.00E+05
Reference stress value	s_ref	[N]	120
SN-curve slope prior to curve break	m1	[-]	4
SN-curve constant prior to curve break	A1	[-]	2.07E+13
Number of cycles at the curve break	N_break	[-]	1.00E+06
Stress at the curve break	s_break	[N]	67.48096
SN-curve slope after curve break	m2	[-]	6
SN-curve constant after curve break	A2	[-]	9.44E+16

Table 4.7 – Parameters for the fatigue damage determination

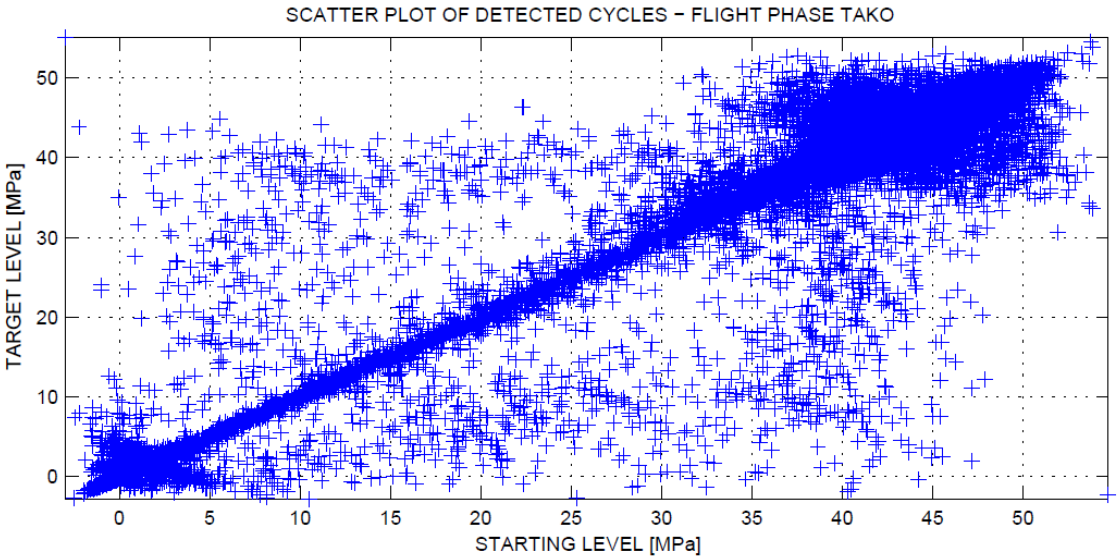

Figure 4.6 – Scatter plot of detected cycles – TAKO

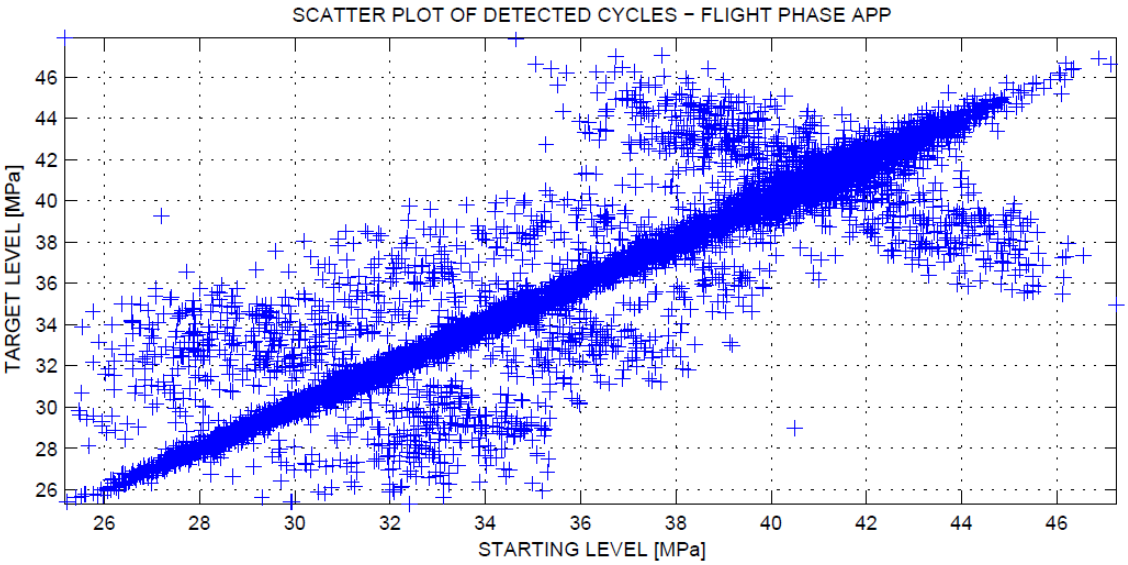

Figure 4.7 – Scatter plot of detected cycles – APP

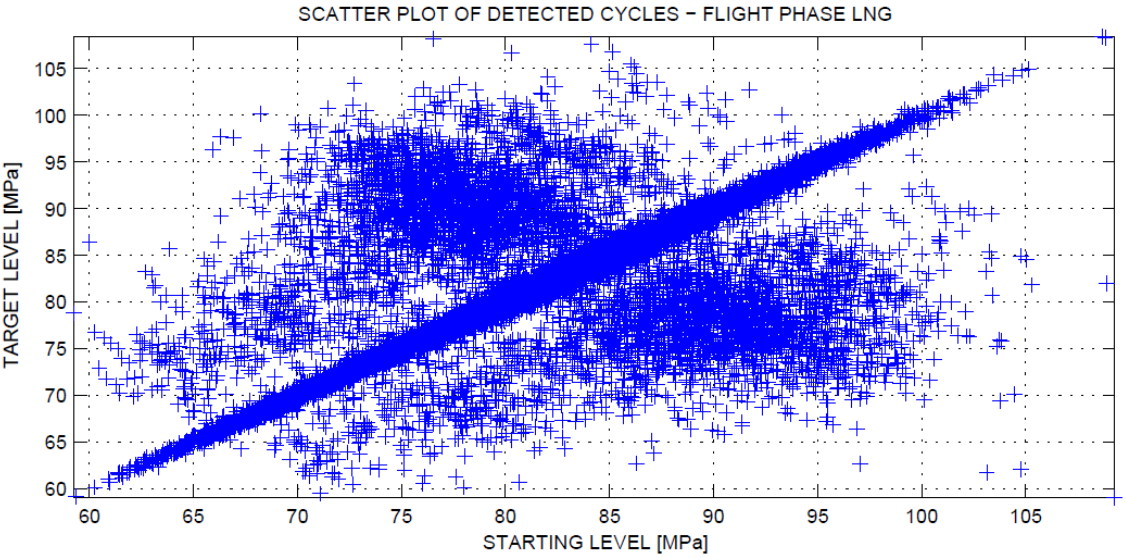

Figure 4.8 – Scatter plot of detected cycles – LNG

Altogether four inputs are accepted to define the mean stress correction method for the computation of an equivalent load/stress:

- ODING for modified Oding
- GERBR for Gerber
- GODMN for Goodman
- SDRBG for Soderberg

The SN-curve is generally assumed as an SN-curve with knee at user-defined knee point $[N_{break}; \sigma_{break}]$. To construct such SN-curve, it is necessary to define the following:

N_{ref}	reference number of cycles to failure
σ_{ref}	reference stress value
m_1	SN-curve slope at the reference point $[N_{ref}, \sigma_{ref}]$
N_{break}	Number of cycles specifying position of the SN-curve knee
m_2	SN-curve slope after the SN-curve break

The rest of parameters are calculated accordingly:

$$A_1 = {\sigma_{ref}}^{m_1} \cdot N_{ref}$$

$$\sigma_{break} = \left(\frac{A_1}{N_{break}}\right)^{\frac{1}{m_1}}$$

$$A_2 = {\sigma_{break}}^{m_2} \cdot N_{break}$$

The absolute frequencies of occurrence of the detected cycles are normalized to fit the user-defined flight phase duration:

$$n_{a\,org} = \frac{t_{TFP}}{t_{org}}$$

where:

$n_{a\,org}$	absolute frequency of occurrence of each detected cycle related to the user-defined flight phase duration
t_{TFP}	user-defined time duration of the flight phase
t_{org}	time duration of the flight phase derived from the in-flight measurement

Together with fatigue damage, the cumulative frequency of occurrence of an equivalent load/stress is determined. Contrary to the fatigue damage, the frequency is related to the duration of the in-flight measurement t_{org}. It means, that each detected cycle is present once per measurement. The cumulative frequency derived from the input data mentioned above with the use of modified Oding method is shown in Figure 4.9 to Figure 4.11.

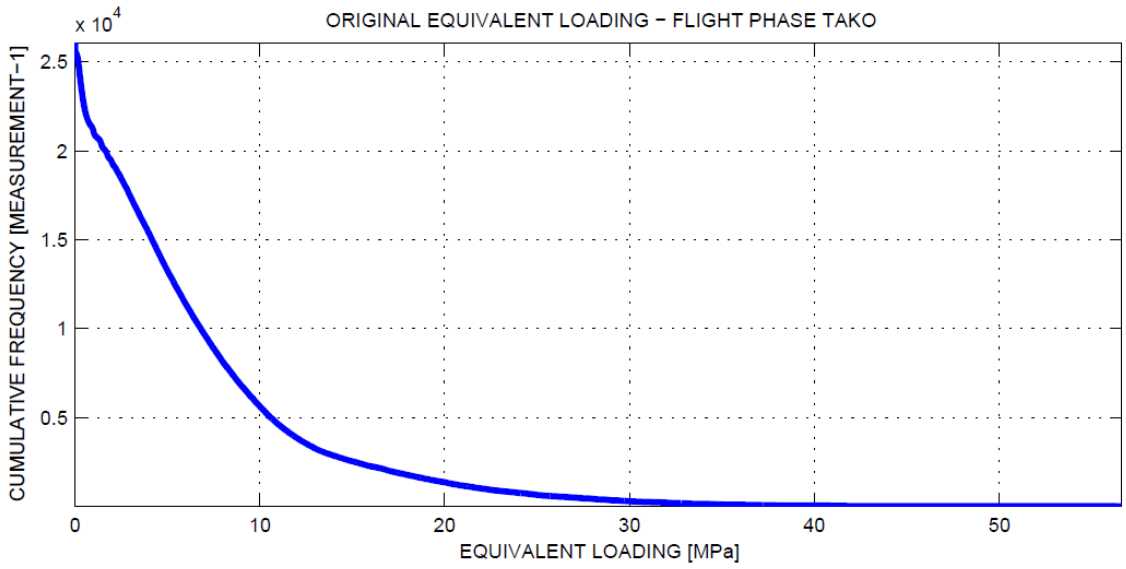

Figure 4.9 – Cumulative frequency of equivalent stress – TAKO

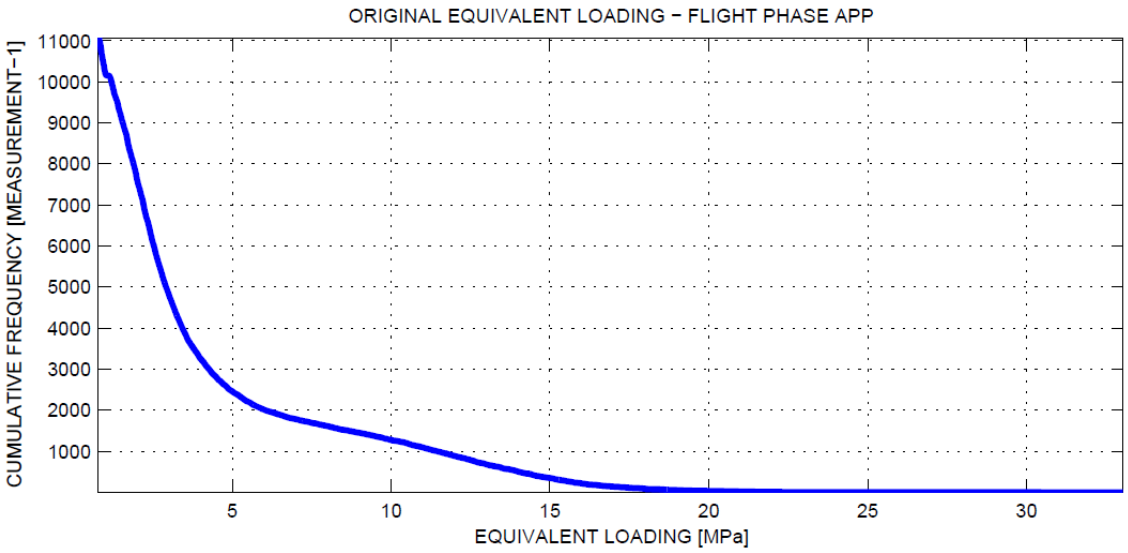

Figure 4.10 – Cumulative frequency of equivalent stress – APP

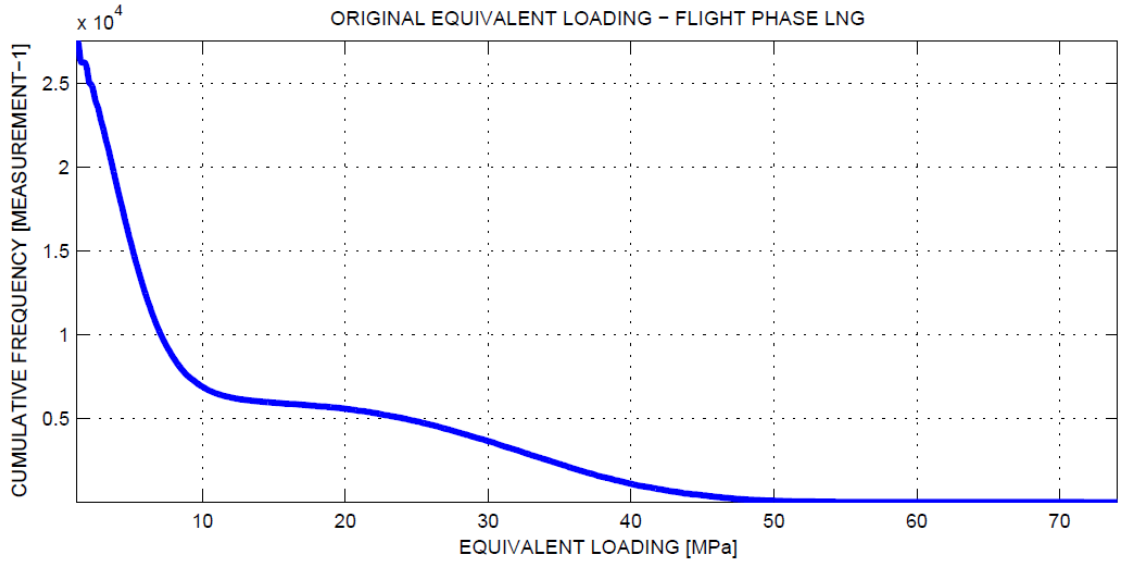

Figure 4.11 – Cumulative frequency of equivalent stress – LNG

Table 4.9 to Table 4.11 show an output summary after calling the script CC.m for each flight phase separately.

	CYCLE COUNTING	
Name of file containing extracted peaks	EP FN	
Number of data points after peaks extraction	N EP [-]	
Name of file containing counted cycles	CC FN	
Number of detected cycles	N CC [-]	
Name of file containg cumulative frequencies	CF_ORG FN	
Name of file containing equivalent loads	EL FN	
Fatigue damage of the original history	FD_ORG [FL-1]	

Table 4.8 – Cycle counting output summary – description

CYCLE COUNTING	
EP FN	TAKO\SLOT_NO_334_SEPARATED PEAKS_TAKO.txt
N EP [-]	52170
CC FN	TAKO\SLOT_NO_334_DETECTED_CYCLES_TAKO.txt
N CC [-]	26084
CF_ORG FN	TAKO\SLOT_NO_334_CUM_FREQ_ORG_TAKO.txt
EL FN	TAKO\SLOT_NO_334_EQ_LOAD_ORG_TAKO.txt
FD_ORG [FL-1]	2.85596E-06

Table 4.9 – Cycle counting output summary – TAKO

CYCLE COUNTING	
EP FN	APP\SLOT_NO_334_SEPARATED PEAKS_APP.txt
N EP [-]	22141
CC FN	APP\SLOT_NO_334_DETECTED_CYCLES_APP.txt
N CC [-]	11070
CF_ORG FN	APP\SLOT_NO_334_CUM_FREQ_ORG_APP.txt
EL FN	APP\SLOT_NO_334_EQ_LOAD_ORG_APP.txt
FD_ORG [FL-1]	3.61493E-07

Table 4.10 – Cycle counting output summary – APP

CYCLE COUNTING	
EP FN	LNG\SLOT_NO_334_SEPARATED PEAKS_LNG.txt
N EP [-]	55158
CC FN	LNG\SLOT_NO_334_DETECTED_CYCLES_LNG.txt
N CC [-]	27578
CF_ORG FN	LNG\SLOT_NO_334_CUM_FREQ_ORG_LNG.txt
EL FN	LNG\SLOT_NO_334_EQ_LOAD_ORG_LNG.txt
FD_ORG [FL-1]	1.30058E-05

Table 4.11 – Cycle counting output summary – LNG

4.4 Bandwidth selection

The loading of flaps and flap's control system is assumed as a stochastic process, as discussed earlier. To deal with a stochastic loading, cycle extrapolation is made. Cycle extrapolation is performed by estimating the PDF of detected cycles in a form of a from-to matrix. Using the PDF, a loading of any length might be generated.

The PDF is estimated by one of the kernel estimation techniques, described in chapter 3.7. The algorithm enables the user to use kernel estimator with constant bandwidth, or an adaptive kernel estimator. As a kernel function, a Normal kernel (also called Gaussian kernel) is used.

Prior to bandwidth selection, all necessary parameters in PARAM spreadsheet and spreadsheets of the investigated flight phases (TAKO, APP and LNG) must be defined. These parameters include:

- **Target life (N_{tgt})** – desired number of flights to be generated after PDF estimation.

- **Method for an automatic bandwidth selection** – only one input accepted by the algorithm is possible in the moment. Enter LSCV for Least square cross validation method.

- **Kernel function** – only one possible input is accepted. Enter NORM for a normal kernel function. This function should be more suitable for cycle extrapolation than Epanechnikov kernel defined in chapter 3.7.4., because the probability of cycle occurrence outside local bandwidth is non-zero in the case of normal kernel function.

- **Reduction factor (RF)** – this factor directly influences the speed of an automatic bandwidth selection. The bandwidth is reduced by the reduction factor in each step of the iteration method, leading to minimizing MISE using LSCV procedure. When entering "DEFAULT", reduction factor is set equal to 3.0.

- **Overrun (OVR)** – defines, how many values of bandwidth will be investigated beyond the recommended value obtained by an automatic bandwidth selection. This parameter enables the user to see the trend of change of the score function M_0 with bandwidth decreasing beneath the recommended value. Only integers are permitted. When entering "DEFAULT", overrun is set equal to 2.

- **Precision of the automatic bandwidth selection (ε_P)** – defines desired precision of bandwidth recommended by an automatic bandwidth selection procedure. The precision is relative to the maximal data range R_{max}:

$$\mathrm{R}_{max} = max\{\sigma\} - min\{\sigma\}$$

The recommended bandwidth h_{rec} found out by the bisection method is set equal to a current bandwidth only if the following condition is satisfied:

$$\varepsilon_i = \frac{|h_L - h_R|}{\mathrm{R}_{max}} \leq \varepsilon_P$$

$$h_{rec} = h_i = \frac{h_L + h_R}{2}$$

Where:

σ	data vector (univariate data)
ε_i	relative error in i-th step
$\langle h_L; h_R \rangle$	interval containing recommended bandwidth
h_i	current bandwidth

When entering "DEFAULT", precision is set equal to 0.05.

- **Maximal permitterd bandwidth** ($\overline{\boldsymbol{h_{max}}}$) – maximal bandwidth permitted by the user. The iteration procedure for recommended bandwidth determination begins by investigating this value. Similarly to desired precision, it is relative to input data range R_{max}. It means, that maximal permitted bandwidth is computed based on the data range as follows:

$$h_{max} = \overline{h_{max}} \cdot \mathrm{R}_{max}$$

When entering "DEFAULT", it is set equal to 0.5.

- **Minimal permitted bandwidth** ($\overline{\boldsymbol{h_{min}}}$) – minimal bandwidth permitted by the user. The iteration procedure is terminated, if the minimum of the score function has not been found till reaching this value. Then, the recommended bandwidth is set equal to minimal permitted value. As well as maximal permitted value, it is relative to input data range R_{max}:

$$h_{min} = \overline{h_{min}} \cdot \mathrm{R}_{max}$$

When entering "DEFAULT", $\overline{h_{min}}$ is set equal to 10^{-3}.

- **Roughness (RGHNS)** – indicates the roughness of generated PDF in a form of a from-to matrix. Roughness specifies number of intervals, into which bandwidth h is divided. It means, that x-axis as well as y-axis of the estimated PDF will be defined by discrete points with spacing Δx and Δy:

$$\Delta x = \Delta y = \frac{h}{RGHNS}$$

When entering "DEFAULT", it is set equal to 5.0.

- **Investigated distance** $(\boldsymbol{DIST})$ – specifies the investigated distance from the most extreme data point obtained by the measurement. This value is relative to current bandwidth, similarly to roughness. Contrary to roughness, it defines the distance to be investigated for an automatic bandwidth selection only. It is not valid for final PDF estimation. Specifying $DIST$, the extremes on the x-axis for univariate PDF function are defined as follows:

$$x_{min} = min\{\sigma\} - DIST \cdot h$$

$$x_{max} = max\{\sigma\} + DIST \cdot h$$

When entering "DEFAULT", the investigated distance $(DIST)$ is set equal to 10.0.

- **Sensitivity factor** – defines the sensitivity of the AKE method to variations in the pilot density, as stated in chapter 3.7.1

- **PDF estimator** – PDF estimator to be used for a subjective choice of bandwidth as well as for the final PDF estimation. Two possible inputs accepted by the algorithm might be entered by the user:

CKE	for Kernel Estimator with Constant bandwidth
AKE	for Adaptive Kernel Estimator

- **Minimal permitted load** – minimal load permitted by the user, which is generated after estimating PDF. This value is used for a subjective choice of bandwidth and for a final choice of bandwidth instead of investigated distance. This value directly indicates the minimal value on x-axis as well as on the y-axis of the estimated PDF. Therefore, it should be set proportionally smaller than the minimal load obtained by the measurement for a particular flight phase.

- **<u>Maximal permitted load</u>** – maximal load permitted by the user. It has the same meaning as the minimal permitted load. It directly indicates the maximal value on x-axis as well as on the y-axis of the estimated PDF. Therefore, it should be set proportionally higher than the maximal load obtained by the measurement for a particular flight phase.

To estimate PDF of detected cycles properly, an optimal bandwidth must be selected. Bandwidth selection is performed in altogether two steps. Firstly, an initial value of bandwidth is recommended by an algorithm for an automatic choice. However, because the automatic choice does not always provide an optimal value, subjective choice of bandwidth must follow.

Summary of all parameters mentioned above is made in the following tables.

	EXTRAPOLATION		
Number of flights to be generated	N_FL	[FL]	30000
Automatic bandwidth selection method	ITER_METHOD	[-]	LSCV
Kernel function	KERNEL	[-]	NORM
Reduction factor for an automatic choice of bandwidth	RED_FACT	[-]	2
Overrun	OVERRUN	[-]	3
Precision of an automatic bandwidth selection	PRECISION	[-]	1.00E-03
Maximal permissible bandwidth	BDWH_MAX	[% dL]	0.3
Minimal permissible bandwidth	BDWH_MIN	[% dL]	0.001
From-to matrix roughness	ROUGHNESS	[-]	5
Investigated distance	INVSTG_DIST	[B]	5
Sensitivity factor	ALFA	[-]	0.5

Table 4.12 – Parameters from PARAM spreadsheet for PDF estimation

	PDF ESTIMATION	
Minimal permitted load	MIN	
Maximal permitted load	MAX	

Table 4.13 – Parameters for PDF estimation – description

4.4.1 Automatic choice

The purpose of the automatic choice of bandwidth is to provide an initial value, recommended by the Least square cross validation procedure for the kernel estimator with constant bandwidth.

Automatic bandwidth selection is initiated by calling the script OSP.m. The flowchart of the procedure is shown in Figure 4.12.

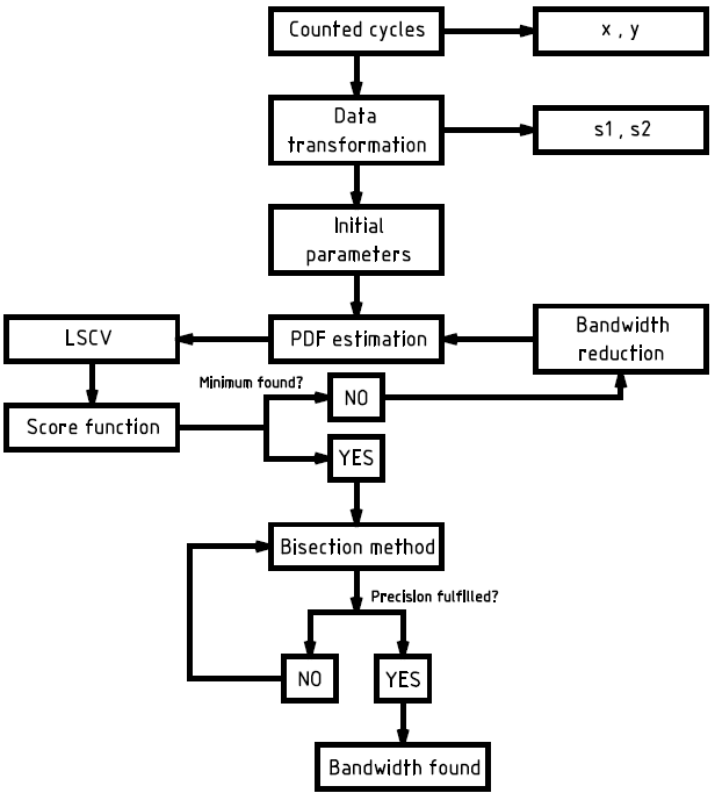

Figure 4.12 – Flowchart of an automatic bandwidth selection

First of all, detected cycles obtained by the cycle counting procedure are loaded. They are in a form of a from-to matrix, which means, that x-variable represents the starting load level and y-variable represents target level of the cycle.

As stated in chapter 3.7.1, it is desirable to pre-scale the multivariate data before estimating their PDF by radially symmetric kernel function. Such scaling is made in the main coordinate system:

- Center of data is translated into the point $[0,0]$ using parameters $\Delta x_T, \Delta y_T$:

$$\Delta x_T = \frac{\sum_{i=1}^{n} x_i}{n_x}$$

$$\Delta y_T = \frac{\sum_{i=1}^{n} y_i}{n_y}$$

$$x_T = x - \Delta x_T$$

$$y_T = y - \Delta y_T$$

- Deviation moment of the data is reduced to zero by rotating the translated coordinates x_T, y_T by an angle φ. Main coordinates x_0, y_0 are therefore obtained:

$$J_{xT} = \frac{\sum_{i=1}^{n} {y_{Ti}}^2}{n_y}$$

$$J_{yT} = \frac{\sum_{i=1}^{n} {x_{Ti}}^2}{n_x}$$

$$D_{xTyT} = \frac{\sum_{i=1}^{n} x_{Ti} \cdot y_{Ti}}{n}$$

$$\varphi = \frac{1}{2} \cdot \tan^{-1} \frac{2 \cdot D_{xTyT}}{J_{yT} - J_{xT}}$$

$$x_0 = x_T \cdot cos\,\varphi + y_T \cdot sin\,\varphi$$

$$y_0 = y_T \cdot cos\,\varphi - x_T \cdot sin\,\varphi$$

- To obtain the same load ranges in both main directions x_0, y_0, the x_0 coordinates are scaled, which provides s_1, s_2 coordinates:

$$SF = \frac{max\{y_{0i}\} - min\{y_{0i}\}}{max\{x_{0i}\} - min\{x_{0i}\}}$$

$$s_1 = min\{y_{0i}\} + (x_0 - min\{x_{0i}\}) \cdot SF$$

$$s_2 = \mathrm{y}_0$$

In the case of an automatic bandwidth selection, variables s_1 and s_2 are analysed separately. As if they were two different univariate data sets. An optimal bandwidth in the sense of minimizing MISE is found for each of them. The bandwidth recommended for further analysis of bivariate data is set equal to greater from both values. Such choice guarantees, that data in any direction shall not be under-smoothed.

Scaling of counted cycles for take-off flight phase can be seen in figures below. The rest of flight phases are transformed in the same way.

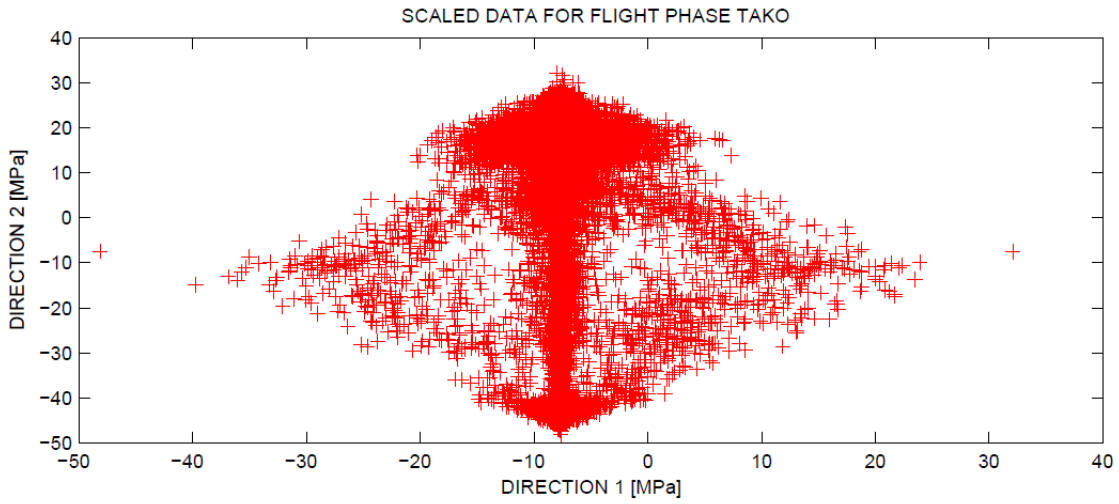

Figure 4.13 – Scatter plot of scaled data for TAKO

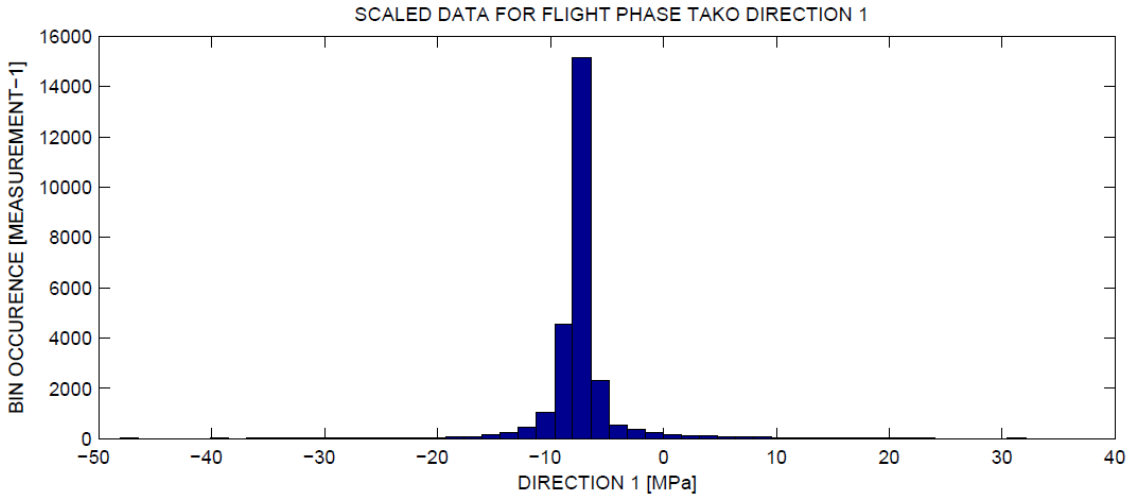

Figure 4.14 – Histogram of scaled data for TAKO – direction n°1

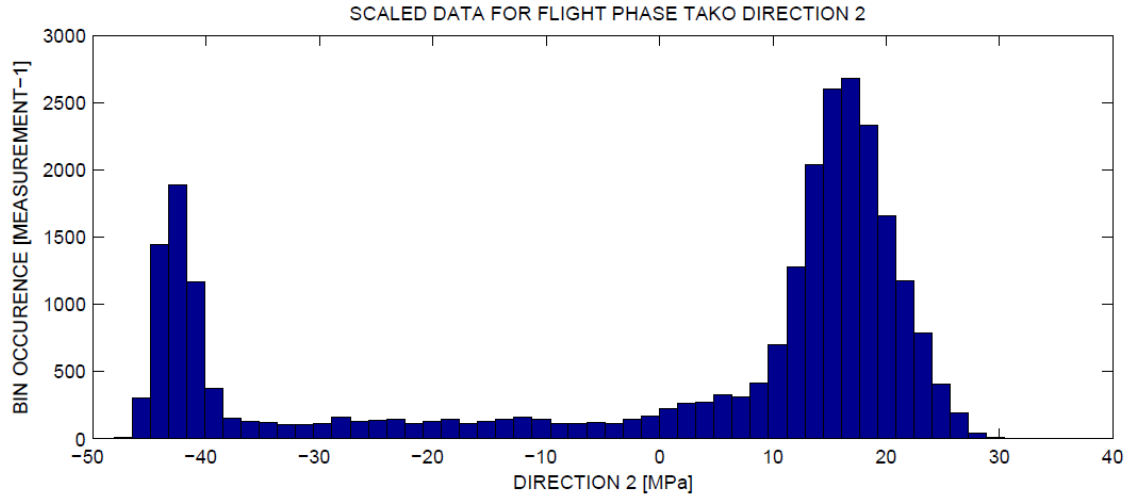

Figure 4.15 – Histogram of scaled data for TAKO – direction n°2

After data transformation, a score function M_0 is computed till its minimum is reached. After that, the bandwidth of desired precision is found by applying the bisection method. Resulting relationship between the score function M_0 and the bandwidth h for each direction of data corresponding to take-off flight phase is shown in Figure 4.16 and Figure 4.17.

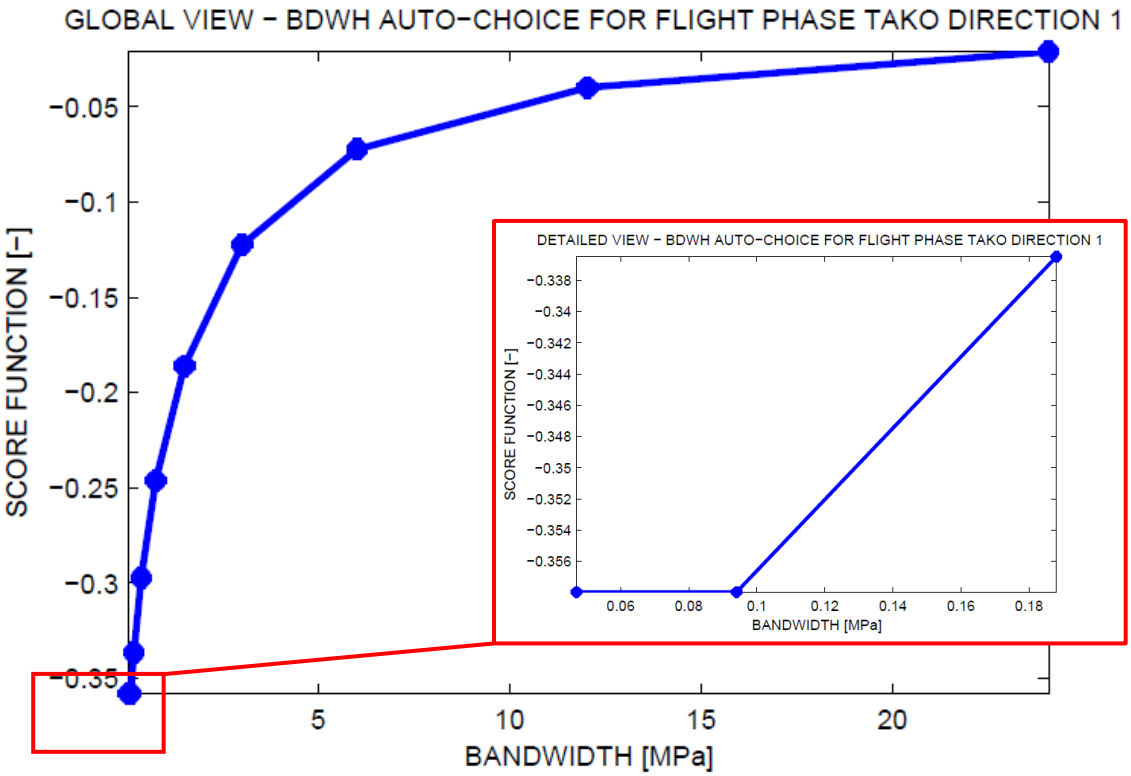

Figure 4.16 – Score function $M_0 = f(h)$ for TAKO – direction n°1

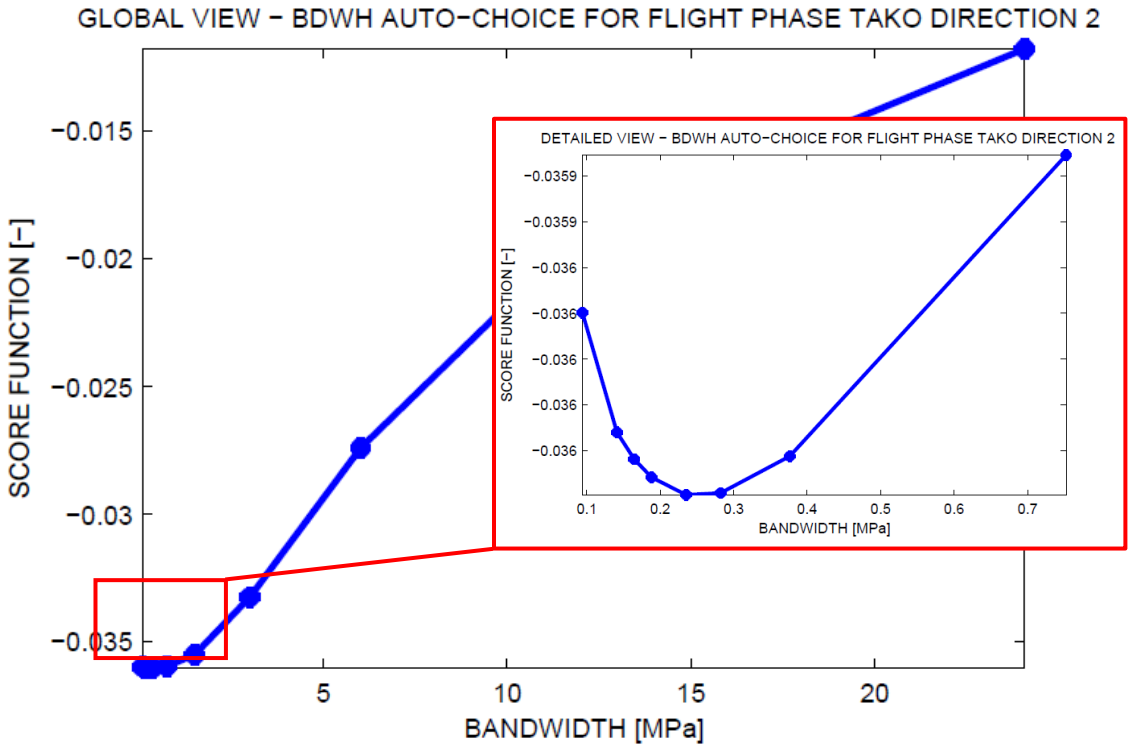

Figure 4.17 –Score function $M_0 = f(h)$ for TAKO – direction n°2

It can be seen, that an optimal bandwidth was not properly established for direction n°1, because the minimum of the score function M_0 was not found. Therefore, the recommended bandwidth was set equal to the user-defined minimal permitted value.

An output of the automatic choice of bandwidth for particular flight phase is shown in Table 4.15 to Table 4.17.

	AUTOMATIC BANDWIDTH SELECTION	
Name of file containg score function for direction n°1 →	DIR 01 FN	
Name of file containg score function for direction n°2 →	DIR 02 FN	
Number of bandwidths analysed for direction n°1 →	N_01 [-]	
Number of bandwidths analysed for direction n°2 →	N_02 [-]	
Automatically chosen bandwidth for direction n°1 →	H_OPT_01	
Automatically chosen bandwidth for direction n°2 →	H_OPT_02	

Table 4.14 – Automatic choice output summary – description

AUTOMATIC BANDWIDTH SELECTION	
DIR 01 FN	TAKO\SLOT_NO_334_BDWH_AC_1_PHASE_TAKO
DIR 02 FN	TAKO\SLOT_NO_334_BDWH_AC_2_PHASE_TAKO
N_01 [-]	10
N_02 [-]	15
H_OPT_01	0.080
H_OPT_02	0.235

Table 4.15 – Automatic choice output summary – TAKO

AUTOMATIC BANDWIDTH SELECTION	
DIR 01 FN	APP\SLOT_NO_334_BDWH_AC_1_PHASE_APP
DIR 02 FN	APP\SLOT_NO_334_BDWH_AC_2_PHASE_APP
N_01 [-]	10
N_02 [-]	22
H_OPT_01	0.031
H_OPT_02	0.317

Table 4.16 – Automatic choice output summary – APP

AUTOMATIC BANDWIDTH SELECTION	
DIR 01 FN	LNG\SLOT_NO_334_BDWH_AC_1_PHASE_LNG
DIR 02 FN	LNG\SLOT_NO_334_BDWH_AC_2_PHASE_LNG
N_01 [-]	10
N_02 [-]	16
H_OPT_01	0.070
H_OPT_02	0.654

Table 4.17 – Automatic choice output summary – LNG

4.4.2 Subjective choice

PDF estimate using bandwidth, which was recommended by the procedure of an automatic bandwidth selection, might not always be the best choice from data extrapolation point of view. Therefore, it is up to the user to define bandwidth which will be used for the final PDF estimate. Generally speaking, it is better to work with a little over-smoothed PDF than with under-smoothed one, because it is impossible to regenerate cycles different from those obtained by the in-flight measurement with a heavily under-smoothed PDF.

From the user's point of view, it is necessary to define criterion, which would designate, that the PDF estimation might be assumed as sufficient enough for cycle extrapolation.

Literature [12] suggests to construct a cumulative frequency distribution (cumulative exceedance diagram) based on a short-term measurement and then to extrapolate the detected cycles to the target life by shifting the short-term spectrum by an extrapolation factor k_{ext} and fitting and projecting the data curve to the upper left corner for higher load estimates. However, it is necessary to reduce the rain-flow cycle count into a simple frequency histogram prior to data extrapolation, by applying any of the mean stress correction methods. As a consequence, an information about the mean load level is lost.

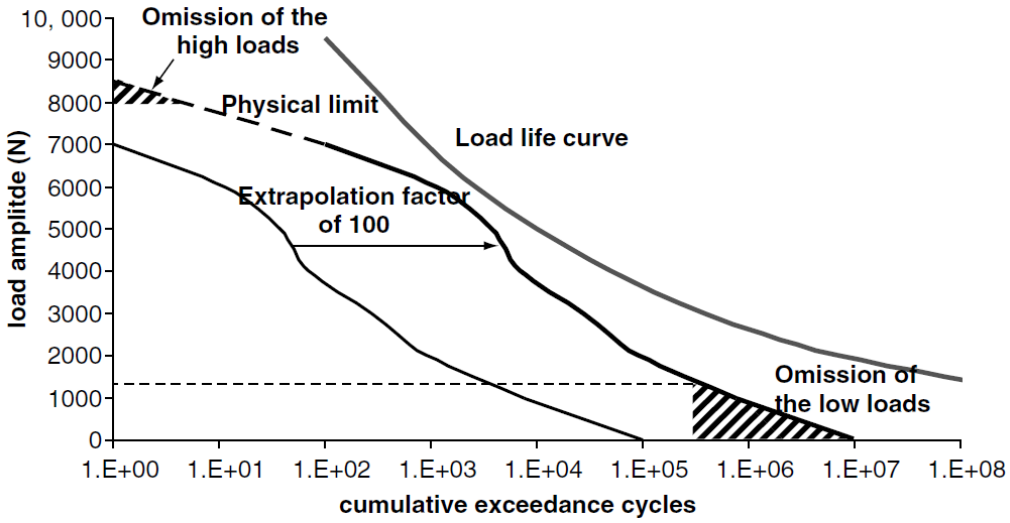

Figure 4.18 – Cycle extrapolation using cumulative exceedance diagram [12]

The proposed procedure of a subjective choice is based on estimating PDFs for various bandwidths and comparing obtained results. For each bandwidth, the following characteristics are determined:

- PDF estimation using user-defined bandwidth
- Determination of fatigue damage matrix
- Production of cumulative exceedance diagram
- Overall fatigue damage

The generated characteristics shall provide all necessary information to decide which bandwidth is the most suitable for cycle extrapolation.

PDF estimation might be performed using CKE or AKE method, based on user's selection. It was suggested in chapter 3.7.4 to use the same bandwidth for the pilot estimate as well as for the final PDF estimate when using AKE method. However, the procedure enables the user to enter different bandwidths for the pilot and the final estimate.

The estimated PDF is normalized to meet the following condition:

$$\sum_{i=1}^{n_x}\sum_{j=1}^{n_y} PDF_{i,j} = 1$$

For each estimated PDF, the fatigue damage per flight is derived from the fatigue damage matrix by summing all local damages:

$$D = n_{FL} \cdot \overline{D} = n_{FL} \cdot \sum_{i=1}^{n_x}\sum_{j=1}^{n_y} D_{i,j}$$

Where:

n_x	number of data points on x-axis
n_y	number of data points on y-axis
$n_{FL} = n_{cc} \cdot \frac{t_{TFP}}{t_{org}}$	overall number of cycles per flight
$D_{i,j} = \overline{D} \cdot PDF_{i,j}$	fatigue damage matrix - local damages relevant to $PDF_{i,j}$

The cumulative exceedance diagram relevant to target life N_{tgt} is determined by two means:

a) Multiplying of already derived cumulative exceedance diagram relevant to measurement length by an extrapolation factor k_{ext}:

$$k_{ext} = \frac{t_{TFP}}{t_{org}} \cdot N_{tgt}$$

b) From PDF estimate by applying user-defined mean stress correction method and multiplying by the number of cycles per target life n_{tgt}:

$$n_{tgt} = n_{FL} \cdot N_{tgt} = n_{cc} \cdot \frac{t_{TFP}}{t_{org}} \cdot N_{tgt}$$

Where:

n_{FL}	Overall number of loading cycles per flight
n_{cc}	Overall number of cycles detected in the particular flight phase of the in-flight measurement

It is up to the user to choose several bandwidths for detailed analysis and enter them into TAKO, APP and LNG spreadsheets, as shown in Table 4.19. The user specifies the PDF method used for detailed analysis (CKE/AKE method) as well. In the case of AKE method, the third column correspond to the bandwidth which is used for the pilot estimate. In the case of CKE method, the third column is not applied. At the same time, the user shall specify an appropriate minimal and maximal permitted load (see Table 4.13)

Table 4.18 shows the input parameters as well as corresponding fatigue damages for take-off flight phase using CKE method.

SUBJECTIVE BANDWIDTH SELECTION			FD [FL-1]	dFD [%]
N_DISP	6	CKE		
H_DISP_01	4		6.261E-06	119.23%
H_DISP_02	2		3.438E-06	20.38%
H_DISP_03	1.5		3.157E-06	10.53%
H_DISP_04	1		2.98E-06	4.35%
H_DISP_05	0.75		2.924E-06	2.37%
H_DISP_06	0.5		2.885E-06	1.03%

PDF ESTIMATION	
MIN	-10
MAX	70

Table 4.18 – Input and output parameters for a subjective choice of bandwidth for CKE method – TAKO

Detailed analysis providing all necessary characteristics for subjective choice of bandwidth is initiated by calling the script PDF_DISPLAY.m. Figure 4.19 to Figure 4.36 show results obtained by the use of the CKE method for the take-off flight phase. Extreme loads and bandwidths mentioned in the Table 4.18 have been used.

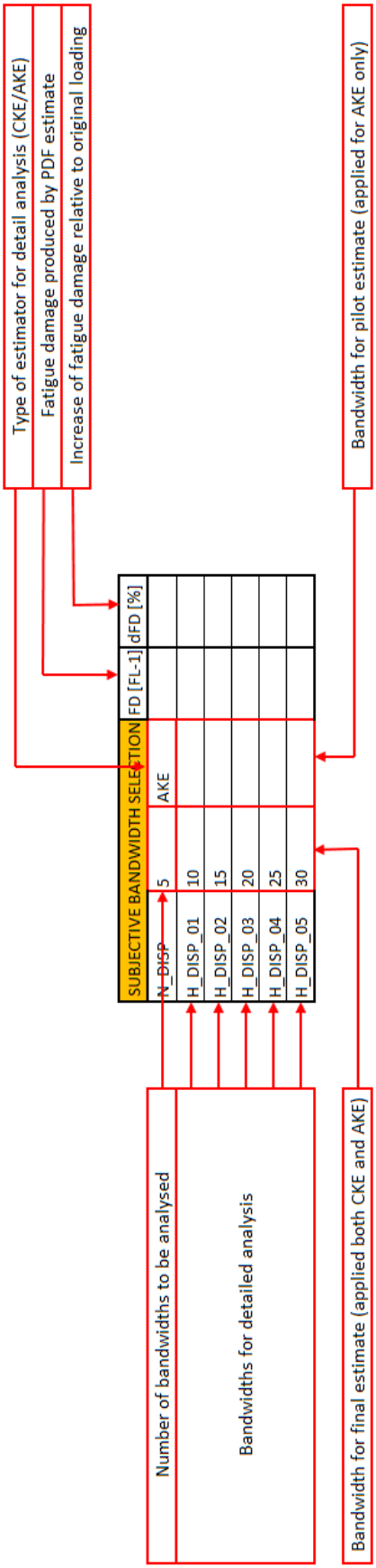

Table 4.19 – Input parameters for subjective choice of bandwidth – description

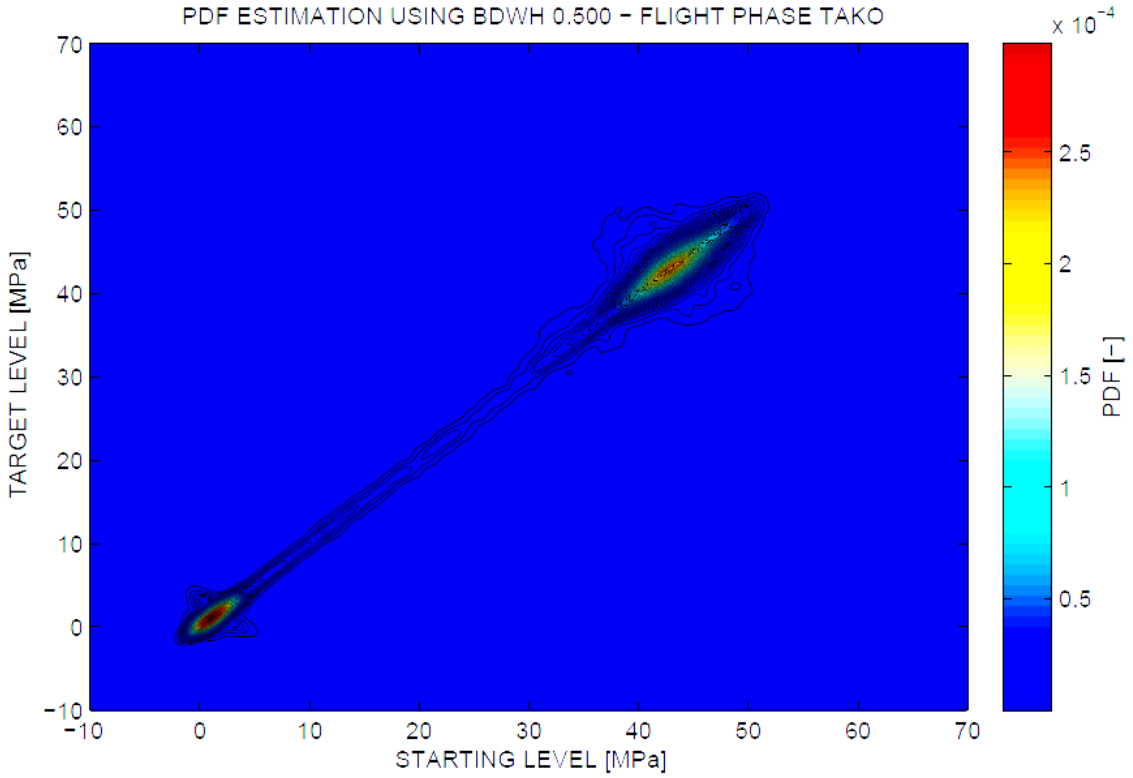

Figure 4.19 – Contour plot of PDF estimate for $h = 0.50\ MPa$

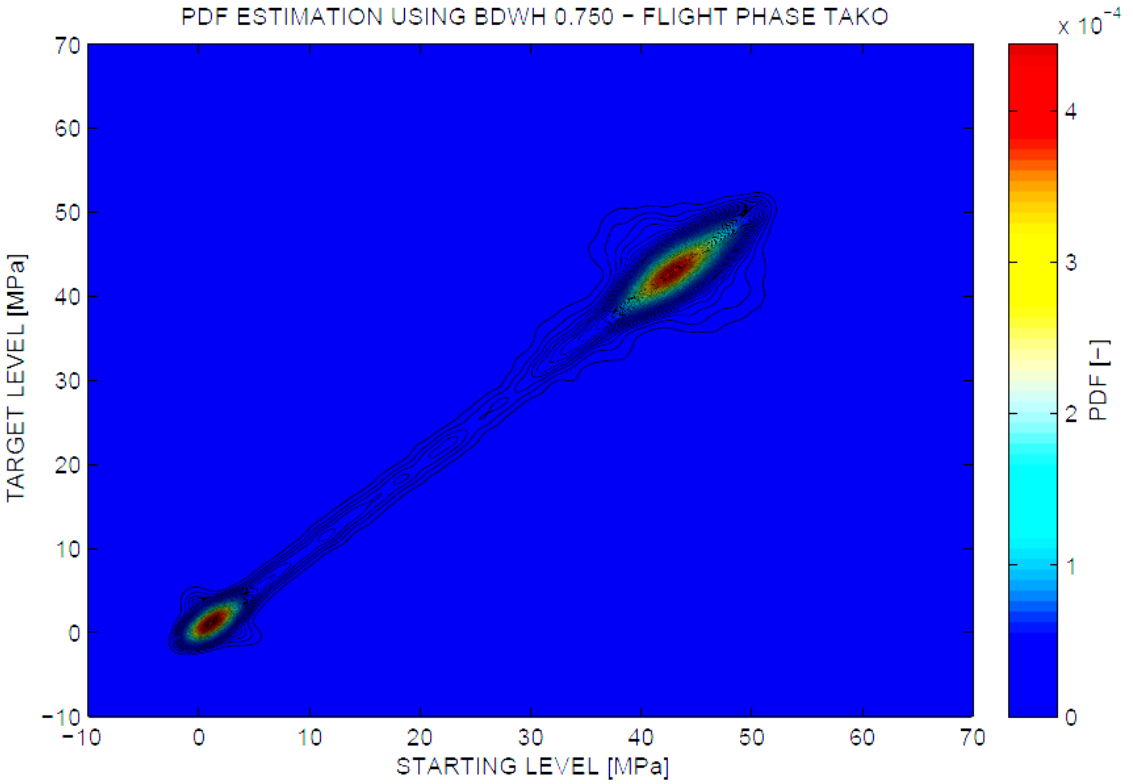

Figure 4.20 – Contour plot of PDF estimate for $h = 0.75\ MPa$

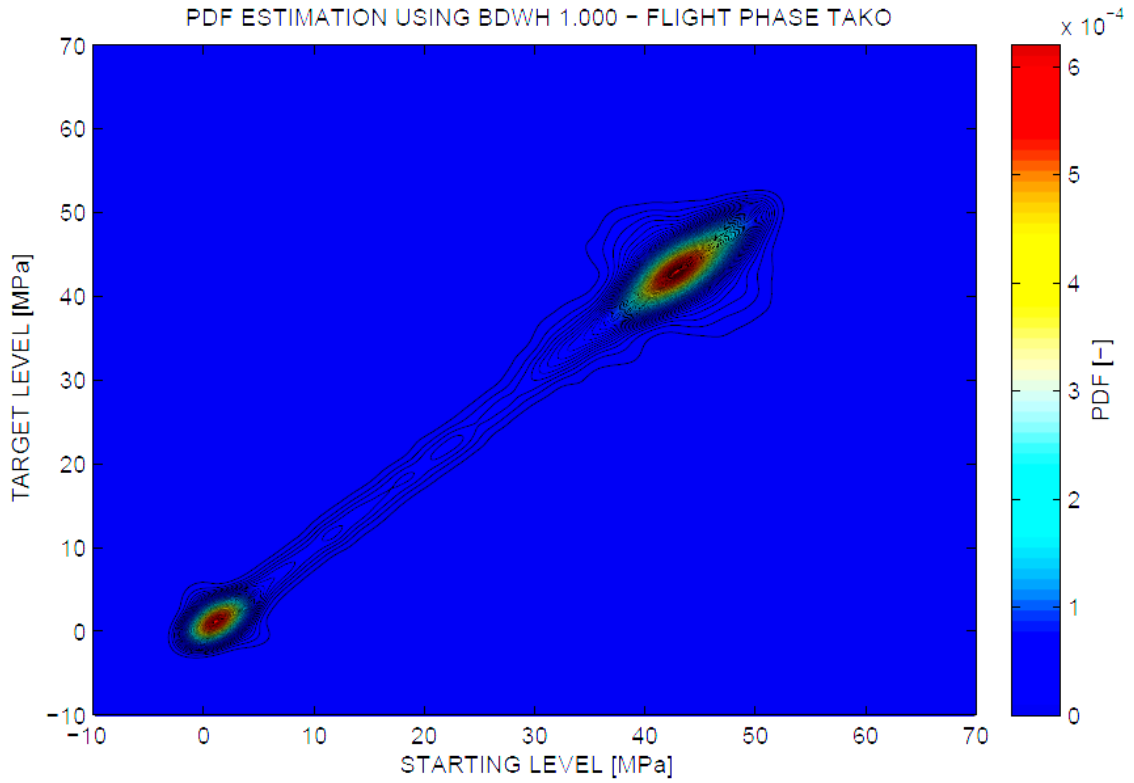

Figure 4.21 – Contour plot of PDF estimate for $h = 1.00\ MPa$

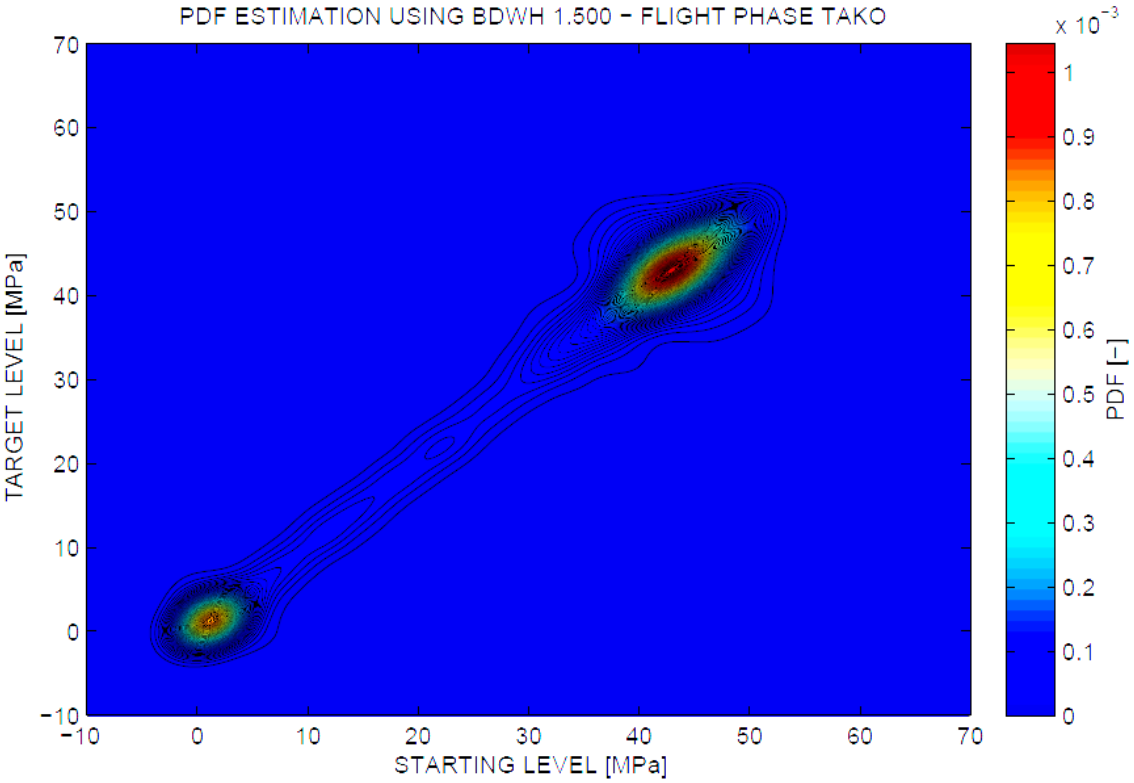

Figure 4.22 – Contour plot of PDF estimate for $h = 1.50\ MPa$

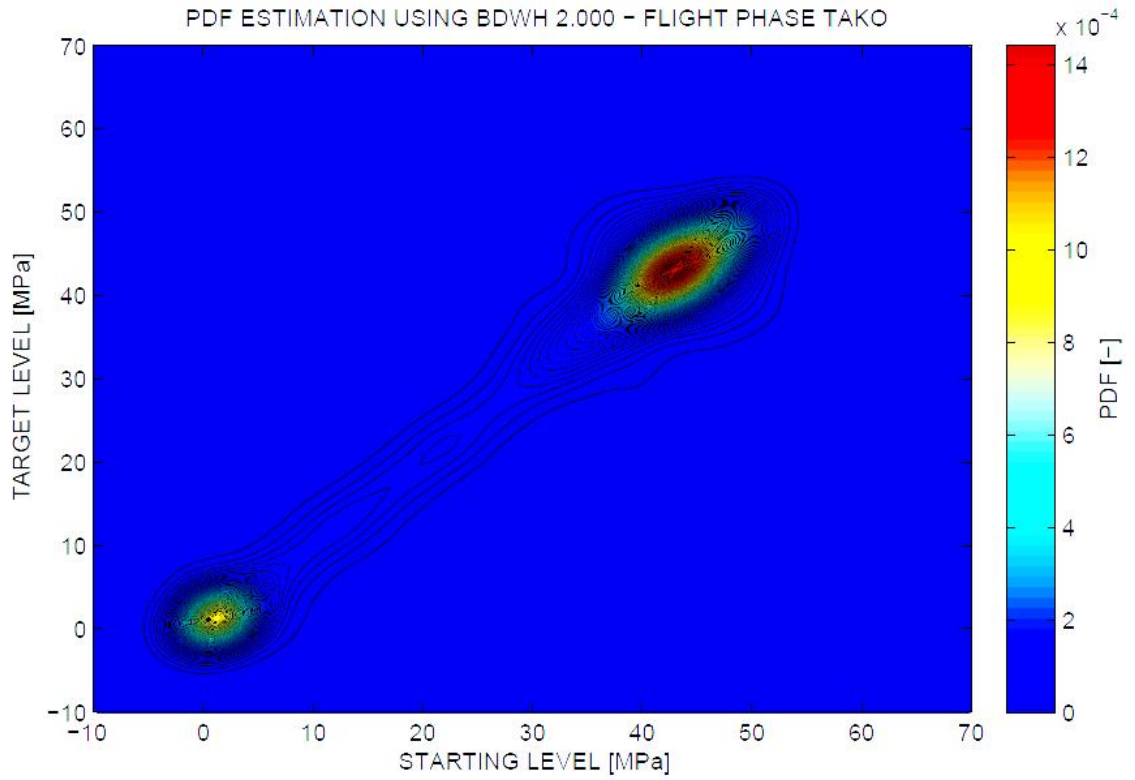

Figure 4.23 – Contour plot of PDF estimate for $h = 2.00\ MPa$

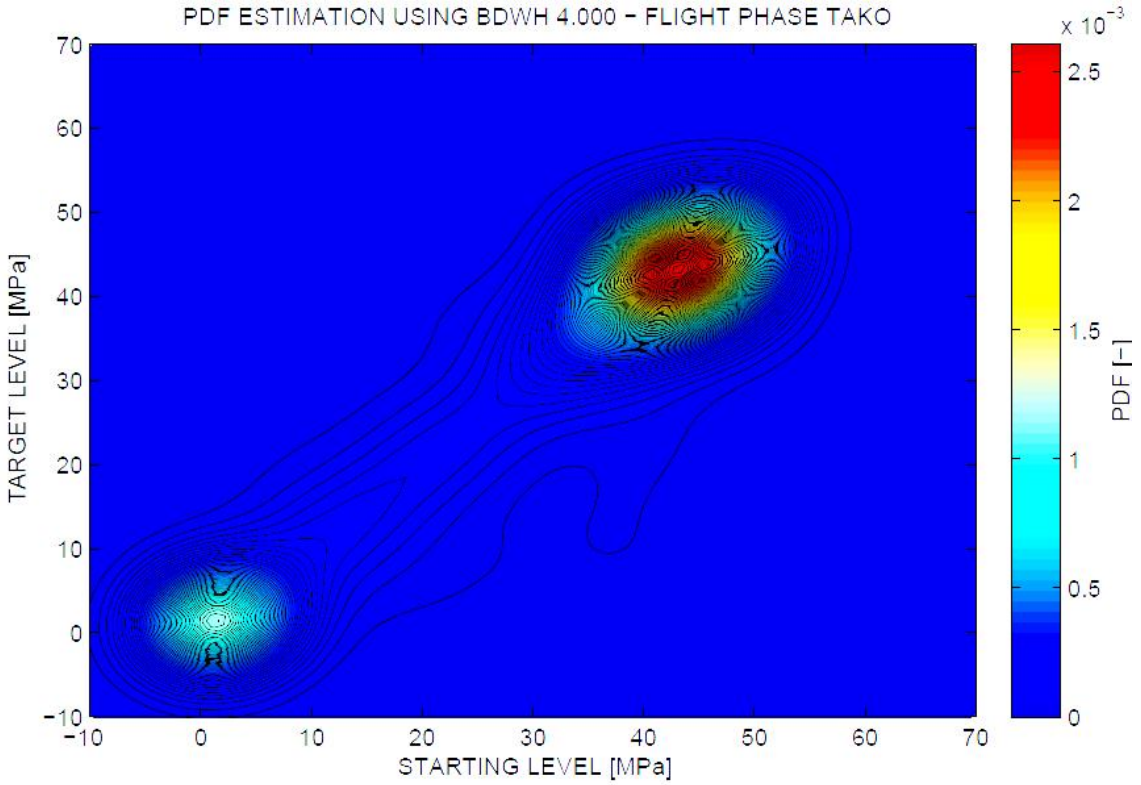

Figure 4.24 – Contour plot of PDF estimate for $h = 4.00\ MPa$

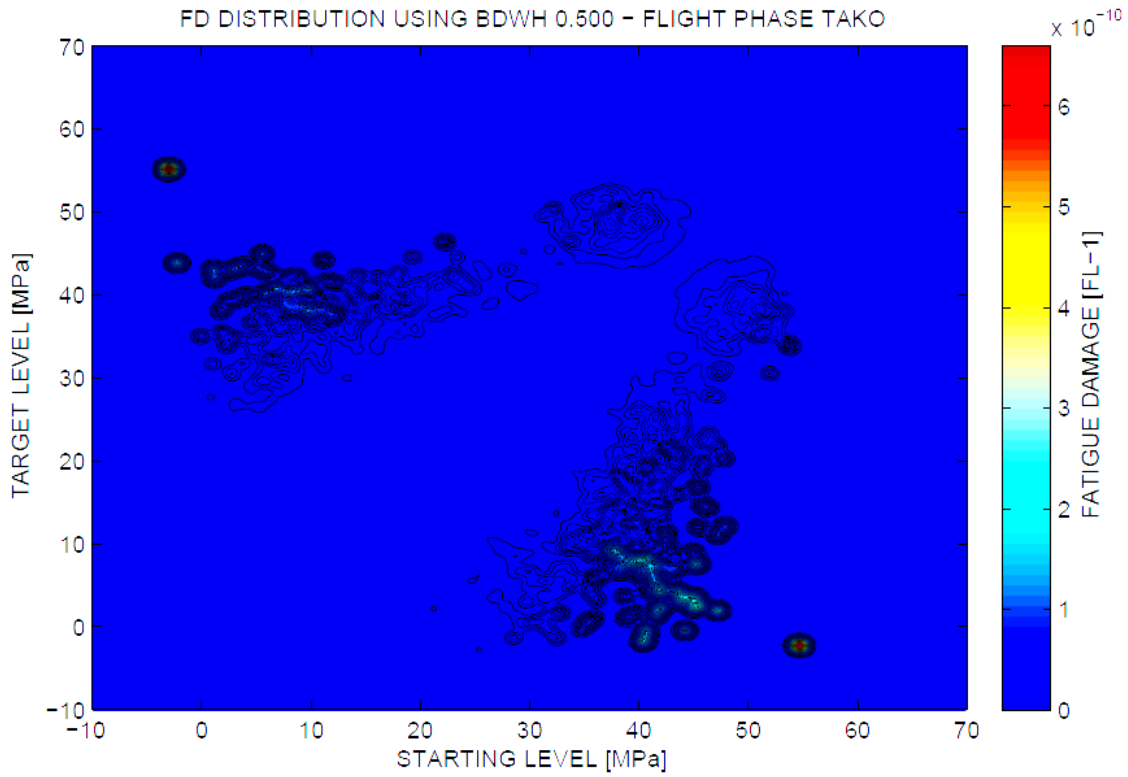

Figure 4.25 – Contour plot of FD distribution for $h = 0.50\ MPa$

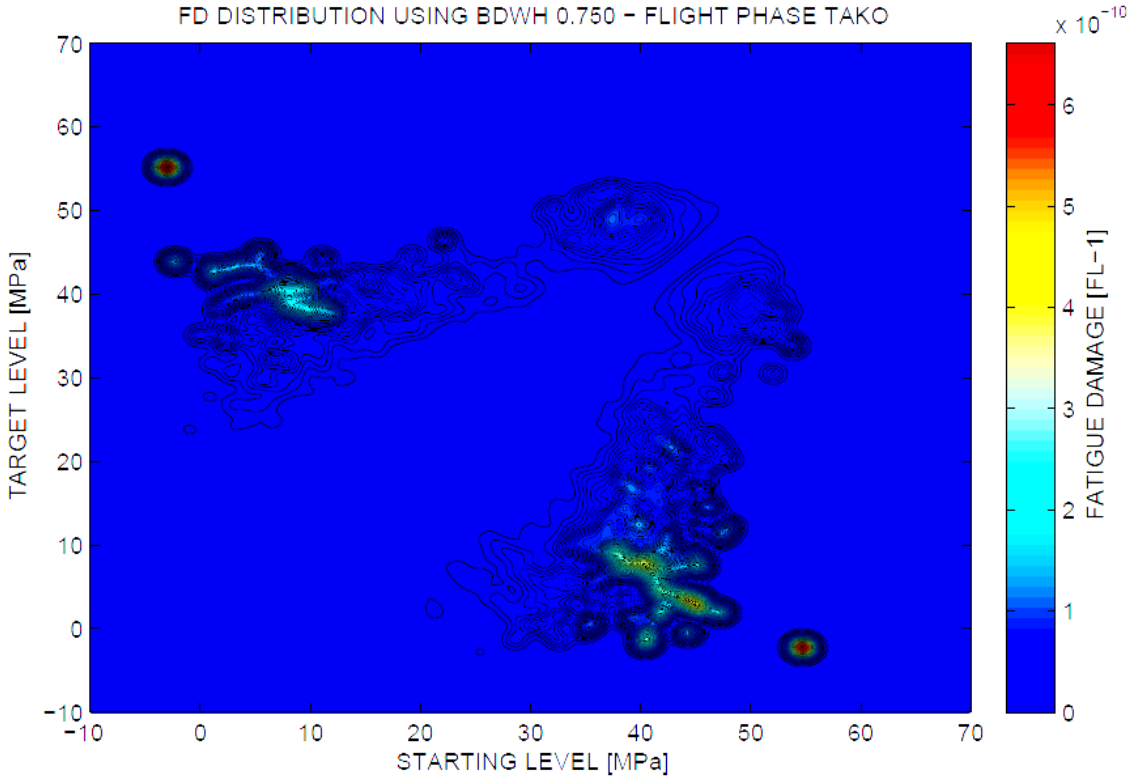

Figure 4.26 – Contour plot of FD distribution for $h = 0.75\ MPa$

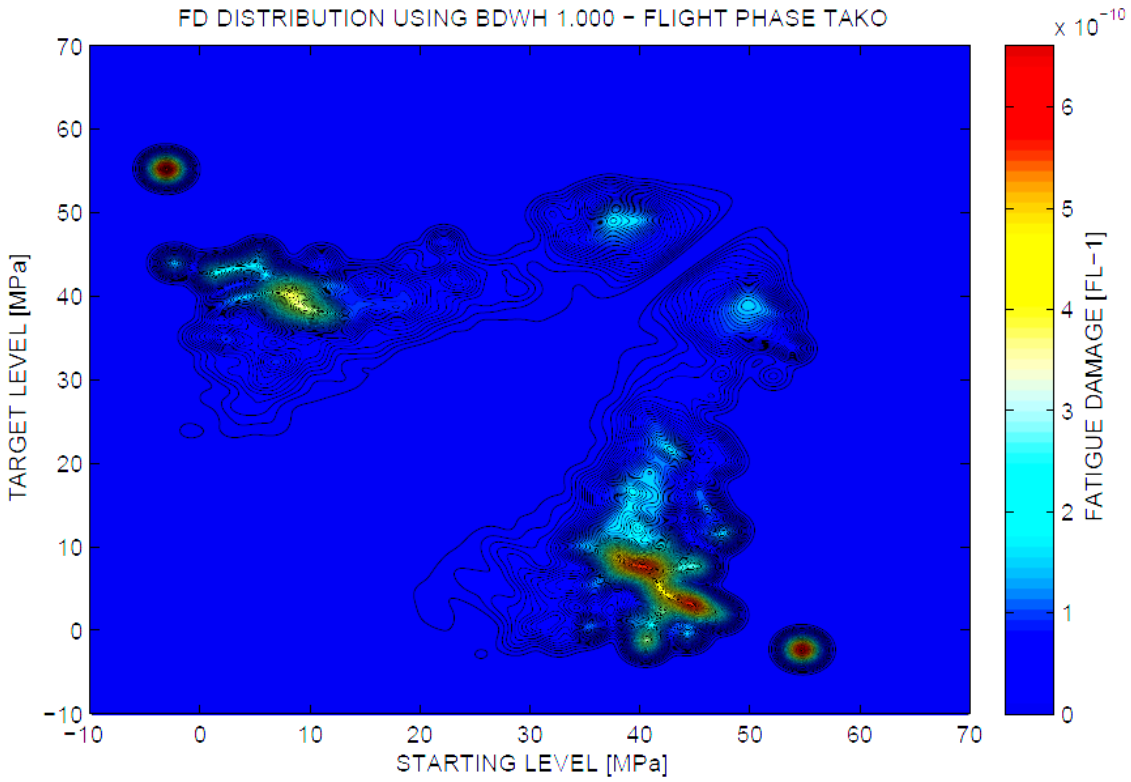

Figure 4.27 – Contour plot of FD distribution for $h = 1.00\ MPa$

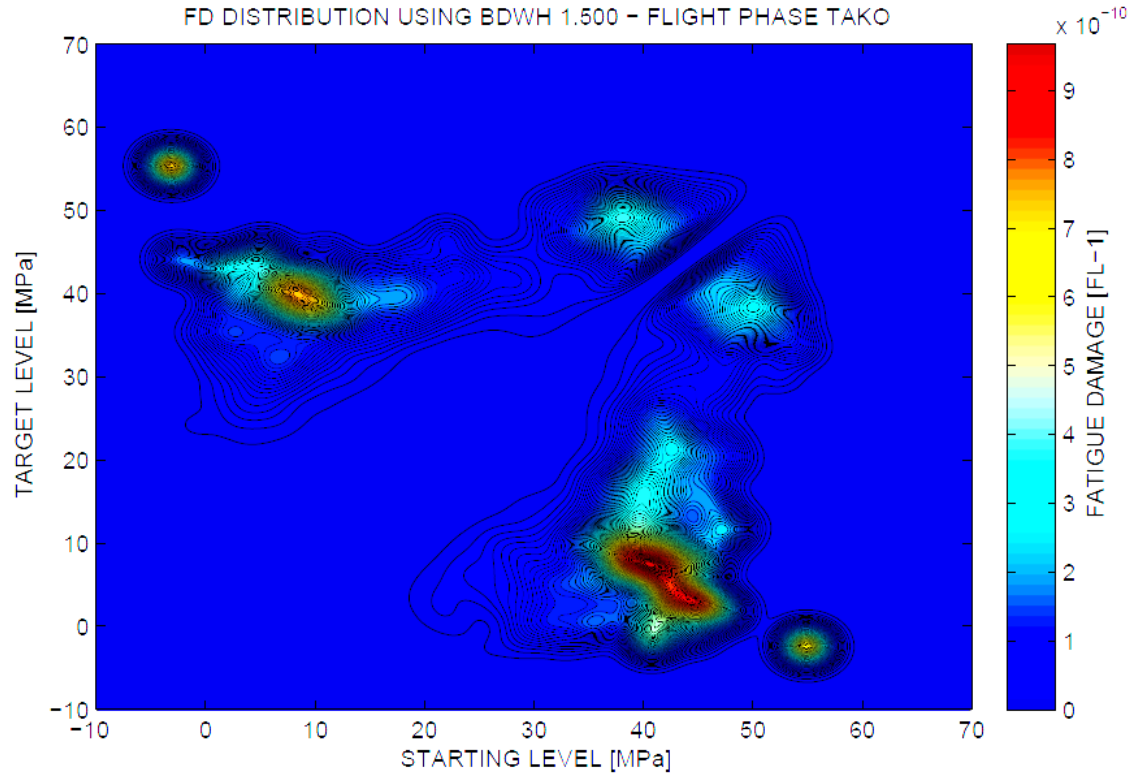

Figure 4.28 – Contour plot of FD distribution for $h = 1.50\ MPa$

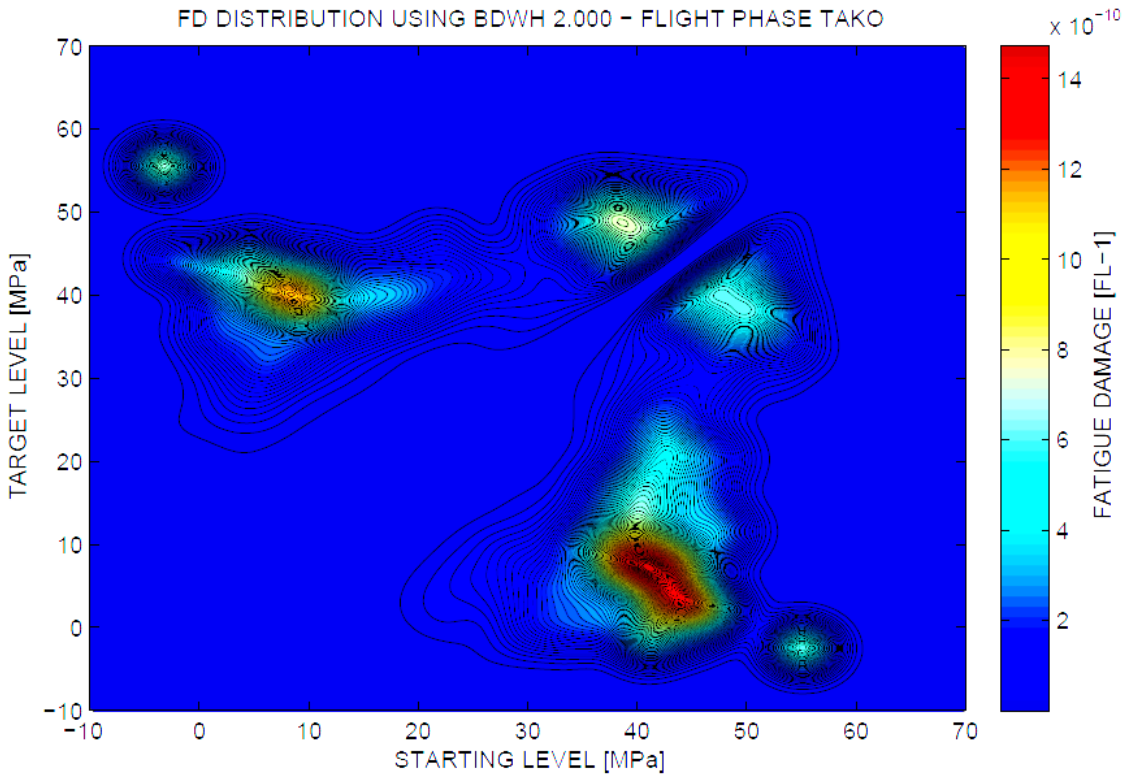

Figure 4.29 – Contour plot of FD distribution for $h = 2.00\ MPa$

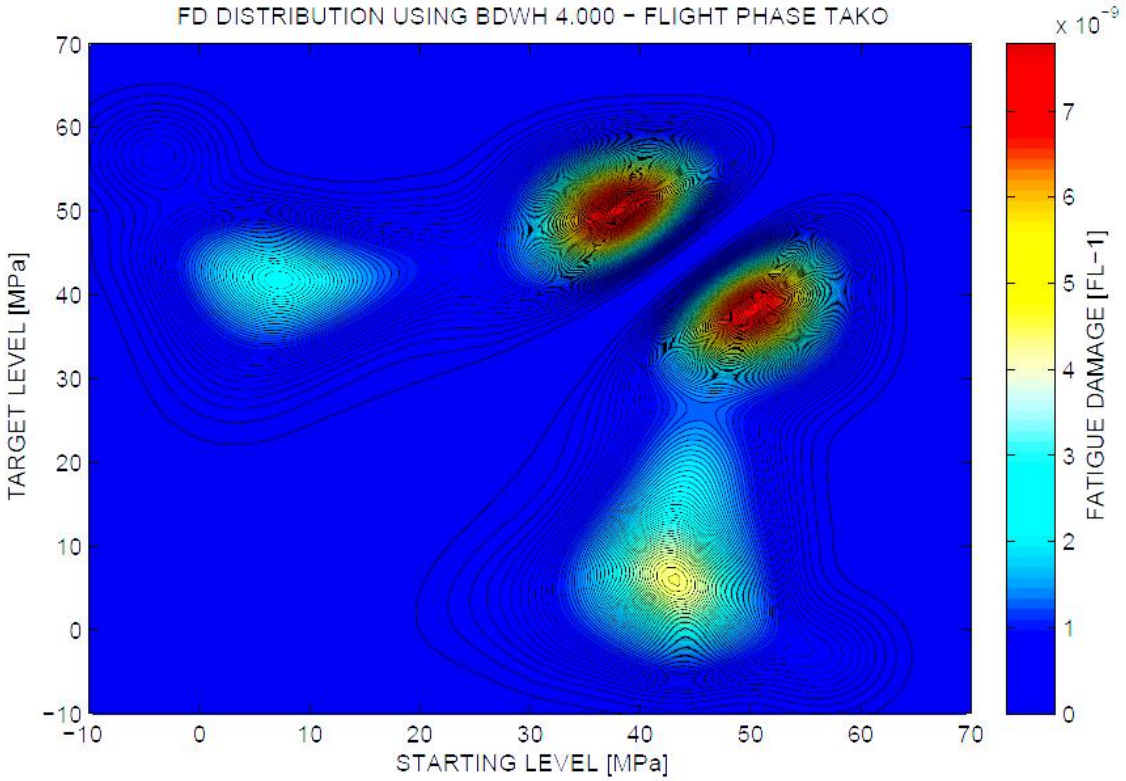

Figure 4.30 – Contour plot of FD distribution for $h = 4.00\ MPa$

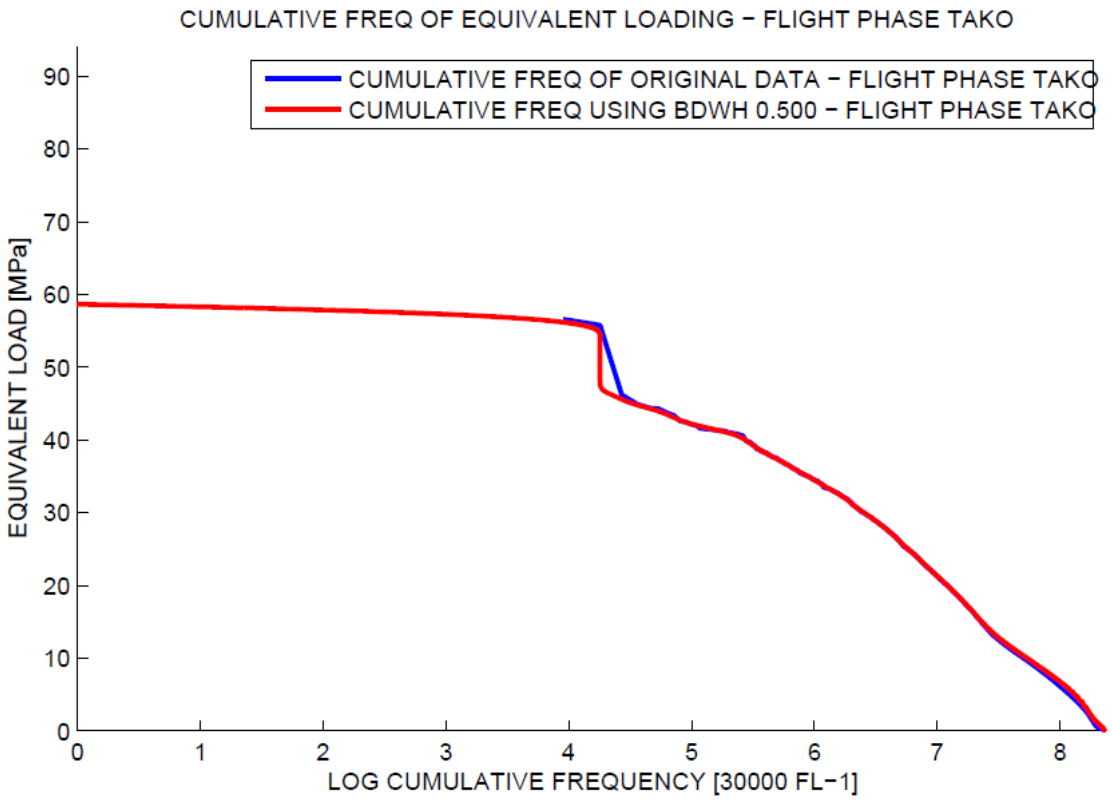

Figure 4.31 – Cumulative exceedance diagram for $h = 0.50\ MPa$

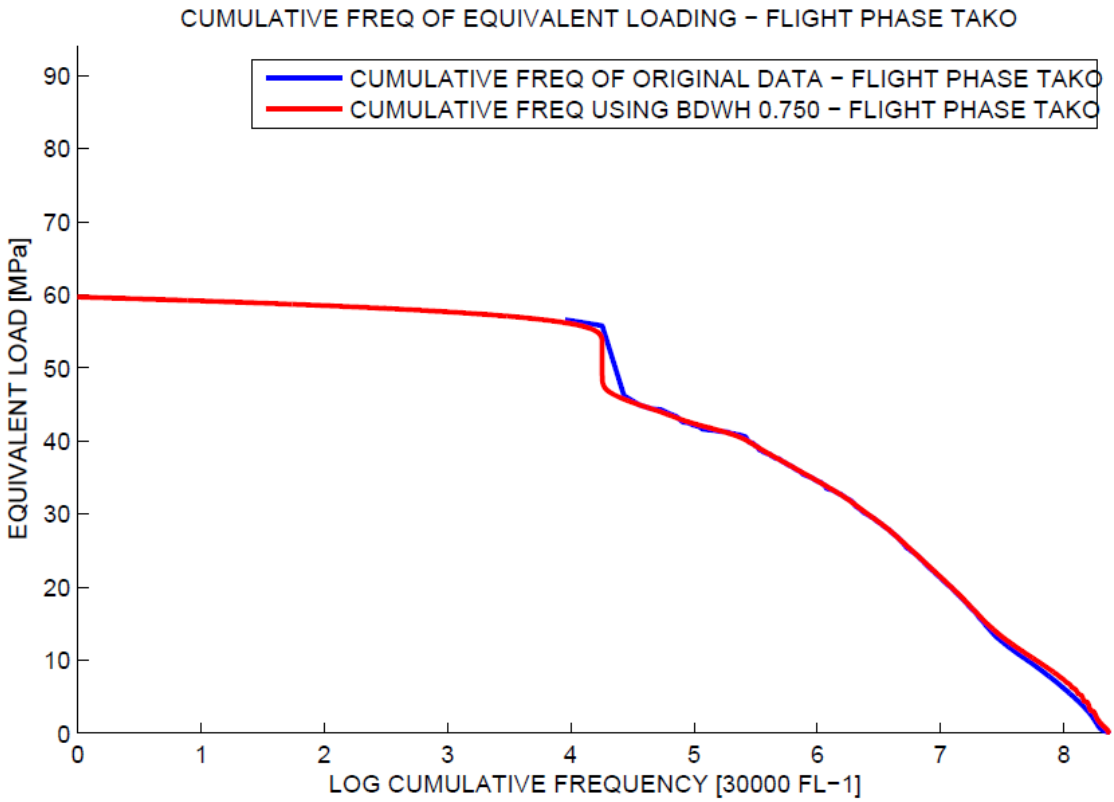

Figure 4.32 – Cumulative exceedance diagram for $h = 0.75\ MPa$

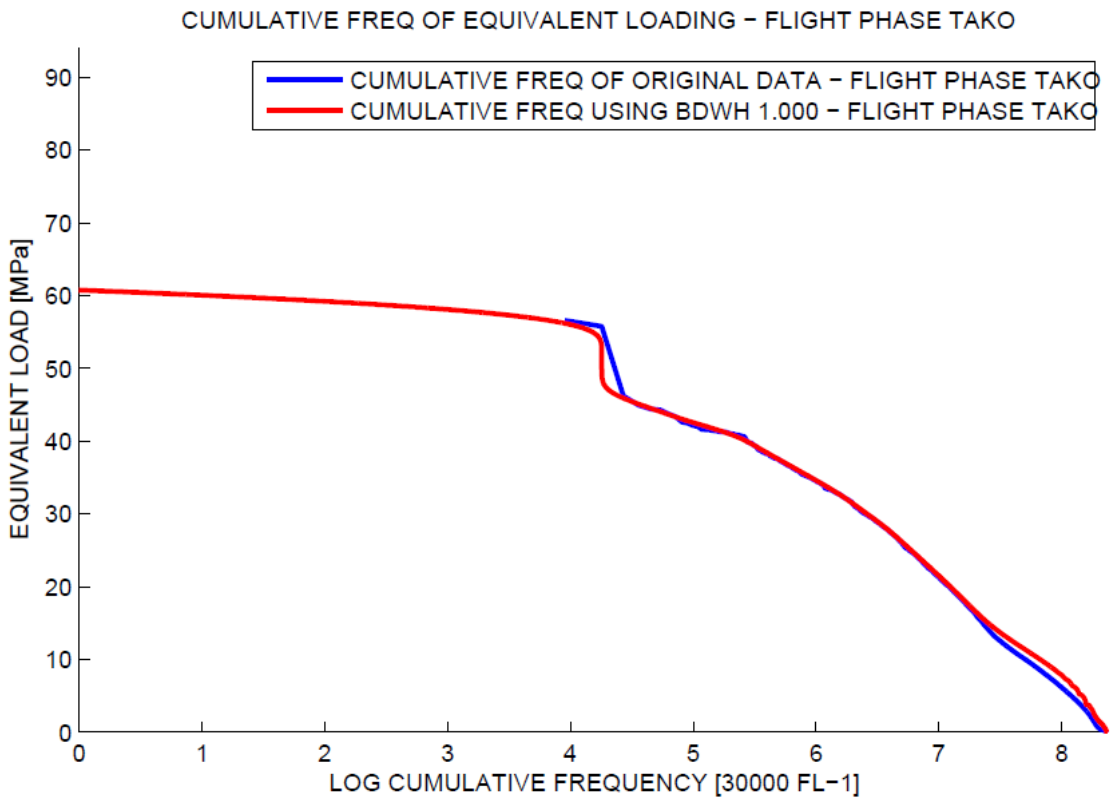

Figure 4.33 – Cumulative exceedance diagram for $h = 1.00\ MPa$

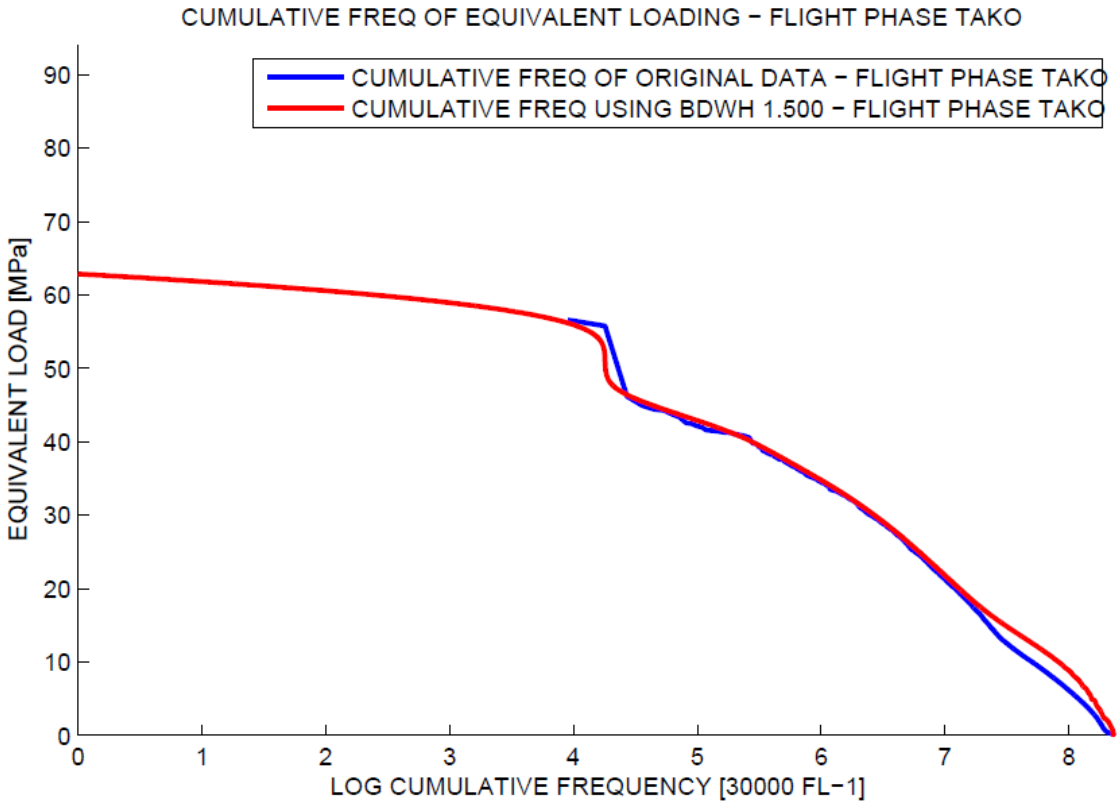

Figure 4.34 – Cumulative exceedance diagram for $h = 1.50\ MPa$

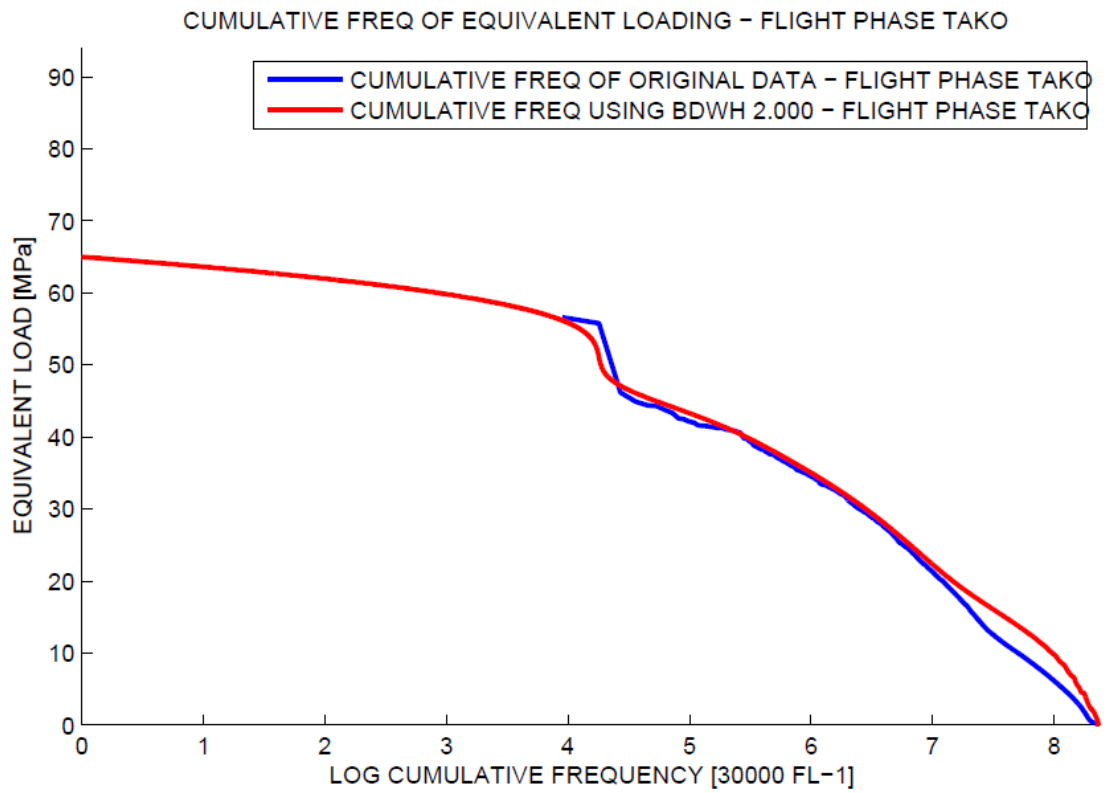

Figure 4.35 – Cumulative exceedance diagram for $h = 2.00\ MPa$

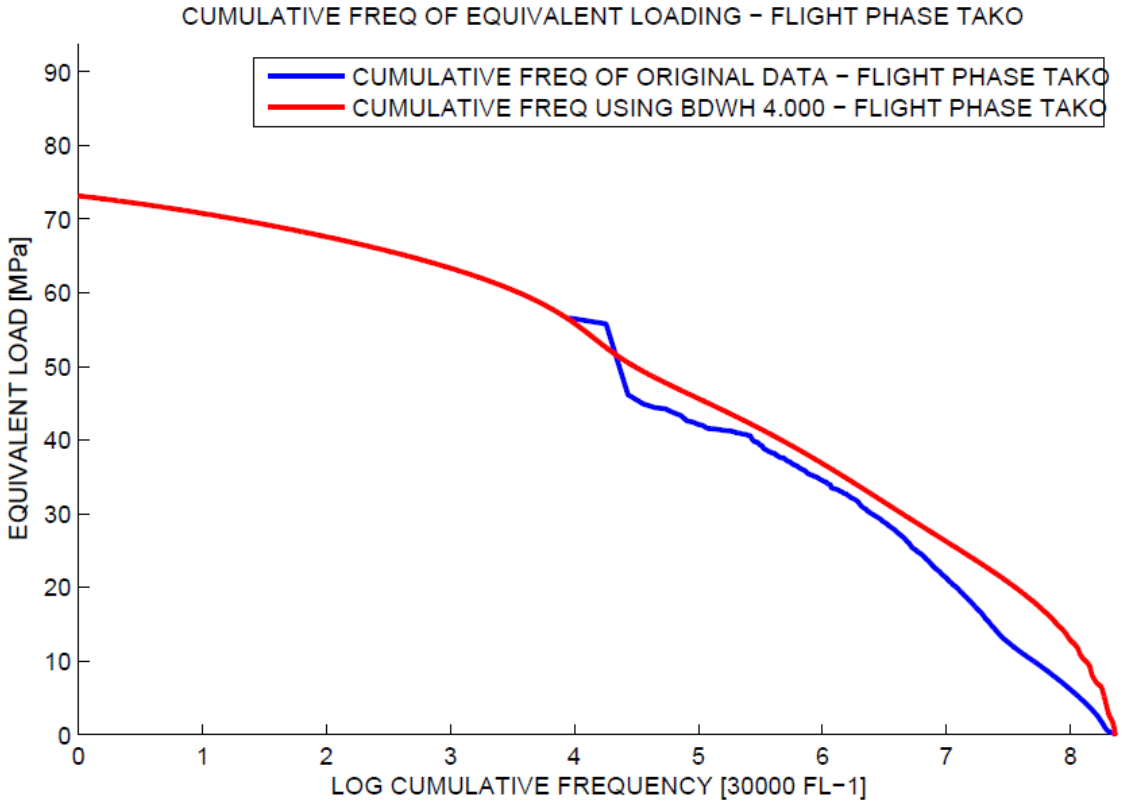

Figure 4.36 – Cumulative exceedance diagram for $h = 4.00\ MPa$

It can be seen, that bandwidth $h = 0.50\ MPa$, which is a higher value than was recommended by an automatic procedure, generates heavily under-smoothed PDF. Such PDF estimate is unacceptable from the cycle extrapolation point of view. On the other hand, PDF estimate produced by CKE with bandwidth $h = 4.00\ MPa$ might be definitely supposed as over-smoothed, because the CED produced from PDF estimate shows a strong deviation from the original CED. Apart from that, fatigue damage distribution changed significantly from the distribution based on PDFs produced by smaller bandwidths. A damaging effect of the basic cycle characterizing the take-off flight phase totally dismissed.

Based on the observation, the general procedure leading to an optimal bandwidth selection was established:

- Increase the bandwidth till the number of peaks in the PDF estimate becomes acceptably small. Too many peaks throughout the PDF is a sign of under-smoothing and is therefore unacceptable.
- Increase the bandwidth till the cumulative exceedance diagram (CED) derived from PDF estimate follows the CED derived from the in-flight measurement in the area of low and moderate amplitude cycles. A significant deviation between CEDs in the area of low and moderate amplitude cycles might be a sign of over-smoothing.
- Isolated “islands” of load cycles with high amplitudes shall not fully dismiss. They usually correspond to envelope cycles of the loading history. Merging of envelope cycles with the rest of the PDF would overestimate the effect of vibrations from the fatigue point of view.
- Growth of fatigue dominant areas with an increasing bandwidth is a natural phenomenon. However, the growth must have its limit. It is unacceptable to permit disappearance of a group of fatigue dominant areas, if it is not replaced by one larger area in their centre.

In line with the established procedure for a subjective choice of an optimal bandwidth, the value $h = 1.50\ MPa$ has been selected for the final PDF estimation of take-off flight phase by using CKE method.

Relationship between the fatigue damage D derived from the PDF estimate obtained by CKE method and corresponding bandwidth h might be seen from the output listed in the excel file AIVIB.xlsx, as shown in Table 4.18.

The PDF estimation using AKE method should be able to describe a long-tail distribution better than CKE method, as already stated in chapter 3.7.1. However, using the same bandwidth for the pilot estimate as well as for the final estimate have not occurred as a reliable way to an optimal PDF estimation. Moreover, in the case of using different bandwidths for the pilot estimate and the final estimate, it becomes tough to find a suitable combination of both parameters.

SUBJECTIVE BANDWIDTH SELECTION			FD [FL-1]	dFD [%]
N_DISP	6	AKE		
H_DISP_01	3	2	6.807E-06	138.33%
H_DISP_02	2	2	1.527E-06	-46.54%
H_DISP_03	1.5	2	7.485E-07	-73.79%
H_DISP_04	1	2	4.459E-07	-84.39%
H_DISP_05	0.75	2	3.833E-07	-86.58%
H_DISP_06	0.5	2	3.53E-07	-87.64%

PDF ESTIMATION	
MIN	-10
MAX	70

Table 4.20 – Input and output parameters for a subjective choice of bandwidth for AKE method – TAKO

Table 4.20 displays the input parameters and resulting fatigue damage of an attempt to estimate PDF for take-off flight phase using constant bandwidth $h = 2.00\ MPa$ for a pilot estimate and various values of bandwidths for the final estimate. The choice of $h = 2\ MPa$ for the pilot estimate comes from the statement mentioned in [22], which claims, that there is not necessary to require some specific smoothness of the pilot estimate to achieve a good result.

Based on the resulting fatigue damage mentioned in Table 4.20 might be stated, that using AKE is much more sensitive to the choice of bandwidth than CKE method. Moreover, contrary to the CKE method, the AKE method does not guarantee, that the conservative result will be obtained. It is quite easy to obtain such PDF estimation by the AKE method which produces lower fatigue damage than the load cycles derived directly from the in-flight measurement.

Figure 4.37 to Figure 4.54 show the contour plots of PDF estimate and FD distribution as well as cumulative exceedance diagrams for take-off flight phase, which were obtained by AKE method in line with parameters mentioned in Table 4.20.

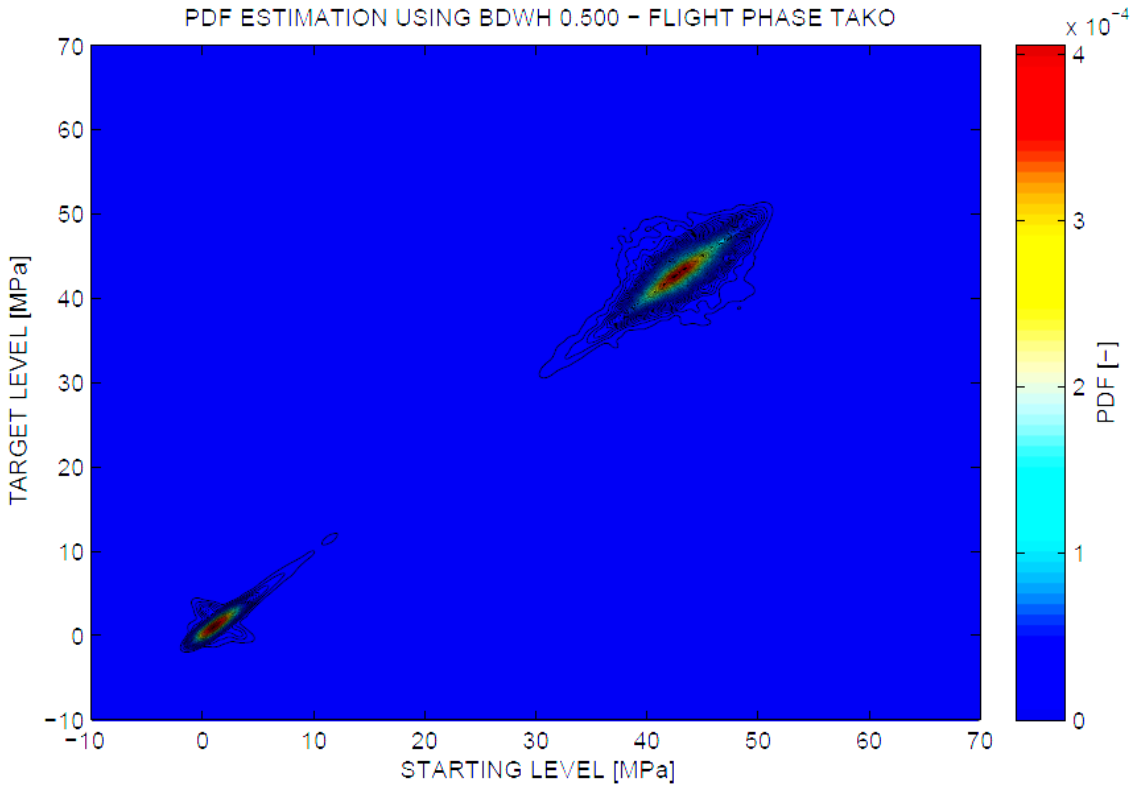

Figure 4.37 – Contour plot of PDF estimate for $h = 0.50\ MPa$

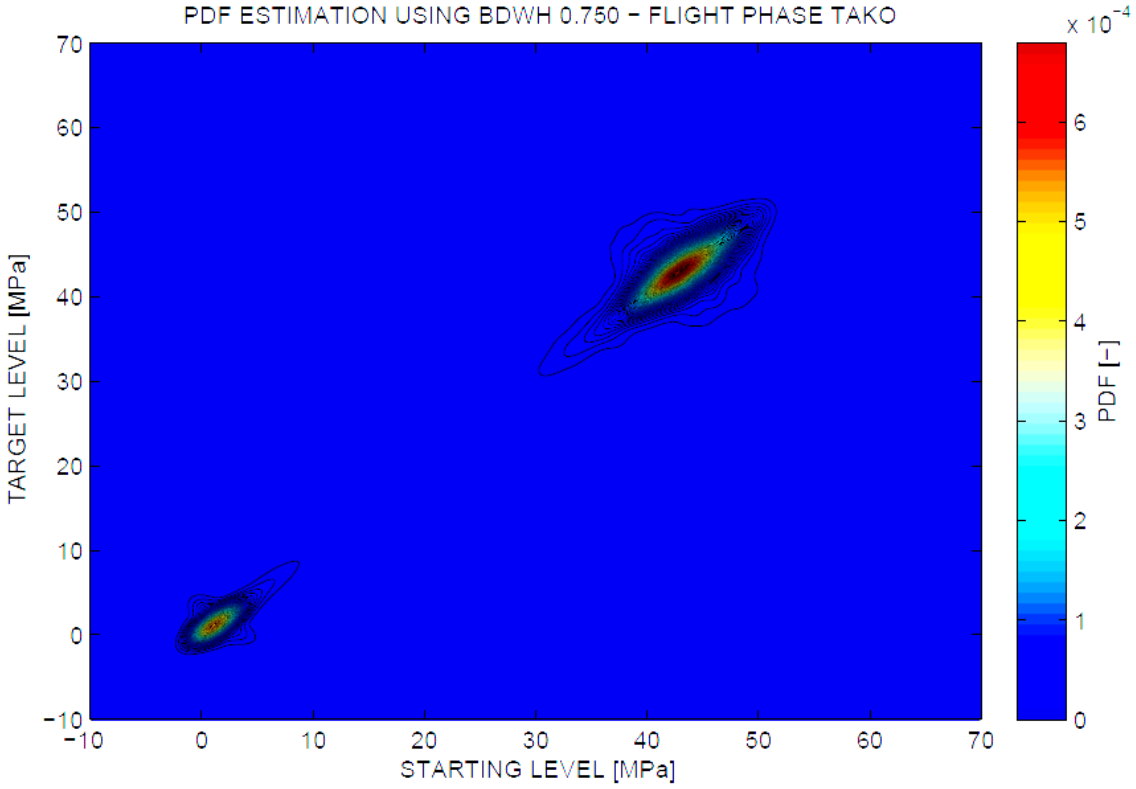

Figure 4.38 – Contour plot of PDF estimate for $h = 0.75\ MPa$

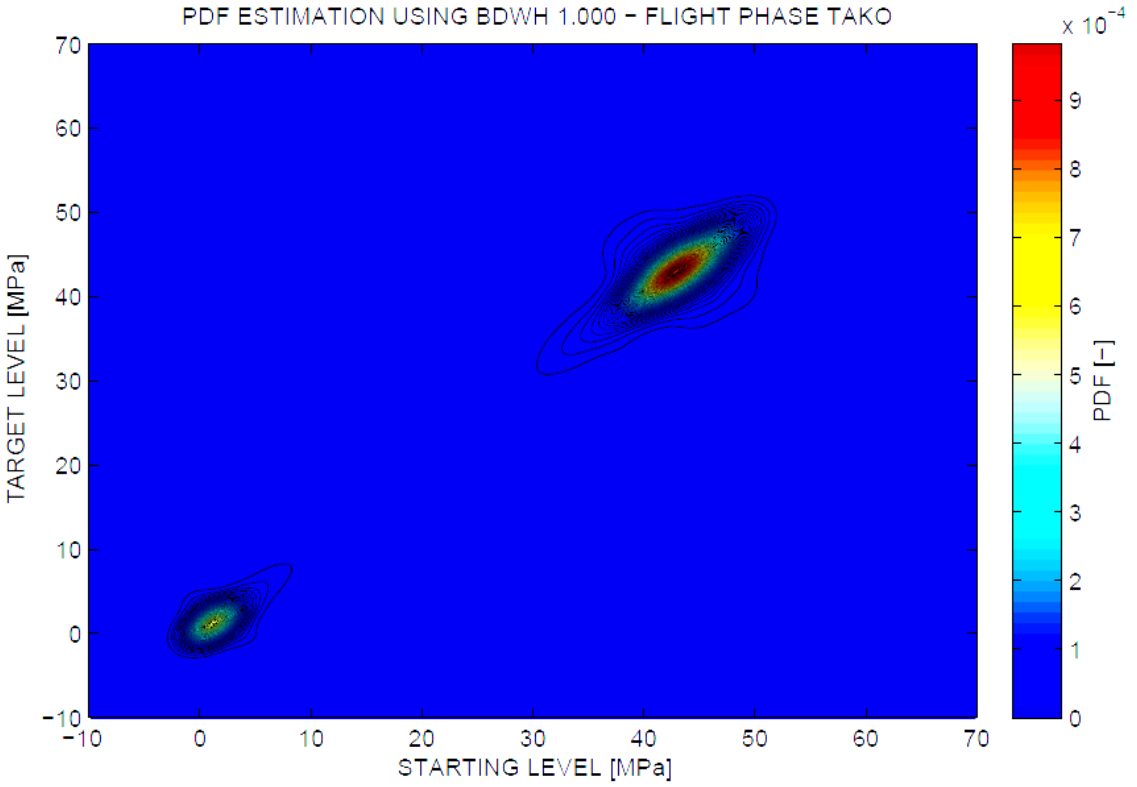

Figure 4.39 – Contour plot of PDF estimate for $h = 1.00\ MPa$

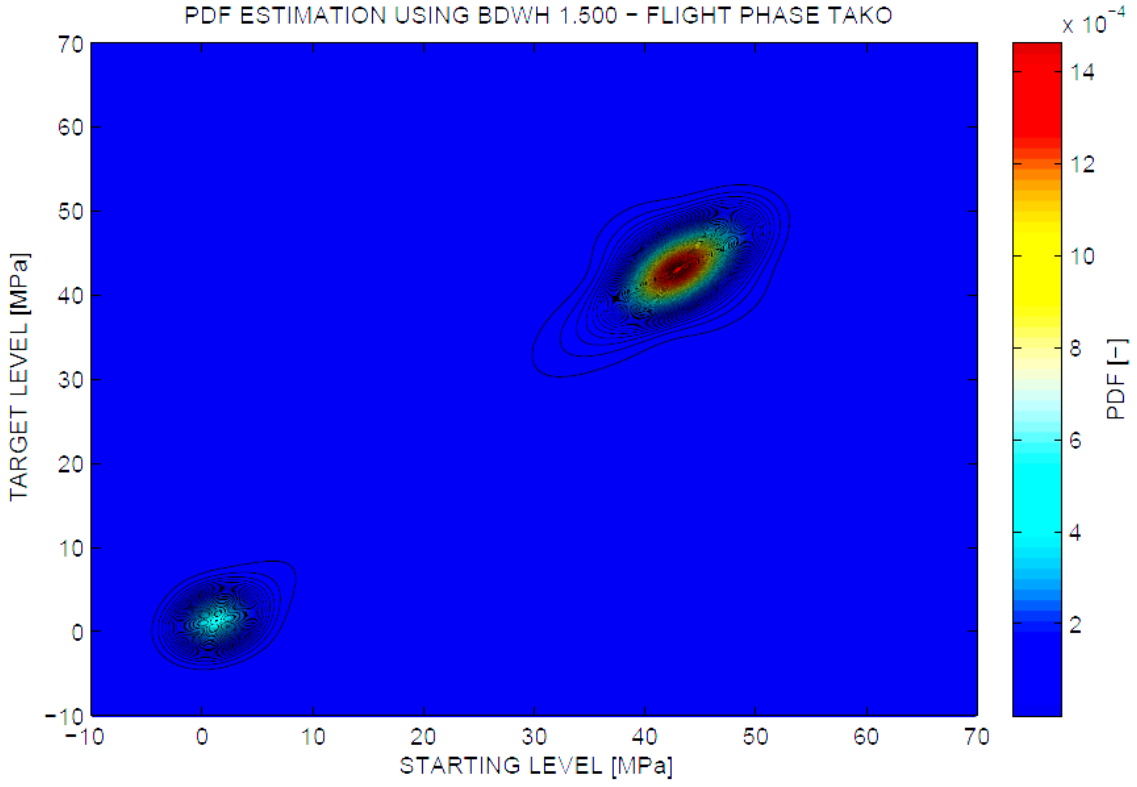

Figure 4.40 – Contour plot of PDF estimate for $h = 1.50\ MPa$

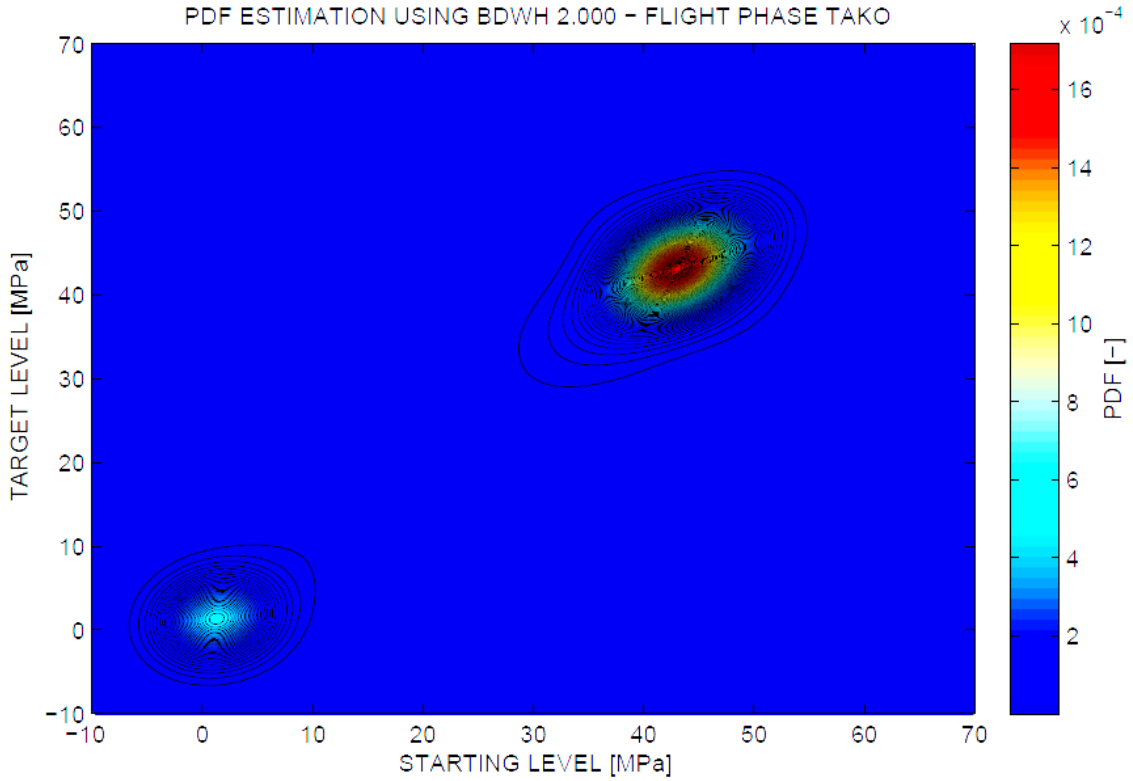

Figure 4.41 – Contour plot of PDF estimate for $h = 2.00\ MPa$

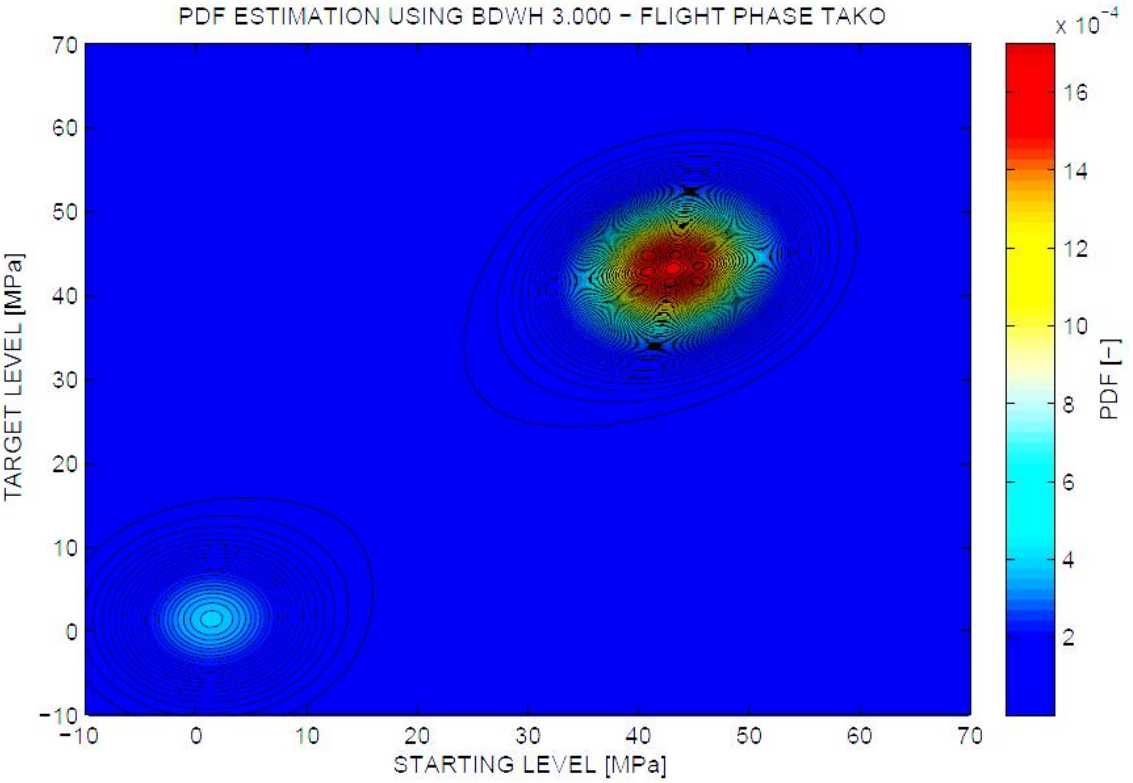

Figure 4.42 – Contour plot of PDF estimate for $h = 3.00\ MPa$

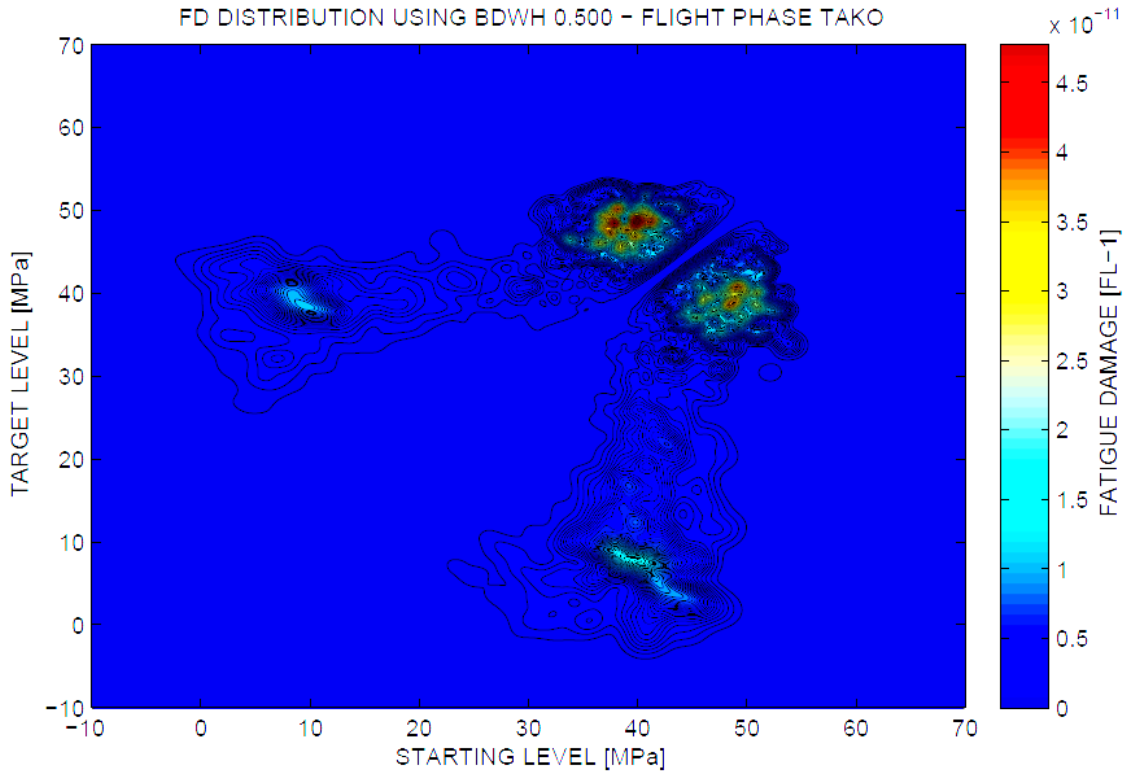

Figure 4.43 – Contour plot of FD distribution for $h = 0.50\ MPa$

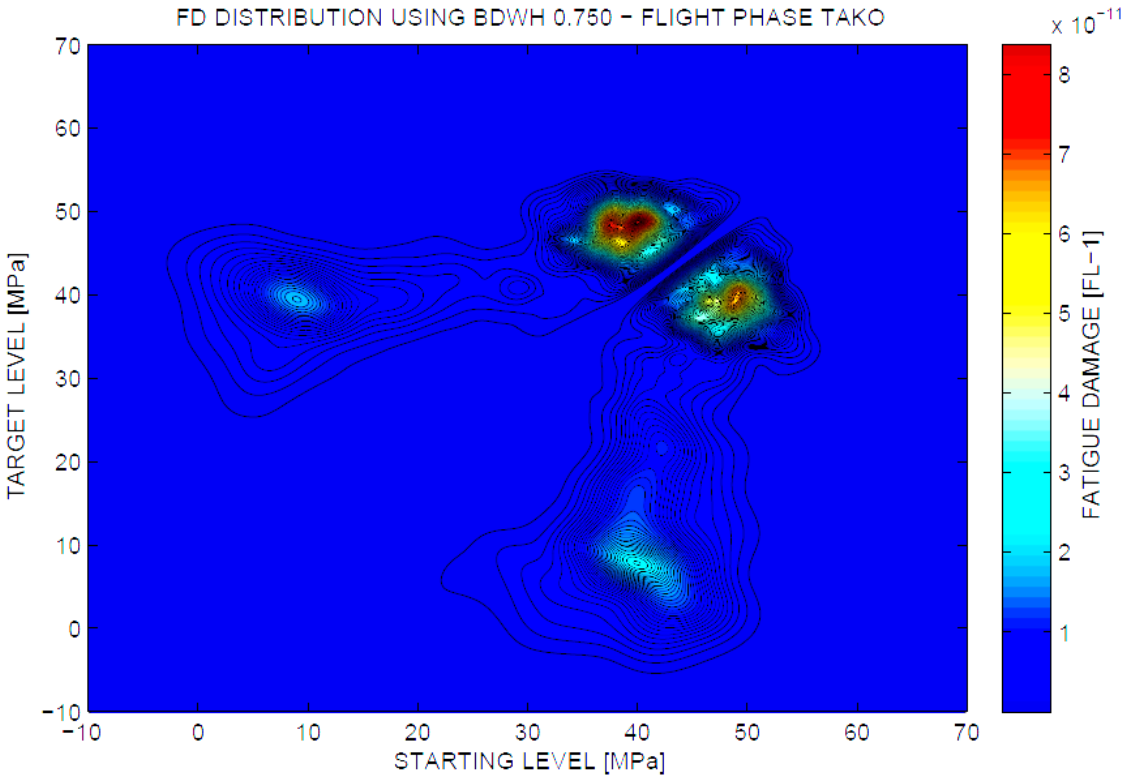

Figure 4.44 – Contour plot of FD distribution for $h = 0.75\ MPa$

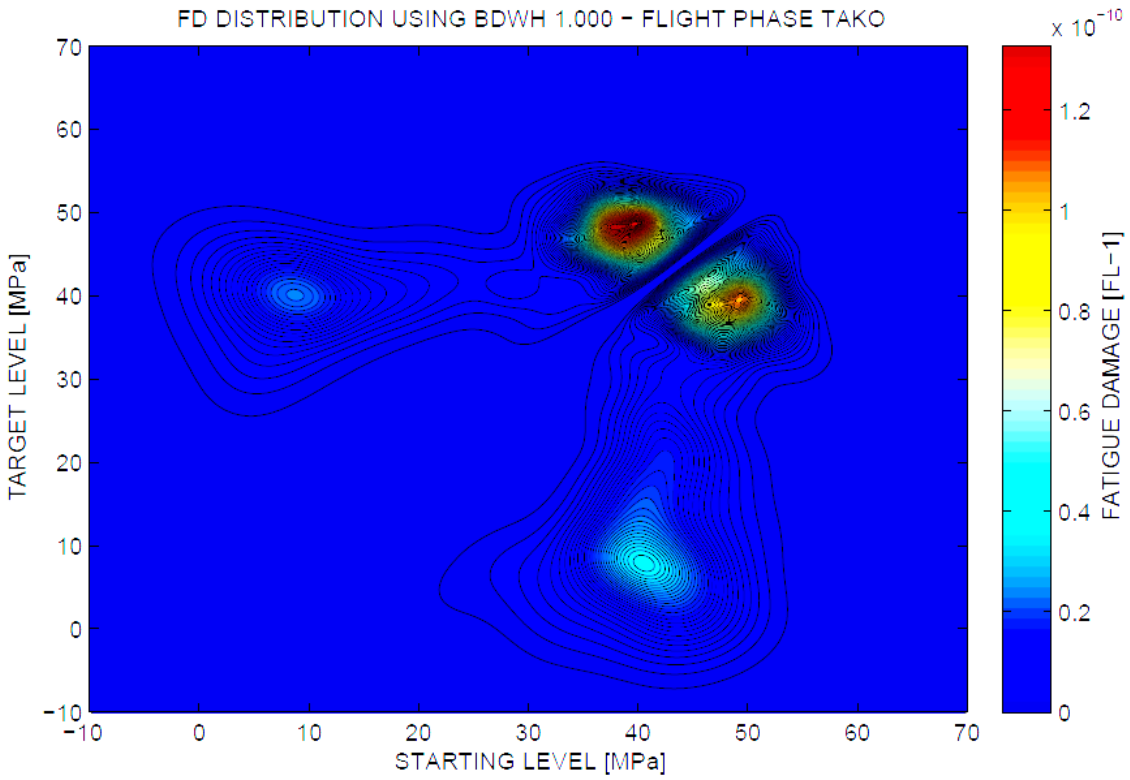

Figure 4.45 – Contour plot of FD distribution for $h = 1.00\ MPa$

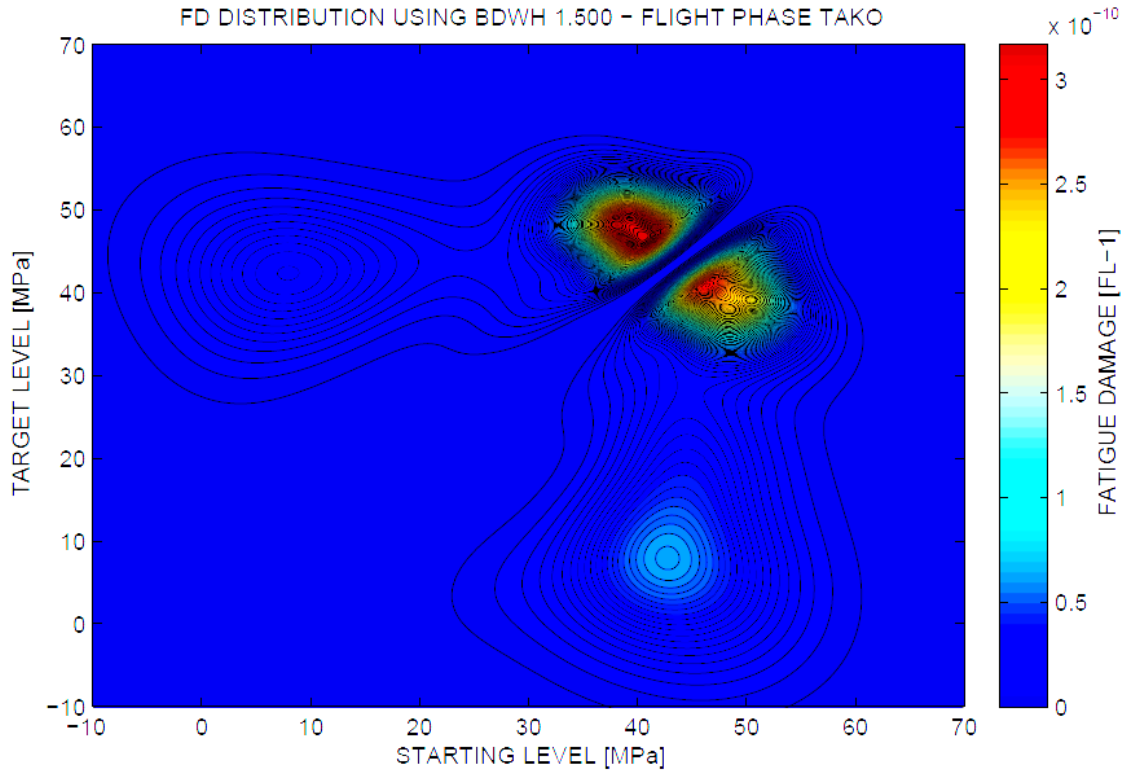

Figure 4.46 – Contour plot of FD distribution for $h = 1.50\ MPa$

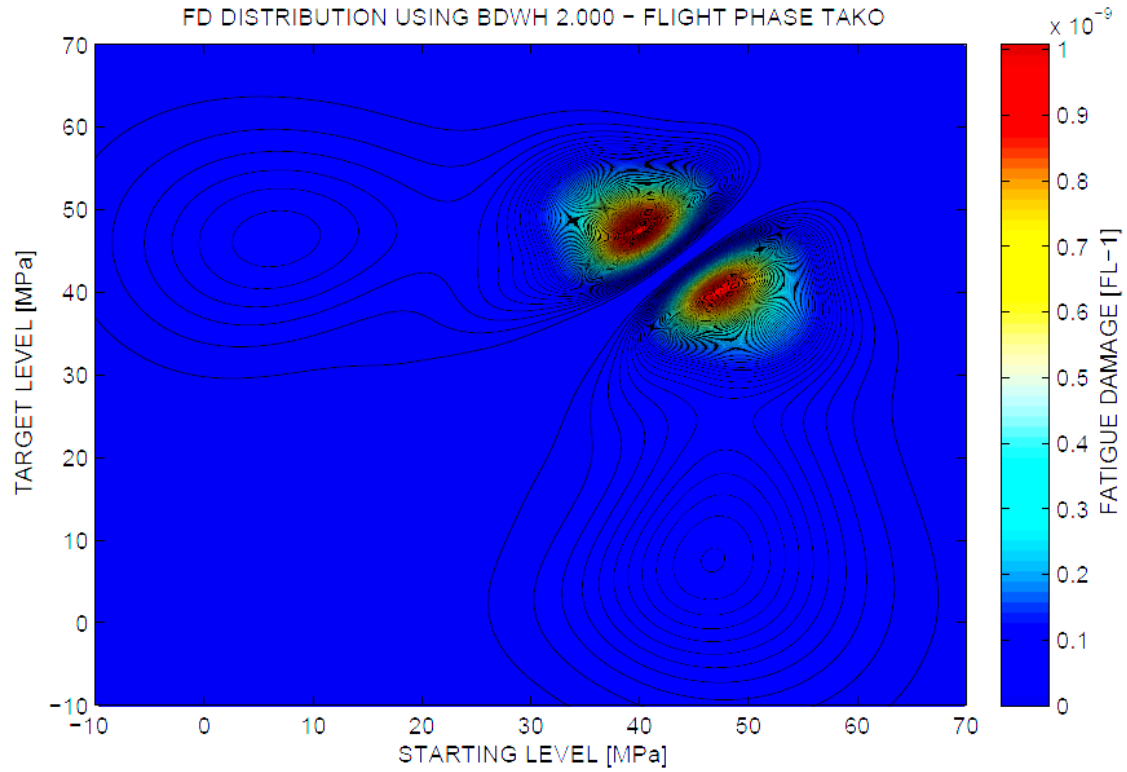

Figure 4.47 – Contour plot of FD distribution for $h = 2.00\ MPa$

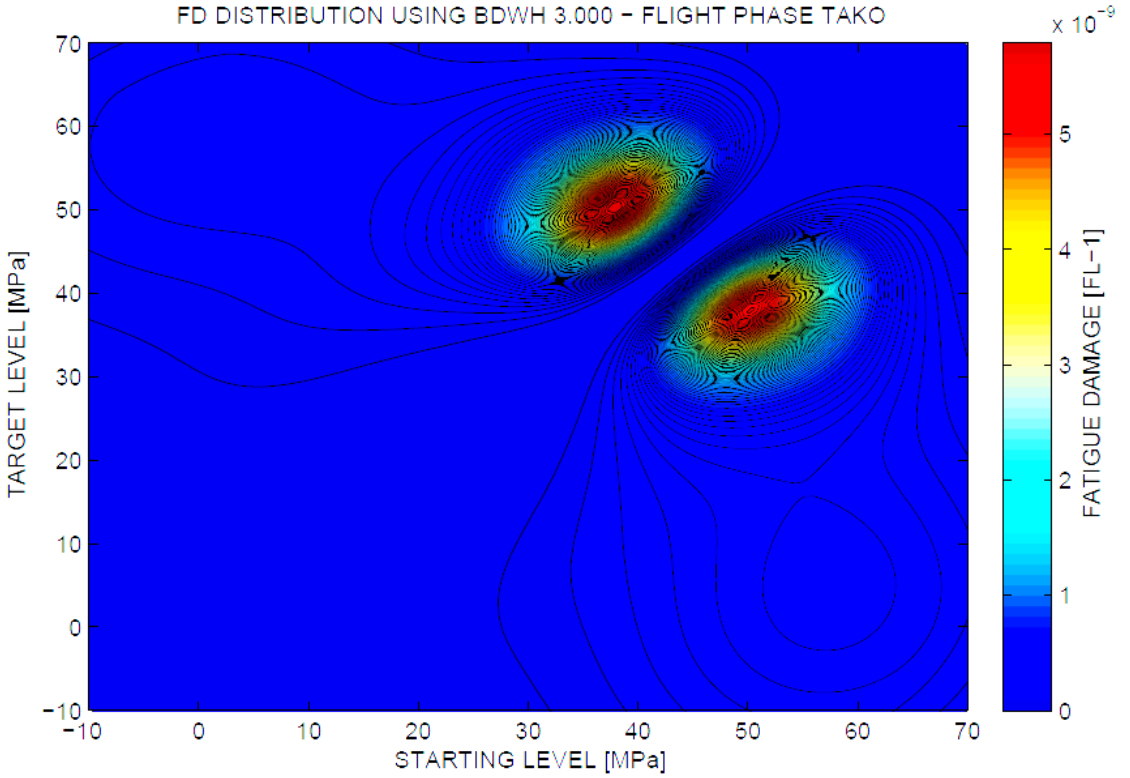

Figure 4.48 – Contour plot of FD distribution for $h = 3.00\ MPa$

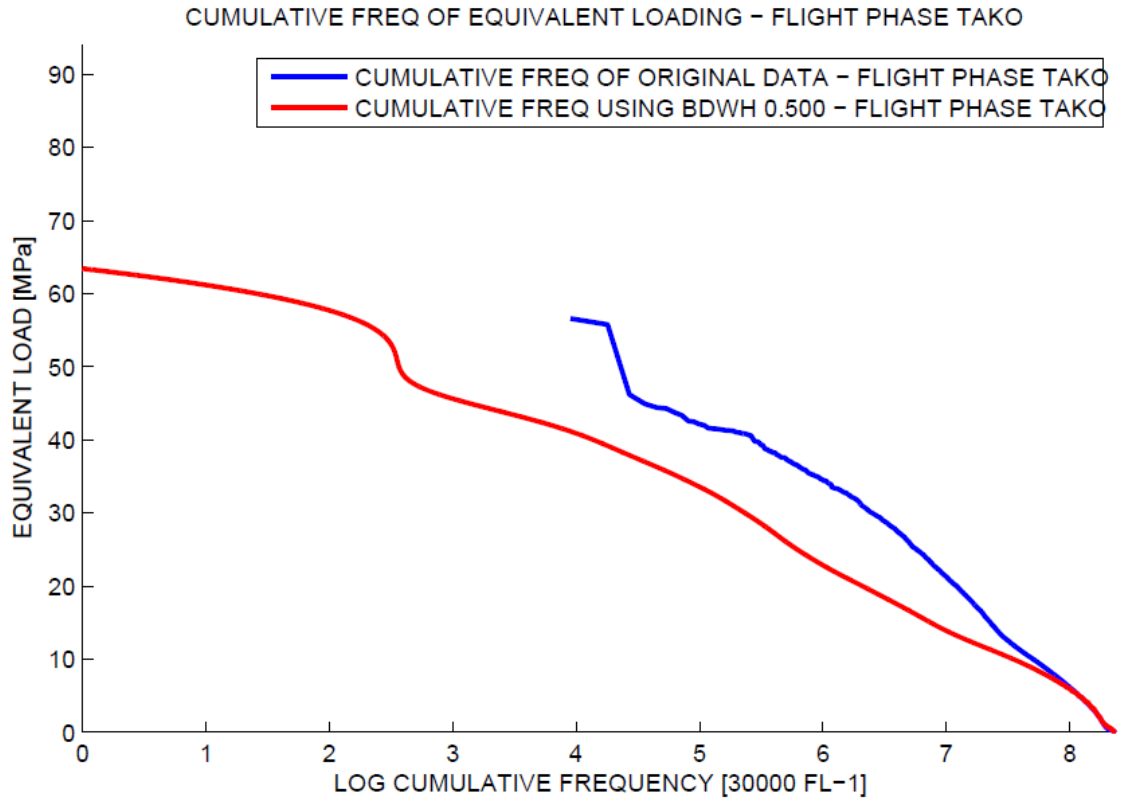

Figure 4.49 – Cumulative exceedance diagram for $h = 0.50\ MPa$

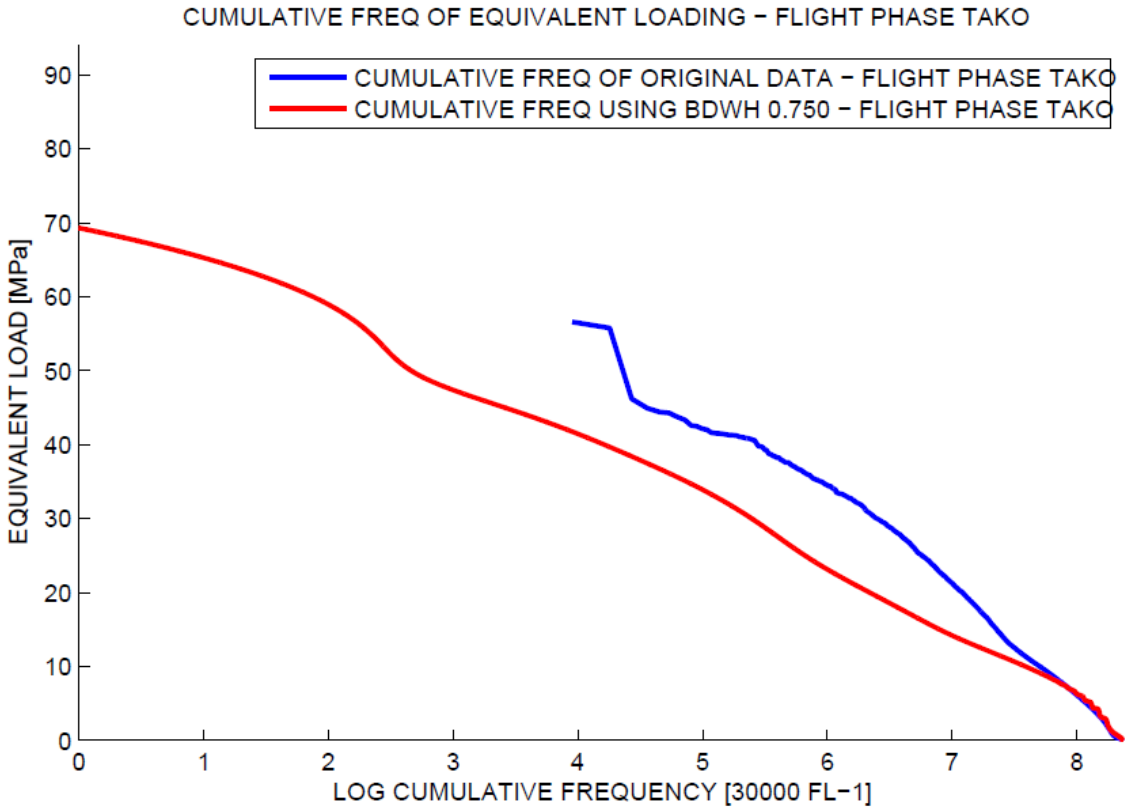

Figure 4.50 – Cumulative exceedance diagram for $h = 0.75\ MPa$

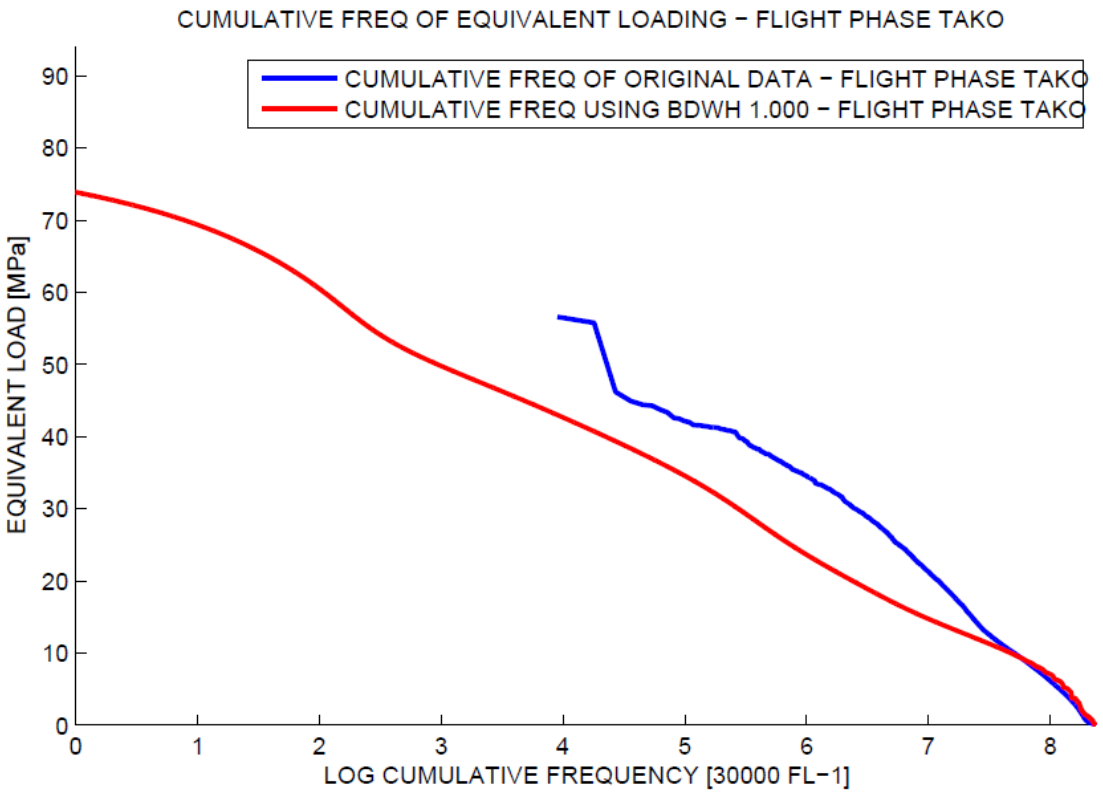

Figure 4.51 – Cumulative exceedance diagram for $h = 1.00\ MPa$

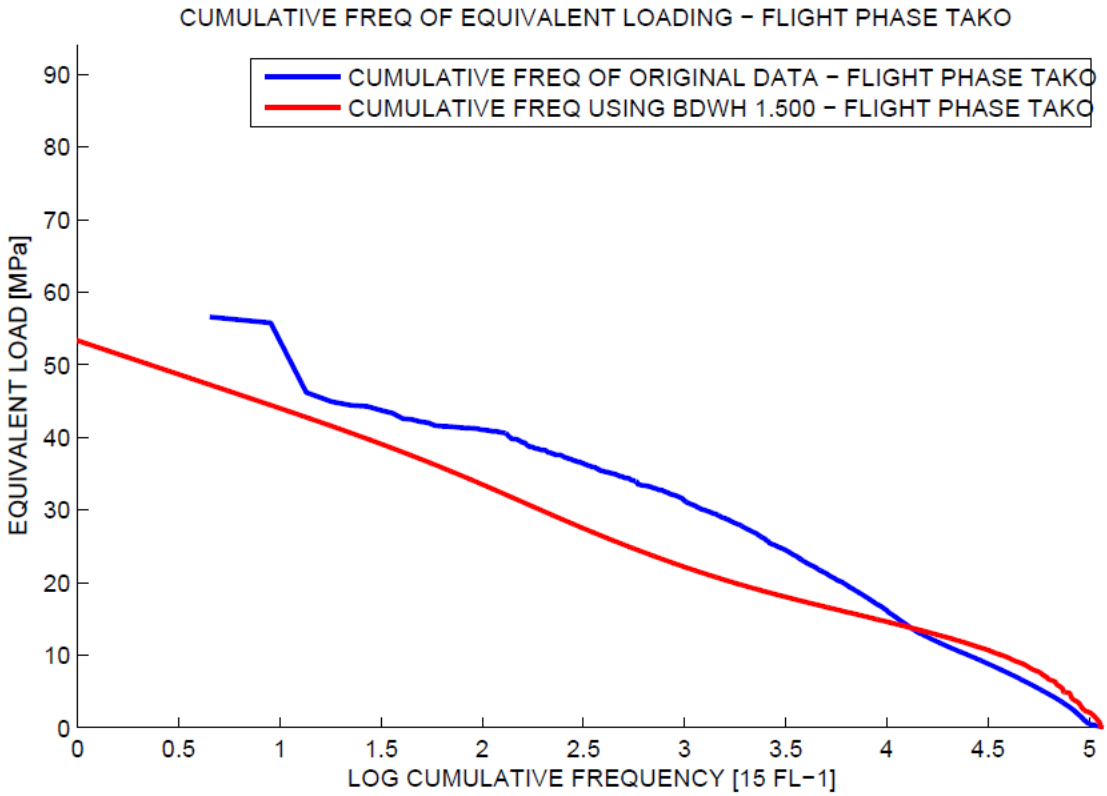

Figure 4.52 – Cumulative exceedance diagram for $h = 1.50\ MPa$

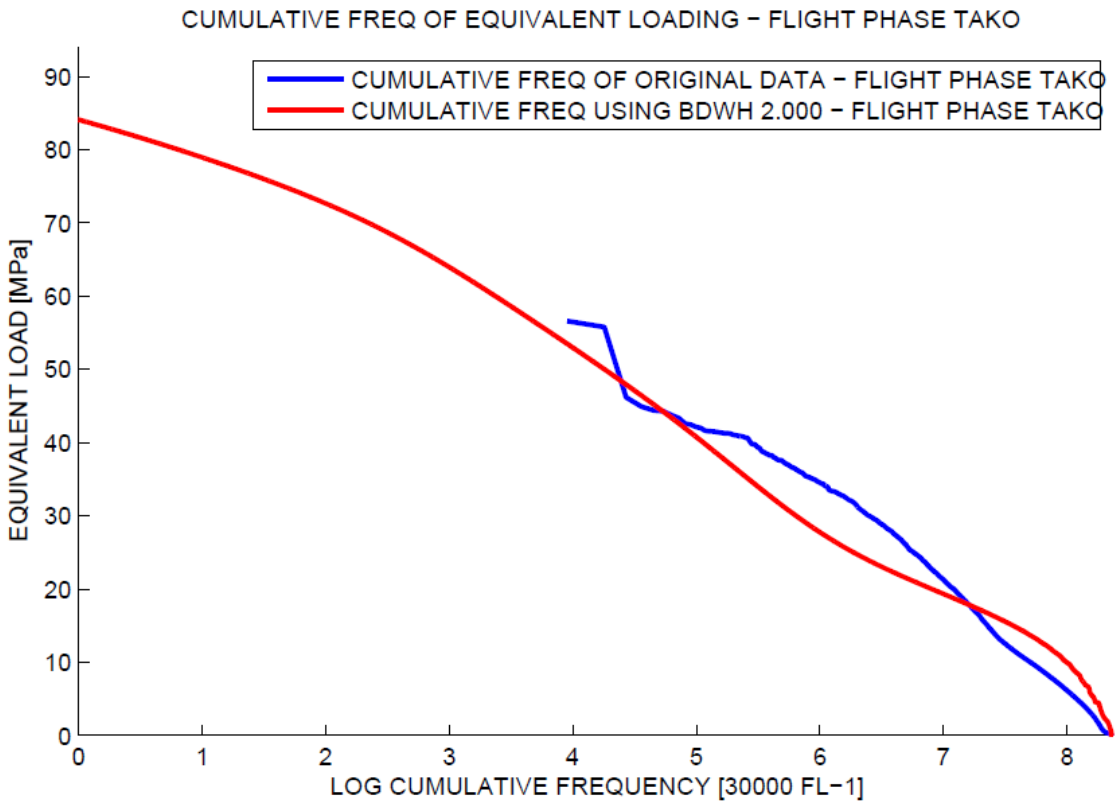

Figure 4.53 – Cumulative exceedance diagram for $h = 2.00\ MPa$

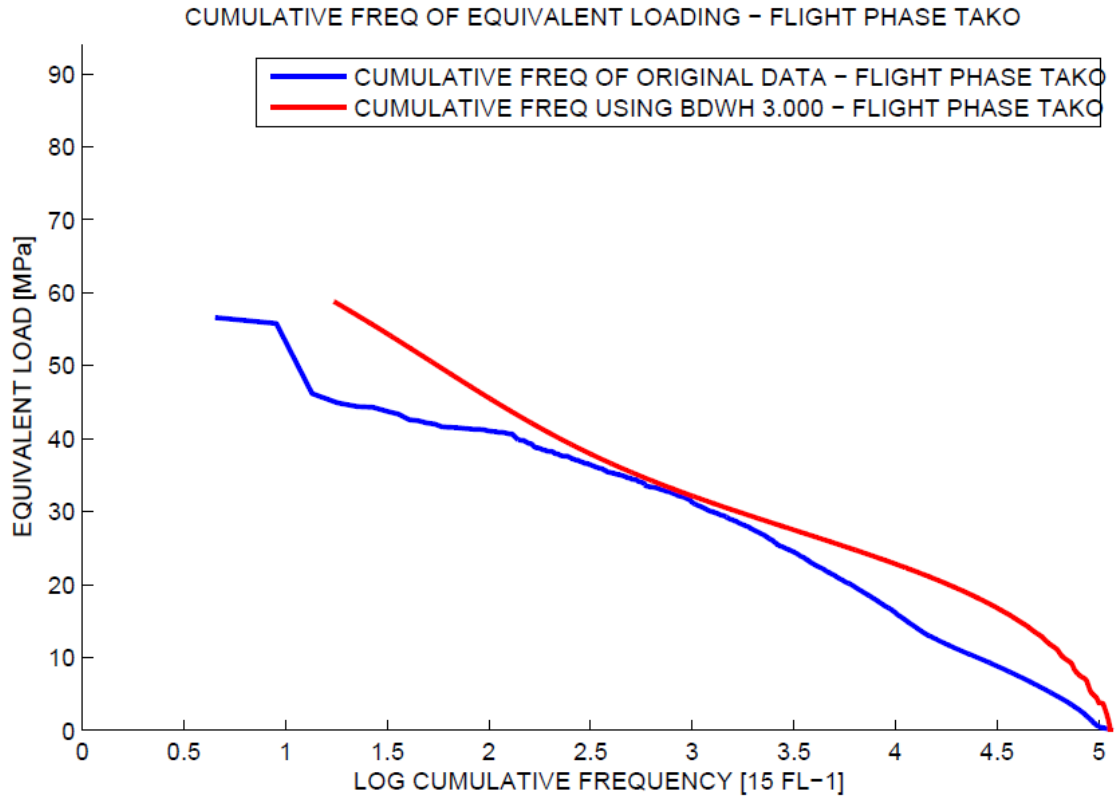

Figure 4.54 – Cumulative exceedance diagram for $h = 3.00\ MPa$

4.5PDF estimation

After the choice of an optimal bandwidth for each investigated flight phase (take-off, approach, landing), the final PDF estimate of load cycles can be determined. Note that the user shall decide, whether to use CKE or AKE method for the final estimation. The chosen bandwidth must be appropriate.

The user has to enter selected bandwidths together with the PDF estimation method and extreme loads into the spreadsheet corresponding to particular flight phase (TAKO, APP, LNG), before calling the script PDF_estimation.m, as shown in Table 4.21.

It is recommended to adapt the extremes of PDF estimate (Minimal and Maximal permitted loads) to the bandwidth selected for the final estimation of the PDF. It is necessary to realize, that limits of starting and target load levels directly affects load cycles, which can be regenerated from the estimated PDF. It is recommended to choose a little bit larger area of PDF than a significantly smaller area. Choice of a small area can inhibit some of the loading cycles outside the investigated range.

	PDF ESTIMATION	
Bandwidth for final PDF estimate	H	
Minimal permitted load	MIN	
Maximal permitted load	MAX	
PDF estimation method (CKE or AKE)	PDF method	
Bandwidth for pilot PDF estimate	Hpilot	

Table 4.21 – User-defined parameters for final PDF estimation - description

The output of the final PDF estimation includes transformation parameters and PDF estimate in a form of a from-to matrix. Matrices of starting level, target level and corresponding values of PDF are exported into text files separately. All output parameters are summarized in the table below.

	PDF ESTIMATION	
Name of file containing matrix of starting load levels	xx_PDF FN	
Name of file containing matrix of target load levels	yy_PDF FN	
Name of file containing matrix of PDF values	fk_PDF FN	
Data rotation angle	FI [rad]	
Data translation in x-direction	xT	
Data translation in y-direction	yT	
Scaling factor	sf [-]	

Table 4.22 – PDF estimation output summary – description

An optimal bandwidth has been selected for the rest of analysed flight phases in the same way as for the take-off flight phase. CKE method has been chosen for the final PDF estimation. Input data and output summary of the final PDF estimation are mentioned in Table 4.23 to Table 4.25.

Figure 4.55 to Figure 4.66 show final PDF estimate and corresponding fatigue damage distribution for each investigated flight phase.

PDF ESTIMATION	
H	1.5
MIN	-10
MAX	70
PDF method	CKE
Hpilot	
xx_PDF FN	TAKO\SLOT_NO_334_xx_PDF_1.500_TAKO.txt
yy_PDF FN	TAKO\SLOT_NO_334_yy_PDF_1.500_TAKO.txt
fk_PDF FN	TAKO\SLOT_NO_334_fk_PDF_1.500_TAKO.txt
FI [rad]	-0.781396983
xT	31.53443986
yT	31.38712568
sf [-]	0.986749252

Table 4.23 – Final PDF estimation – TAKO

PDF ESTIMATION	
H	1
MIN	15
MAX	60
PDF method	CKE
Hpilot	
xx_PDF FN	APP\SLOT_NO_334_xx_PDF_1.000_APP.txt
yy_PDF FN	APP\SLOT_NO_334_yy_PDF_1.000_APP.txt
fk_PDF FN	APP\SLOT_NO_334_fk_PDF_1.000_APP.txt
FI [rad]	-0.784131286
xT	35.77262313
yT	35.84352864
sf [-]	1.231796966

Table 4.24 – Final PDF estimation – APP

PDF ESTIMATION	
H	2
MIN	40
MAX	130
PDF method	CKE
Hpilot	
xx_PDF FN	LNG\SLOT_NO_334_xx_PDF_2.000_LNG.txt
yy_PDF FN	LNG\SLOT_NO_334_yy_PDF_2.000_LNG.txt
fk_PDF FN	LNG\SLOT_NO_334_fk_PDF_2.000_LNG.txt
FI [rad]	-0.782415474
xT	82.49670756
yT	82.61962296
sf [-]	1.201085567

Table 4.25 – Final PDF estimation – LNG

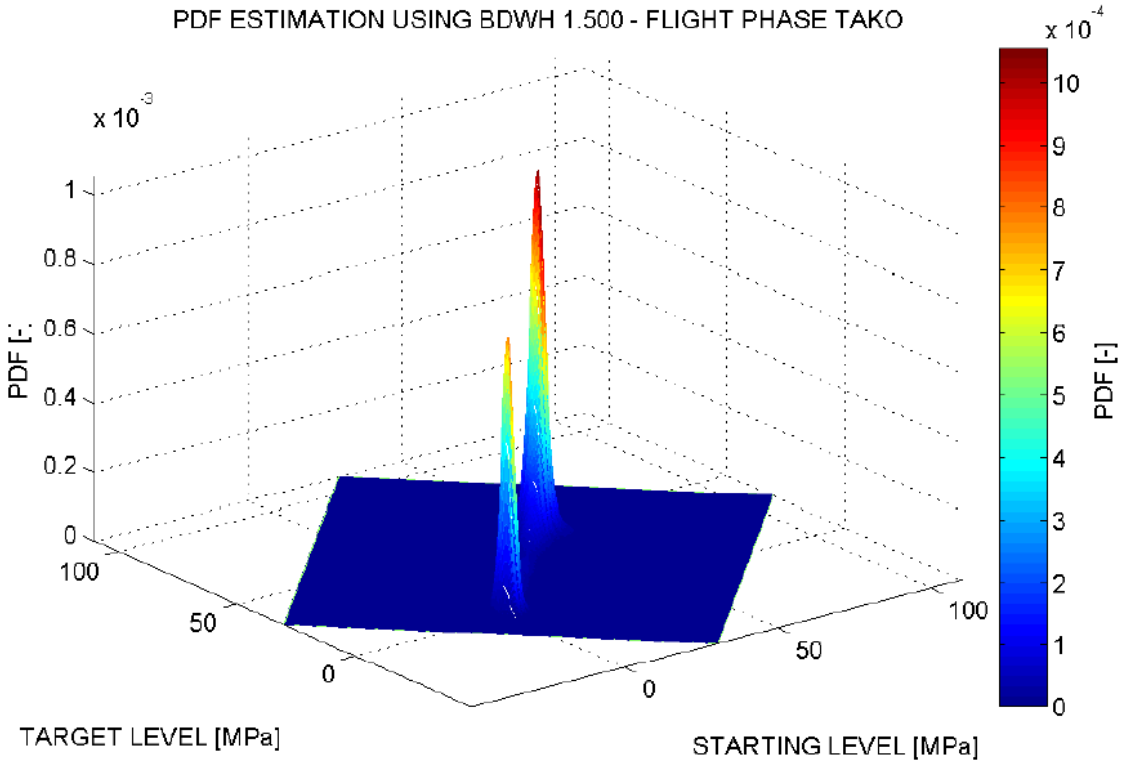

Figure 4.55 – Meshz plot of the final PDF estimate – TAKO

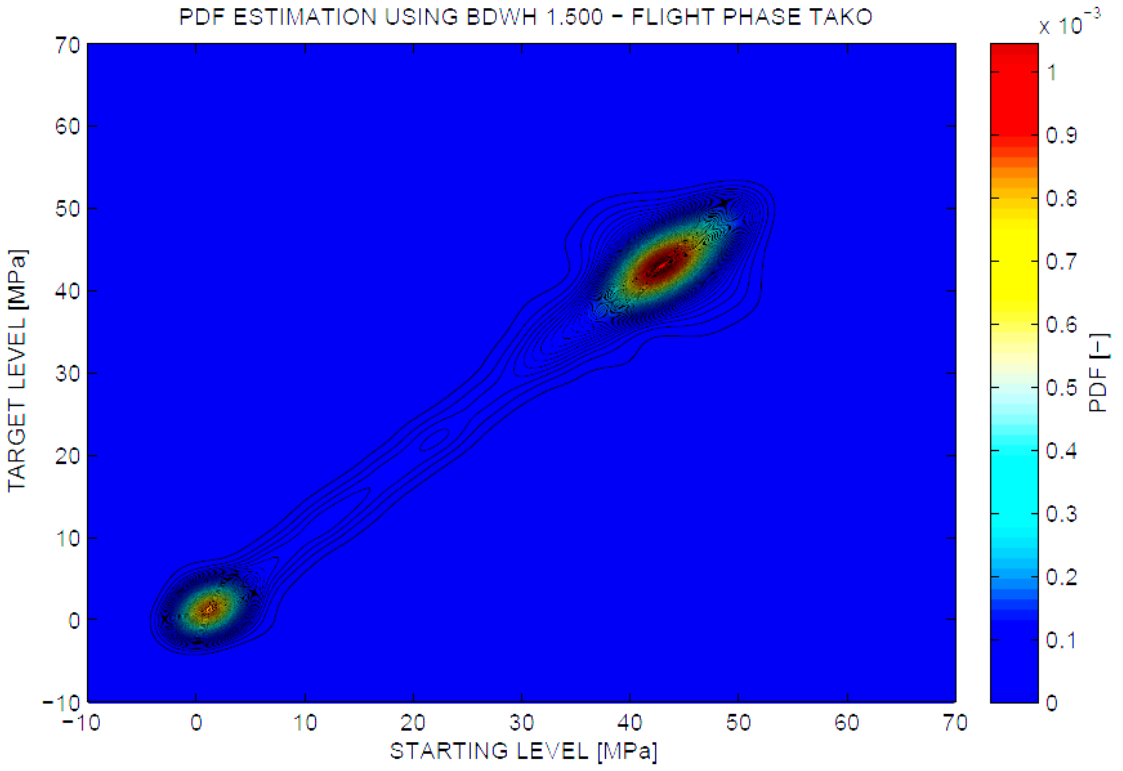

Figure 4.56 – Contour plot of the final PDF estimate – TAKO

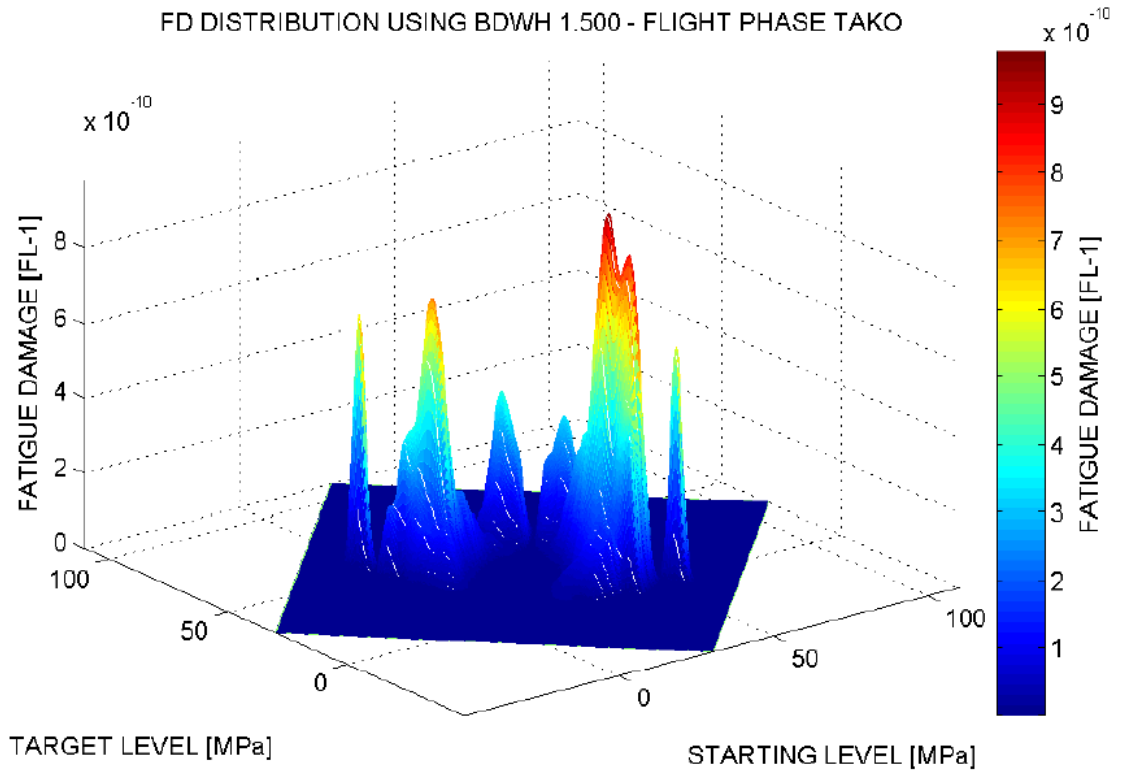

Figure 4.57 – Meshz plot of the final fatigue damage distribution – TAKO

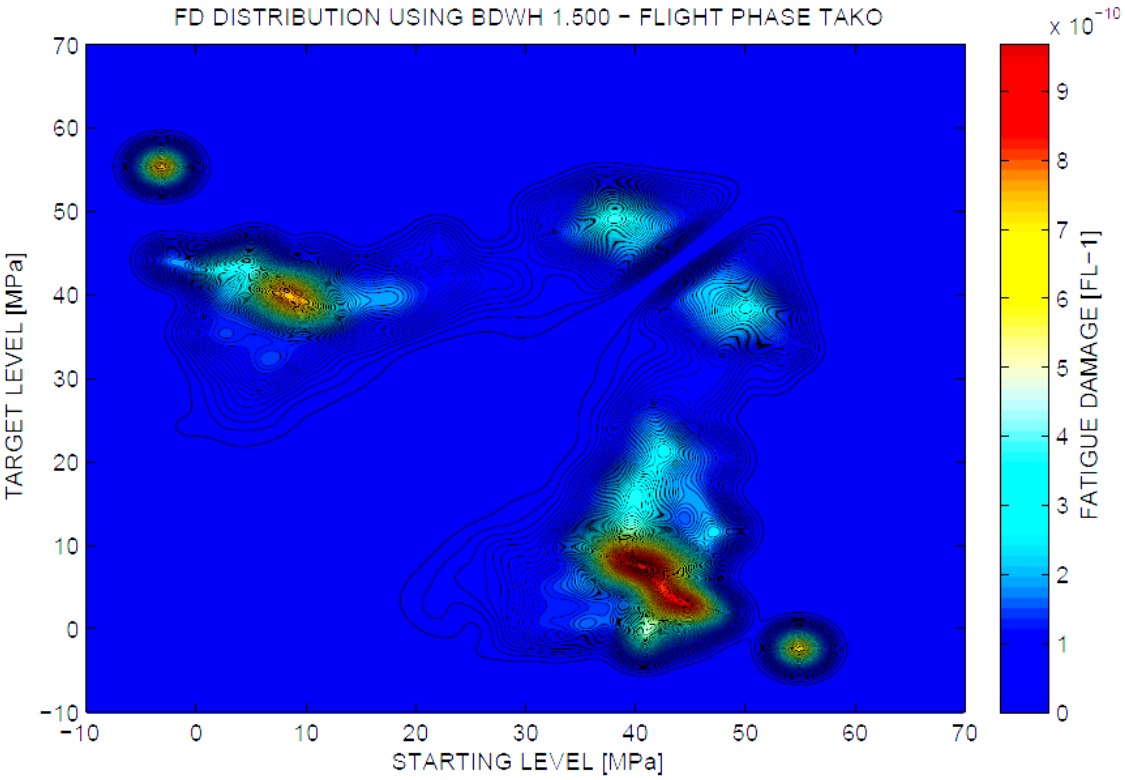

Figure 4.58 – Contour plot of the final fatigue damage distribution– TAKO

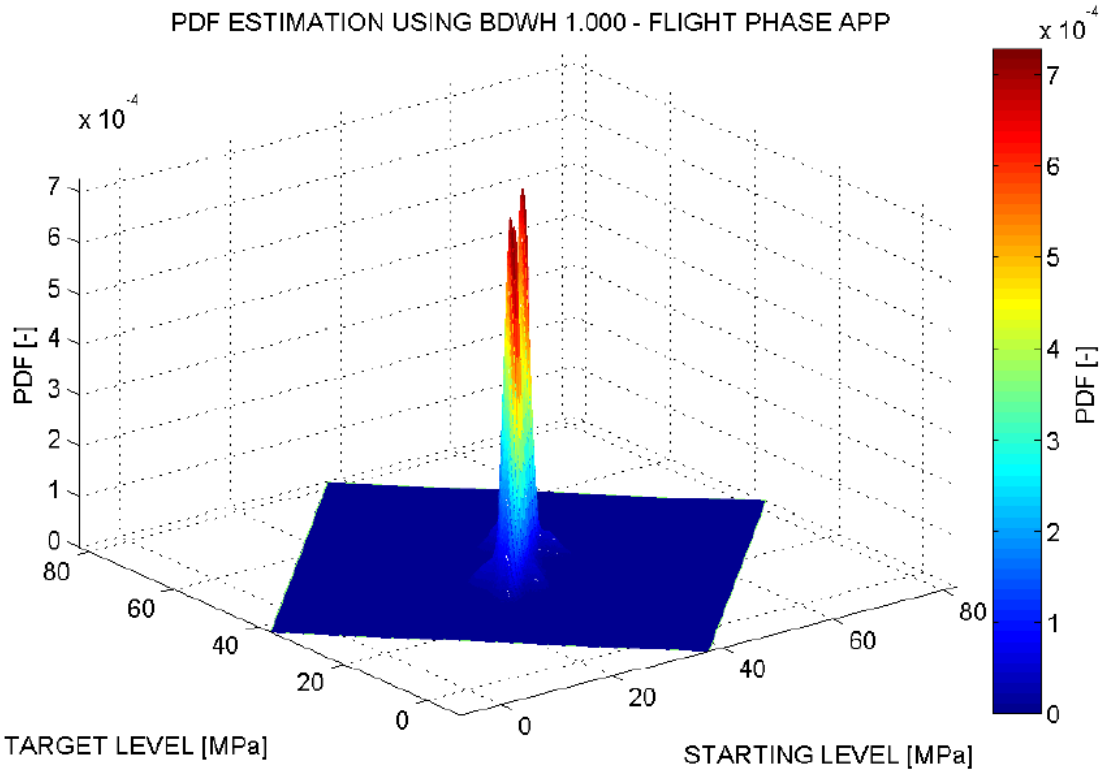

Figure 4.59 – Meshz plot of the final PDF estimate – APP

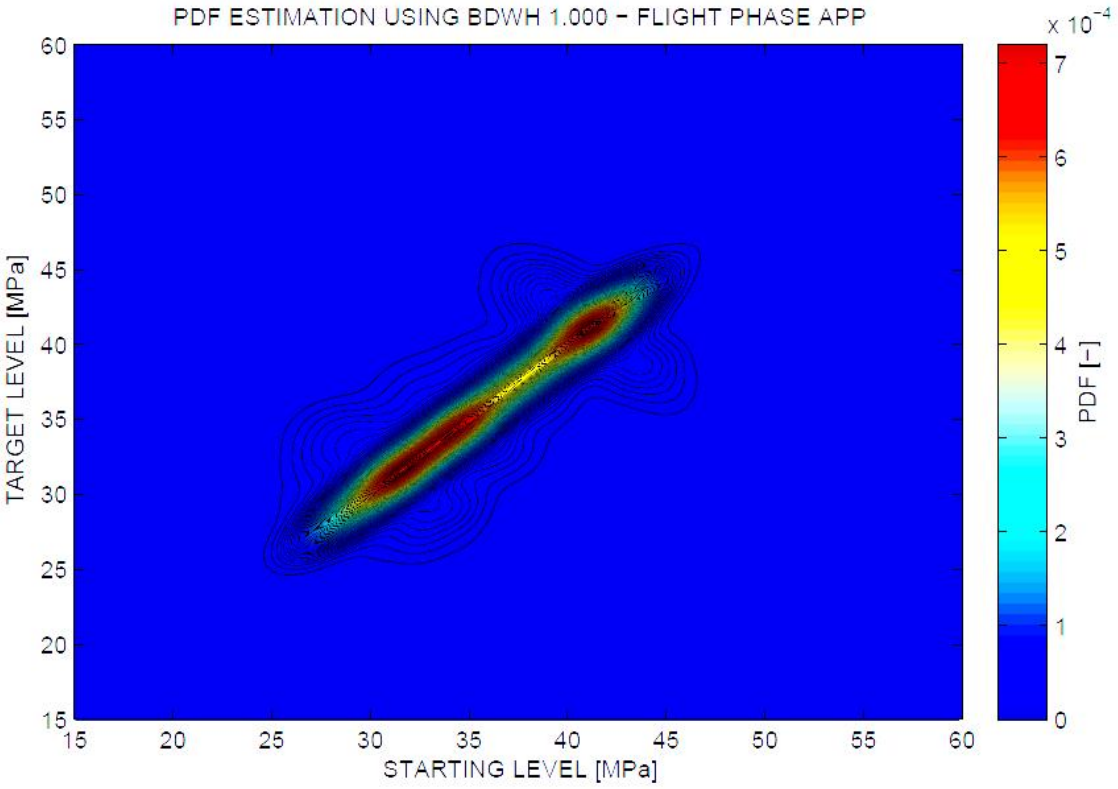

Figure 4.60 – Contour plot of the final PDF estimate – APP

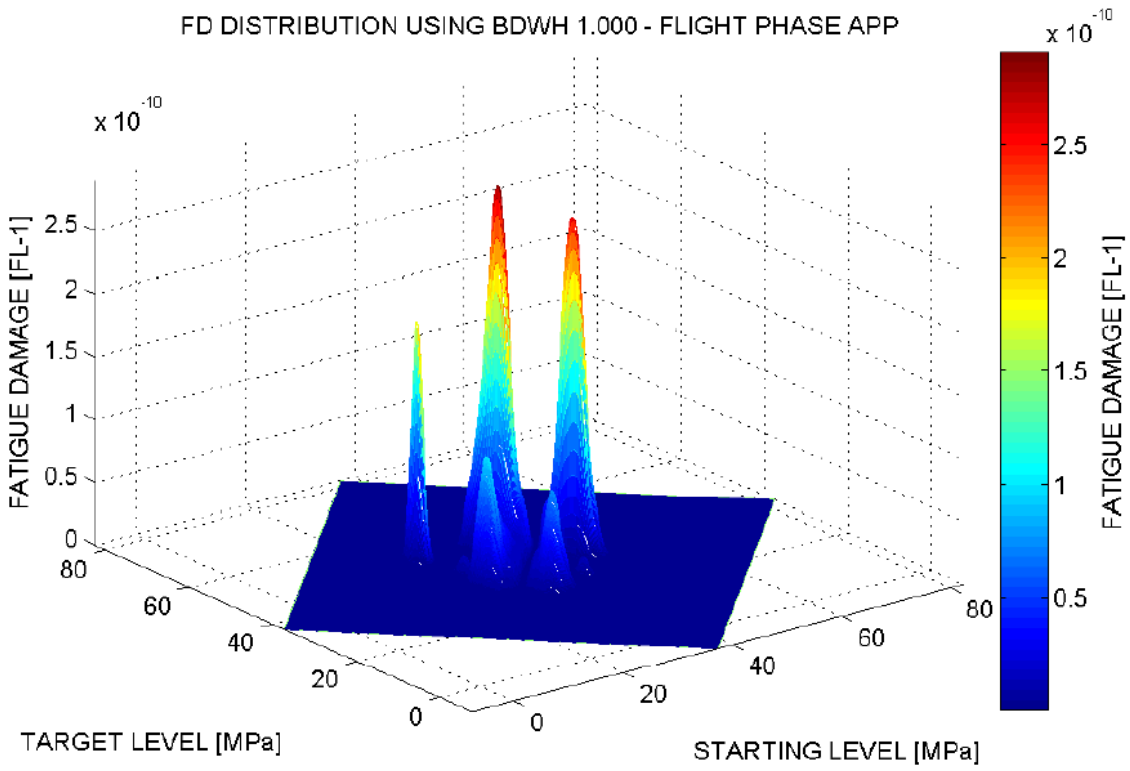

Figure 4.61 – Meshz plot of the final fatigue damage distribution – APP

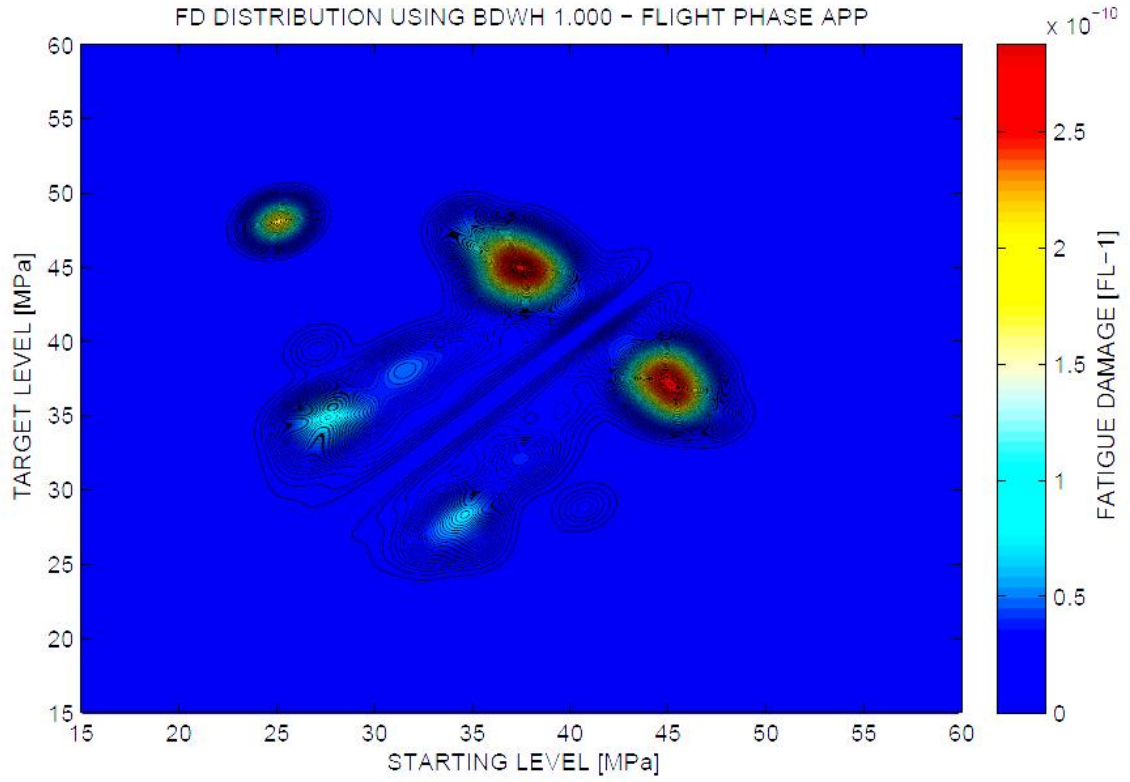

Figure 4.62 – Contour plot of the final fatigue damage distribution– APP

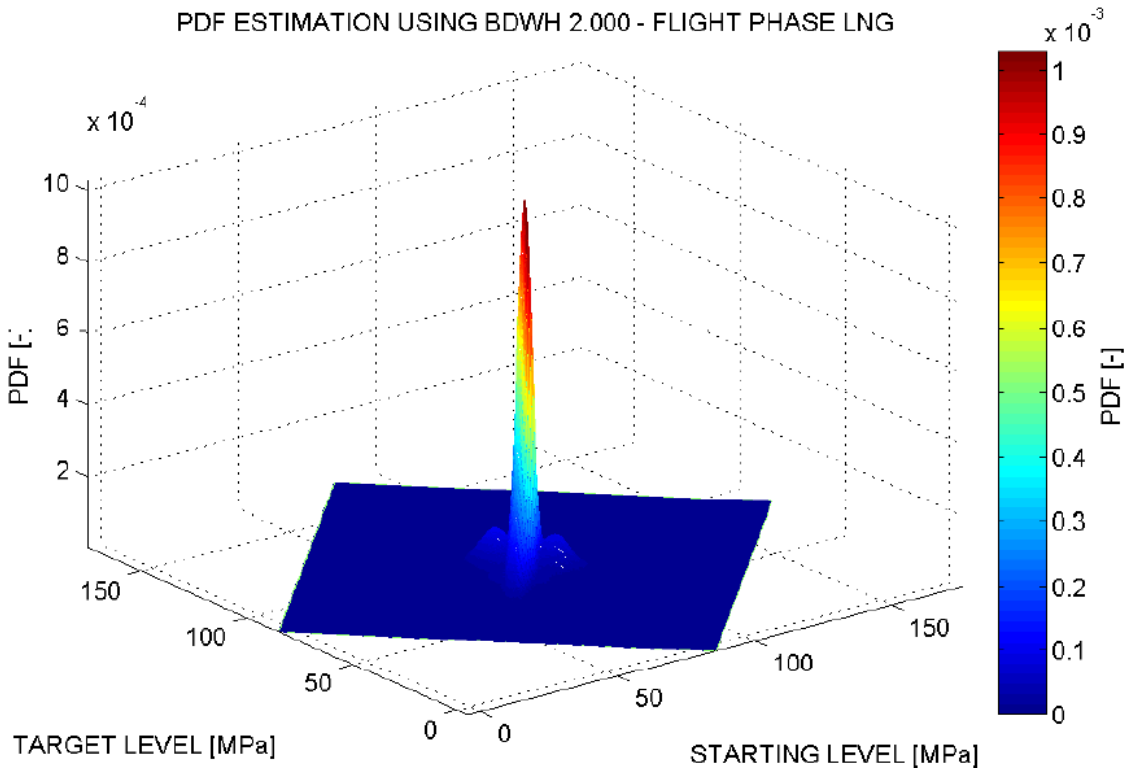

Figure 4.63 – Meshz plot of the final PDF estimate – LNG

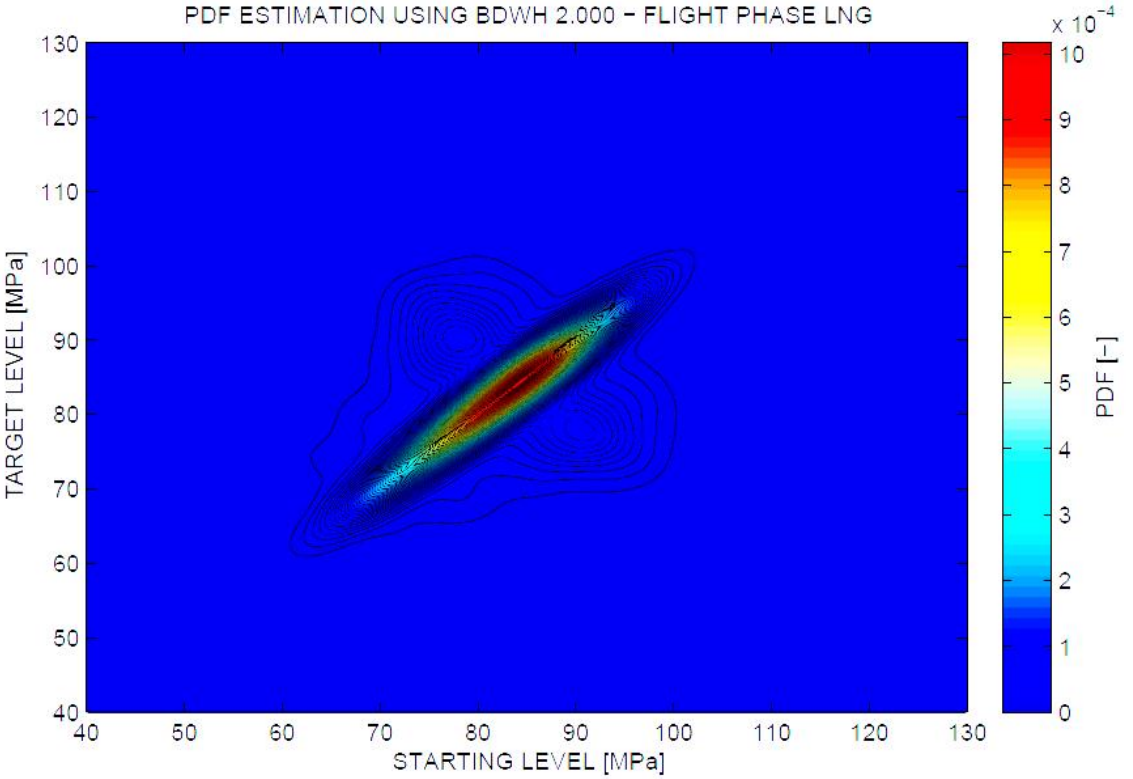

Figure 4.64 – Contour plot of the final PDF estimate – LNG

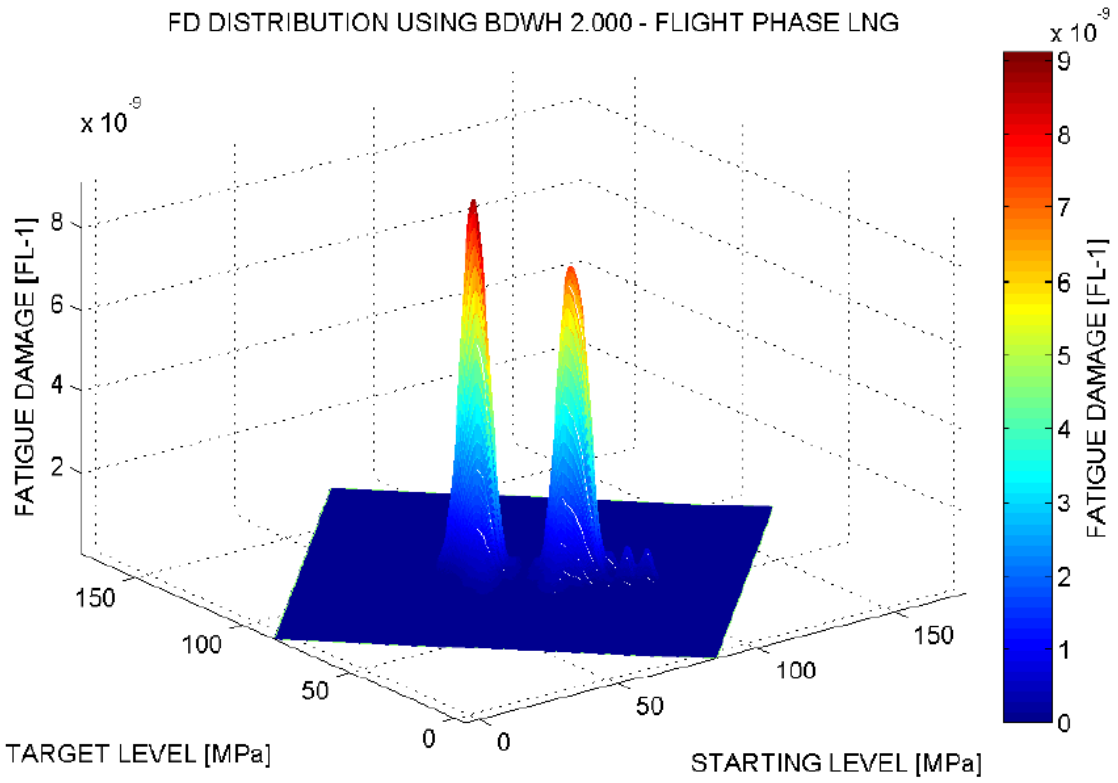

Figure 4.65 – Meshz plot of the final fatigue damage distribution – LNG

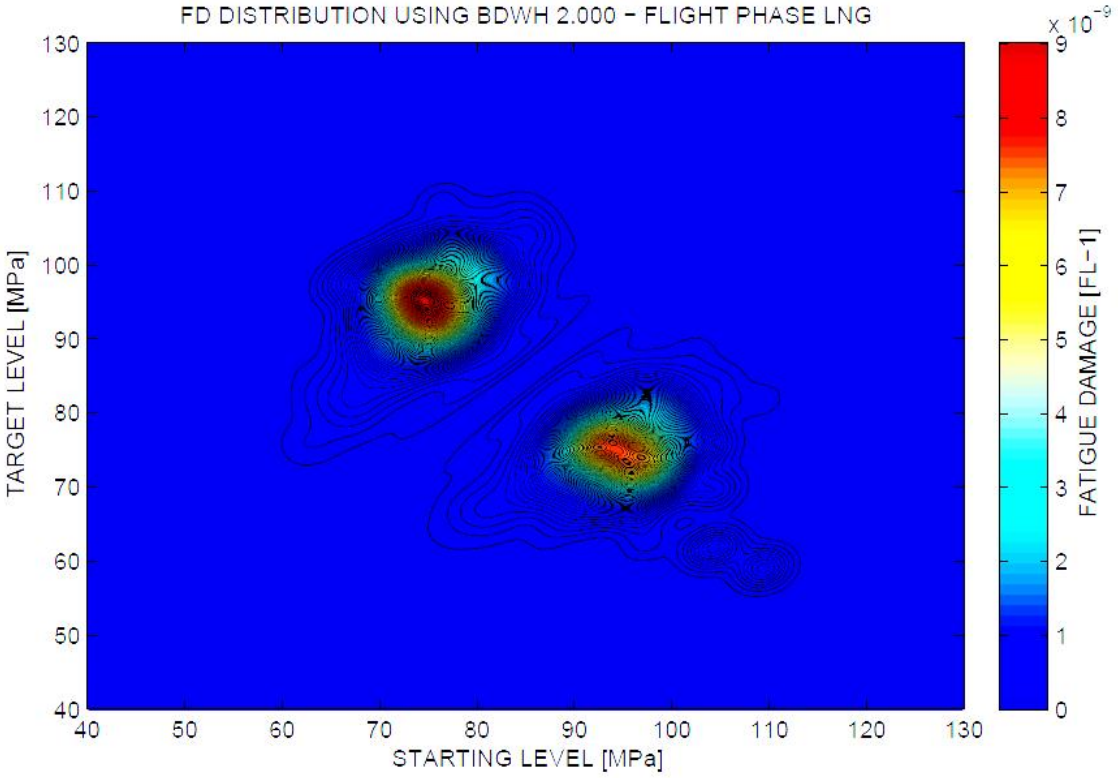

Figure 4.66 – Contour plot of the final fatigue damage distribution– LNG

4.6 Reconstruction of loading history

After the PDF is estimated for each investigated flight phase, the loading history of particular length might be reconstructed. The reconstruction of loading history is initiated by calling the script RECON.m.

After load reconstruction, the fatigue damage caused by flap-duty cycles as well as an overall fatigue damage are computed. Apart from the fatigue damage, AFGROW loading sequence is generated. The process might be seen in a form of a flowchart in the figure below.

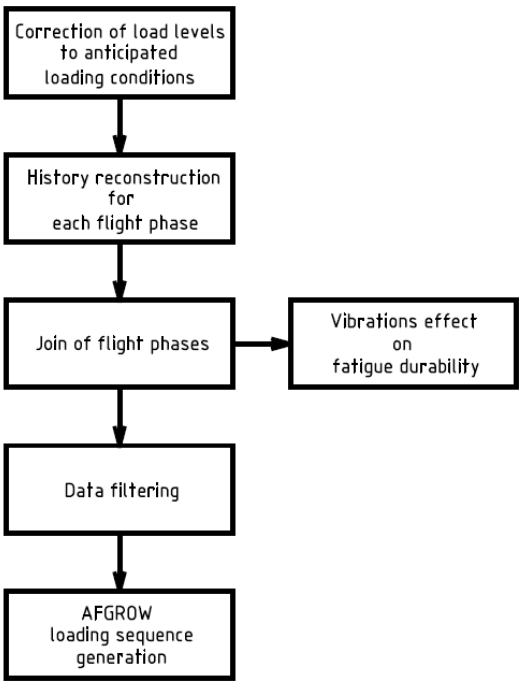

Figure 4.67 – Flowchart of loading history reconstruction

Data filtering is performed prior to sequence generation to reduce the volume of data.

An input for the flight phase load reconstruction in a form of the mean stress/load of the most frequent cycle was determined at the same time as the final PDF estimation. Apart from that, text files containing fatigue damage distribution and cumulative frequencies of equivalent stress/load were created. An overall fatigue damage due to appropriate flight phase was computed. Corresponding increase of fatigue damage in comparison to the original load history detected from the in-flight measurement was determined as well. The summary of input data is displayed in the following tables.

	FATIGUE DAMAGE OF THE RECONSTRUCTED HISTORY	
Name of file containing fatigue damage distribution	FDM FN	
Name of file containing cumulative frequencies of cycles	CF FN	
Fatigue damage after data extrapolation	FD_EXT [FL-1]	
Mean load/stress of the most frequent cycle	MPL	
Relative increase of fatigue damage	dFD [%]	

Table 4.26 – Input for flight phase load reconstruction – description

FATIGUE DAMAGE OF THE RECONSTRUCTED HISTORY	
FDM FN	TAKO\SLOT_NO_334_FDM_1.500_TAKO.txt
CF FN	TAKO\SLOT_NO_334_CF_1.500_TAKO.txt
FD_EXT [FL-1]	3.15682E-06
MPL	43.03
dFD [%]	10.53%

Table 4.27 – Input for flight phase load reconstruction – TAKO

FATIGUE DAMAGE OF THE RECONSTRUCTED HISTORY	
FDM FN	APP\SLOT_NO_334_FDM_1.000_APP.txt
CF FN	APP\SLOT_NO_334_CF_1.000_APP.txt
FD_EXT [FL-1]	4.40751E-07
MPL	31.62
dFD [%]	21.93%

Table 4.28 – Input for flight phase load reconstruction – APP

FATIGUE DAMAGE OF THE RECONSTRUCTED HISTORY	
FDM FN	LNG\SLOT_NO_334_FDM_2.000_LNG.txt
CF FN	LNG\SLOT_NO_334_CF_2.000_LNG.txt
FD_EXT [FL-1]	1.42864E-05
MPL	84.17
dFD [%]	9.85%

Table 4.29 – Input for flight phase load reconstruction – LNG

4.6.1 Load levels correction

Because the in-flight measurement does not always correspond to loading presumed by the analysis, the algorithm enables the user to define his own loading conditions. The loading conditions are entered in the PARAM spreadsheet as shown in Table 4.30.

	LOADING CONDITIONS		
	MANOUVER ONLY		
Anticipated load level - take off	S_TAKO	[N]	default
Anticipated load level - initial approach	S_APPR	[N]	default
Anticipated load level - final approach	S_LANG	[N]	default
Anticipated load level - taxiing	S_GRND	[N]	0
Anticipated load level - cruise flight	S_CRUSE	[N]	0

Table 4.30 – User-defined loading conditions

The user has to specify at least load levels during taxiing and cruise flight with flaps retracted, because these flight phases are not investigated in detail. Load levels of the rest of flight phases might be chosen as "default," which means, that load levels of the reconstructed history will correspond precisely to the load levels obtained by the measurement.

To match detected cycles in a form of the PDF estimate with the anticipated loading for the current flight phase, the following procedure has been developed:

- PDF estimate in a form of from-to matrix is transformed into a mean-amplitude matrix. The mean values $\sigma_{m\,i,j}$ and amplitudes $\sigma_{a\,i,j}$ are derived from the starting levels $x_{\,i,j}$ and target levels $y_{\,i,j}$:

$$\sigma_{m\,i,j} = \frac{x_{\,i,j} + y_{\,i,j}}{2}$$

$$\sigma_{a\,i,\mathrm{j}} = \frac{y_{\,i,j} - x_{\,i,j}}{2}$$

- The mean value of the most frequent cycle $\sigma_{m\,fmax}$ is determined
- Derived mean load/stress $\sigma_{m\,fmax}$ is matched with the anticipated loading condition σ_{ALC}

There are altogether two ways, how to match the mean load/stress with the anticipated loading condition:

a) By translating the mean values by a factor of $k_{ALC\,TRANS}$:

$$\sigma_{m\,i,j} = \sigma_{m\,i,j} + k_{ALC\,TRANS}$$

$$k_{ALC\,TRANS} = \sigma_{ALC} - \sigma_{m\,fmax}$$

b) By multiplying the mean values by a factor of $k_{ALC\ MULTI}$:

$$\sigma_{m\,i,j} = \sigma_{m\,i,j} \cdot k_{ALC\ MULTI}$$

$$k_{ALC\ MULTI} = \frac{\sigma_{ALC}}{\sigma_{m\,fmax}}$$

The first option is based on the assumption, that anticipated load level might be higher due to higher airspeed. Higher airspeed affect the mean load only. It does not have any effect on load amplitude, which is mostly affected by airspeed variability. The variability of airspeed might be caused by lateral gusts or airflow acceleration due to propeller providing thrust of the aircraft.

The second option has been introduced to deal with the take-off flight phase, where the first option is not fully applicable. In the case of TAKO, the mean load increases continuously from small value acting on the ground up to the loading acting upon flaps and flap's control system during the initial climb. The airspeed increases in the same way as mean stress/load. Simple translation of load levels upwards does not correspond to reality, because loading on the ground would become higher, which was not observed.

The method of matching load levels with the anticipated load must be defined by the user in the spreadsheet corresponding to particular flight phase (TAKO, APP, LNG), as shown below. Two possible inputs are accepted: MULTI for multiplication, or TRANS for translation of load levels.

	FATIGUE DAMAGE OF THE RECONSTRUCTED HISTORY	
Method for matching of load levels with anticipated load →	METHOD	MULTI

Table 4.31 – Correction of load levels

Note that the load level's correction mentioned above shall be made only in the case, that anticipated load is higher than mean load of the highest absolute frequency derived from the in-flight measurement. Otherwise the anticipated load shall be set to "default" value.

For presentation of the algorithm, anticipated loading conditions have been selected as shown in Table 4.30.

4.6.2 Flight phase load reconstruction

The load history is reconstructed for each flight phase separately, based on the estimated PDF. The flowchart of the flight phase load reconstruction is shown in the figure below.

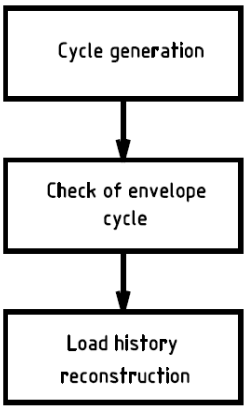

Figure 4.68 – Flowchart of flight phase load reconstruction

Firstly, cycles from the estimated PDF are generated in line with their probability of occurrence. The number of generated cycles n_{FL} is proportional to the user-defined flight phase duration t_{TFP}, duration of the in-flight measurement t_{org} and overall number of cycles detected from the in-flight measurement n_{cc}:

$$n_{FL} = n_{cc} \cdot \frac{t_{TFP}}{t_{\mathrm{d}rtn}}$$

After cycle generation, it is necessary to check, if an envelope cycle exists. An envelope cycle is any cycle which starting load level is the same or lower than starting level of the rest of generated cycles and at the same time, its target load level is the same or higher than the target level of the rest of generated cycles. The existence of an envelope cycle is a mandatory condition for a proper functionality of the reconstruction method mentioned in chapter 3.6.

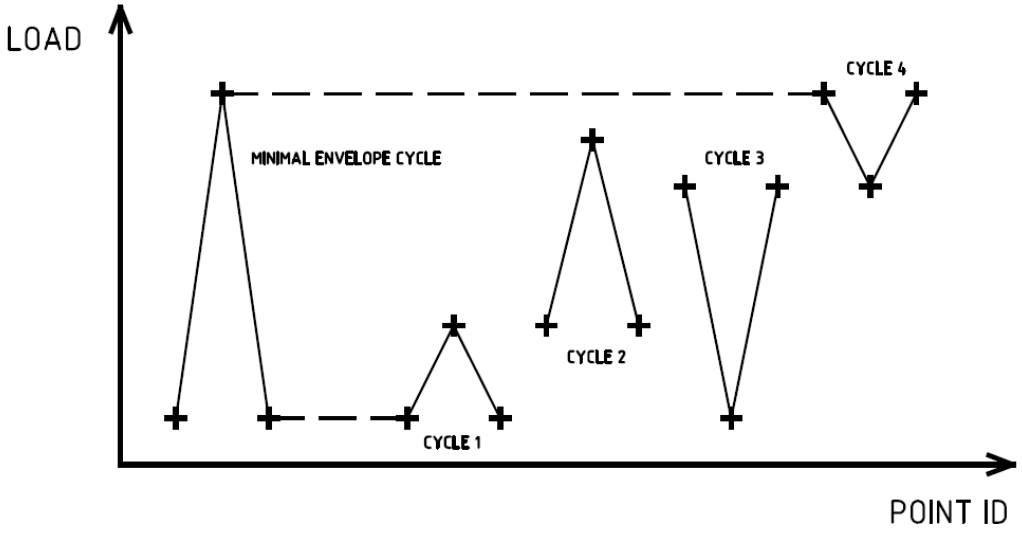

Figure 4.69 – Envelope cycle

In the most cases, an envelope cycle does not exist. Therefore, it is necessary to create an envelope cycle in addition. The additionally created envelope cycle replaces a random cycle from the already generated cycle ensemble.

A scheme of an envelope cycle for an ensemble of four different load cycles is displayed in Figure 4.69. The additionally created envelope cycle is always created from the lowest and the highest load level which is present in the cycle ensemble.

The loading reconstruction is made in line with the procedure stated in chapter 3.6. The only difference is the order of cycle insertion. Load cycles in a form of two vectors representing starting and target levels are ordered according to their load range in the descending order prior to load reconstruction. The cycle with the highest load range is inserted first. After that, cycles with smaller load ranges are inserted. This practice guarantees full functionality of the reconstruction algorithm, similarly to the method proposed in chapter 3.6, which works with a from-to matrix.

User-defined number of data sets N_{tgt} (corresponding to desired number of flights) is generated. Desired number of flights to be generated must be specified in the PARAM spreadsheet, as shown in Table 4.12.

The following parameters are determined for each generated data set:

- Minimum load/stress
- Maximum load/stress
- Mean value of load/stress
- Mean load/stress of the most frequent cycle

Variability of the defined parameters is displayed on the following figures for the take-off flight phase. Total number of flights $N_{tgt} = 15$ was generated.

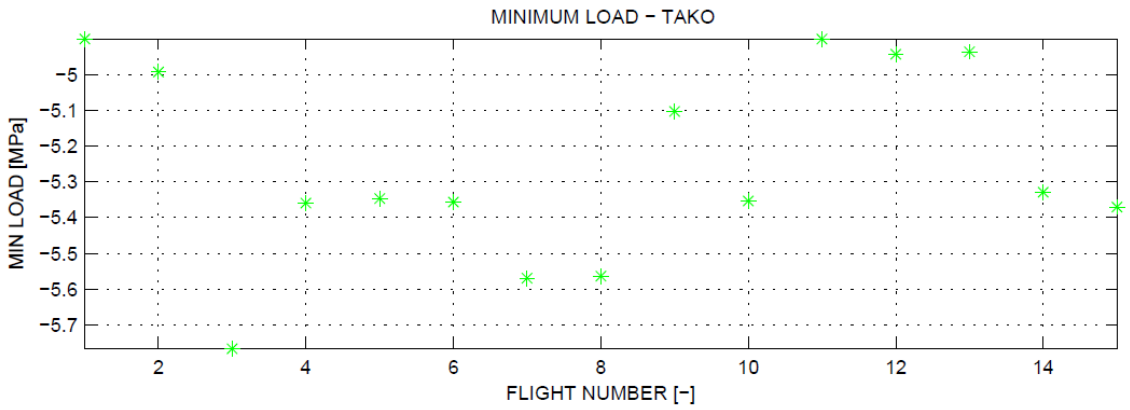

Figure 4.70 – Variability of minimum load – TAKO

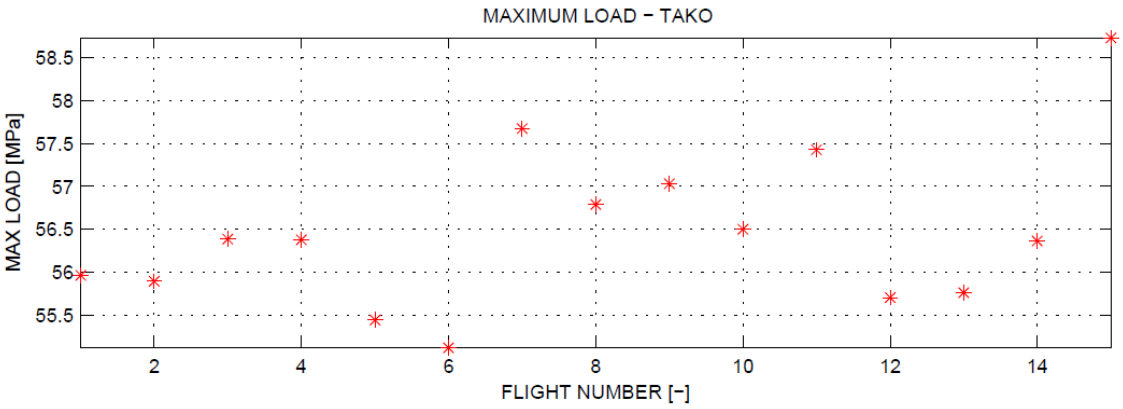

Figure 4.71 – Variability of maximum load – TAKO

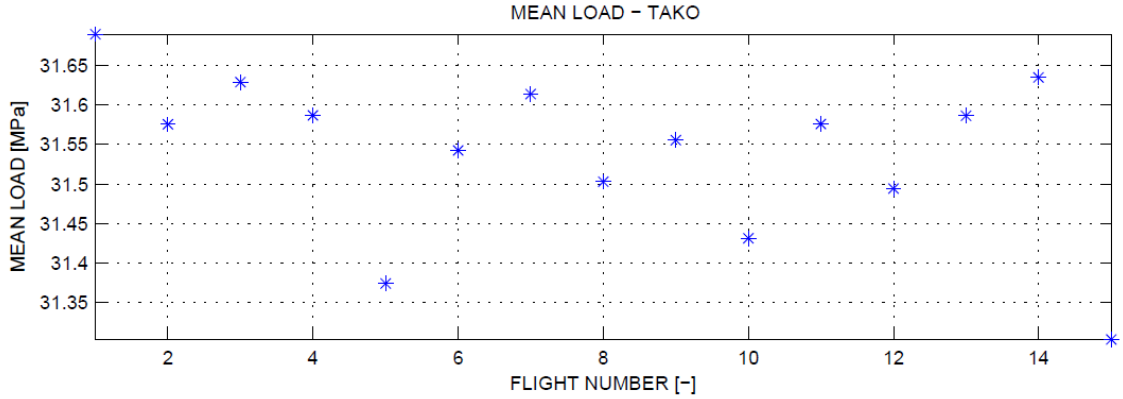

Figure 4.72 – Variability of mean loading – TAKO

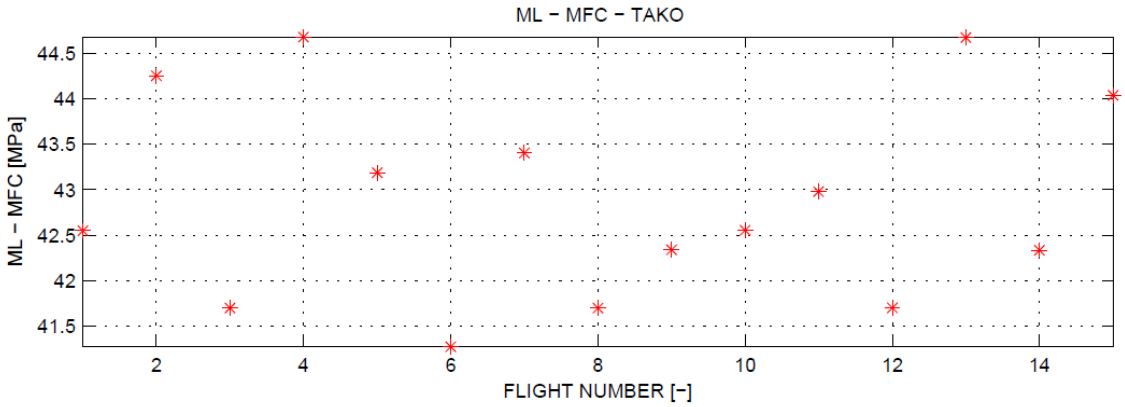

Figure 4.73 – Variability of mean load of the most frequent cycle- TAKO

An output of the flight phase load reconstruction comprises text file containing reconstructed loading history for desired number of flights N_{tgt} and overall number of cycles in the reconstructed loading history, as can be seen in tables below.

	FATIGUE DAMAGE OF THE RECONSTRUCTED HISTORY	
Name of file containing reconstructed load history	RH FN	
Number of data points in the reconstructed history	DPN [FL-1]	

Table 4.32 – Output of the flight phase load reconstruction – description

FATIGUE DAMAGE OF THE RECONSTRUCTED HISTORY	
RH FN	TAKO\SLOT_NO_334_PH_seq_TAKO.txt
DPN [FL-1]	15653

Table 4.33 – Output of the flight phase load reconstruction – TAKO

FATIGUE DAMAGE OF THE RECONSTRUCTED HISTORY	
RH FN	APP\SLOT_NO_334_PH_seq_APP.txt
DPN [FL-1]	47741

Table 4.34 – Output of the flight phase load reconstruction – APP

FATIGUE DAMAGE OF THE RECONSTRUCTED HISTORY	
RH FN	LNG\SLOT_NO_334_PH_seq_LNG.txt
DPN [FL-1]	4515

Table 4.35 – Output of the flight phase load reconstruction – LNG

4.6.3 Join of the reconstructed loading histories

After the load history is reconstructed for each flight phase, join of the flight phases is performed to create a loading history of the entire flight. An initial value of the loading history for each flight is made of the user-defined ground loading condition (see Table 4.30).

Reconstructed loading history for the take-off flight phase is inserted after the ground loading condition.

User-defined cruise flight loading condition (see Table 4.30) is inserted inside the take-off flight phase. The area of insertion of the cruise flight loading condition is found by applying a simple procedure:

The history being reconstructed is analysed backwards. After the load range with the same mean stress/load as the mean stress/load of the most frequent cycle of take-off flight phase is found, the cruise flight loading condition is inserted after this range and before the consecutive point.

The reconstructed history for approach is inserted after the cruise flight loading condition and before the rest of the loading history. The reconstructed history of the landing flight phase is inserted in the same way after the approach flight phase. At the end of the loading history, the ground loading condition is inserted again, which guarantees, that the simplified rainflow counting method for repeating loading histories provides the same fatigue damage as the rain-flow counting method.

The scheme of data insertion technique for each flight is shown in Figure 4.74. After the loading history of the entire flight length is reconstructed, data peaks are separated. Such data processing might cause a creation of some additional cycles in particular flight phase. However, these cycles might produce just an insignificant fatigue damage comparing to the rest of cycles in the corresponding flight phase.

The algorithm is repeated till the desired number of flights N_{FL} is created. For each flight, the following parameters are defined:

- Lower and upper load of flap duty cycle n°1
- Lower and upper load of flap duty cycle n°2
- Fatigue damage due to flap duty cycle n°1
- Fatigue damage due to flap duty cycle n°2
- Sum of fatigue damages caused by flap duty cycles
- Overall fatigue damage caused by the reconstructed history for the whole flight

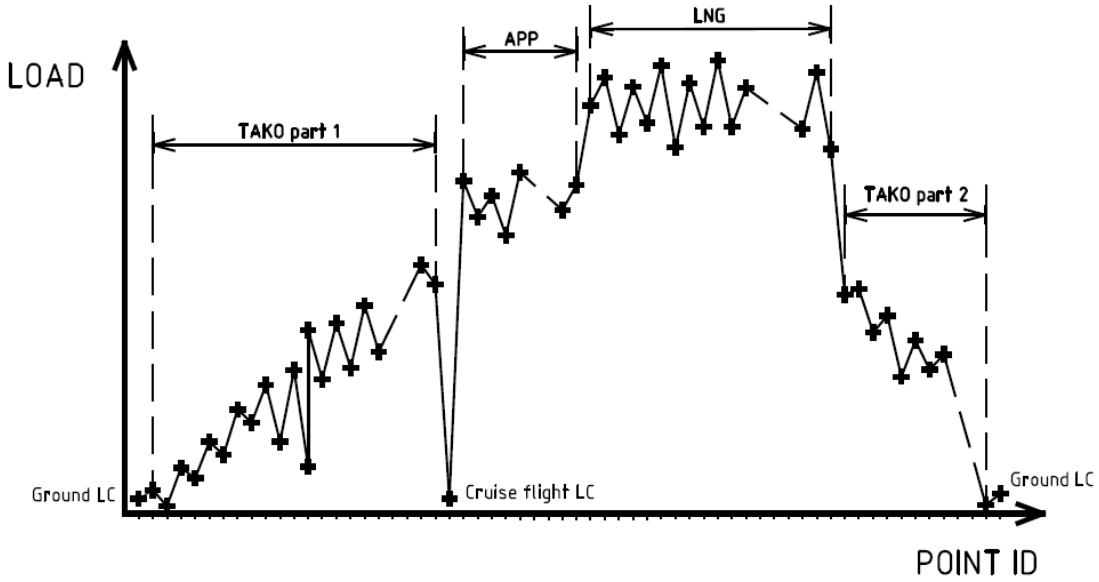

Figure 4.74 – Data insertion technique

The lower load of flap duty cycle n°1 is set equal to the user-defined loading condition for the cruise flight. The upper load of flap duty cycle n°1 is set equal to the mean load of the most frequent cycle in the take-off flight phase.

The lower load of flap duty cycle n°2 is equal to the user-defined loading condition for taxiing (user-defined ground load). The upper load of flap duty cycle n°2 is set equal to the mean load of the most frequent cycle in the landing flight phase.

Figure 4.74 and Figure 4.75 show the resulting loading history for a random flight and the ensemble consisting of altogether 15 flights.

Figure 4.77 to Figure 4.80 display variability of all parameters derived from the reconstructed history.

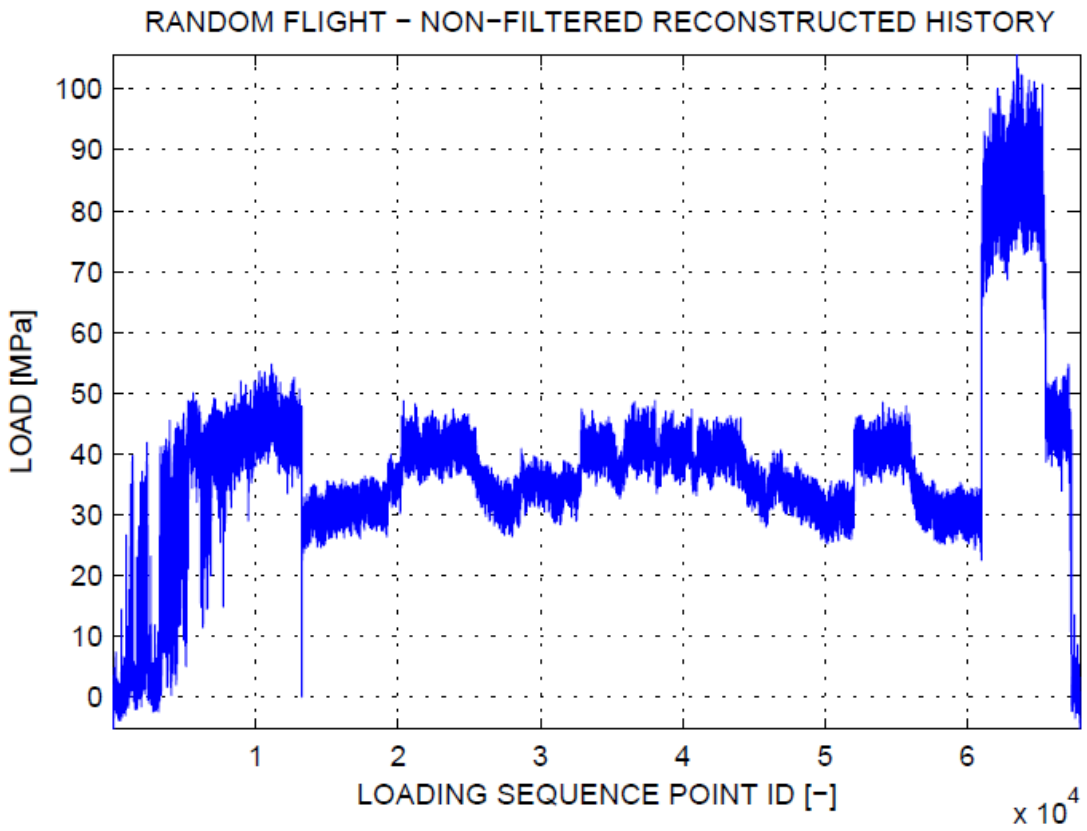

Figure 4.75 – Non-filtered loading history of a random flight

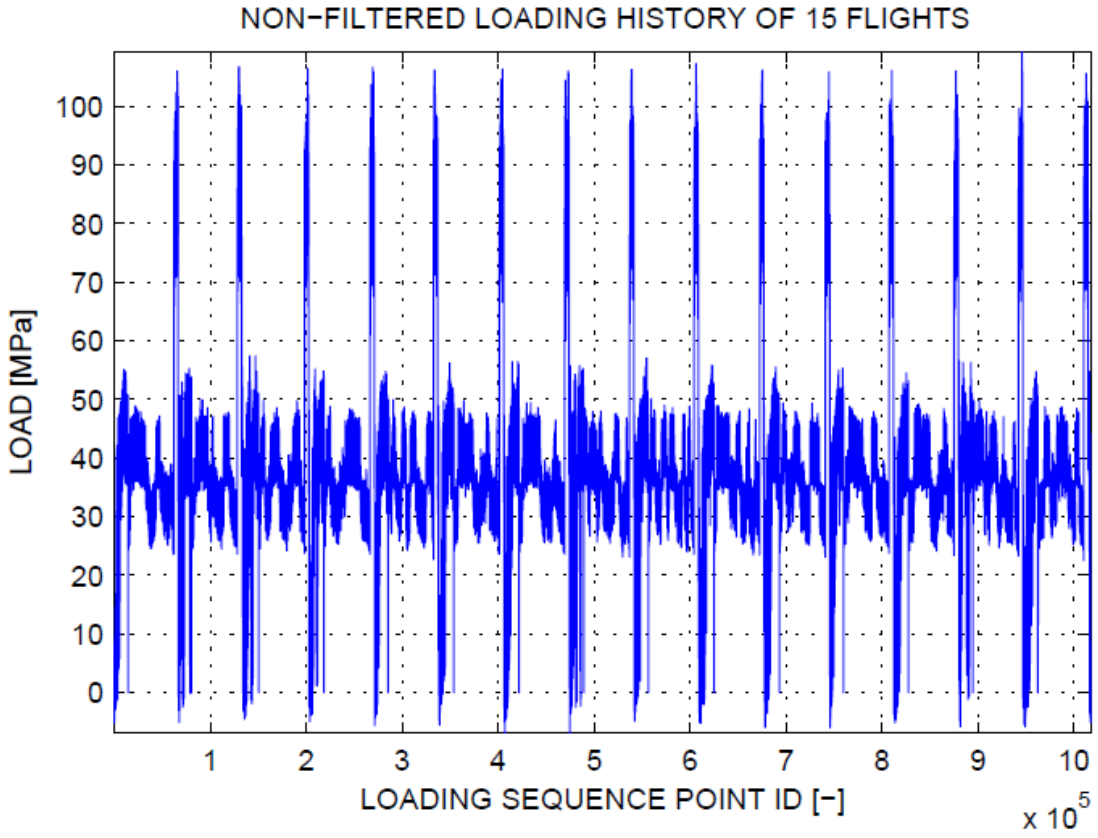

Figure 4.76 – Non-filtered loading history of N_{FL} flights

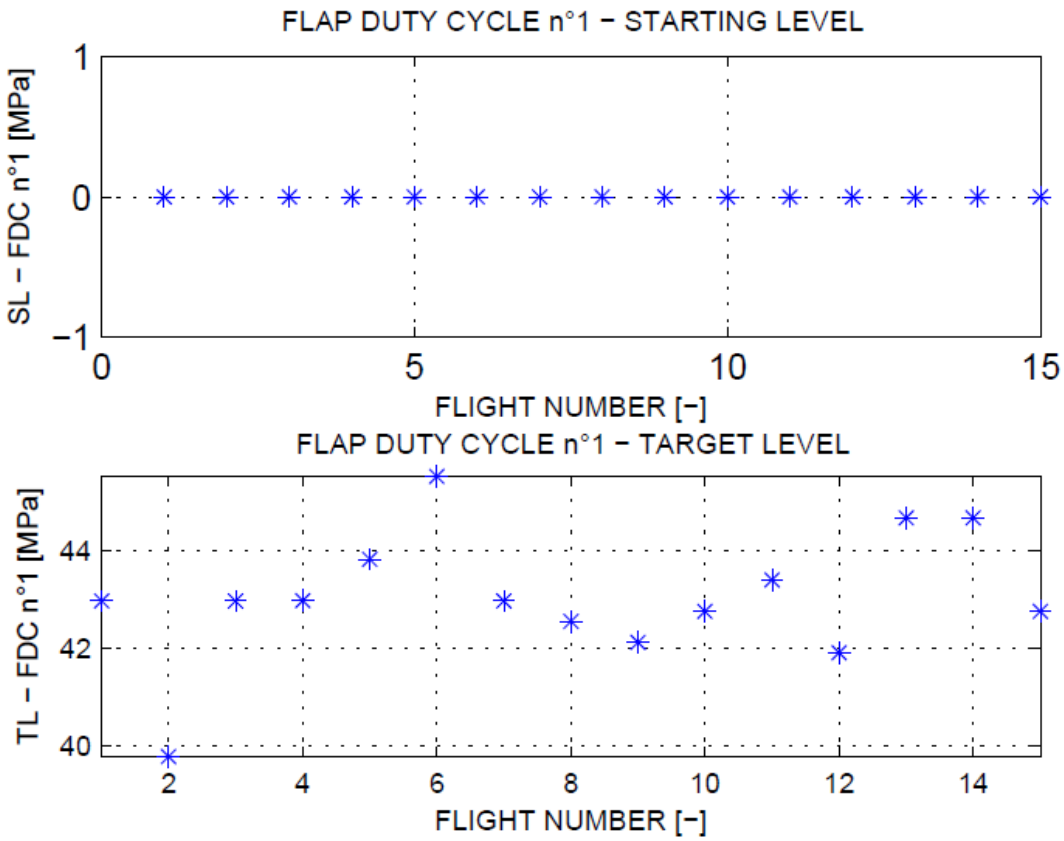

Figure 4.77 – Variability of flap duty cycle n°1

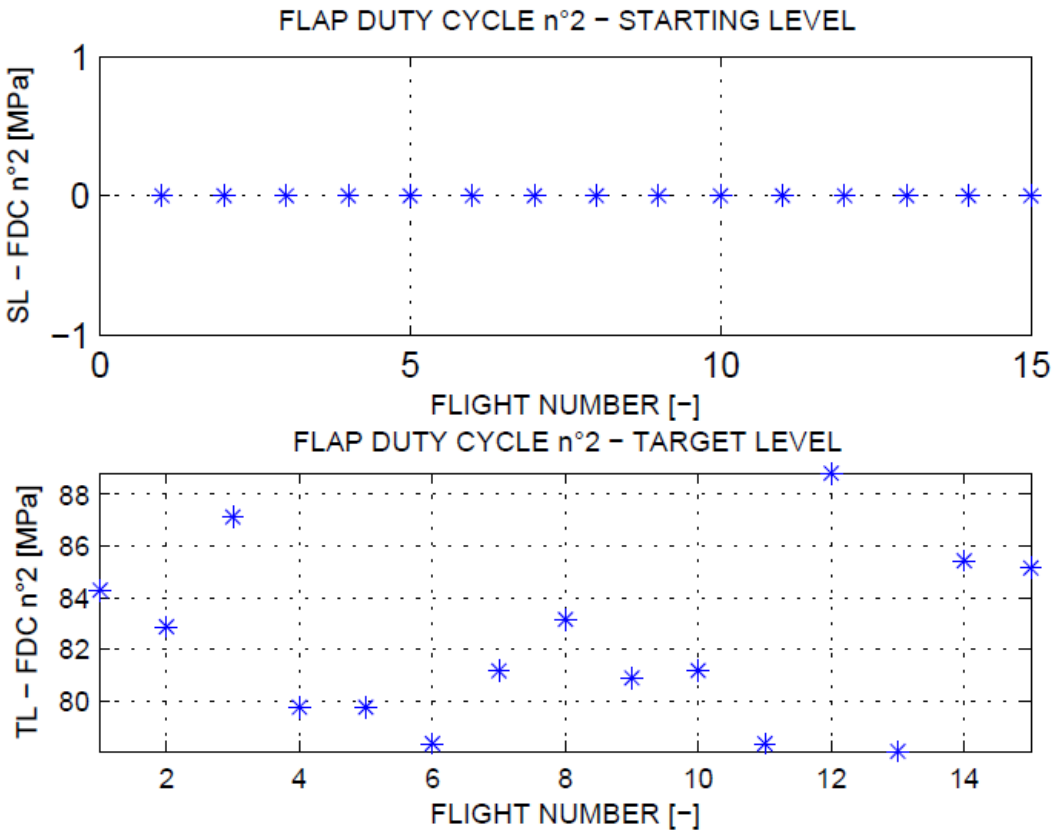

Figure 4.78 – Variability of flap duty cycle n°2

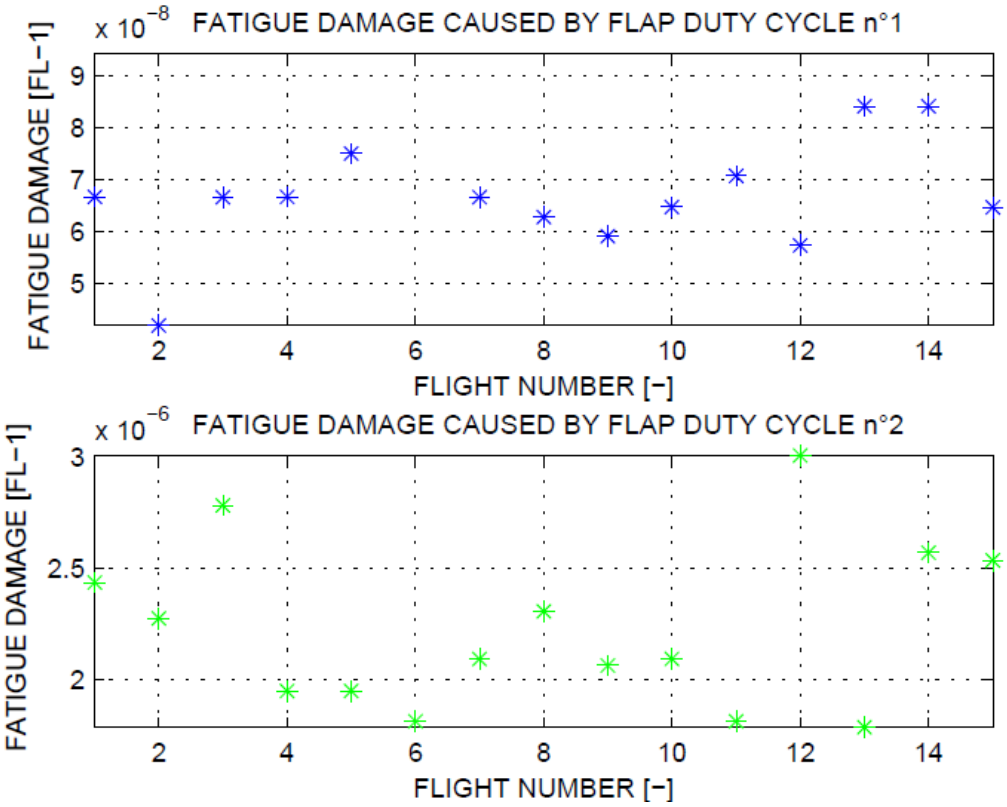

Figure 4.79 – Variability of fatigue damage due to flap duty cycle n°1 and n°2

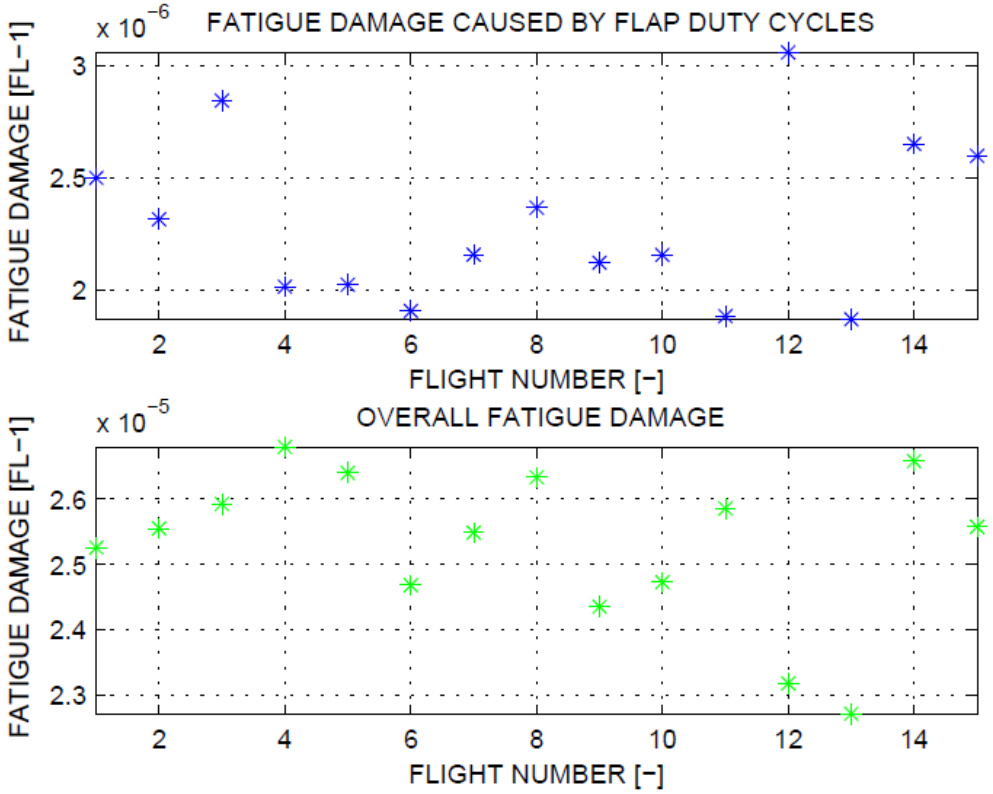

Figure 4.80 – Variability of overall fatigue damage and fatigue damage due to both flap duty cycles

4.6.4 Data filtration

Prior to generation of loading sequence for crack growth calculations using AFGROW, data filtration is performed to reduce volume of data. A parameter controlling the amount of filtration is the relative fatigue damage reduction due to data filtering:

$$\Delta D_{rel} = \frac{D_c - D_{c\,filtered}}{D_c}\ [\%]$$

The user defines maximal permitted value $\Delta D_{rel\,permitted}$ in AIVIB.xlsx file, as shown in Table 4.36.

	RAINFLOW FILTERING		
Maximal permitted error in fatigue damage	Permitted FD error	[%]	0.5

Table 4.36 – Input data from PARAM spreadsheet for data filtration

After $\Delta D_{rel\,permitted}$ is specified, determination of maximal permissible load range $max\{R_{min}\}$ is made. The selection of $max\{R_{min}\}$ is made in line with the flowchart displayed in the following figure.

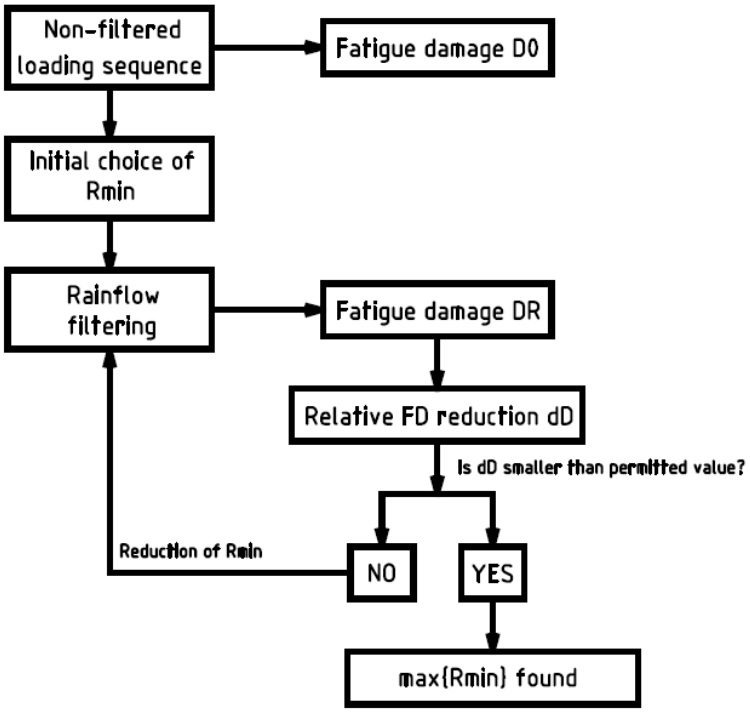

Figure 4.81 – Determination of $max\{R_{min}\}$

An initial value of R_{min} is set to $R_{min} = \frac{R_{max}}{2}$ where R_{max} is a maximal load range in the loading history σ_i consisting of n points:

$$R_{max} = \max\{\sigma_i\}_{i=1}^{n} - min\{\sigma_i\}_{i=1}^{n}$$

If the relative fatigue damage reduction assuming the current R_{min} value is not smaller than maximal permitted value defined by the user, the filtering parameter R_{min} is multiplied by a factor of 0.5. In the other way, $max\{R_{min}\}$ is set equal to current R_{min} value.

An output of data filtering contains a plot of a relationship $D_{c\ filtered} = f(R_{min})$, plot of filtered loading history and AFGROW loading sequence derived from non-filtered and filtered loading histories.

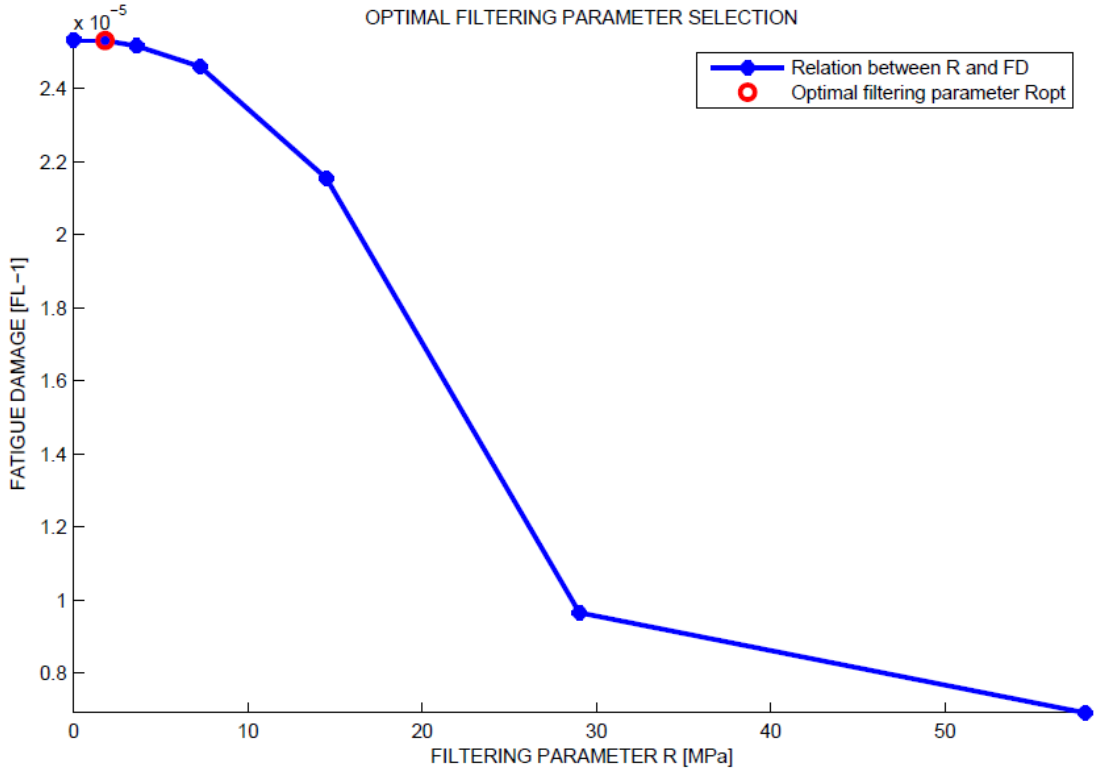

Figure 4.82 – Determination of $max\{R_{min}\}$

The AFGROW loading sequence is generated in line with chapter 2.4. The title is identical with a file output notation defined by the user in INPUT_DATA spreadsheet (see Table 4.2). The sub-spectrum label defines overall number of flights, which form the loading sequence. Type of spectrum is always entered as CYCLExCYCLE, which means, that each cycle is present only once in the loading sequence. Only one .sub file is always created.

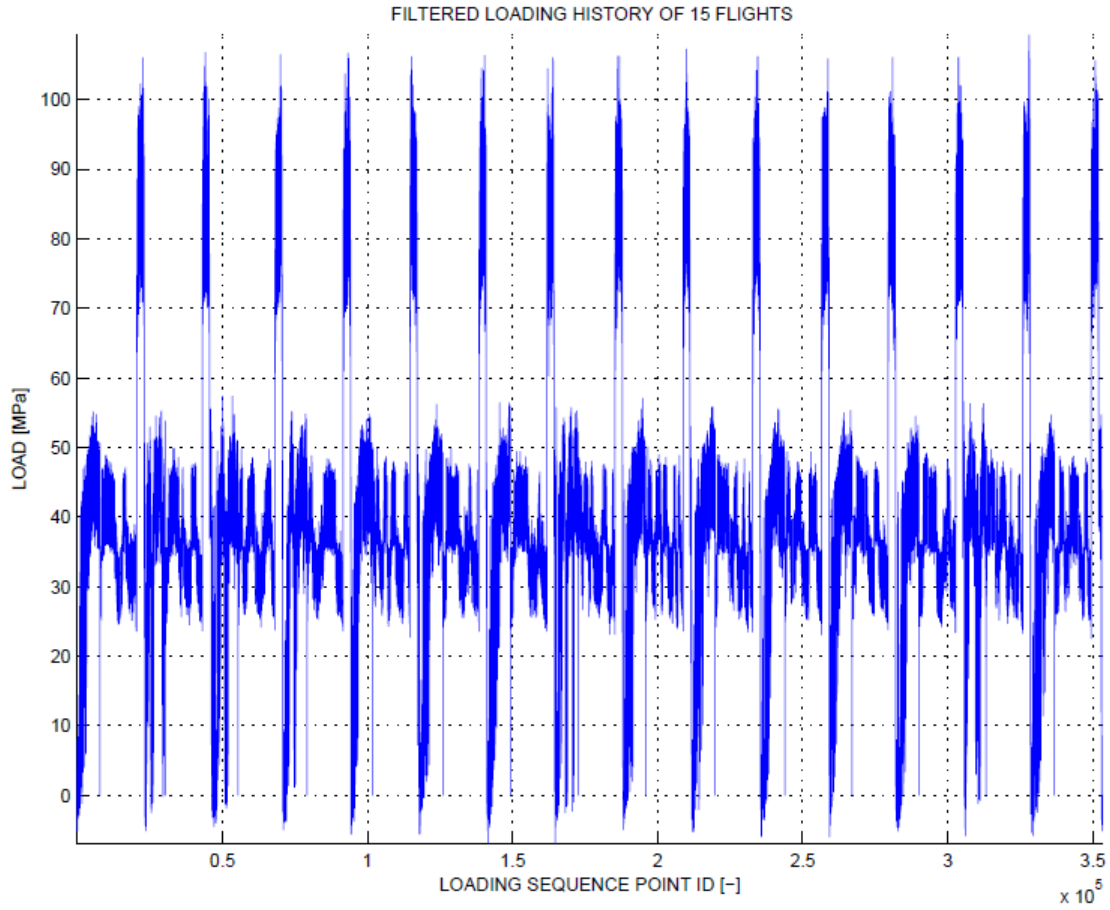

Figure 4.83 – Filtered loading history of N_{FL} flights

4.7 Effect of vibrations on the fatigue life and crack propagation

Similarly to an alternative approach mentioned in the report [26], the effect of vibrations on the fatigue life is defined as the ratio between fatigue damage due to vibrations D_{vib} and the fatigue damage due to flap-duty cycles D_{FDC} (analogy with basic cycle):

$$k_{vib} = \frac{D_{vib}}{D_{FDC}}$$

Fatigue damage due to flap duty cycles is a sum of damages caused by both flap duty cycles computed directly from the measurement, or determined by the user in a form of anticipated loading conditions (see Table 4.30):

$$D_{FDC} = D_{FDC\,1} + D_{FDC\,2}$$

User-defined loading of flaps during taxiing and cruise flight is required, because the test evidence providing sufficient information about these phases is missing at the moment. The loading of flaps in the retracted position is believed to be much less damaging than loading with flaps extended.

Fatigue damage due to vibrations is derived from fatigue damage accumulated during the entire flight D_c reduced by the fatigue damage due to flap duty cycles and fatigue damage due to gusts and variability of the airspeed D_{gust}:

$$D_{vib} = D_c - D_{FDC} - D_{gust}$$

The fatigue damage accumulated during the entire flight is computed using the load spectra obtained by the load reconstruction. It is evident, that the in-flight measurement always cover gust loads. Fatigue damage due to gusts might be exerted by the usage of gust spectra defined for particular aircraft, or other relevant method. It is required to specify the fatigue damage due to gusts by the user.

The effect of vibration cycles on the fatigue crack growth might be observed by comparing the crack growth curve due to flap duty cycles, and the crack growth curve due to flap duty cycles including vibrations. To gain such curves, a loading sequence derived from the in-flight measurement is used for crack growth calculations.

Assuming, that each flight contains two flap duty cycles, the crack growth curves might be normalized into the same units and then easily compared.

Spreadsheet OUTPUT of the AIVIB.xlsx file contains an information about fatigue damage due to vibrations. It contains also a link on a text file with an AFGROW loading sequence derived both from non-filtered and filtered reconstructed loading history.

User-defined number of flights N_{tgt} is always generated. The summary of output parameters is shown in Table 4.37 and Table 4.38.

	OUTPUT SEQUENCE FOR AFGROW ANALYSIS		
Name of file containing reconstructed loading history	Reconstructed history FN	[-]	
Number of points of the reconstructed loading history	RH PN	[-]	
Name of file containing non-filtered AFGROW sequence	Non-filtered sequence FN	[-]	
Number of points of the non-filtered AFGROW sequence	NFS PN	[-]	
Name of file containing filtered reconstructed history	Filtered reconstructed history FN	[-]	
Number of points of the filtered reconstructed history	FRH PN	[-]	
Name of file containing filtered AFGROW sequence	Filtered sequence FN	[-]	
Number of points of the filtered AFGROW sequence	FS PN	[-]	
Maximal permissible filtering parameter	Optimal filtering parameter R	[-]	
Average fatigue damage after data filtration	Average fatigue damage after filtration	[FL-1]	

Table 4.37 – AFGROW loading sequence determination – description

All parameters in Table 4.38 are average values derived from the reconstructed loading history. The only exception is a fatigue damage caused by gusts, which must be entered by the user.

	VIBRATION EFFECT ON FATIGUE DAMAGE			
	FLAP DUTY CYCLES 01 , 02			
Lower stress/load of the flap duty cycles n°1	sd_01	[MPa]	0.00	
Upper stress/load of the flap duty cycles n°1	sh_01	[MPa]	43.06	
Stress/load amplitude of the flap duty cycles n°1	sa_01	[MPa]	21.53	
Mean stress/load of the flap duty cycles n°1	sm_01	[MPa]	21.53	
Equivalent stress/load of the flap duty cycles n°1	s_eq_01	[MPa]	43.06	
Lower stress/load of the flap duty cycles n°2	sd_02	[MPa]	0.00	
Upper stress/load of the flap duty cycles n°2	sh_02	[MPa]	82.29	
Stress/load amplitude of the flap duty cycles n°2	sa_02	[MPa]	41.14	
Mean stress/load of the flap duty cycles n°2	sm_02	[MPa]	41.14	
Equivalent stress/load of the flap duty cycles n°2	seq_02	[MPa]	82.29	
	FATIGUE DAMAGE DUE TO FDC			
Mean fatigue damage due to flap duty cycles	FD_01	[FL-1]	6.842E-08	
	FD_02	[FL-1]	2.232E-06	
	FD_FDC	[FL-1]	2.300E-06	
	OVERALL FATIGUE DAMAGE BY LOADING HISTORY			
Mean fatigue damage due to the reconstructed history	FDc_mean	[FL-1]	2.530E-05	
	FD DUE TO FLIGHT VARIABILITY, GUSTS INCLUDING VIBRATION			
Fatigue damage due to gusts including vibrations	FD_vib+gust	[FL-1]	2.300E-05	
	FD DUE TO GUSTS AND OTHER FLIGHT VARIABILITY			
User-defined fatigue damage due to gusts	FD_gust	[FL-1]	0.000E+00	
	FD DUE TO VIBRATION			
Fatigue damage due to vibrations	FD_vib	[FL-1]	2.300E-05	
	kvib	[FL-1]	10.00	

Table 4.38 – Effect of vibrations on fatigue durability

As can be seen in Table 4.38, zero fatigue damage due to guts is assumed. Such assumption causes an overestimation of vibrations effect. In the case of fictitious example, the resulting fatigue damage due to vibrations is ten times higher than fatigue damage due to flap-duty cycles.

5 CONCLUSION

The master thesis presents a methodology proposed to involve the effect of vibrations into the analysis of fatigue life and crack growth propagation in the structure of flaps and flap's control system on L 410 NG airplane. An approach based on strain gauge survey of analysed locations has been selected. Results of the survey are treated by the means of the time-domain techniques.

As dominant loading cycles of flaps and flaps control system were identified so called flap-duty cycles, which are caused by repeated extension and deflection of flaps during take-off and landing. Loading of flaps in retracted position during straight taxiing and cruise flight is supposed to be significantly lower.

Because only a finite number of flights can be made during the strain gauge survey, an extrapolation of the results is made. Hence, the flight is divided into altogether three phases - take-off, approach and landing. PDF of cyclic loading is estimated for each flight phase by a non-parametric density method.

Different time durations of in-flight measurements from those of the typical flight profile might occur. Therefore, the loading history of user-specified length is regenerated from the estimated PDFs.

The output of the proposed algorithm contains a loading sequence for further crack growth calculations using AFGROW and a ratio between fatigue damage due to vibrations and fatigue damage due to flap-duty cycles k_{vib}.

The effect of vibrations on the fatigue durability is directly expressed in the form of k_{vib} ratio. The effect of vibrations on the crack propagation in particular structural element might be established by comparing the two different crack growth curves. The first one consists of flap-duty cycles only, the second one is derived from the reconstructed loading history which covers apart from the flap-duty cycles also the vibration cycles.

Further development of the algorithm might include the following tasks:

- Enabling to cover other flight phases (cruise flight, taxiing, etc.) specified by the user into the analysis
- Simplification of the PDF estimation process
- Development of a comfortable user-interface for data processing

REFERENCES

[1] ROZSÁR, Peter, et al. *Supplemental Inspection Document Development Program for the aircraft L 410 NG.* Initial release. Kunovice: Aircraft Industries, 2012. MOSTA.0439.A.U.MD.

[2] PELIKÁN, František and Pavel PIŠTĚCKÝ. *Základní aerodynamické a geometrické podklady.* Rev.B. Kunovice: Aircraft Industries, 2011. MOSTA.0101.A.A.TR.

[3] ČASTULÍK, Lubomír. *F&DT analysis of flaps control system*. Initial release. Kunovice: Aircraft Industries, 2016. MOSTA .04105.A.U.TR.

[4] ZVĚŘINA, Ondřej and Jiří VLÁČIL. *Strength analysis of the wing flaps of the L 410 NG airplane.* Rev.B. Kunovice: Aircraft Industries, 2015. MOSTA.0333.A.S.TR.

[5] PIŠTĚCKÝ, Petr. Zatížení vztlakové klapky v zasunuté poloze od vzdušných sil. Initial release. Kunovice: Aircraft Industries, 2012. MOSTA.0112.A.A.TR.

[6] PELIKÁN, František and Peter JUREK. *Typical flight profile.* Rev.G. Kunovice: Aircraft Industries, 2015. MOSTA.0103.A.A.PD.

[7] GE AVIATION. *GE H85 Turboprop engine*. [online] Prague: GE Aviation Business & General Aviation, 2012. [cit. 2017-05-14] AE-65674

[8] GE AVIATION. *GE H80 Turboprop engine*. [online]. Prague: GE Aviation Business & General Aviation, 2012. [cit. 2017-05-14] AE-57856

[9] FEDERAL AVIATION ADMINISTRATION (FAA). *Federal Aviation Regulation (FAR): Part 23*. Washington.

[10] FEDERAL AVIATION ADMINISTRATION (FAA). *Advisory circular AC 25.571-1D*. Washington, 2011.

[11] NEUGEBAUER, Martin. *Měření maximální velikosti osových sil na táhlech ovládání vztlakových klapek letounu L410UVP-E20 s motory H80-200.* Initial release. Kunovice: Aircraft Industries, 2014. L410UVP-E.Z693.VZ01/13

[12] LI LEE, Yung, Jwo PAN, Richard B. HATHAWAY and Mark E. BARKEY. *Fatigue testing and analysis (Theory and Practice)*. Burlington: Elsevier, 2005. ISBN 0-7506-7719-8

[13] RŮŽIČKA, Milan, Miroslav HANKE and Milan ROST. *Dynamická pevnost a životnost*. Praha: Ediční středisko ČVUT, 1987, 212 p.

[14] ASTM E1049-85(2011)e1, *Standard Practices for Cycle Counting in Fatigue Analysis*, ASTM International, West Conshohocken, PA, 2011.

[15] KHOSROVANEH, A. K. and N. E. DOWLING. *Fatigue Loading History Reconstruction Based on the Rain-flow Technique*. Blacksburg: Virginia Polytechnic Institute and State University, 1989. NASA contractor report 181942

[16] KHOSROVANEH, A. K. and N. E. DOWLING. Analysis and Reconstruction of Helicopter Load Spectra. *Paper for the American Helicopter Society National Technical Specialists Meeting on Advanced Rotorcraft Structures*. Williamsbrug, VA, 1988

[17] PERRETT, B. An Evaluation of a Method for Reconstructing Fatigue Test Loading Sequences From Load Data Acquired via Rainflow Counting. *Proceeedings of the 14th ICAF Symposium*. Ottawa, Ontario, 1887

[18] VLČEK, Dalibor. *L 410 NG Fatigue & Damage Tolerance Compliance Guidelines.* Initial release. Kunovice: Aircraft Industries, 2015. MOSTA.0463.A.U.MD.

[19] KAHÁNEK, Václav. *Únavová životnost letadlových konstrukcí*. Bratislava: ALFA, 1977. 262 p.

[20] SCHIJVE, Jaap. *Fatigue of Structures and Materials*. 2nd ed. Dordrecht: Springer, 2008. ISBN 978-1-4020-6807-2

[21] JOHANESSON, P. and M. SPECKERT. Guide to Load Analysis for Durability in Vehicle Engineering. [online]. John Wiley & Sons, 2013. [cit. 2017-05-14] ISBN 978-1-118-64831-5

[22] SILVERMAN, B. W. Density Estimation for Statistics and Data Analysis. Dordrecht: Springer, 1986, ISBN 978-0-412-24620-3

[23] TSYBAKOV, Alexandre B. *Introduction to Nonparametric Estimation*. New York: Springer, 2009. ISBN 978-0-387-79051-0

[24] BOWMAN, A.W. *An alternative method of cross-validation for the smoothing of density estimates*. Biometrika, 1984, **71**, 353-360.

[25] VLČEK, Dalibor. *Methodology of Crack Growth and Residual Strength Analyses*. Initial release. Kunovice: Aircraft Industries, 2014. MOSTA.0464.A.U.MD.

[26] BURIAN, Petr. *Vliv vibrací na únavovou pevnost a rychlost šíření únavové trhliny v Al-slitinách.* R-2695/1992. Praha: VZLÚ, 1992. 42 p.

[27] HARTER, James A. *AFGROW Users Guide and Technical Manual*. Version 5.02.01.18. Dayton: LexTech Inc., 2014. 321 p.

[28] EATON, John W., David BATEMAN, Soren HAUBERG and Rik WEHBRING. *GNU Octave Free Your Numbers*. 4th edition for Octave version 4.0.1. [online]. 2015 [cit. 2017-05-14]

DEFINITIONS AND ABBREVIATIONS

Value Abbreviation	*Units*	*Description*
A	$[MPa^m]$	Constant of S-N curve
a	$[\mathrm{m}]$	Crack length
AC	$[-]$	Advisory Circular
AKE	$[-]$	Adaptive Kernel Estimator
ALC	$[-]$	Anticipated Loading Conditions
ALT	$[-]$	Altitude
APP	$[-]$	Approach flight phase
CED	$[-]$	Cumulative Exceedance Diagram
CKE	$[-]$	Kernel Estimator with Constant bandwidth
D	$[FL^{-1}]$	Fatigue damage
D_c	$[FL^{-1}]$	Fatigue damage due to all cycles during a flight
D_{vib}	$[FL^{-1}]$	Fatigue damage due to vibration cycles
D_{FDC}	$[FL^{-1}]$	Fatigue damage due to flap duty cycles
D_{gust}	$[FL^{-1}]$	Fatigue damage due to gusts
D_{xy}	$[unit^4]$	Deviation moment of axis x, y
DF	$[-]$	Distribution Function
DSG	$[-]$	Design Service Goal
DT	$[-]$	Damage Tolerance
DTA	$[-]$	Damage Tolerance Approach
F&DT	$[-]$	Fatigue and Damage Tolerance
F(x)	$[-]$	Distribution function of a process $X(t)$
$f(x)$	$[-]$	Probability density function of a process $X(t)$
$\hat{f}(x)$	$[-]$	Probability density estimate
FAR	$[-]$	Federal Acquisition Regulation
FC	$[-]$	Flight Cycle
FDC	$[-]$	Flap Duty Cycle
FH	$[-]$	Flight Hour

GE	$[-]$	General Electric
h	$[-]$	Smoothing parameter
IAS	$[-]$	Indicated Air Speed
ISA	$[-]$	International Standard Atmosphere
J	$[unit^4]$	Quadratic moment relative to particular axis
K	$[\mathrm{MPa} \cdot \sqrt{m}]$	Stress intensity factor
K(x)	$[-]$	Kernel function
k_{ext}	$[-]$	Extrapolation factor
k_q	$[-]$	Dynamic pressure increase coefficient
LC	$[-]$	Loading Condition
LNG	$[-]$	Landing flight phase
LSCV	$[-]$	Least Square Cross Validation
m	$[-]$	S-N curve slope
MISE	$[-]$	Mean Integrated Square Error
MSE	$[-]$	Mean Square Error
MTOW	$[-]$	Maximum Take Off Weight
N	$[-]$	Number of cycles to failure
n	$[-]$	Number of cycles in the loading spectrum
n_{cc}	$[-]$	Original number of cycles per flight phase
n_{Fi}	$[-]$	Number of data points in the input file of index i
n_{FL}	$[-]$	Number of cycles per flight phase (normalized to the user-defined flight phase duration)
n_{RD}	$[-]$	Number of input files for particular flight phase
n_{org}	$[-]$	Original number of points in the flight phase
n_{tgt}	$[-]$	Number of cycles per user-defined number of flights
N_{tgt}	$[FC]$	User-defined number of flights
OAT	$[-]$	Outside Air Temperature
PDF	$[-]$	Probability Density Function
Pxx	$[-]$	Residual Stress Strength Requirement
q	$[\mathrm{Pa}]$	Dynamic pressure

R	$[N]$	Load range
R_{max}	$[N]$	Maximal load range in a data set
R_e	$[\mathrm{MPa}]$	Yield strength
R_m	$[\mathrm{MPa}]$	Ultimate strength
RPM	$[-]$	Revolutions Per Minute
SF	$[-]$	Scaling factor
SG	$[-]$	Strain Gauge
SHP	$[-]$	Shaft Horse Power
SLA	$[-]$	Safe Life Approach
SMF	$[-]$	Stress Multiplication Factor
S_{VD}	$[\mathrm{m}^2]$	Propeller disc area
T	$[s]$	Time period
t	$[s]$	Time
TAKO	$[-]$	Take-off flight phase
TAS	$[-]$	True Air Speed
t_{Fi}	$[s]$	time duration of the input data of index i
t_{org}	$[s]$	Time duration of a flight phase during measurement
t_{TFP}	$[s]$	User-defined time duration of flight phase
V_∞	$[\mathrm{m} \cdot \mathrm{s}^{-1}]$	Air speed
w_0	$[\mathrm{m} \cdot \mathrm{s}^{-1}]$	Induced air speed
x	$[-]$	First coordinate of general bivariate data set
y	$[-]$	Second coordinate of general bivariate data set
z	$[-]$	Number of propeller blades
β	$[-]$	Shape function
δ_{FL}	$[\mathrm{deg}]$	Flap's deflection
ε	$[-]$	Relative error
λ	$[-]$	Local bandwidth factor
μ(x)	$[-]$	Mean value of a process $X(t)$
σ	$[\mathrm{MPa}]$	Stress
σ_a	$[\mathrm{MPa}]$	Stress amplitude

$\sigma_{h,ekv}$	$[\mathrm{MPa}]$	Maximum stress of equivalent loading with $R = 0$
σ_m	$[\mathrm{MPa}]$	Mean stress
σ_N	$[\mathrm{MPa}]$	Normal stress
σ_X	$[-]$	Standard deviation of a process $X(t)$
σ_X^2	$[-]$	Variance of a process $X(t)$
φ	$[deg]$	Rotation angle
ω	$[Hz]$	Frequency

LIST OF APENDICES

Appendix A: Extraction of flight phases from an in-flight measurement

The appendix contains the flight phases, which were extracted from the strain gauge survey performed on L410 UVP-E20. General recommendations for flight phase extraction are also covered.

Altogether two flights have been carried out on L410 UVP-E20, denoted as F2202_01 and F2202_02. Take-off, approach and landing flight phase have been extracted from each flight record. Extracted flight phases are shown below.

General recommendations for proper functionality of the proposed algorithm are the following:

a) TAKE-OFF flight phase:
    a. The flight phase begins with the beginning of an acceleration period of the aircraft
    b. The flight phase is terminated by a load decrease due to flap's retraction
    c. The time period before the aircraft's acceleration should be minimal
    d. The extracted record should be cut before the sudden decrease of load due to flap's retraction

b) APPROACH flight phase:
    a. The flight phase begins with the flap's extension into position $\delta_{FL} = 18°$
    b. The flight phase is ended by the flap's extension into position $\delta_{FL} = 42°$
    c. The extracted record should not contain a continuous increase of load due to flap's extension

c) LANDING flight phase:
    a. The flight phase begins with the flap's extension into position $\delta_{FL} = 42°$
    b. The flight phase is ended by a sudden decrease of load due to touch down
    c. The extracted record should not contain a continuous increase of load due to flap's extension
    d. The extracted record should not contain a sudden decrease of load due to touch down

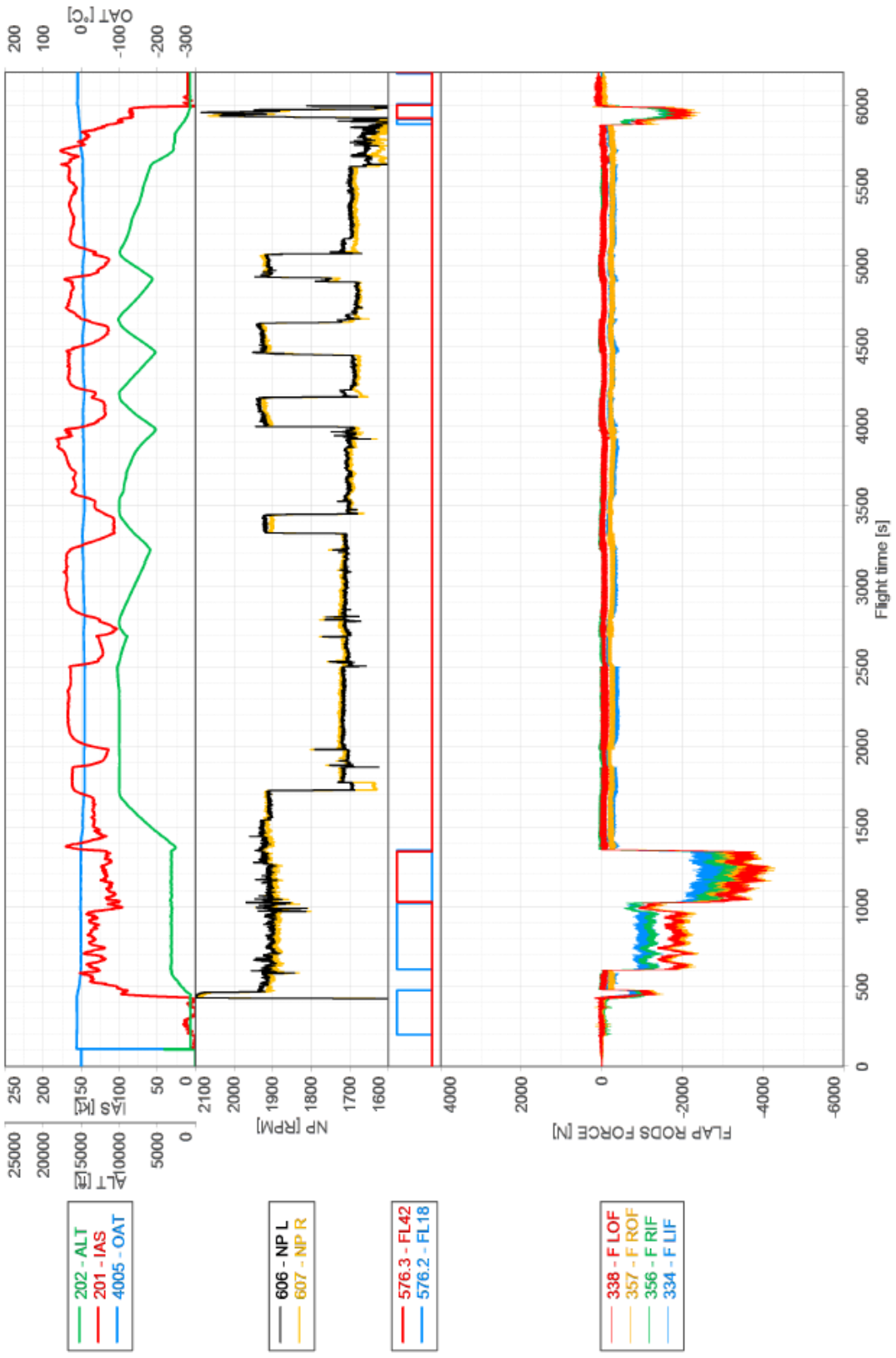

Entire flight record F2202_01

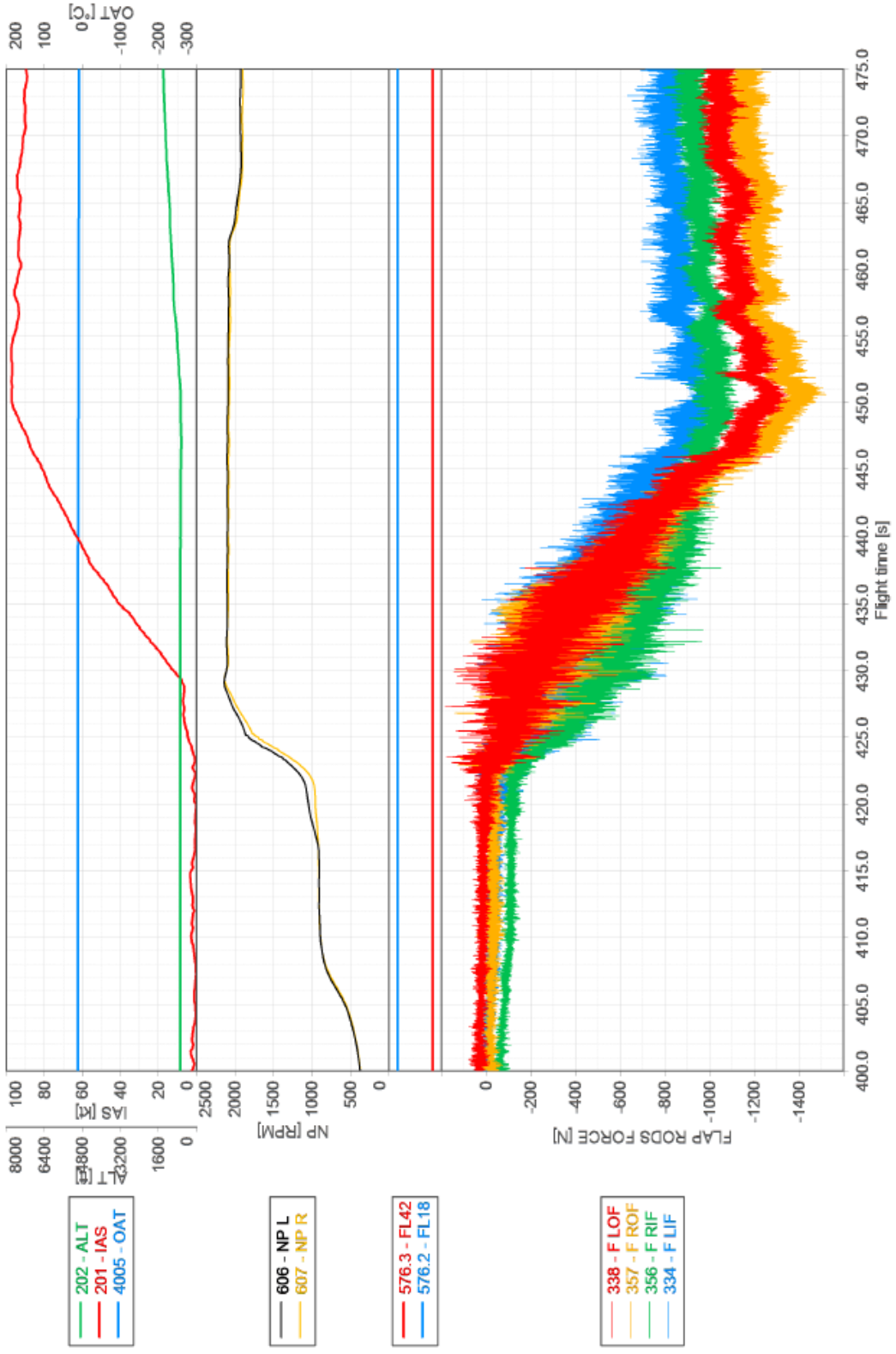

Take-off flight phase extracted from the flight record F2202_01

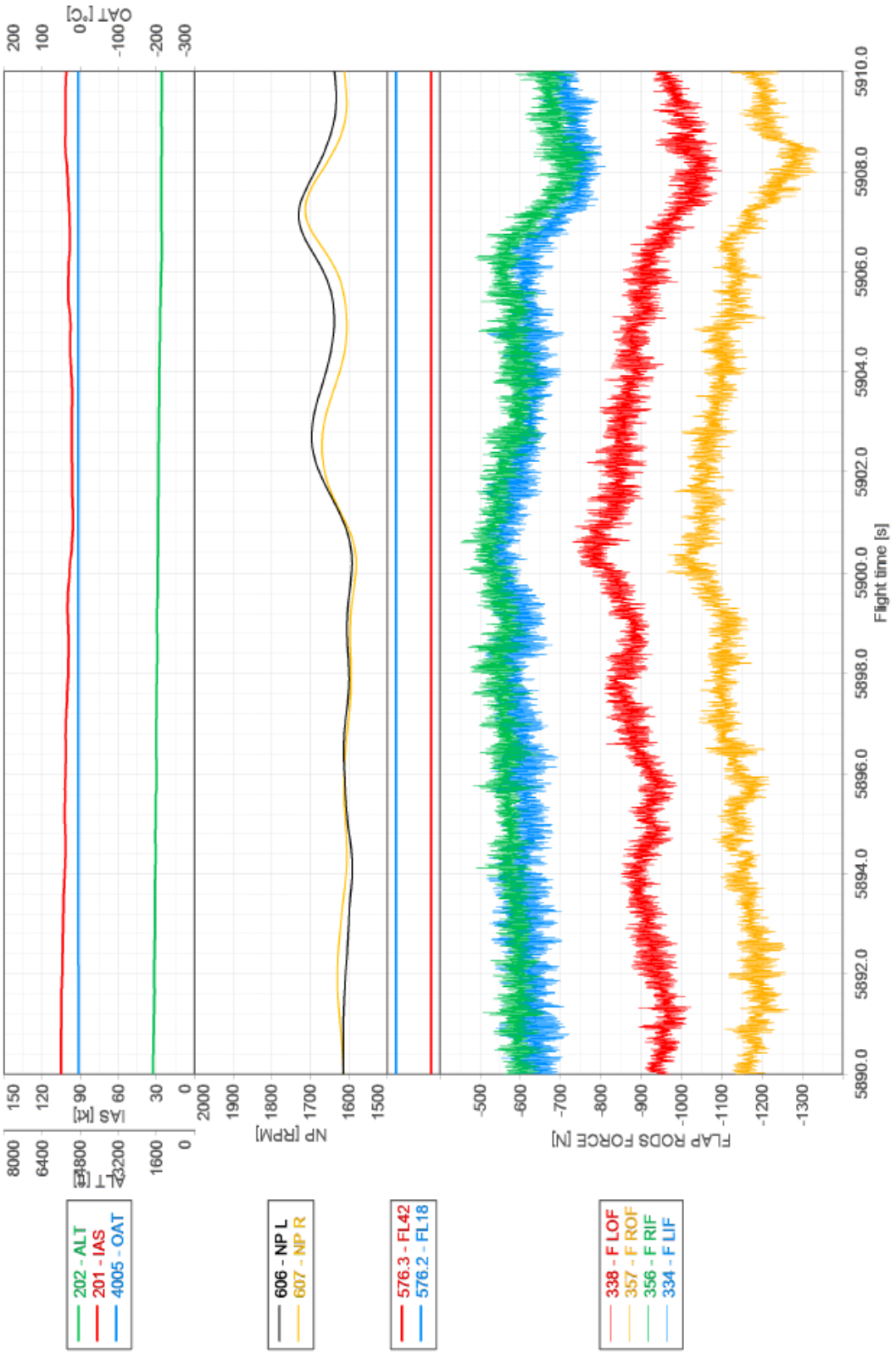

Approach flight phase extracted from the flight record F2202_01

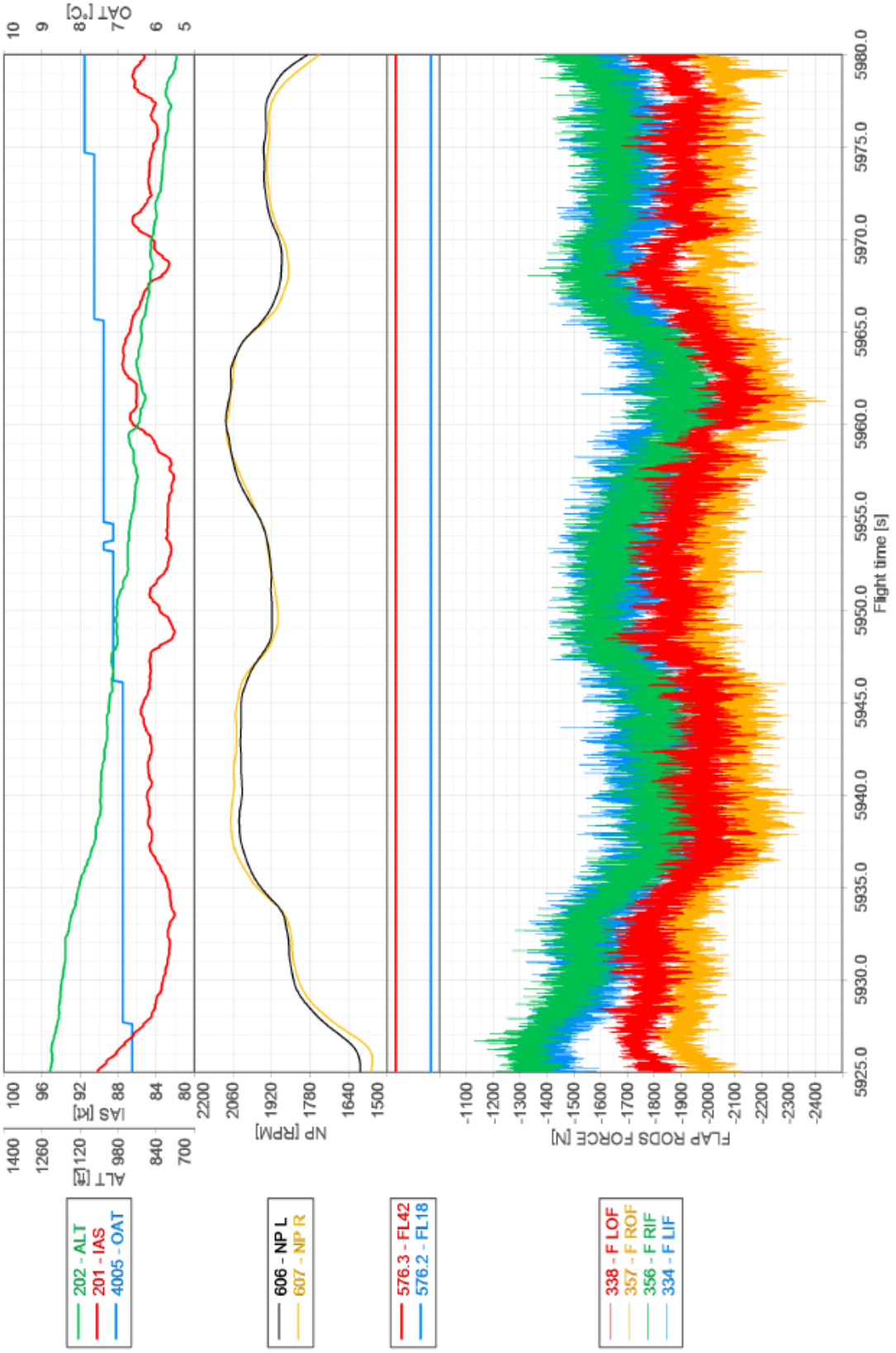

Landing flight phase extracted from the flight record F2202_01

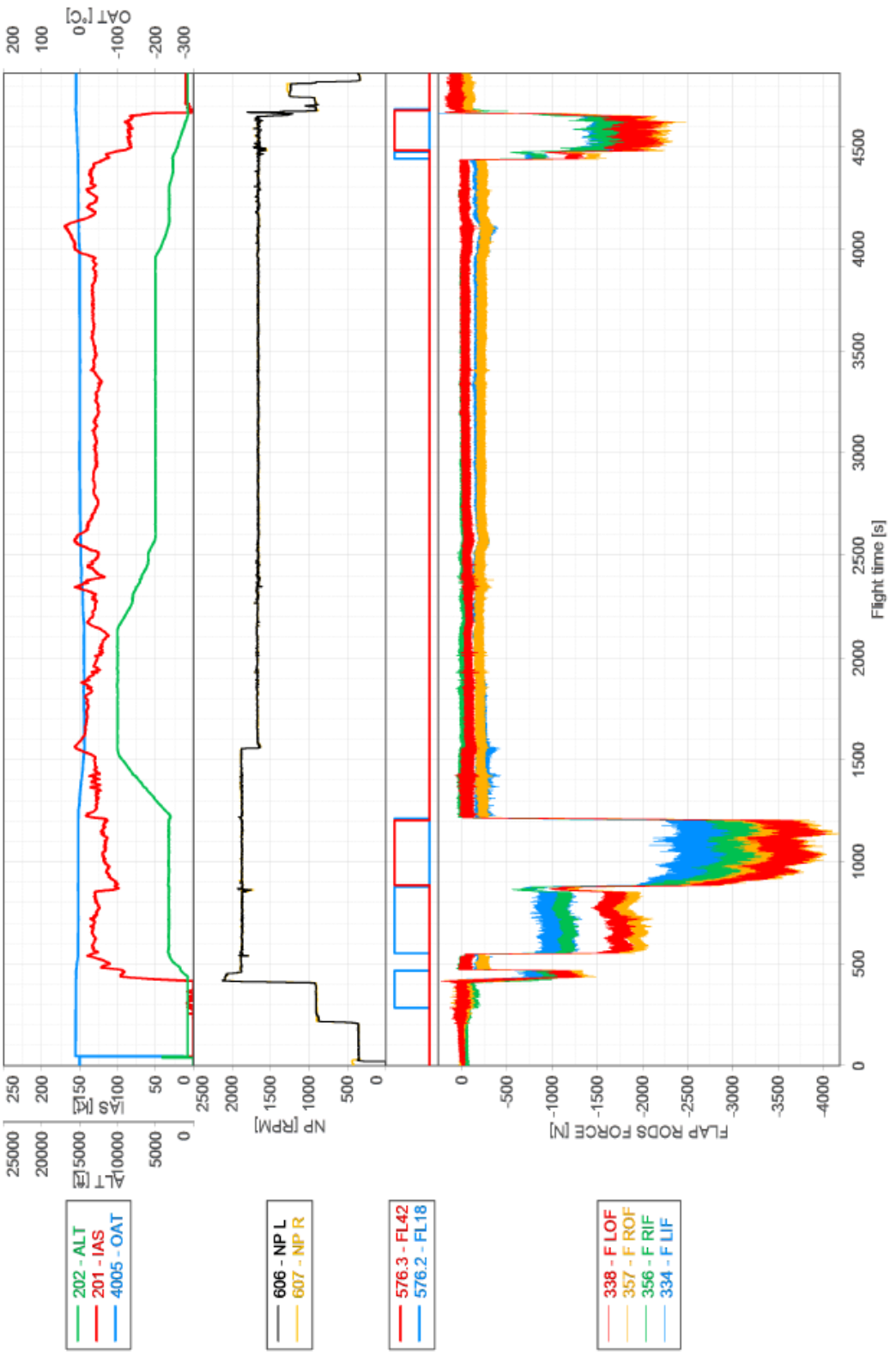

Entire flight record F2202_02

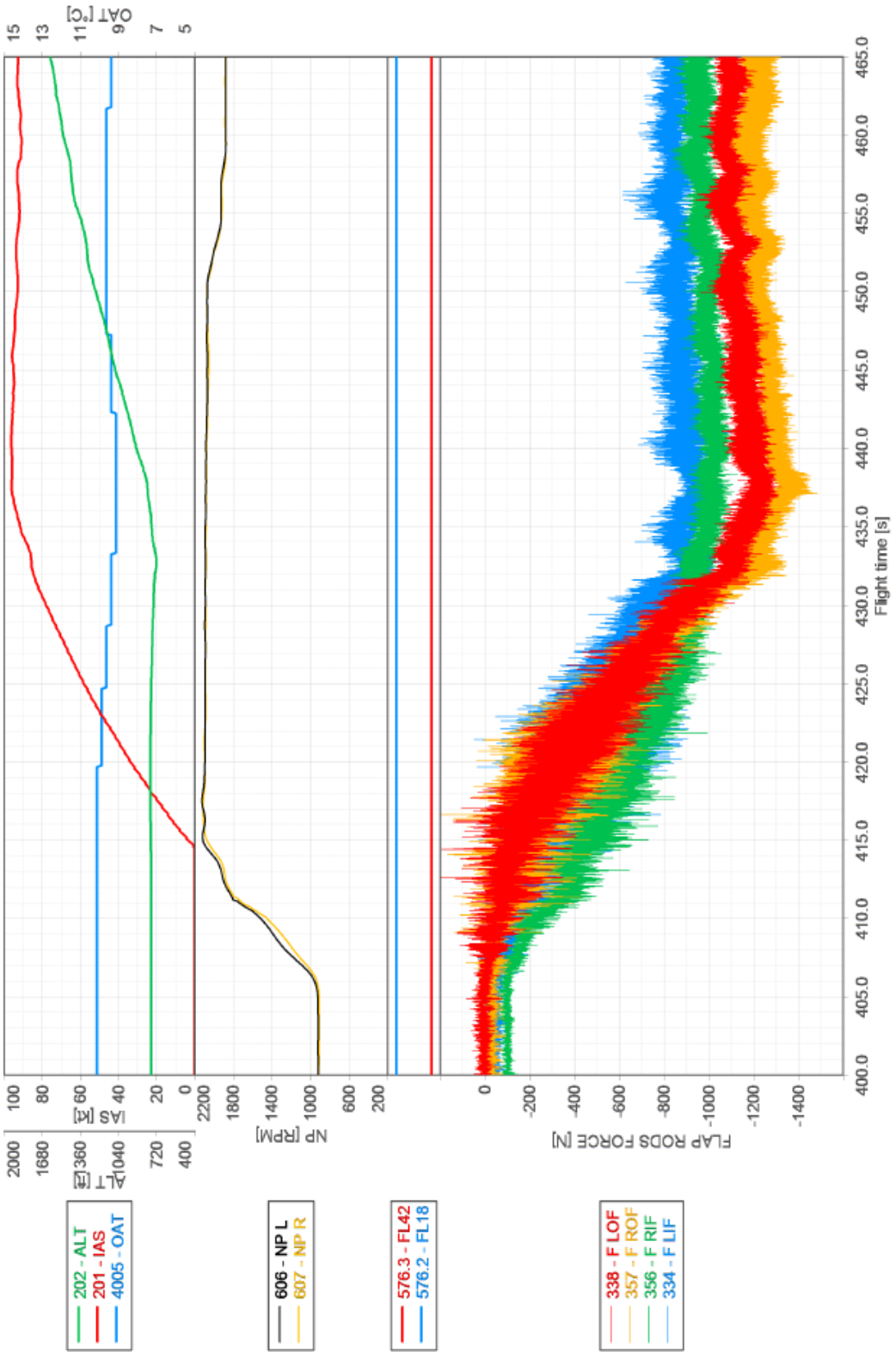

Take-off flight phase extracted from the flight record F2202_02

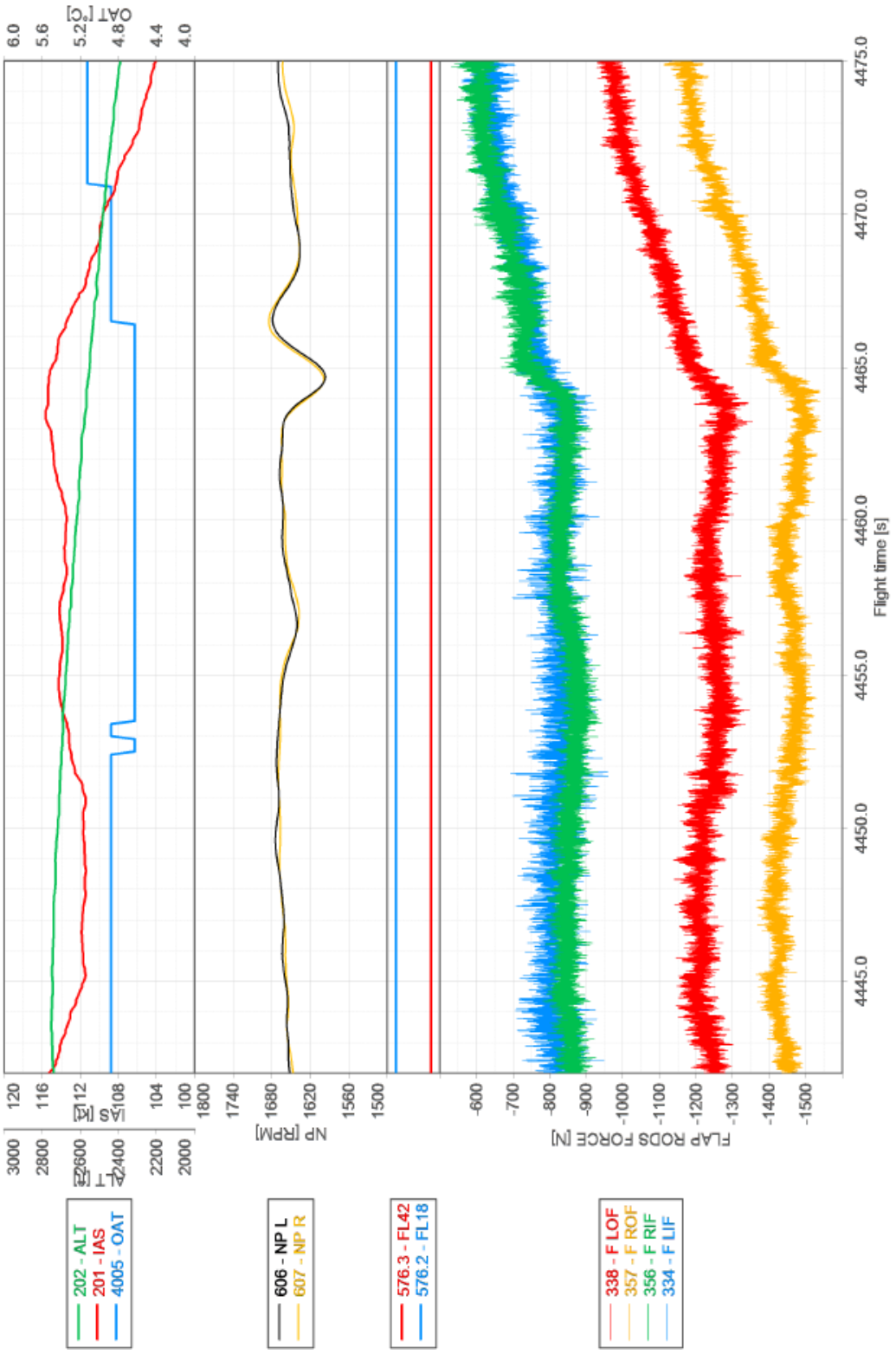

Approach flight phase extracted from the flight record F2202_02

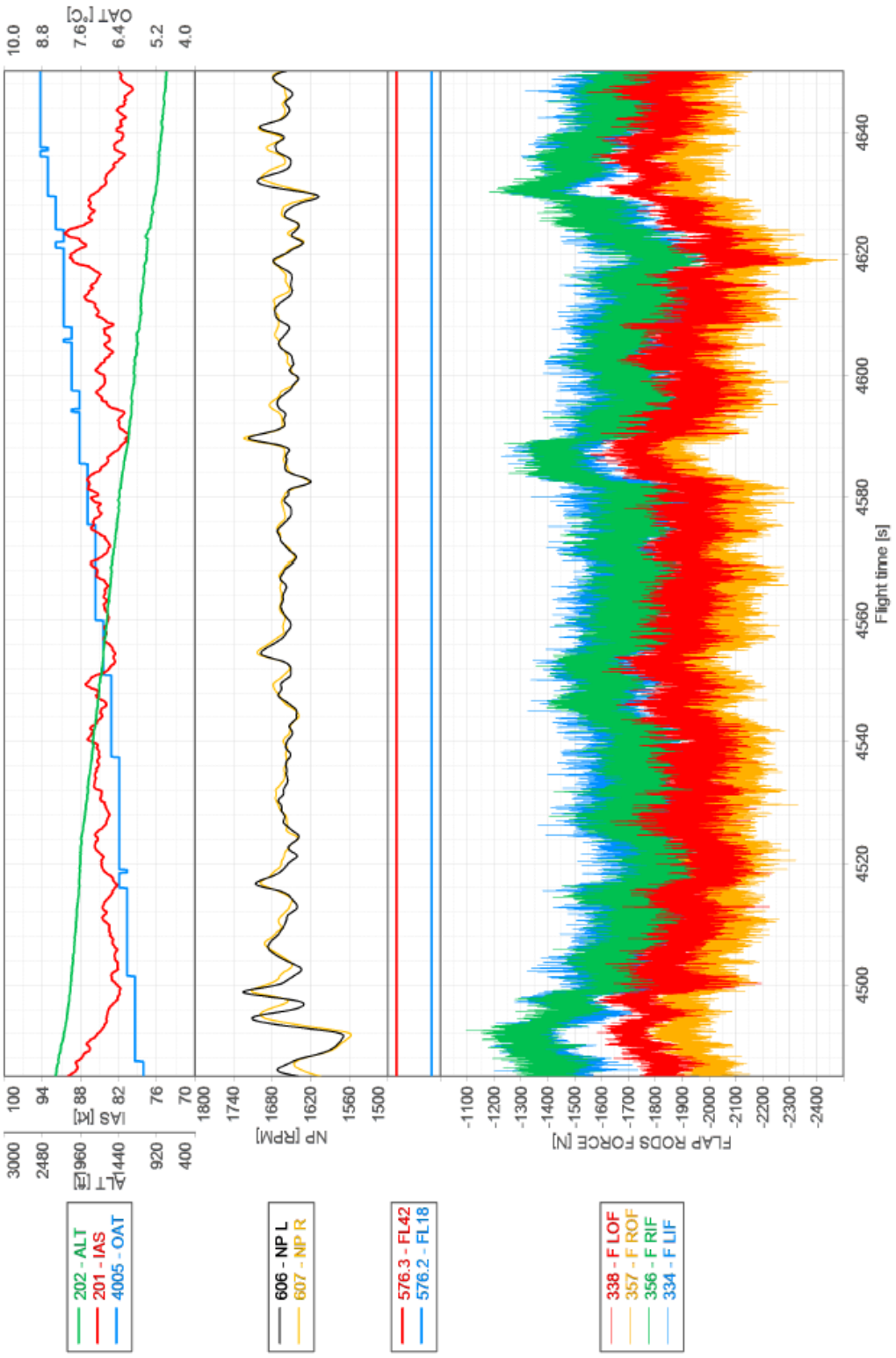

Landing flight phase extracted from the flight record F2202_02

Appendix B: Standard input file description

There is described a standard format of an input file in this appendix. This format must be met for successful loading of an input file. Only mandatory parts are mentioned. Only excel files are accepted (.xls or .xlsx file). Spreadsheet containing data from the in-flight measurement must be named "Data." All other spreadsheets containing any relevant data and descriptions are optional and are not further processed by the algorithm.

The following formats of time units are accepted:

- $[s]$ for seconds
- $[m]$ for minutes
- $[h]$ for hours